Title
Application of Tyrosinase-Mediated Oxidative Coupling to Site-Selective Surface Bioconjugation

Author
Ramsey, Alexandra

Publication Date
2021

Peer reviewed|Thesis/dissertation

Application of Tyrosinase-Mediated Oxidative Coupling to Site-Selective Surface Bioconjugation

By

Alexandra Victoria Ramsey

A dissertation submitted in partial satisfaction of the

requirements for the degree of

Doctor of Philosophy

in

Chemistry

in the

Graduate Division

of the

University of California, Berkeley

Committee in charge:

Professor Matthew B. Francis, Chair
Professor Michael Marletta
Professor Markita Landry

Spring 2021

Application of Tyrosinase-Mediated Oxidative Coupling
to Site-Selective Surface Bioconjugation

By: Alexandra Victoria Ramsey

Abstract

Application of Tyrosinase-Mediated Oxidative Coupling
to Site-Selective Surface Bioconjugation

by

Alexandra Victoria Ramsey

Doctor of Philosophy in Chemistry

University of California, Berkeley

Professor Matthew B. Francis, Chair

Bioconjugation is key to enabling the diverse applications that biomolecules are capable of mediating. While strategies for solution-phase bioconjugation are of critical importance, many applications of biomolecules require surface immobilization. Thus, efficient surface bioconjugation strategies are required in order to enable the full potential of biomolecules, particularly proteins. Many current immobilization methods are not site-specific. Although non-site-specific methods are sometimes effective, such as the new approach for tyrosinase immobilization provided herein, site-specificity is often critical to maintaining protein activity once immobilized. This work focuses on a new method for surface bioconjugation that employs an enzymatic oxidative coupling strategy. The method was optimized on gold nanoparticles, and it was demonstrated that phenol functional groups on gold nanoparticle surfaces can be directly oxidized by the enzyme tyrosinase to enable subsequent site-selective bioconjugation of proteins, including multivalent protein assemblies, and DNA. Cellulose was also explored as a solid support, and small molecule oxidative coupling is described. Appropriate optimization may allow the oxidative coupling approach to be efficient for biomolecule immobilization on cellulose substrates. Progress was also made toward oxidative coupling of proteins on gold chips, with the goal of generating reversible Surface Plasmon Resonance sensor chips to study biomolecule interactions. Overall, the work herein offers a new route for protein immobilization on a range of surfaces, which expands the toolbox of surface bioconjugation and may improve or enable a variety of devices, diagnostics, and other systems that require efficient protein immobilization strategies.

Dedicated to my parents, Chuck and Renee,
who are always on the sideline cheering me on.

Table of Contents

Chapter 1: Protein Bioconjugation Strategies for Modification of Native Amino Acid Residues

1.1 Introduction....2
1.2 General Considerations....2
1.3 Modification Chemistries....5
1.3.1 Lysine Modification....5
1.3.2 Cysteine Modification....7
1.3.3 Tyrosine Modification....9
1.3.4 Aspartic Acid, Glutamic Acid, and C-terminal Carboxylate Modification....10
1.3.5 Tryptophan Modification....12
1.4 Conclusion....14
1.5 References....15

Chapter 2: Immobilization of Tyrosinase for Solution-Phase Oxidative Coupling

2.1 Introduction....21
2.1.1 Enzymatic Oxidative Coupling....21
2.1.2 Immobilized Enzymes....22
2.2 Results and Discussion....23
2.2.1 Design and Initial Characterization of Resin-Bound abTyr....23
2.2.2 Kinetics of Resin-Bound abTyr....26
2.2.3 Stability and Reusability of Resin-Bound abTyr....27
2.2.4 Protein Oxidation by Resin-Bound abTyr....28
2.2.5 Alex's Magic Mushroom Powder....30
2.3 Conclusion and Future Outlook....30
2.4 Materials and Methods....31
2.5 References....33

Chapter 3: Enzyme Activated Gold Nanoparticles for Versatile Site-Selective Bioconjugation

3.1 Introduction....37
3.2 Results and Discussion....39
3.2.1 Generating Phenol Monolayers on 5 nm AuNPs....39
3.2.2 Oxidative Coupling of Proteins and a Small Molecule to Phenol-AuNPs....40
3.2.3 Oxidative Coupling of DNA to Phenol-AuNPs....43
3.2.4 Oxidative Coupling of an Aniline-Containing Multivalent Protein Assembly...45
3.3 Conclusion and Future Outlook....49
3.4 Materials and Methods....50
3.5 References....57
3.6 Supplementary Figures....62

Chapter 4: Oxidative Coupling as a New Method for Conjugating Small Molecules and Biomolecules to Cellulose

4.1 Introduction....74

4.2 Results and Discussion....76
4.2.1 Cellulose Activation with Tosyl Chloride....76
4.2.2 Small Molecule Oxidative Coupling on Aniline(TsCl)-Cellulose....78
4.2.3 Oxidative Coupling of Biomolecules to Aniline(TsCl)-Cellulose....81
4.2.4 Aniline-Functionalization of Cellulose with Isatoic Anhydride....83
4.2.5 Cellulose Activation with 4-Nitrophenyl Chloroformate and Carbonyldiimidazole....86
4.2.6 Cellulose Functionalization through Oxime Ligation....89
4.2.7 Catechol and Phenol Functionalization of Cellulose....92
4.3 Conclusion and Future Outlook....94
4.4 Materials and Methods....95
4.5 References....102
4.6 Supplementary Figures....105

Chapter 5: Progress Towards Regenerable SPR Chips and a Universal Biotinylation Strategy
5.1 Introduction....112
5.2 Results and Discussion....114
5.2.1 Streptavidin Immobilization via Binding to Biotin-Coated Gold Chips....114
5.2.2 Switchavidin Immobilization via Direct Covalent Conjugation....118
5.2.3 Tyrosine-Tagged IL-1β Constructs for Universal Biotinylation....119
5.3 Conclusion and Future Outlook....121
5.4 Materials and Methods....121
5.5 References....126
5.6 Supplementary Figures....129

Acknowledgments

This work and the past five years would not have been possible without an incredible group of people that embarked on my graduate school journey with me. I want to first and foremost thank Matt Francis for welcoming me into his lab and for being the most wonderful advisor that I could have ever asked for. He has provided constant support and mentorship during my time as a PhD student and has helped me grow both personally and professionally. I greatly appreciate his open mind on my career path and his ability to see each of his students as an individual person with unique capabilities and interests. Matt also hosts the best Christmas parties, ski trips, and hiking adventures, all of which are just extra perks of having joined his lab.

During graduate school, I have made some of the most incredible friends and colleagues. I want to thank each and every member, current and former, of the Francis lab for their thoughtful discussions, advice, and kindness. I came to the lab with little knowledge of chemical biology, but my labmates always allowed me to seek advice and ask questions without feeling judged, and for that I will forever be thankful.

I especially want to thank my labmate, roommate, and dear friend, Johnathan, for his endless support from my very first day of graduate school to my very last. From weekly Wednesday dinners and stuying for PhysOrg quizzes; to cleaning and setting up our very own lab benches, troubleshooting experiments, and writing a book chapter; to making cherry cobbler and embarking on evening adventures to Costco – Johnathan helped make my graduate school experience the joy that it was. He cheered me on when I needed it most, and together, we celebrated our accomplishments and trudged through the hardships. I will always value Johnathan's support, advice, and friendship. His incredible and transformative work with tyrosinase also propelled the lab into a new direction and paved the way for many exciting projects.

In addition to Johnathan, I joined the Francis lab with two very talented and wonderful people, Dan and Vanessa. As group barista, Dan has been key to the function of our lab. Lady Gaggia, our group espresso machine, was arguably the most important instrument in the lab, and props to Dan for keeping her operational. Dan proved his loyalty as a friend when he stuck with me on the slopes during our first group ski trip that ended in collisions, wipe outs, and utter exhaustion (though was a great time regardless). He also provided invaluable advice when I dove into the world of cloning during my last several months in the lab. Vanessa played her part in keeping the lab motivated by providing the best vegan treats to fuel the lab when the coffee wore out. She also provided key advice and support during my cloning adventures, in addition to being a genuinely kind and thoughtful person and friend. I will miss Vanessa's smiles, as well as our hallway conversations and laughs. Vanessa is also an inspiration for trying new things – Surfboarding? Rock climbing? Renovating a van? Vanessa has literally done it all.

Vanessa's primary baking competition has been Nick, who is the vegan cupcake master. Chocolate raspberry cupcakes? You bet. Sour patch kids cupcakes? Don't mind if I do. Nick was also the lab's resident NMR expert and helped me on countless occasions when I attempted NMR after a three year hiatus from synthesis.

Amanda provided yet more support when I was facing cloning qualms, but more importantly, she is one of the kindest people that I have ever had the pleasure of meeting.

It has been an absolute joy to work with her and get to know her over the past several years, and I feel incredibly fortunate to have had the chance to write a paper with her. She constantly inspired me through her dedication to scientific rigor and learning new things while also maintaining her incredibly kind and pleasant personality. I will miss our chats about science and life and Amanda's always positive outlook, but I'm also looking forward to seeing what amazing things she does in the lab and beyond!

Our now third years, Derek, Wendy, Jamie, and Paul, have been a wonderful addition to the lab. Whether building a snowman or providing (yet more) cloning advice, Derek showed nothing short of endless kindness and compassion and was always willing to lend a helping hand. Wendy, my lyophilizer mentee and safety officer buddy, was the incognito baker of the lab, and I'm confident that she will keep the lab fueled once Vanessa and Nick depart. Wendy always radiated positivity and support, and she was a true joy to have as a labmate and friend. I greatly appreciated Jamie's down to earth nature – and her cats, which always brightened subgroup and group meetings. She was also a fabulous lab social committee chair and kept our lab moral high. Being a naturally terrible speller, I was constantly in awe of Paul's mad skills with words. I can only dream of one day stacking up to half his expertise.

Gone from the lab but certainly not forgotten, Emily was one of my first mentors in graduate school and remains an amazing mentor and friend to this day. She supported me through my qualifying exam preparation and always found a way to ask how I was doing, how I was *really* doing. I also want to thank my other first mentor in the lab, Sarah, who helped me run my very first bioconjugation reaction. She always installed a sense of calmness, despite approaching science, running, and everything she did with maximum vigor. Another mentor and dear friend of mine, Rachel, always provided, and still provides, fresh perspectives on situations. She has always been positive, real, and inspiring, and I take her advice with utmost consideration. I also want to thank Kristin for helping me to organize my qual studies and for motivating me with cat-shaped sticky tabs. Marco enlivened 726 from the first day of my rotation until the day he set off to start his own company. We bonded over our hair and the miracles of coconut oil for keeping it tame, and we shared in our passion for inter-winding business and science. I thank Laura for installing my obsession with Giant Microbes and also for the collection of small toys that appeared in mystery on my desk over the course of several months. Jing was always a beacon of cheerfulness and high spirit, not to mention yet another incredible baker and cook. We all swooned at her macaroons and boba (with homemade tapioca!). Joel must be thanked for passing on his superb guacamole making skills to the lab. As softball coach during my first summer in grad school, Joel also taught me how to hit (or at least swing at) flying objects. Teaching me how to catch such objects was less successful, but that was not due to lack of effort on Joel's part.

We have had many wonderful post-docs over the years who have provided support and mentorship, so thank you to each and every one of them. Special shout-out to Ayo for helping me run my first grad-school column and helping me trouble-shoot my first synthesis. And special thank you to Celine for just plain being the coolest post-doc and person and to Erik for always showing kindness and willingness to help.

My friends and mentors were key to my graduate school experience, but I was also incredibly fortunate to mentor an undergraduate student, Jesus. His passion for learning

and dedication to excellence have been an inspiration to me, and it was an absolute joy to work with him during my time at Berkeley. I'm excited to see the incredible things that he is bound for!

Due to the timing of the COVID pandemic, I unfortunately did not have the opportunity to interact extensively with Paige or Deborah, but they are clearly passionate and very capable scientists, and I'm sure that they will contribute greatly to the lab. I do want to give a shout-out to my biosafety officer protégé, Deborah, for her willingness to jump in on biosafety duties, especially when I was deep in thesis writing.

Outside of the lab, I want to thank Laura for Taco Bell lunches, horseback riding adventures, treks through Tilden and up Mount Diablo, and sharing in the joys and toruture of a half marathon; Jared for early morning runs and coffee shop adventures; Naomi for Sweetgreen lunch dates; Bonnie, Steve, and Ken for being my RSF family; and Zach for ice cream dates and deep conversations about science and life. Each and every one of these people provided support and helped me to navigate the graduate school experience, while also giving me a source of out-of-the-lab adventures.

I also want to thank Michelle Douskey, who I had the great pleasure of teaching with on four different occasions. She not only taught me how to be a compassionate teacher and how to navigate sensitive situations, but she gave me the agency to take charge and allowed me to discover my potential as a teacher and manager. I only hope that someday I can repay everything that she has helped me to learn and achieve by delivering the same level of mentorship that she has provided to me.

Finally, I want to thank my family – my dad, Chuck, my mom, Renee, my brother, Spencer, and my sister, Paige Gibbons. Each of you helps me to see the beauty in the world and inspires me to wake up every morning and put my best foot forward. You make me feel loved and special and capable. You give me the motivation to pursue my dreams and the strength to never give up. You pick me up when I fall down and are the glue that puts me back together. Thank you for always believing in me, even when I struggle to believe in myself. It is to each of you that I owe everything I have been able to achieve.

Chapter 1

Protein Bioconjugation Strategies for Modification of Native Amino Acid Residues

Abstract

Proteins are magnificent biomolecules that are capable of achieving a vast range of functions. Bioconjugation is an essential tool for exploiting these biomolecules and gaining access to the numerous applications that proteins can enable. Thus it is vital to maintain a bioconjugation toolbox with a wide variety of strategies that can be selected based on the specific application at hand. This chapter presents a popular set of such strategies that target lysine, cysteine, tyrosine, carboxylate, and tryptophan residues. When native residues are not accessible or cannot yield desired selectivity, the reported methods are also effective toward modification of engineered residues. Applications toward surface bioconjugation are also considered and highlight an unmet need that is addressed in the following chapters of this work.

1.1 Introduction

Proteins drive the regulation and function of every organ and tissue in the human body. While derived from a basis set of only 20 amino acids, proteins exhibit incredible diversity owing to the multitude of ways in which the amino acids can be combined. Each permutation leads to a specific three-dimensional folding structure that is critical to the particular role that a protein carries out. Because of the diverse functions attributed to proteins, these biomolecules have found extensive utility in a vast range of fields from drug delivery to diagnostics and even nanomaterials. To broaden the participation in these applications, it is often critical to first append a functional moiety to the protein to generate a "bioconjugate." Common functional moieties include fluorophores, cytotoxic drugs, nanoparticles, radiolabels, polymers, surfaces, and even other biomolecules. The process (termed "bioconjugation") of appending these moieties is key to chemical biology and adjacent fields, and thus much effort has been devoted to developing methods for constructing bioconjugates.[1]

While the majority of new chemistries focus on solution-phase chemistry, novel methods for protein immobilization are equally critical, particularly for advancing the fields of diagnostics and therapeutics where immobilized proteins find a wide range of applications. For example, enzyme-linked immunosorbent assays (ELISA) require initial immobilization of antibodies or other analyte detection elements. Many detection devices, such as lateral flow assays and microfluidic devices, rely on immobilization of antibodies or DNA aptamers on cellulose-based substrates and/or metal nanoparticles. Other applications of immobilized proteins include phage display, which has implications in immunotherapy,[2] and solid phase enzymes, which can enhance the efficiency of purification processes and large-scale industrial applications of enzymes.[3] Despite the vast number of applications, many immobilization strategies are inefficient and lead to loss of native function that is critical to the performance of the device or system.

1.2 General Considerations

Highly stable amide bonds form the backbone of protein structure, but pH and temperature can drastically affect protein folding and thus function. While protein refolding is possible, it can be cumbersome, time consuming, and difficult to achieve. Generally, protein structure is maintained between pH 6 and 8.5 and from 0 ºC to 37 ºC, and thus bioconjugation reactions involving proteins should be carried out in these pH and temperature ranges. Reactions should also employ buffered aqueous conditions, although small quantities (up to 10% by volume) of organic co-solvents such as dimethylformamide and dimethyl sulfoxide can be included. This is necessary when small molecule coupling partners, such as fluorophores, are not soluble in aqueous solvents.

Although protein synthesis has become vastly more scalable in recent years, proteins remain relatively rare and costly when compared to organic small molecule compounds that are produced on massive scales. Because of the valuable nature of proteins, as well as the low concentrations of biomolecules in nature, most bioconjugation reac-

tions occur at low micromolar in protein substrate and correspondingly low concentrations of coupling partners. Similar to proteins, the coupling partners can be quite costly and, as mentioned, exhibit limited solubility. These low concentrations necessitate the use of chemistries with very favorable kinetics, which exemplifies one of the key hurdles in developing new bioconjugation reactions.

Another obstacle in the field of bioconjugation methodology is developing site-specific chemistries, i.e. strategies that target only one residue on a protein that may consist of over 1,000 amino acids. Needless to say, this can be a challenging task. While many methods target a specific residue type, proteins often display multiple solvent-exposed copies of a particular amino acid. This is especially true for lysine, tyrosine, and carboxylic acid residues and can lead to heterogeneous modification.[4] Furthermore, cross-reactivity can be observed, especially when using reagents that can react with multiple nucleophilic residues. Depending on the application, heterogeneous modification may be acceptable, but in many cases, it can greatly affect the properties of the protein, including native activity and solubility. Achieving homogeneous modification often requires genetic manipulation to install reactive residues (either canonical or noncanonical) at specific locations in the protein structure. While an effective strategy, it can be cumbersome, and the success is highly dependent on the nature of the protein and the ease at which it is expressed and purified. As a result, the application of the final conjugate and the need for homogeneous versus heterogeneous modification should be considered before choosing a bioconjugation method (Figure 1). While not discussed in this chapter, it should be noted that many modification strategies developed for protein modification can also be used in the context of DNA conjugation. However, the higher inherent stability of DNA allows for greater flexibility in the reaction conditions, including a broader range of reaction temperatures and the use of higher quantities of organic co-solvents.

Generally, surface bioconjugation faces the same obstacles as solution-phase bioconjugation, with the added complication that surface chemistry is inherently less efficient because it can be difficult for biomolecules to access the surface functional groups. This necessitates constant agitation during reaction. Protein adsorption is another commonly encountered issue, and thus a surface passivation technique, alongside a surface functionalization approach, is often required. Additionally, even when site-specificity is achieved, immobilization can obstruct active sites and hinder substrate access, leading to activity loss. It can also be difficult to control the surface density of immobilized proteins, which may affect the performance of the resulting device or system as an exceedingly dense protein layer can also impede substrate access. A final complication from a practical standpoint is that characterizing and quantifying the extent of surface immobilization can be difficult, making it challenging to optimize reaction conditions.

This chapter will cover traditional and contemporary protein modification chemistries that target lysine, tryptophan, and carboxylic acid residues. Standard modification of cysteine and tyrosine residues will also be discussed. When relevant, applications toward surface modification are considered.

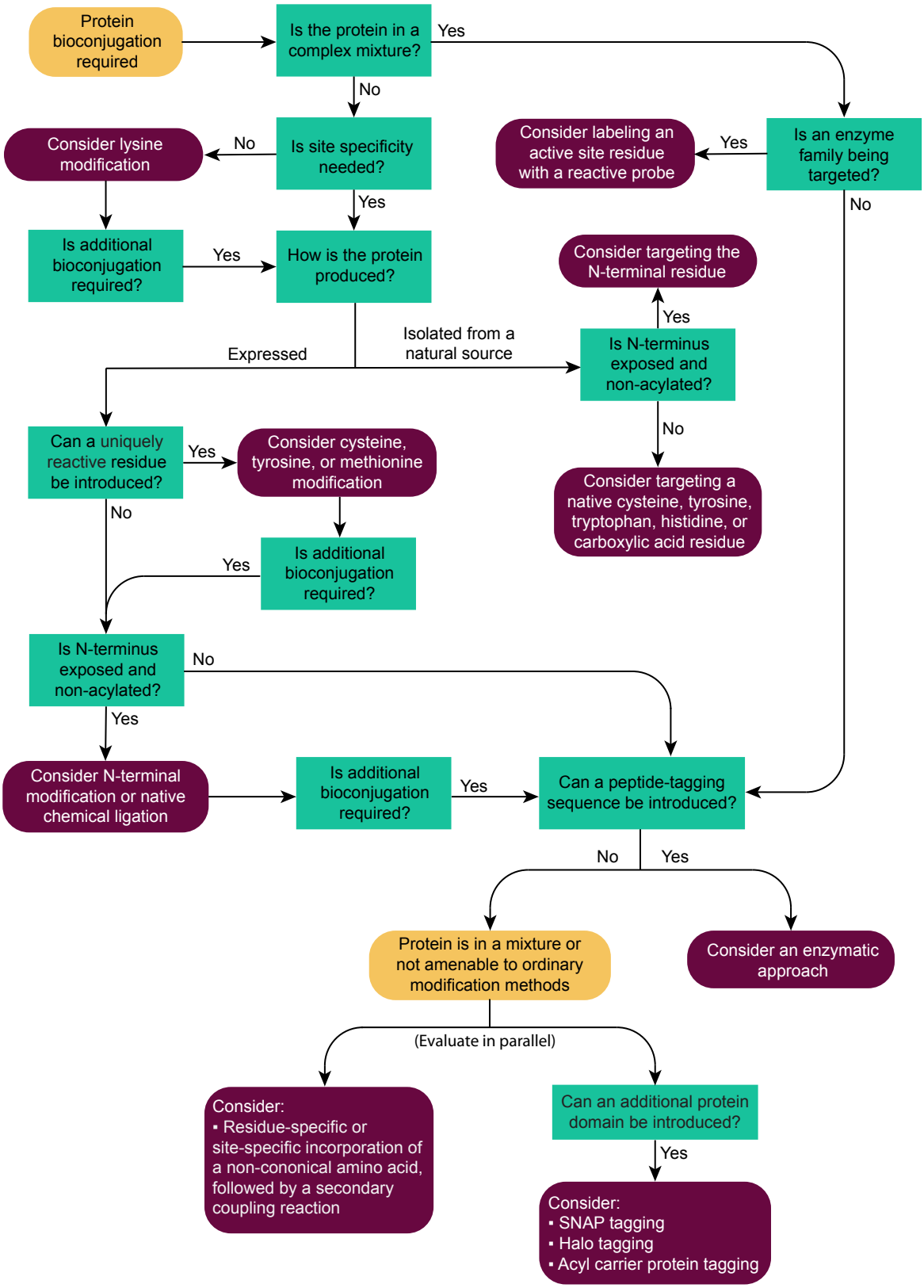

Figure 1. Flowchart to determine the optimal bioconjugation strategy for constructing a desired protein bioconjugate. (Figure is based on a previously published figure.[5])

1.3 Modification Chemistries

1.3.1 Lysine Modification

Within protein sequences, lysine is the 7th most abundant amino acid, and it occurs in over 90% of proteins.[6] This frequency makes lysine a commonly targeted residue for protein modification, especially in cases for which the protein sequence is unknown or cannot be easily altered. The majority of lysine residues are surface-exposed and have a pK_a of roughly 10.5.[7] However, the exact value of the amine pK_a depends on its location and microenvironment. As one striking example, buried lysine residues have been shown to have pK_a values as low as 5.3, representing a 100,000-fold decrease in basicity.[8] For the most part, however, the amines of lysine residues remain largely protonated at physiological pH and exhibit low reactivity. As the pH is raised, increasing numbers of free amines become accessible as reactive nucleophiles. However, this is balanced by protein stability considerations and the fact that many amine-reactive reagents are susceptible to hydrolysis at elevated pH. In practice, therefore, the optimum pH for lysine bioconjugation is roughly 8.5 to 9.5.[9] Since hydrolysis still occurs readily under these conditions, it is common to use large stoichiometric excesses of amine-reactive reagents—particularly when the targeted lysine residue is less reactive due to either limited solution exposure or an increased pK_a value. It is thus recommended to screen varying pH values and reagent stoichiometries to determine the optimal conditions for the case at hand. As an additional consideration, buffers free of amines and other small, nucleophilic molecules must be used.[9]

While lysine modification chemistry is widely applicable across a vast range of proteins, important limitations exist. The high occurrence of this residue almost always leads to heterogeneous modification products. This highlights the key trade-off in lysine bioconjugation chemistry: convenience versus heterogeneity. For example, lysine chemistry is often used as a facile and rapid method for protein immobilization on surfaces, but the inherent heterogeneity can lead to randomly oriented proteins. This can lead to variable protein activities, and, for enzymes or binding proteins, obstruction of active sites or binding regions. An additional limitation of lysine bioconjugation is that other nucleophilic residues, such as exposed cysteines, can cross react with amine-reactive reagents. Despite these limitations, lysine chemistry remains the most common approach for protein modification with tracking labels, polymers, and many other chemical functional groups.

Perhaps the easiest route for lysine modification is the use of *N*-hydroxysuccinimide (NHS) activated esters (Figure 2A).[10] The electrophilic carbonyl of these esters reacts readily with side chain amines to form highly stable amide bonds. While the extent of modification can be controlled by tuning the stoichiometry of the NHS ester components, heterogeneous modification is typically obtained. However, NHS chemistry is very convenient as reactions are typically completed in one hour at room temperature under mild aqueous reaction conditions. Additionally, there exist many commercially available NHS esters, including fluorophores, biotin, and a variety of cross-linkers. NHS esters can also be synthesized from carboxylic acids by initial activation with dicyclohexylcarbodiimide

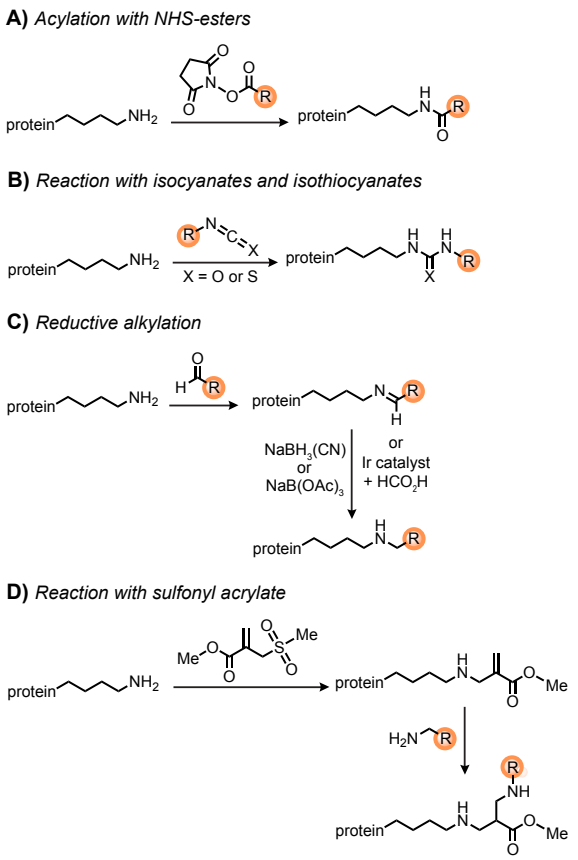

Figure 2. Chemical modification of lysine. (A) Lysine residues can be acylated with NHS-esters. (B) Isocyanates and isothiocyanates react readily with lysine residues. However, isothiocyanates are more readily available. (C) Reductive alkylation of lysine residues can be carried out with borane- and borohydride-based reducing reagents or an iridium-based catalyst and formate ion. (D) A more recent lysine strategy involves reaction with sulfonyl acrylates. (Some components of this figure are derived from a previously published figure.[4])

(DCC), diisopropylcarbodiimide (DIC), or *N*-3-dimethylaminopropyl-*N'*-ethylcarbodiimide (EDC), to form an anhydride intermediate, followed by reaction with NHS-OH. With DCC, the use of dichloromethane as the solvent during the formation step facilitates the removal of the resulting urea byproduct. EDC, on the other hand, offers the advantage of water solubility. For protein immobilization, there are many commercially available resins that are pre-activated with NHS esters. The wide accessibility of these derivatives and ease of use make NHS modification a common and widely used strategy. NHS chemistry is also one of the most common methods for activating surfaces for subsequent bioconjugation. Typically, a monolayer of carboxylic acids is first formed, and these carboxylic acids are subsequently activated through the addition of NHS and EDC.

Lysine residues can also be acylated using isocyanates and isothiocyanates (Figure 2B). Many isothiocyanates, especially fluorophores, are commercially available, while there are fewer isocyanates due to difficulties in storing these reagents. Reaction conditions for isothiocyanates are comparable to those for NHS esters, but the thiourea linkage that forms is often less hydrolytically stable than an amide bond and can degrade over time;[9] thus NHS chemistry is typically preferred.

Reductive alkylation is another method used for lysine modification (Figure 2C). This strategy involves the condensation of an aldehyde with the side chain amine to form a transient imine, which is then reduced with a mild reducing agent, such as sodium cyanoborohydride. The resulting alkylamine linkage has enhanced hydrolytic stability relative to the imine. Despite its widespread use, sodium cyanoborohydride is water sensitive and requires a desiccant for storage. In addition, this reductant has been found to reduce disulfides as well as imines,[9] making it potentially problematic for the modification of antibodies and other proteins with critical disulfide bonds. As a workaround, a variety of borane and borohydride reductants have been developed that display varying water sensitivity, solubility, and reactivity.[11] Additionally, an iridium catalyst that is less water

sensitive than traditional reagents has been reported for reductive alkylation under mild reaction conditions with formate anion as a hydride source.[12]

An important advantage of reductive alkylation approaches is their ability to maintain the overall charge of the proteins, in contrast to acylation strategies that reduce the degree of positive charge with each modification. However, even with effective reducing reagents, reductive alkylation can suffer from long reaction times (often up to 24 h) and moderate-to-low conversion, making it a low efficiency reaction.

Overall, reductive alkylation has found its greatest utility in coupling amines to oligosaccharides.[9] The C-C bond between adjacent hydroxyl groups in sugars can be oxidatively cleaved using sodium periodate, generating two free aldehydes that can then undergo reductive alkylation with amine bearing cargo or proteins. This strategy has found use in the construction of vaccines, including the development of Salmonella vaccines that conjugate glycosylated *S. typhimurium* O-antigens to the carrier protein CRM197.[13,14] The ability to easily generate aldehydes from oligosaccharides has also given reductive alkylation extensive use in conjugating proteins to cellulose. In this case, the 2,3-diol bond of glucose is cleaved.[15] Oxidative activation of cellulose for subsequent reductive alkylation remains one of the most commonly employed strategies for immobilization of proteins to generate cellulose-based biosensors and diagnostics (further discussed in Chapter 3).

Although several long-standing chemistries remain in use, new methods for lysine modification are still being developed. Recently, a chemo- and regio-selective two-step modification strategy (Figure 2D) was shown to target a single lysine residue on five different proteins, including the anti-cancer mAb trastuzumab.[16] The first step is the addition of a sulfonyl acrylate reagent, which is attacked by the most reactive lysine on the protein. This reaction proceeds rapidly at mild reaction conditions (pH 8, 37 °C, 1-2 h), requires only 1 eq of the sulfonyl acrylate, and produces quantitative and irreversible conversion. Selectivity is driven by a hydrogen bond between the side chain amino group and the sulfonyl group. The second step is modification through an aza-Michael addition that can be carried out with an amine-based compound, resulting in conjugation of fluorophores, drugs, or PEG chains. New reactions like this pave the way for the site-selective targeting of this ubiquitous and highly accessible amino acid, as do efforts to improve our understanding of how local environment effects can influence the ability of lysine residues to participate in reactions.

1.3.2 Cysteine Modification

Cysteine residues are attractive targets for site-selective modification owing to their low surface abundance, especially in comparison to lysine. If surface exposed cysteine residues do not exist in the native protein, they can be readily introduced through site-directed mutagenesis. In addition to site-specificity, cysteine residues are active nucleophiles at neutral pH due to their characteristic pK_a of ~8. Furthermore, the S-H bond is relatively weak, allowing access to single-electron mechanisms. Taken together, cysteine

is one of the most sought-after targets when site-specificity is required.

One of the most common methods for cysteine modification is disulfide formation. A prominent example of this is reaction with 5,5-dithio-bis-(2-nitrobenzoic acid) (also known as DTNB or Ellman's reagent, Figure 3A). Because the 2-nitro-5-thiobenzoate anion acts as a highly efficient leaving group, reaction with DTNB can enhance reactivity of exposed cysteine residues, making them more amenable to disulfide formation with other thiols. DTNB can also serve to cap cysteine residues and prevent cross-reaction while other conjugation is carried out.[17] The cysteine can then be liberated by reducing the disulfide bond with a reducing reagent such as dithiothreitol (DTT) or tris(2-carboxyethyl) phosphine (TCEP). The reducible nature of disulfides makes them common in the context of cleavable linkers and drug delivery. For example, incorporation of disulfides in linkers between a drug carrier and a cargo molecule allows targeted release of the drug upon entering the natural reducing environment of cells.[18] Alternatively, *in vitro* reduction can be achieved with DTT or TCEP.

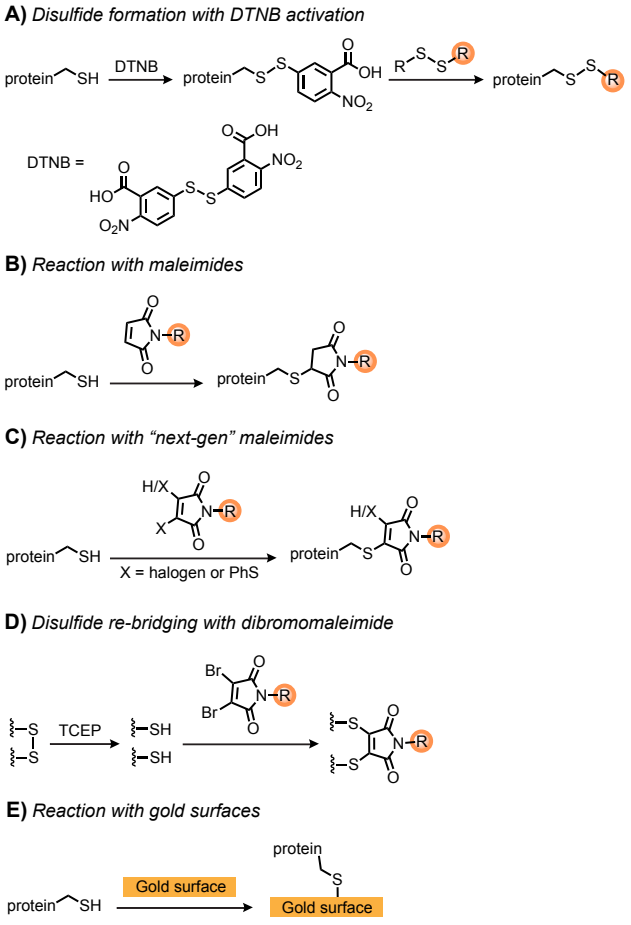

Figure 3. Chemical modification of cysteine. (A) Cysteine residues can be modified through disulfide formation, which is often facilitated by initial reaction with DTNB. (B) Maleimides, either "traditional" (B) or "next-gen" (C), are common reagents for targeting cysteine residues. (D) Dibromomaleimide is a version of next-gen maleimides that is used to modify disulfides. (E) Sulfur atoms form spontaneous bonds with gold, allowing for convenient immobilization of proteins on gold surfaces. (Some components of this figure are derived from a previously published figure.[4])

Maleimide chemistry is another common method for modifying cysteine residues (Figure 3B) and is often employed for functionalizing proteins with cargo molecules. Similar to NHS, many dyes, cross-linkers, and small molecules are commercially available as maleimides, making this chemistry convenient and widely applicable. However, a key limitation of maleimide chemistry is that the linkage is susceptible to hydrolysis and can also be reversed in the presence of competing thiols.[19] In the latter case, the maleimide can be completely transferred to the competing thiol or cysteine residue. This is particularly problematic for *in vivo* applications where glutathione or endogenous proteins can reduce the stability of the maleimide linkage. In the context of surface chemistry, maleimides are a common choice for generating functional monolayers that allow for subsequent bioconjugation.[20,21]

The stability concerns associated with maleimides have led to the development of "next-generation" maleimides,[22] which exhibit enhanced stability on the protein, although some can still be reversed under appropriate conditions.[23] These "next-gen" maleimides feature halogens (typically bromine, but can also be iodine or chlorine) or aryl sulfides in place of one or both of the vinyl hydrogens (Figure 3C). In addition to single cysteine modification, next-gen maleimides can be used to modify disulfides, which is particularly useful in the context of antibody modification.[24] The disulfides are first reduced with low equivalents of TCEP, followed by "re-bridging" with a next-gen maleimide (Figure 3D). Dibromomaleimide is typically used for this application, although other types of re-bridging reagents are also being explored.[25-29] Many of these new re-bridging reagents are aiming to address the reversible nature of maleimides, although deliberate hydrolysis after re-bridging with dibromomaleimide leads to a relatively stable linkage.[30] Disulfide re-bridging is particularly useful for generating antibody-drug conjugates (ADCs) as they allow the ADCs to be generated with control over the drug-to-antibody ratio (DAR).[31] The DAR can range from one to four, corresponding to the number of reduced disulfides. The exact DAR depends on the equivalents of reductant, identity of reductant, and time of reduction. While in theory this should allow precise control over the conjugate, in practice it can be quite difficult to achieve a very specific and uniform DAR. Nonetheless, this strategy has been highly successful in the context of ADCs.

A convenient characteristic of thiols is that they form spontaneous bonds with gold. While this has historically been viewed as a chemisorption interaction with loss of a hydrogen atom from the sulfur, more recent characterization indicates that chemisorption is actually quite rare and the majority of interactions occur through physisorption,[32] although the strength of interaction depends on a multitude of factors. While the gold-thiol interaction is often used in the context of forming functional self-assembled monolayers, this interaction also allows direct immobilization of proteins on gold surfaces (Figure 3E). This can occur through either an engineered cysteine residue[33] or, in the case of antibodies, through reduction of disulfide bonds.[34] This allows direct immobilization of proteins on gold nanoparticles or other gold supports, but it can still be difficult to control the surface density of the protein, and, depending on the application, background adsorption can be particularly problematic.

1.3.3 Tyrosine Modification

Tyrosine is a relatively rare amino acid in proteins with an abundance of 3%[35] and, along with tryptophan and phenylalanine, is one of only three aromatic amino acids (excluding histidine). Owing to the aromatic nature of tyrosine, electrophilic aromatic substitution (EAS) is the primary mechanism by which tyrosine residues are modified.[4] Tyrosine exhibits a relatively high pK_a value of 10.5, and thus most tyrosine residues remain neutral at physiological pH. Tyrosine modification thus imparts little impact on the overall protein charge and minimally affects protein solubility and other charge-dependent characteristics. This, along with other aforementioned characteristics, makes tyrosine a very attractive target for site-specific conjugation. However, tyrosine residues are often buried in the protein structure and thus, not solvent exposed.[36] In the absence of accessible

residues, genetic engineering of tyrosine residues, often at the N- or C-terminus, can enable access to this prime bioconjugation target.

Historically, tyrosine modification has been achieved through aryldiazonium salt coupling (Figure 4A).[37] In this reaction, a diazonium compound reacts with tyrosine residues through an EAS mechanism. The speed of the reaction can be enhanced by installing electron withdrawing groups at the *para* position of the diazonium.[38,39] While diazonium coupling has been highly successful, one drawback of this approach for tyrosine modification is that cross-reactivity with histidine is often observed. Additionally, the highly reactive diazonium compounds must be generated immediately before use, which requires exposing an aniline precursor to strongly acidic conditions.

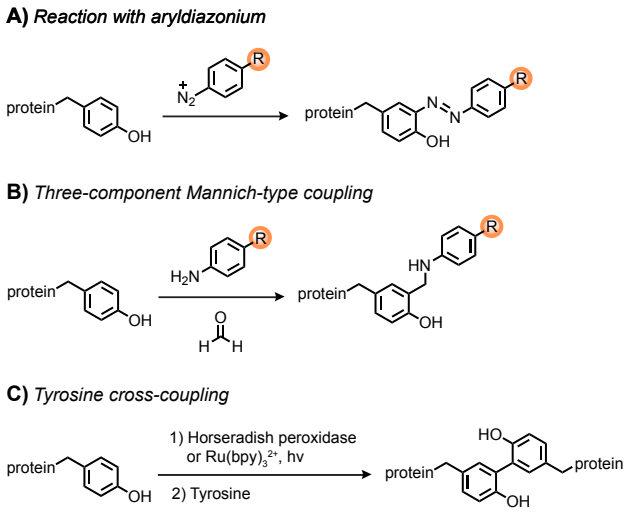

Figure 4. Chemical modification of tyrosine. (A) Tyrosine residues can be modified via reaction with aryldiazonium by way of an electrophilic aromatic substitution (EAS) mechanism. (B) EAS also facilitates the three-component Mannich-type coupling that yields a new carbon-carbon bond. (C) Tyrosine cross-coupling can be mediated either enzymatically or photochemically. (Some components of this figure are derived from a previously published figure.[4])

A three-component Mannich-type coupling reaction can also be used to modify tyrosine residues (Figure 4B). The three components of this reaction are the protein bearing an accessible tyrosine residue, an aldehyde (often formaldehyde), and an aniline.[40] A Schiff base is formed through condensation of the aldehyde and aniline, and this reactive imine then undergoes reaction with the tyrosine residue through a Mannich-type EAS mechanism to form a new carbon-carbon bond. While native lysine residues can also undergo condensation with the aldehyde, control over reaction pH can tune selectivity for condensation with the aniline.

Another common method for targeting tyrosine residues is tyrosine cross-coupling (Figure 4C). In this strategy, a radical is generated in the phenol ring, which then dimerizes with a tyrosine residue on another protein. Formation of the radical can be facilitated by enzymes such as horseradish peroxidase[41,42] or can be photo-mediated in the presence of water soluble metal complexes such as $Ru(bpy)_3^{2+}$.[43] Tyrosine cross-coupling is a convenient method for generating protein-protein conjugates and even multivalent protein polymers.[41] Additionally, this conjugation strategy has recently been employed in the context of protein immobilization. Streptavidin was immobilized on a polyvinylphenol surface in the presence of horseradish peroxidase.[44] Importantly the streptavidin maintained its ability to bind biotin, highlighting tyrosine cross-coupling as a strategy that can maintain native activity of immobilized proteins.

1.3.4 Aspartic Acid, Glutamic Acid, and C-terminal Carboxylate Modification

Aspartic acid, glutamic acid, and the C-terminus present carboxylic acids that can participate in modification reactions. Both of the acidic amino acid residues are highly abundant and are frequently found on protein surfaces. The C-terminus and aspartic acid groups have very similar pK_a values (3.5 and 3.3, respectively), while glutamic acid exhibits a slightly higher pK_a of 4.2.[7] Similar to lysine residues, the pK_a values of individual carboxylate groups are highly influenced by the local environment. In general, however, the small differences in these pK_a values are insufficient to allow selective modification based on this parameter alone. As a result, very few site-specific conjugation chemistries for acidic residues and the C-terminus exist.

Carboxylic acids, whether at the C-terminus or displayed on aspartate and glutamate residues, can exhibit enhanced electrophilicity when pre-activated with reagents like EDC and NHS (Figure 5A). As discussed in the lysine section, these activated esters subsequently react to form highly stable amide bonds with amine-based reagents. However, the activated carboxylates are susceptible to hydrolysis, making these couplings inefficient. Furthermore, amide bond formation is rarely selective for a single residue, making the construction of well-defined conjugates very difficult using this approach. In the context of surface chemistry, carboxylate residues can be activated with EDC/NHS and then coupled to amine-functionalized surfaces.

As a reactive alternative, a method has been developed that esterifies carboxyl groups using diazo compounds (Figure 5B).[45,46] In this case, the carboxylate acts as a nucleophile and proceeds through an S_N1-like pathway with positive charge developing on the electrophilic diazo group in the transition state. The diazo reagents were evolved such that esterification with carboxylates is preferred over unproductive hydrolysis. This preference is based on the basicity of the diazo compound, with low basicity leading to little reaction and high basicity preferring hydrolysis; balancing these factors allows esterification to be favored. The diazo compounds were also selected on the basis of preferential reaction with carboxylates over reaction with other amino acids, such as cysteine and serine. With ribonuclease A, the diazo reaction was shown to proceed to almost full conversion in 4 h with 10 eq of the diazo compound and under modest pH (5.5) and temperature (37 ºC) conditions.[46] Depending on accessibility and pK_a, this reaction can target any carboxylate residue, leading to heterogeneous modification.

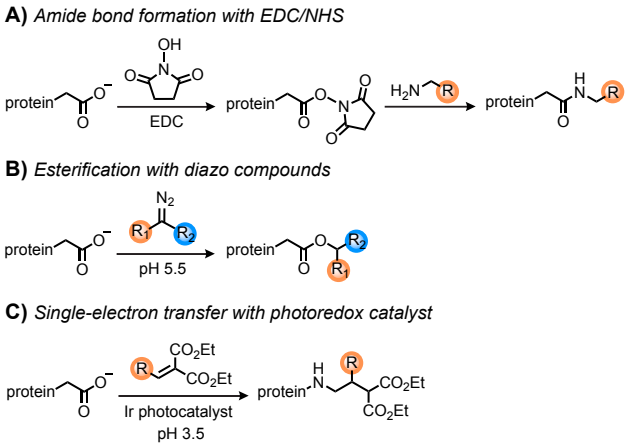

Figure 5. Chemical modification of glutamic acid, aspartic acid, and the C-terminus. (A) Carboxylates in all three residues can be modified through amide bond formation with EDC/NHS. (B) Carboxylate residues can also be modified through esterification with diazo compounds. (B) The C-terminus can be specifically targeted with a single-electron transfer reaction that requires a photoredox catalyst.

Additionally, the ester bond that is formed is much less stable than an amide bond and is susceptible to hydrolysis. However, this can be used to advantage by mediating release of cargo when in specific environments. Esterification has also been used to shield negative charges on proteins, leading to enhanced cytosolic delivery.[47]

The protein C-terminus is an attractive target for site-selective modification owing to the fact that every protein exhibits a single instance of this site. It is often solvent exposed and has been modified selectively over aspartate and glutamate side chains on the basis of redox potential differences.[48] Specifically, the redox potentials of aspartic and glutamic acids are ~1.25 V, while the C-terminal redox potential is ~0.95 V.[49] This observation recently led to development of a single-electron transfer reaction that solely targets the C-terminal carboxylate (Figure 5C).[49] Using a photocatalyst, this strategy produces a transient radical species that adds to conjugated olefins. Results have shown that yields are reduced when the C-terminal residue is histidine, tyrosine, or lysine, and the most efficient coupling is produced at pH 3.5. Importantly, the light-mediated reaction proceeds with up to 50% conversion on human insulin, and small peptides can achieve yields of almost 70% using this strategy. This highlights the potential for exclusive modification at the C-terminus, making the C-terminus an exciting new target for site-selective bioconjugation.

Another approach to C-terminal modification is native chemical ligation (NCL). While this strategy can generate protein-protein conjugates and has been incredibly successful, it requires initial conversion of the C-terminus to a thioester[50] and thus does not target native C-termini. NCL also necessitates an N-terminal cysteine on the protein coupling partner, making this approach less widely applicable. If NCL is to be used, the C-terminal thioester can be generated by adjacent intein domains introduced during protein expression.

1.3.5 Tryptophan Modification

Tryptophan is the rarest amino acid, constituting just over 1% of all residues in proteins.[51] Despite its low abundance, at least one tryptophan residue is found in ~90% of proteins, typically within the folded protein core or at binding interfaces.[52] Of all the aromatic residues, tryptophan is the strongest contributor to the A_{280} absorbance of proteins.[6] Additionally, the indole ring exhibits unique chemical properties.[4] For example, tryptophan is the most fluorescent amino acid, and its emission wavelength can be correlated with its level of aqueous exposure and thus the folding state of the protein. Tryptophan is also known to mediate electron transfer, which can allow for unique, radical-based methods for targeted modification. Finally, because of the hydrogen donating ability of the nitrogen in the indole ring, tryptophan is commonly involved in ligand binding. Thus, the chemical modification of tryptophan offers an avenue by which ligand binding can be tuned.

The unique properties and rarity of tryptophan, combined with its low abundance on protein surfaces, make it a promising target for site-specific protein modification if new instances can be introduced using site directed mutagenesis. However, there are significant

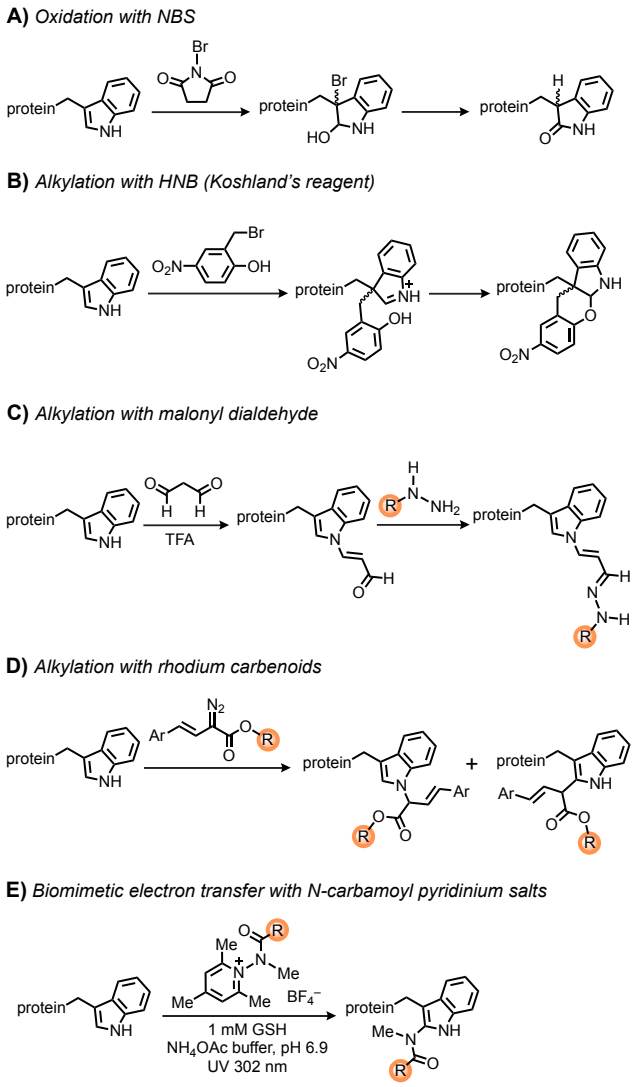

Figure 6. Chemical modification of tryptophan. (A) Tryptophan residues can be oxidized with NBS. Alkylation of tryptophan can be carried out with (B) HNB, (C) malonyl dialdehyde, or (D) rhodium carbenoids. (E) A newer tryptophan modification involves biomimetic electron transfer with *N*-carbamoyl pyridinium salts. (Some components of this figure are derived from a previously published figure.[4])

challenges with targeting tryptophan that have limited its widespread application. In general, tryptophan exhibits low reactivity because the nitrogen atom of the indole ring exhibits delocalized electron density. This leads to lower nucleophilicity than other amino acids, such as lysine and cysteine, which can lead to cross-reactivity when electrophilic reagents are used for modification. To enhance reactivity, harsh conditions, including high temperatures and organic solvents, are often employed. Many of these conditions are not compatible with biomolecules and thus most tryptophan conjugation strategies are directed toward peptides rather than proteins with secondary structure. Because of the inherent hurdles, targeting tryptophan for protein immobilization on surfaces is not reported in the literature.

The electron-rich ring makes tryptophan susceptible to oxidation. Historically, oxidation has been carried out with *N*-bromosuccinimide (NBS, Figure 6A) or 2-hydroxy-5-nitrobenzyl bromide (HNB, Figure 7B). NBS oxidation can be used to determine the tryptophan content within a protein by comparing the ratio of A_{280} absorptions of the indole ring and the oxidized oxindole product.[53] The oxindole has a weaker A_{280} signal, and this decrease can be correlated to the number of tryptophan residues. NBS oxidation is also used to study ligand binding and the involvement of tryptophan in protein active sites.[54] Like with NBS, HNB (also known as "Koshland's reagent") can be used to quantify the number of tryptophan residues by comparing the A_{280} signal with the A_{410} signal of the oxidative conjugate.[55] Another application of HNB oxidation is to study protein conformational changes.[55] It should be noted that HNB can also react with cysteine, histidine, and tyrosine, but it is five-times more selective for tryptophan relative to cysteine.[55] While common historically and still used today, tryptophan oxidation tends to employ harsh conditions (including the use of strong acids) and, as mentioned, can have cross reactivity with other amino acids.[56] Newer oxidation reagents have improved upon these limitations, but in general, oxidation is still limited due to common cross-reactivity with

other residues such as methionine and tyrosine.[56]

Beyond oxidation, the nitrogen of the indole ring can be targeted for modification with malondialdehyde (MDA, Figure 6C). Reversal of this reaction can be obtained by cleavage with hydrazine or phenylhydrazine.[57] Alternatively, secondary modification can be carried out by forming a hydrazone with a hydrazide-containing compound.[4] MDA tagging has been an important tool for quantifying peptide levels in mass spectrometry and proteomics. However, full conversion can be difficult to achieve, and the formation of a Schiff base can occur, leading to undesired cross-linking. To combat these limitations, the reaction is often carried out under highly acidic conditions (3 M HCl or 50% TFA),[56] which prevents its use in many bioconjugation reactions.

The C-2 position of the indole ring is typically the most reactive and has been heavily targeted for tryptophan modification.[58] Transition metal complexes, including those with Pd, Rh, Ru, Au, Mn, and Co, are particularly common catalysts for this type of modification.[56] However, many reactions with these catalysts require high temperature and/or organic solvents. Recent developments have led to reactions with milder conditions for peptide modification; these reactions rely on Pd[59,60] or Ru[61] catalysts. One of the most successful transition metal catalyst transformations for tryptophan modification utilizes Rh carbenoids (Figure 6D).[62,63] The reaction can be performed with both peptides and proteins under mild conditions. In early studies, low pH (~3.5) was required to generate an *in situ* carbenoid intermediate from a diazo precursor.[52] This low pH led to protein denaturation and limited the reaction scope. However, it was later found that the addition of N-(tert-butyl)hydroxylamine allows the reaction to proceed at a much more modest pH of 6-7.[63] The reaction has since been applied to various protein and peptide substrates[64-66] and reacts almost exclusively with tryptophan with modest conversion.

Despite challenges in the past, many research groups are actively pursuing new tryptophan modification strategies that utilize its unique chemical properties. New strategies include radical processes like trifluoromethylation,[67-70] photocatalytic methods for beta position conjugation,[71] and non-photocatalytic methods that proceed through photoinduced electron transfer (PET).[72] The PET reaction (Figure 6E) is particularly exciting and relies on interactions with *N*-carbamoyl pyridinium salts that can be functionalized with a variety of desired cargo groups. UV-B light is also required, and glutathione (1 mM) can elevate the efficiency. While explored mostly with peptides, this photochemical strategy provides up to 94% conversion on lysozyme in 45 min under aqueous conditions. Although this method displays good selectivity for tryptophan, the need to functionalize cargo with N-carbamoyl pyridinium salts is a potential hindrance to widespread adoption of this technique. However, it still represents a compelling example of the future direction for selective tryptophan modification.

1.4 Conclusion

A wide variety of bioconjugation strategies exist for constructing protein bioconjugates. While the majority of these strategies target native amino acid residues, achieving

site-specific modification may require genetic engineering to install residues at specific, accessible locations. Thus in many cases, there is a trade-off between selectivity and convenience. Additionally, the appropriate bioconjugation method depends widely on the application, and many techniques exhibit specific limitations that necessitate further development of new strategies. Effective bioconjugation in the context of surface immobilization can be particularly difficult to achieve due to inherent obstacles encountered with surface chemistry. While some solution-based methods can be applied to surface modification, the majority of these approaches are not site-specific, resulting in minimal control over orientation and surface density. Thus, there is a need for new biomolecule immobilization strategies that address these limitations, as well as expand the repertoire for protein immobilization. Adding to the current toolbox for bioconjugation on surfaces, this thesis will explore oxidative coupling as a novel method for biomolecule immobilization on cellulose and gold surfaces. This, alongside other new approaches, will help enable the full scope of surface-based protein applications.

1.5 References

(1) Hermanson, G. T. Bioconjugate Techniques: Third Edition. *Elsevier Inc.* **2013**.
(2) Bazan, J.; Całkosiński, I.; Gamian, A. Phage Display—A Powerful Technique for Immunotherapy. *Hum. Vaccin. Immunother.* **2012**, *8* (12), 1817–1828.
(3) Datta, S.; Christena, L. R.; Rajaram, Y. R. S. Enzyme Immobilization: An Overview on Techniques and Support Materials. *3 Biotech* **2013**, *3* (1), 1–9.
(4) Begley, T. P.; Tilley, S. D.; Joshi, N. S.; Francis, M. B. Proteins: Chemistry and Chemical Reactivity. In *Wiley Encyclopedia of Chemical Biology*, T.P. Begley (Ed.); American Cancer Society. **2008**, 1–16.
(5) Stephanopoulos, N.; Francis, M. B. Choosing an Effective Protein Bioconjugation Strategy. *Nat. Chem. Bio.* **2011**, *7* (12), 876–884.
(6) Nelson, D.; Cox, M. Principles of Biochemistry, 7th ed.; W.H. Freeman and Company, **2017**.
(7) Grimsley, G. R.; Scholtz, J. M.; Pace, C. N. A Summary of the Measured PK Values of the Ionizable Groups in Folded Proteins. *Protein Sci.* **2009**, *18* (1), 247–251.
(8) Isom, D. G.; Castañeda, C. A.; Cannon, B. R.; E, B. G.-M. Large Shifts in pK_a Values of Lysine Residues Buried inside a Protein. *PNAS* **2011**, *108* (13), 5260–5265.
(9) Koniev, O.; Wagner, A. Developments and Recent Advancements in the Field of Endogenous Amino Acid Selective Bond Forming Reactions for Bioconjugation. *Chem. Soc. Rev.* **2015**, *44* (15), 5495–5551.
(10) Anderson, G. W.; Zimmerman, J. E.; Callahan, F. M. The Use of Esters of N-Hydroxysuccinimide in Peptide Synthesis. *J. Am. Chem. Soc.* **1964**, *86* (9), 1839–1842.
(11) Ambrogelly, A.; Cutler, C.; Paporello, B. Screening of Reducing Agents for the PEGylation of Recombinant Human IL-10. *Protein J.* **2013**, *32* (5), 337–342.
(12) McFarland, J. M.; Francis, M. B. Reductive Alkylation of Proteins Using Iridium Catalyzed Transfer Hydrogenation. *J. Am. Chem. Soc.* **2005**, *127* (39), 13490–13491.
(13) Stefanetti, G.; Rondini, S.; Lanzilao, L.; Saul, A.; MacLennan, C. A.; Micoli, F. Impact of Conjugation Chemistry on the Immunogenicity of S. Typhimurium Conju-

gate Vaccines. *Vaccine* **2014**, *32* (46), 6122–6129.
(14) Rondini, S.; Micoli, F.; Lanzilao, L.; Gavini, M.; Alfini, R.; Brandt, C.; Clare, S.; Mastroeni, P.; Saul, A.; MacLennan, C. A. Design of Glycoconjugate Vaccines against Invasive African Salmonella Enterica Serovar Typhimurium. *Infect .Immun.* **2015**, *83* (3), 996–1007.
(15) Hong, W.; Jeong, S.-G.; Shim, G.; Kim, D. Y.; Pack, S. P.; Lee, C.-S. Improvement in the Reproducibility of a Paper-Based Analytical Device (PAD) Using Stable Covalent Binding between Proteins and Cellulose Paper. *Biotechnol. Bioproc. E* **2018**, *23* (6), 686–692.
(16) Matos, M. J.; Oliveira, B. L.; Martínez-Sáez, N.; Guerreiro, A.; Cal, P. M. S. D.; Bertoldo, J.; Maneiro, M.; Perkins, E.; Howard, J.; Deery, M. J.; Chalker, J. M.; Corzana, F.; Jiménez-Osés, G.; Bernardes, G. J. L. Chemo- and Regioselective Lysine Modification on Native Proteins. *J. Am. Chem. Soc.* **2018**, *140* (11), 4004–4017.
(17) Rosen, C. B.; Kwant, R. L.; MacDonald, J.I.; Rao, M.; Francis, M.B. Capture and Recycling of Sortase A through Site-Specific Labeling with Lithocholic Acid. *Angew Chemie Int. Ed.* **2016**, *55* (30), 8585–8589.
(18) Wang, Q.; Guan, J.; Wan, J.; Li, Z. Disulfide Based Prodrugs for Cancer Therapy. *RSC Adv.* **2020**, *10* (41), 24397–24409.
(19) Renault, K.; Fredy, J.W.; Renard, P.Y.; Sabot, C. Covalent Modification of Biomolecules through Maleimide-Based Labeling Strategies. *Bioconjugate Chem*. **2018**, *29* (8), 2497–2513.
(20) Ferrero, V. E. V.; Andolfi, L.; Di Nardo, G.; Sadeghi, S. J.; Fantuzzi, A.; Cannistraro, S.; Gilardi, G. Protein and Electrode Engineering for the Covalent Immobilization of P450 BMP on Gold. *Anal. Chem.* **2008**, *80* (22), 8438–8446.
(21) Oliverio, M.; Perotto, S.; Messina, G. C.; Lovato, L.; De Angelis, F. Chemical Functionalization of Plasmonic Surface Biosensors: A Tutorial Review on Issues, Strategies, and Costs. *ACS Appl. Mater. Interfaces* **2017**, *9* (35), 29394–29411.
(22) Smith, M. E. B.; Schumacher, F. F.; Ryan, C.P.; Tedaldi, L. M.; Papaioannou, D.; Waksman, G.; Caddick, S.; Baker, J. R. Protein modification, bioconjugation, and disulfide bridging using bromomaleimides. *J. Am. Chem. Soc.* **2010**, *132* (6), 1960-1965.
(23) Nathani, R. I.; Chudasama, V.; Ryan, C.P.; Moody, P. R.; Morgan, R. E.; Fitzmaurice, R. J.; Smith, M. E. B.; Baker, J. R.; Cakkick, S. Reversible protein affinity-labelling using bromomaleimide-based reagents. *Org. Biomol. Chem.* **2013**, *11* (15), 2408-2411.
(24) Kuan, S.L.; Wang, T.; Weil, T. Site-Selective Disulfide Modification of Proteins: Expanding Diversity beyond the Proteome. *Chem - A Eur J.* **2016**, *22* (48), 17112-17129.
(25) Bahou, C.; Richards, D. A.; Maruani, A.; Love, E. A.; Javaid, F.; Caddick, S.; Baker, J. R.; Chudasama, V. Highly Homogeneous Antibody Modification through Optimisation of the Synthesis and Conjugation of Functionalised Dibromopyridazinediones. *Org. Biomol. Chem.* **2018**, *16* (8), 1359–1366.
(26) Bryant, P.; Pabst, M.; Badescu, G.; Bird, M.; McDowell, W.; Jamieson, E.; Swierkosz, J.; Jurlewicz, K.; Tommasi, R.; Henseleit, K.; Sheng, X.; Camper, N.; Manin, A.; Kozakowska, K.; Peciak, K.; Laurine, E.; Grygorash, R.; Kyle, A.; Morris, D.;

Parekh, V.; Abhilash, A.; Choi, J.; Edwards, J.; Frigerio, M.; Baker, M. P.; Godwin, A. In Vitro and In Vivo Evaluation of Cysteine Rebridged Trastuzumab–MMAE Antibody Drug Conjugates with Defined Drug-to-Antibody Ratios. *Mol. Pharm*. **2015**, *12* (6), 1872–1879.
(27) Sun, S.; Akkapeddi, P.; Marques, M. C.; Martínez-Sáez, N.; Torres, V. M.; Cordeiro, C.; Boutureira, O.; Bernardes, G. J. L. One-Pot Stapling of Interchain Disulfides of Antibodies Using an Isobutylene Motif. *Org. Biomol. Chem.* **2019**, *17* (7), 2005–2012.
(28) Griebenow, N.; Dilmaç, A. M.; Greven, S.; Bräse, S. Site-Specific Conjugation of Peptides and Proteins via Rebridging of Disulfide Bonds Using the Thiol–Yne Coupling Reaction. *Bioconjugate Chem.* **2016**, *27* (4), 911–917.
(29) Walsh, S. J.; Omarjee, S.; Galloway, W. R. J. D.; Kwan, T. T.-L.; Sore, H. F.; Parker, J. S.; Hyvönen, M.; Carroll, J. S.; Spring, D. R. A General Approach for the Site-Selective Modification of Native Proteins, Enabling the Generation of Stable and Functional Antibody–Drug Conjugates. *Chem. Sci.* **2019**, *10* (3), 694–700.
(30) M. Nunes, J. P.; Morais, M.; Vassileva, V.; Robinson, E.; S. Rajkumar, V.; B. Smith, M. E.; Barbara Pedley, R.; Caddick, S.; R. Baker, J.; Chudasama, V. Functional Native Disulfide Bridging Enables Delivery of a Potent, Stable and Targeted Antibody–Drug Conjugate (ADC). *Chem. Comm*. **2015**, *51* (53), 10624–10627.
(31) Badescu, G.; Bryant, P.; Bird, M.; Henseleit, K.; Swierkosz, J.; Parekh, V.; Tommasi, R.; Pawlisz, E.; Jurlewicz, K.; Farys, M.; Camper, N.; Sheng, X.; Fisher, M.; Grygoras, R.; Kyle, A.; Abhilash, A.; Frigerio, M.; Edwards, J.; Godwin, A. Bridging disulfides for stable and defined antibody drug conjugates. *Bioconjugate Chem*. **2014**, *25* (6), 1124-1136.
(32) Pacchioni, G. A Not-so-Strong Bond. *Nat. Rev. Mat*. **2019**, *4* (4), 226–226.
(33) Liu, S.; Lämmerhofer, M. Functionalized Gold Nanoparticles for Sample Preparation: A Review. *Electrophoresis* **2019**, *40*, 2438–2461.
(34) Karyakin, A. A.; Presnova, G. V.; Rubtsova, M. Yu.; Egorov, A. M. Oriented Immobilization of Antibodies onto the Gold Surfaces via Their Native Thiol Groups. *Anal. Chem.* **2000**, *72* (16), 3805–3811.
(35) Leier, S.; Richter, S.; Bergmann, R.; Wuest, M.; Wuest, F. Radiometal-Containing Aryl Diazonium Salts for Chemoselective Bioconjugation of Tyrosine Residues. *ACS Omega* **2019**, *4* (26), 22101–22107.
(36) Sato, S.; Matsumura, M.; Kadonosono, T.; Abe, S.; Ueno, T.; Ueda, H.; Nakamura, H. Site-Selective Protein Chemical Modification of Exposed Tyrosine Residues Using Tyrosine Click Reaction. *Bioconj. Chem.* **2020**, *31* (5), 1417–1424.
(37) Pauly, H. Über die Konstitution des Histidins: I. Mitteilung. *Hoppe Seylers Z Physiol. Chem.* **1904**, *42* (5-6), 508-518.
(38) Hooker, J. M.; Kovacs, E. W.; Francis, M. B. Interior Surface Modification of Bacteriophage MS2. *J. Am. Chem. Soc*. **2004**, *126* (12), 3718–3719.
(39) Schlick, T. L.; Ding, Z.; Kovacs, E. W.; Francis, M. B. Dual-Surface Modification of the Tobacco Mosaic Virus. *J. Am. Chem. Soc*. **2005**, *127* (11), 3718–3723.
(40) Joshi, N. S.; Whitaker, L. R.; Francis, M. B. A Three-Component Mannich-Type Reaction for Selective Tyrosine Bioconjugation. *J. Am. Chem. Soc*. **2004**, *126* (49), 15942–15943.

(41) Minamihata, K.; Yamaguchi, S.; Nakajima, K.; Nagamune, T. Tyrosine Coupling Creates a Hyperbranched Multivalent Protein Polymer Using Horseradish Peroxidase via Bipolar Conjugation Points. *Bioconjugate Chem.* **2016**, *27* (5), 1348–1359.
(42) Minamihata, K.; Goto, M.; Kamiya, N. Site-Specific Protein Cross-Linking by Peroxidase-Catalyzed Activation of a Tyrosine-Containing Peptide Tag. *Bioconj. Chem*. **2011**, *22* (1), 74–81.
(43) Fancy, D. A.; Denison, C.; Kim, K.; Xie, Y.; Holdeman, T.; Amini, F.; Kodadek, T. Scope, Limitations and Mechanistic Aspects of the Photo-Induced Cross-Linking of Proteins by Water-Soluble Metal Complexes. *Chem. Biol.* **2000**, *7* (9), 697–708.
(44) Tonami, H.; Nishiuchi, H. Protein Immobilization on Polyvinylphenol via Tyrosine Oxidation of Proteins Catalyzed by Horseradish Peroxidase. *J. Appl. Polym. Sci*. **2021**, *138* (21), 50475.
(45) Mix, K. A.; Raines, R. T. Optimized Diazo Scaffold for Protein Esterification. *Org. Lett.* **2015**, *17* (10), 2358–2361.
(46) McGrath N, Andersen K, Davis A, Lomax J, Raines R. Diazo Compounds for the Bioreversible Esterification of Proteins. *Chem. Sci.* **2015**, *6* (1), 752–755.
(47) Mix, K. A.; Lomax, J.; Raines, R. T. Cytosolic Delivery of Proteins by Bioreversible Esterification. *J. Am. Chem. Soc*. **2017**, *139* (41), 14396–14398.
(48) Shadish, J. A.; DeForest, C. A. Site-Selective Protein Modification: From Functionalized Proteins to Functional Biomaterials. *Matter* **2020**, *2* (1), 50–77.
(49) Bloom, S.; Liu, C.; Kölmel, D. K.; Qiao, J. X.; Zhang, Y.; Poss, M. A.; Ewing, W. R.; MacMillan, D. W. C. Decarboxylative Alkylation: An Approach to Site-Selective Bioconjugation of Native Proteins via Oxidation Potentials. *Nat. Chem.* **2018**, *10* (2), 205–211.
(50) Dawson, P. E.; Muir, T .W.; Clark-Lewis, I.; Kent, S. B. H. Synthesis of proteins native chemical ligation. *Science* **1994**, *266* (5186), 776–779.
(51) Petersen, J.; Christensen, K. E.; Nielsen, M. T.; Mortensen, K. T.; Komnatnyy, V. V.; Nielsen, T. E.; Qvortrup, K. Oxidative Modification of Tryptophan-Containing Peptides. *ACS Comb. Sci.* **2018**, *20* (6), 344–349.
(52) Koniev, O.; Wagner, A. Developments and Recent Advancements in the Field of Endogenous Amino Acid Selective Bond Forming Reactions for Bioconjugation. *Chem. Soc. Rev*. **2015**, *44* (15), 5495–5551.
(53) Spande, T.; Witkop, B. Determination of the tryptophan content of proteins with N-bromosuccinimide. *Methods Enzymol.* **1967**, *11*, 498–506.
(54) Cannon, L. E.; Woehler, M. E.; Lovins, R. E. N-Bromosuccinimide Oxidation and Amino Acid Content of Isoelectrofocused Fractions from a DNP Antibody Population. *Immunology* **1974**, *26* (6), 1171–1182.
(55) Horton, H. R.; Koshland, D. E. A Highly Reactive Colored Reagent with Selectivity for the Tryptophan Residue in Proteins. 2-Hydroxy-5-Nitrobenzyl Bromide. *J. Am. Chem. Soc.* **1965**, *87* (5), 1126–1132.
(56) Hu, J.; He, P.; Li, Y. Chemical Modifications of Tryptophan Residues in Peptides and Proteins. *J. Pep. Sci.* **2020**, e3286.
(57) Foettinger, A.; Melmer, M.; Leitner, A.; Lindner, W. Reaction of the Indole Group with Malondialdehyde: Application for the Derivatization of Tryptophan Residues in

Peptides. *Bioconj. Chem.* **2007**, *18* (5), 1678–1683.
(58) Weng, Y.; Song, C.; Chiang, C.-W.; Lei, A. Single Electron Transfer-Based Peptide/ Protein Bioconjugations Driven by Biocompatible Energy Input. *Commun. Chem*. **2020**, *3* (1), 1–11.
(59) Zhu, Y.; Bauer, M.; Ploog, J.; Ackermann, L. Late-Stage Diversification of Peptides by Metal-Free C-H Arylation. *Chem. Eur. J.* **2014**, *20* (41), 13099-13102.
(60) Zhu, Y.; Bauer, M.; Ackermann, L. Late-Stage Peptide Diversification by Bioorthogonal Catalytic C-H Arylation at 23 °C in H_2O. *Chem. Eur. J.* **2015**, *21* (28), 9980–9983.
(61) Schischko, A.; Ren, H.; Kaplaneris, N.; Ackermann, L. Bioorthogonal Diversification of Peptides through Selective Ruthenium(II)-Catalyzed C–H Activation. *Angewandte Chemie* **2017**, *129* (6), 1598–1602.
(62) Antos, J. M.; Francis, M. B. Selective Tryptophan Modification with Rhodium Carbenoids in Aqueous Solution. *J. Am. Chem. Soc.* **2004**, *126* (33), 10256–10257.
(63) Antos, J. M.; McFarland, J. M.; Iavarone, A. T.; Francis, M. B. Chemoselective Tryptophan Labeling with Rhodium Carbenoids at Mild PH. *J. Am. Chem. Soc*. **2009**, *131* (17), 6301–6308.
(64) Popp, B.; Ball, T. Proximity-driven metallopeptide catalysis: Remarkable side-chain scope enables modification of the Fos bZip domain. *Chem. Sci*. **2011**, *2*, 690–695.
(65) Ball, Z. Designing Enzyme-like Catalysts: A Rhodium(II) Metallopeptide Case Study. *Acc. Chem. Res*. **2012**, *46* (2), 560–570.
(66) Vohidov, F.; Coughlin, J.; Ball, Z. Rhodium(II) Metallopeptide Catalyst Design Enables Fine Control in Selective Functionalization of Natural SH3 Domains. *Angew. Chem. Int. Ed.* **2015**, *54*, 4587-4591.
(67) Cheng, M.; Zhang, B.; Cui, W.; Gross, M. L. Laser-Initiated Radical Trifluoromethylation of Peptides and Proteins: Application to Mass-Spectrometry-Based Protein Footprinting. *Angew. Chem. Int. Ed.* **2017**, *56* (45), 14007–14010.
(68) Imiołek, M.; Karunanithy, G.; Ng, W.-L.; Baldwin, A. J.; Gouverneur, V.; Davis, B. G. Selective Radical Trifluoromethylation of Native Residues in Proteins. *J. Am. Chem. Soc.* **2018**, *140* (5), 1568–1571.
(69) Ding, B.; Weng, Y.; Liu, Y.; Song, C.; Yin, L.; Yuan, J.; Ren, Y.; Lei, A.; Chiang, C.-W. Selective Photoredox Trifluoromethylation of Tryptophan-Containing Peptides. *Eur. J. Org. Chem.* **2019**, *2019* (46), 7596–7605.
(70) Kee, C. W.; Tack, O.; Guibbal, F.; Wilson, T. C.; Isenegger, P. G.; Imiołek, M.; Verhoog, S.; Tilby, M.; Boscutti, G.; Ashworth, S.; Chupin, J.; Kashani, R.; Poh, A. W. J.; Sosabowski, J. K.; Macholl, S.; Plisson, C.; Cornelissen, B.; Willis, M. C.; Passchier, J.; Davis, B. G.; Gouverneur, V. 18F-Trifluoromethanesulfinate Enables Direct C–H 18F-Trifluoromethylation of Native Aromatic Residues in Peptides. *J. Am. Chem. Soc.* **2020**, *142* (3), 1180–1185.
(71) Yu, Y.; Zhang, L. K.; Buevich, A. V.; Li, G.; Tang, H.; Vachal, P.; Colletti, S. L.; Shi, Z.-C. Chemoselective Peptide Modification via Photocatalytic Tryptophan β-Position Conjugation. *J. Am. Chem. Soc.* **2018**, *140* (22), 6797–6800.
(72) Tower, S. J.; Hetcher, W. J.; Myers, T. E.; Kuehl, N. J.; Taylor, M. T. Selective Modification of Tryptophan Residues in Peptides and Proteins Using a Biomimetic Electron Transfer Process. *J. Am. Chem. Soc.* **2020**, *142* (20), 9112–9118.

Chapter 2

Immobilization of Tyrosinase for Solution-Phase Oxidative Coupling

Abstract

Immobilized enzymes feature a variety of advantages, including the ability to remove the enzymes from solution, enhance long-term stability, and even reuse the enzymes over multiple catalytic cycles. In this chapter, we report a facile method for resin immobilization of tyrosinase, a key mediator of oxidative coupling in the context of bioconjugation. The immobilization strategy is a non-site-specific reaction between native lysine residues on tyrosinase and commercially available NHS-activated Sepharose 4 Fast Flow. The resin-bound tyrosinase was characterized by its ability to oxidize small molecule phenols for conjugation to an N-terminal proline sfGFP. The enzyme was quickly and efficiently removed from solution after reaction through spin filtration, thus mitigating complications from over-oxidation. Kinetic parameters for the oxidative coupling reaction mediated by resin-bound tyrosinase were also estimated. Resin-bound tyrosinase could be stored at 4 °C for extended periods of time, and a single aliquot was reused up to six times and still able to mediate oxidative coupling. Finally, the resin-bound tyrosinase was applied to oxidation of a C-terminal tyrosine tag on an scFv.

Portions of this chapter are based on the following publication:

Maza, J. C.; Ramsey, A. V.; Mehare, M.; Krska, S. W.; Parish, C. A.; Francis, M. B. Secondary Modification of Oxidatively-Modified Proline N-Termini for the Construction of Complex Bioconjugates. *Org. Biomol. Chem*. **2020**, *18* (10), 1881–1885.

2.1 Introduction

2.1.1 Enzymatic Oxidative Coupling

Over the years, our lab has developed a rapid and efficient oxidative coupling strategy for biomolecules through the reactions of reactive *ortho*-quinoid intermediates with specific nucleophiles of interest (Figure 1).[1] The *ortho*-quinoids can be accessed by potassium ferricyanide ($K_3Fe(CN_6)$) or sodium periodate oxidation of *ortho*-phenolic compounds, such as catechols, aminophenols, and methoxyphenols.[4-6] This versatile chemistry has enabled the construction of various bioconjugates that tether proteins, peptides, and nucleic acids to small molecules, other biomolecules, and even surfaces, such as glass[7] and gold electrodes.[8]

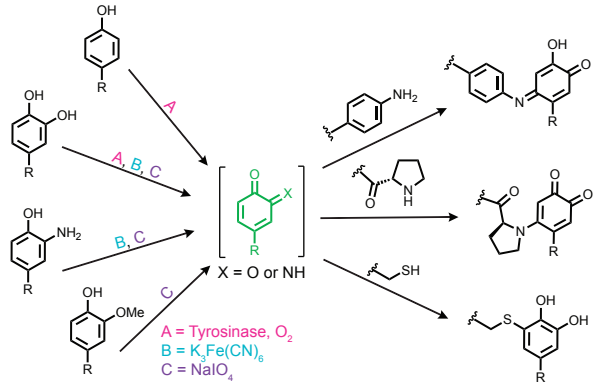

Figure 1. Oxidative coupling reactions. A variety of oxidants can be used to oxidize phenol based moieties to *ortho*-quinoid intermediates (green). These intermediates can undergo subsequent reactions with both amine- and thiol-based nucleophiles.

Recently, we have developed an enzymatic version of the oxidative coupling reaction that allows *ortho*-quinones to be accessed from water soluble and highly stable phenols.[9] The enzyme employed, tyrosinase, features a binuclear copper active site and is responsible for the formation of melanin. During this process, tyrosine is oxidized to dopaquinone, which then cyclizes to form dopachrome (Figure 2). This process is also responsible for the browning of food, reducing the appeal of produce, such as fresh cut apples, when exposed to oxygen for extended periods of time. For the purposes of oxidative coupling, our lab employs tyrosinase isolated from the common button mushroom, *Agaricus bisporus*. This enzyme (abTyr) is commercially available in its active form. Past work has demonstrated that abTyr can oxidize phenols on a variety of substrates, including small molecules, peptides, and proteins. Importantly, the enzymatic version of this reaction allows thiols to be used as nucleophiles without competing side reaction pathways.[10] Our lab has also demonstrated successful oxidative couplings with a smaller (35.5 kDa versus ~120 kDa for abTyr) tyrosinase, megaTyr, from *Bacillus megaterium*.[11]

While oxidative coupling with abTyr has been widely successful, it is important to note that we have encountered steric- and charge-based limitations of phenol activation

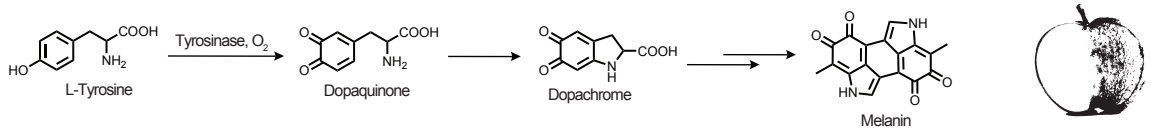

Figure 2. Formation of melanin. In nature, tyrosinase is responsible for oxidation of L-tyrosine. This generates dopaquinone, which cyclizes to form dopachrome, a key intermediate in the synthesis of melanin. Melanin is responsible for skin color and the browning of foods, such as fresh cut apples.

as the abTyr active site cavity is relatively small and features negatively charged residues. Thus abTyr prefers relatively small and positively charged substrates. MegaTyr, however, exhibits a less sterically hindered active site and can oxidize both positively and negatively charged substrates. Mutations to the active site of megaTyr can further tune the specificity of the enzyme for substrate charge, allowing precise control over oxidation activity. Taken together, our lab is building a repository of tyrosinases that allow access to a vast range of substrates for numerous applications.

2.1.2 Immobilized Enzymes

The native function and catalytic behavior of enzymes depend heavily on proper folding and three-dimensional confirmation. This makes enzymes sensitive to storage conditions and can lead to significant activity loss over time. Additionally, the folding properties of enzymes can be very sensitive to reaction conditions, thus necessitating aqueous conditions and narrow pH and temperature ranges. This can limit their usability, particularly in synthesis-based applications. One way to improve stability is to immobilize enzymes on a surface, leading to enhanced durability. More importantly, surface immobilization can allow an enzyme to be removed from solution after a reaction is complete and can even permit an enzyme to be reused for multiple catalytic cycles.[12]

As noted in the previous section, our lab has re-purposed the natural enzyme tyrosinase (both abTyr and megaTyr) to catalyze a wide range of oxidative bioconjugation reactions. In the majority of cases, soluble abTyr and megaTyr are highly effective. However, in some cases, excess tyrosinase in solution can lead to over-oxidation. Additionally, it can be necessary to remove tyrosinase after oxidative coupling if the conjugate is to be used in subsequent cell-based assays where excess oxidation could be particularly detrimental. Immobilization of tyrosinase could address these limitations while also harvesting the other benefits of immobilized enzymes, namely superior stability and the ability to reuse the enzyme.

In the literature, tyrosinase has been immobilized on a variety of surfaces for various purposes. For example, tyrosinase has been immobilized on silica for use in chromatography to screen drug candidates;[13] it has been immobilized on glass for removal of phenols from aqueous solutions;[14] and it has been immobilized on porous silicon for phenolic detection.[15] Strategies for tyrosinase immobilization typically target native lysine residues. For example, surfaces are commonly activated with EDC/NHS[15] or epoxy,[16] or the protein is cross-linked to the surface with glutaraldehyde.[14]

In this chapter, we report immobilization of abTyr on sepharose resin and demonstrate that the resin-bound abTyr exhibits performance comparable to that of soluble tyrosinase, with the added benefit of quick and easy removal of the enzyme through spin filtering. We also show that the immobilized enzyme can be reused for multiple catalytic cycles and can be stored for at least a month at 4 °C. Additionally, kinetic studies reveal a V_{max} for resin-bound abTyr that is comparable to literature reported values.

2.2 Results and Discussion

2.2.1 Design and Initial Characterization of Resin-Bound abTyr

In initial studies, a commercially available NHS-activated sepharose resin was chosen as the solid support. This allowed for a quick and convenient method of tyrosinase immobilization that did not require pre-activation of the resin or manipulation of native abTyr. However, this immobilization strategy targeted native lysine residues and thus was not site-specific. This could be problematic if solvent-exposed lysine residues reside near the abTyr active site. Immobilization through these lysine resides could lead to blocking or obstruction of the active site, rendering the abTyr ineffective or with reduced activity. Thus we initially intended to develop a site-specific immobilization strategy if initial results with lysine chemistry were promising.

A

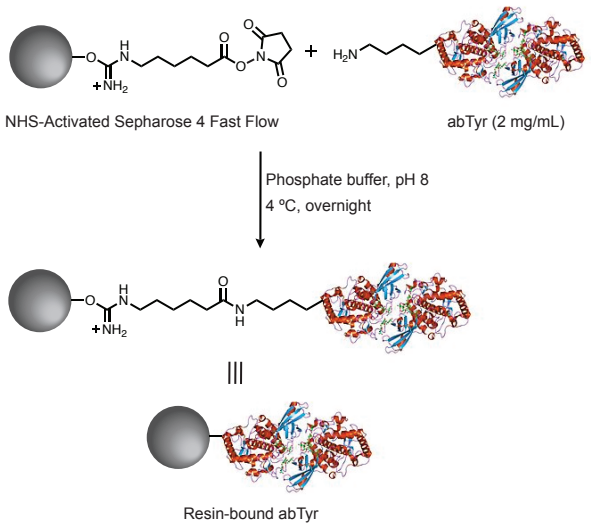

B

Sample	Initial abTyr concentration (mg/mL)	Final abTyr concentration (mg/mL)	% abTyr coupled
NHS-Activated Sepharose 4 Fast Flow	1.52	-0.19	100%
CL-4B resin (negative control)	1.52	0.46	~70%

Figure 3. Immobilization and surface quantification of abTyr. (A) Commercially available NHS-Activated Sepharose 4 Fast Flow was reacted with native lysine residues on abTyr (at 2 mg/mL) to generate resin-bound abTyr. (B) The amount of abTyr immobilized on Sepharose 4 Fast Flow was quantified using a Bradford Assay. While a significant quantity of abTyr also appeared to be immobilized on CL-4B resin, this negative control did not catalyze oxidative coupling reactions (see Figure 4).

The lysine-targeted immobilization strategy was based on a protocol provided by Cytiva. Briefly, the NHS-activated resin was combined with abTyr in phosphate buffer at pH 8 and allowed to react overnight at 4 °C (Figure 3A). This was followed by blocking of unreacted NHS with ethanolamine. As a negative control, we repeated the immobilization process with CL-4B resin. CL-4B is a cross-linked 4% agarose resin, the same core material as the NHS-activated sepharose resin.

We next sought to quantify the amount of protein immobilized on the resin. A common way to quantify protein immobilized on surfaces is through a depletion assay that compares protein concentration of the coupling solution before and after immobilization.[17] After conjugation, flow through from washings of the functionalized resin was collected, lyophilized, and resuspended in a small amount of phosphate buffer. A Bradford Assay was then used to quantify the amount of protein in the collected flow through (Figure 3B). For the NHS-activated sepharose resin, no protein was detected in the flow through, indicating that all protein was coupled to the resin. For an initial 1.5 mg/mL solution of abTyr, this corresponds to 0.15 mg of abTyr coupled to 100 µL of resin. As a comparison, we also quantified protein in the flow through from abTyr conjugation with the CL-4B negative control resin. As

expected, protein was detected in the flow through, but surprisingly, the concentration was less than the concentration in the initial coupling solution. Comparison of the abTyr concentrations before and after incubation indicated that ~70% of the protein was coupled (Figure 3B). However, this is likely due to background adsorption of abTyr or natural protein loss during resin washings. To confirm this, the CL-4B resin was tested for activity in the oxidative coupling reaction but was ineffective in mediating conjugation. This is discussed below in more detail.

While a concentration of 1.5 mg/mL was used for the immobilized protein quantification assay, an abTyr concentration of 2 mg/mL was used in subsequent preparations of the resin. The Bradford Assay was not repeated for a 2 mg/mL concentration, but immobilization always appeared successful by eye (i.e. while the initial abTyr coupling solution was brown, all flow through after coupling was colorless). Thus it is likely that the upper limit of immobilization is greater than 0.15 mg of abTyr per 100 µL of resin. However, this was not investigated further.

We next explored the activity of resin-bound abTyr. Given the steric limitations of abTyr encountered in solution, it was possible that immobilization could further hinder access to the active site. Activity was tested by carrying out a bioconjugation reaction between superfolder GFP with an engineered proline N-terminus (pro-sfGFP[4,18]) and rhodamine- or biotin-phenol (Figure 4A) in phosphate buffer at pH 6.5. The resin-bound abTyr or CL-4B control was added to 25% (v/v) (though later results revealed that 10% (v/v) produces efficient coupling) and removed prior to analysis by filtering the reaction through a 0.22 µm cellulose acetate spin filter. After 1 h at room temperature, the conversions to coupled products were 85% and 95% for rhodamine- and biotin-phenol, respectively (Figure 4B). This is comparable to catalysis by solution abTyr (Figure 4C). In contrast, no product was detected when the reaction was carried out with the CL-4B resin negative control (Figure 4D). The double additions observed in the presence of resin-bound and soluble abTyr are likely from participation of a solvent-exposed lysine or cysteine residue in the oxidative coupling reaction. Overall, immobilization did not hinder the native activity of abTyr, and thus resin-bound abTyr can be used as a convenient alternative to soluble abTyr in applications where soluble abTyr is effective.

To explore the scope of resins that are compatible with tyrosinase immobilization, we also immobilized tyrosinase on NHS-activated acrylamide-PEG (PEGA) resin. The same immobilization procedure was followed as that for NHS-activated sepharose resin. Once coupled, the resin was used to conjugate rhodamine- or biotin-phenol to pro-sfGFP. Percent conversions were comparable to those achieved with sepharose resin (~90% conversion for both rhodamine and biotin conjugates, Figure 4E), demonstrating that tyrosinase activity is not dependent on the resin. Similar to sepharose resin, we included a negative control of PEGA resin that was not activated with NHS but was exposed to the same abTyr immobilization conditions as NHS-activated PEGA resin. This negative control yielded no coupling with rhodamine-phenol, but ~40% conversion was observed with biotin-phenol (Figure 4F). A depletion assay may lend insight into the source of this activity and the possibility of abTyr adsorption that could explain the observed conju-

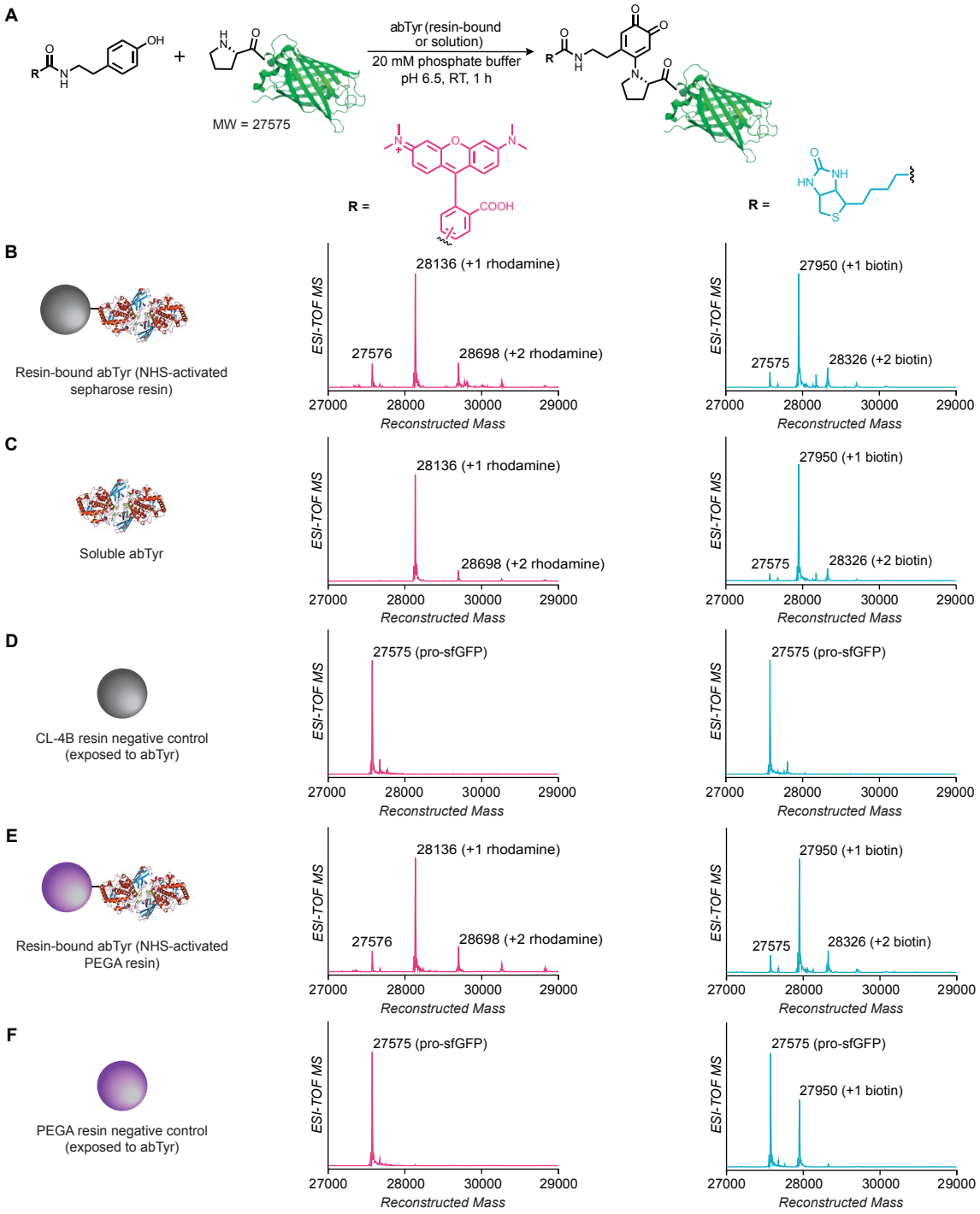

Figure 4. Oxidative coupling of biotin- and rhodamine-phenol to pro-sfGFP with resin-bound abTyr. (A) A small molecule biotin- or rhodamine-phenol (100 μM or 400 μM, respectively) was coupled to pro-sfGFP (10 μM) in the presence of resin-bound abTyr at 10% (v/v). (B) The pro-sfGFP reaction proceeded to 85–90% conversion in the presence of resin-bound abTyr. (C) As comparison, the pro-sfGFP proceeded to nearly complete conversion in the presence of soluble abTyr (200 nM). (D) CL-4B resin (negative control resin with no NHS-activation) did not catalyze the oxidative coupling reaction, even though the resin was exposed to the same abTyr immobilization conditions as the Sepharose 4 Fast Flow resin. (E) abTyr immobilized on NHS-activated acrylamide-PEG (PEGA) resin also catalyzed the oxidative coupling reaction, leading to high conversion. (F) Similar to CL-4B resin, PEGA resin that was not NHS-activated did not lead to production of rhodamine-sfGFP. However, the PEGA resin negative control did lead to product when phenol-biotin was reacted with pro-sfGFP. This is likely due to background adsorption of abTyr on PEGA resin.

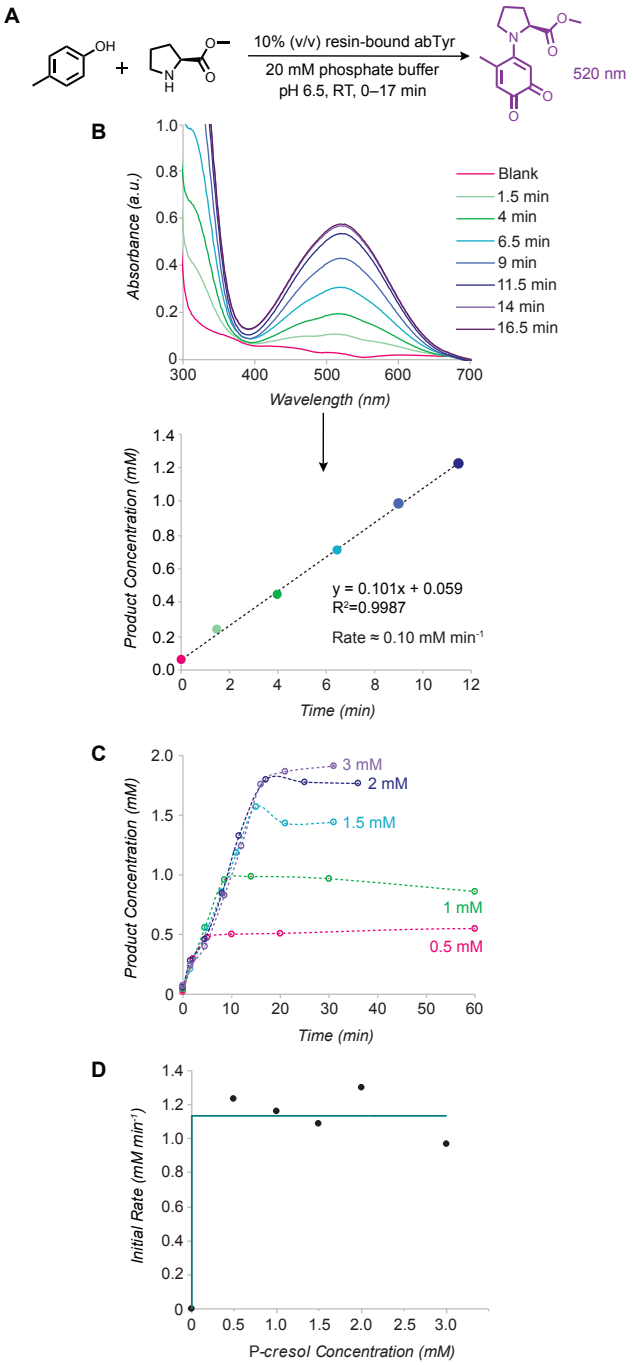

Figure 5. Kinetics of small molecule oxidative coupling mediated by resin-bound abTyr. (A) Couplings were performed with 1.5 mM *p*-cresol and 100 mM L-proline methyl ester in the presence of 10% (v/v) resin-bound abTyr. The product of this reaction absorbs at 520 nm. (B) Product concentration was determined by obtaining the UV-vis absorbance of the reaction at time intervals from 0 to 17 min. Absorbance values were converted to product concentrations (ε_{520}= 3,500 M^{-1} cm^{-1}) and used to calculate initial reaction rates. (C) To determine kinetic parameters, reaction rates were determined for various starting concentrations (0.5, 1, 1.5, 2, and 3 mM) of *p*-cresol. (D) Initial rates were plotted as a function of *p*-cresol concentration to generate a Michaelis-Menten plot.

gation. While immobilization with PEGA resin was successful, we chose to pursue sepharose resin for future studies due to more effective negative controls and commercial availability of the resin in an NHS-activated form.

2.2.2 Kinetics of Resin-Bound abTyr

In some instances, immobilizing enzymes can affect activity due to changes in confirmation and/or obstruction of active sites.[19,20] We were thus interested in further characterizing the rate and activity of immobilized abTyr. To this end, a calorimetric activity assay was developed that was based on the reaction between *p*-cresol and L-proline methyl ester (Figure 5A). This reaction produces a deep purple product that absorbs at 520 nm, which allows the formation of product to be monitored over time. We initially tested an analogous reaction with 4-methyl catechol instead of *p*-cresol, and while this reaction produced the same colored product, we chose to pursue the reaction with *p*-cresol because 4-methyl catechol is readily oxidized by air. Since the rate limiting step of oxidative coupling with abTyr is oxidation of the phenolic compound, the rate of the overall reaction can be directly correlated to oxidation events and thus activity of the enzyme. Therefore, background oxidation of 4-methyl catechol could lead to an observed activity that is misconstrued.

When pursuing *p*-cresol as the substrate, we recognized that 4-methyl-*o*-benzoquinone (the oxidized form of *p*-cresol) can react with unoxidized *p*-cresol and polymerize, which could reduce the 520 nm signal and thus diminish the apparent activity of resin-bound abTyr. To minimize this effect, the reaction was carried out with a 100-fold excess of

L-proline methyl ester so that *ortho*-quinone species would be immediately quenched. It should be noted that initially, 1,000x L-proline methyl ester was tested, but this produced little to no product. L-proline methyl ester is provided as an HCl salt, and thus at a 1,000x concentration, the HCl was likely disrupting the buffer pH and quenching the reaction.

To correlate the small molecule reaction with resin-bound abTyr activity, aliquots of the reaction were removed at various time points, and the reactions were stopped by spin filtering to remove the resin. The absorbance measurements at each time point were converted to product concentration, and the initial reaction rates were determined (Figure 5B). Initial tests with the calorimetric activity assay and 2 mM *p*-cresol revealed that the reaction was nearly complete after 15 min. This was the case for the majority of *p*-cresol concentrations tested. In order to further assess enzyme activity, V_{max} and K_m were estimated. The formation of product was monitored over time for concentrations of *p*-cresol ranging from 0.5 to 3 mM (Figure 5C). The initial rates for each concentration were then plotted to generate a Michaelis-Menten curve. However, when fitting the data, a line with a 90-degree angle, rather than a curve, was obtained (Figure 5D). This is because the initial velocities for each concentration were very similar, indicating that V_{max} was already reached at a substrate concentration of 0.5 mM. Thus we were able to estimate a V_{max} of 113 μM/min, but a K_m value could not be determined. Initial velocities for lower substrate concentrations would be needed to generate an accurate K_m value. However, because saturation occurred at 0.5 mM substrate, the K_m value lies between zero and 0.5 mM. The V_{max} and K_m values for resin-bound abTyr are comparable to the literature, which reports a V_{max} of 45–185 μM/min for tyrosinase immobilized on epoxy-silica,[16] and a K_m of 0.96–11 mM, depending on the substrate (*p*-cresol[14] or L-DOPA[16]) and surface used for immobilization (glass[14] or epoxy-silica[16]). In fact, the K_m value of our resin-bound abTyr is likely lower than that reported in the literature.

As noted in section 3.2.1, efforts to quantify the amount of immobilized abTyr revealed possible adsorption of abTyr to the negative control resin. Thus we wanted to ensure that the observed activity of resin-bound abTyr originated from activity of immobilized abTyr versus adsorbed abTyr that was leaching into solution during storage. To test this, the initial rate of resin-bound abTyr (stored for ~3 d at 4 °C) was determined and compared to the rate of a reaction catalyzed by the supernatant from the same batch of resin. For the supernatant, negligible amount of product was formed over the course of 15 min, and thus the rate was determined to be zero. In contrast, the rate of the reaction catalyzed with resin was ~106 μM/min, which aligned with results from kinetic studies.

2.2.3 Stability and Reusability of Resin-Bound abTyr

Motivation for abTyr immobilization was driven by the desire to quickly and efficiently remove abTyr from solution after reaction. However, as previously noted, another advantage of immobilizing enzymes is the ability to store the enzymes at 4 °C for extended periods of time, as well as reuse the same enzyme for multiple catalytic cycles. To test long-term stability of resin-bound abTyr, a batch of tyrosinase resin was stored at 4 °C, and the calorimetric activity assay was carried out every three to four days. While there

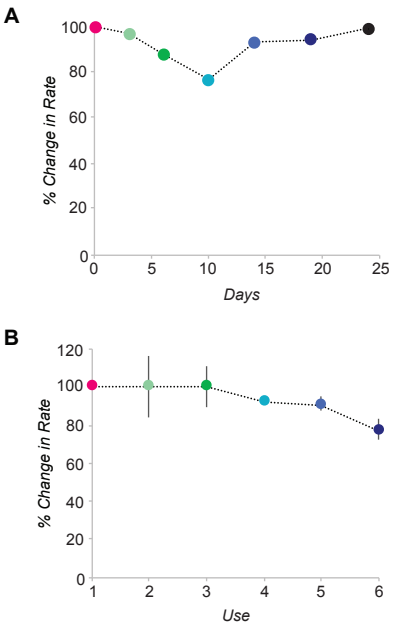

Figure 6. Long-term storage and reusability of resin-bound abTyr. (A) The colorimetric activity assay described in Figure 5A was used to monitor the activity of a single batch of resin-bound abTyr stored at 4 °C for 25 days. (B) Reusability studies were carried out with a single aliquot of resin-bound abTyr. The resin was collected after each reaction, washed four times with 50 mM phosphate buffer at pH 8, and then used to catalyze the next reaction. Error bars represent standard deviation for n = 2.

were some fluctuations in measurements, the initial rate after 25 days was the same as the initial rate on the day of resin preparation (Figure 6A). Thus resin-bound abTyr can be stored at 4 °C for at least 25 days with negligible loss in activity, negating the need for storage of soluble abTyr at -20 or -80 °C. In the literature, tyrosinase immobilized on epoxy-silica and stored at 4 °C exhibited an activity loss of 20% to 60% (depending on the immobilization method) over a 21 day storage period.[16] For tyrosinase immobilized via entrapment in alginate, comparable activity losses were observed over a similar time frame, but the entrapped resin could be stored at 21 °C.[21] While we did not test long-term stability at room temperature, our stability data is in line with, and in some cases superior, to those reported in the literature. In many cases, the resin-bound abTyr exhibits minimal activity loss even after several months of storage at 4 °C. This, combined with the ability to filter out the enzyme, makes oxidative coupling with resin-bound abTyr very user-friendly.

For testing reusability, a single aliquot of resin-bound abTyr was used to catalyze multiple reactions, and the initial rate of each reaction (based on the calorimetric activity assay) was determined. The first three reactions exhibited nearly identical rates, after which a slight decline in rate was observed (Figure 6B). However, the rate of the sixth reaction decreased by only 20% relative to the first reaction. Thus, if desired, the resin can be reused up to three times without any loss of activity. If reusing more than three times, the reaction time may need to be extended or the amount of resin may need to be increased to allow for maximum conversion to product. Depending on the surface, immobilized tyrosinase in the literature maintains 65% to 100% of activity over 10 catalytic cycles,[22,23] although when immobilized on aminopropyl glass, 100% activity was observed after 40 cycles.[14] Despite the ability to reuse resin-bound abTyr, we typically do not recycle the resin due to the low cost of the enzyme and the facile method for immobilization.

2.2.4 Protein Oxidation by Resin-Bound abTyr

Having demonstrated successful oxidation of several small molecules, we wanted to test the ability of resin-bound abTyr to oxidize tyrosine residues on proteins. We anticipated that the increased steric hindrance around these residues combined with the bulk of the resin might reduce the efficiency of the reaction. Our model protein was a sin-

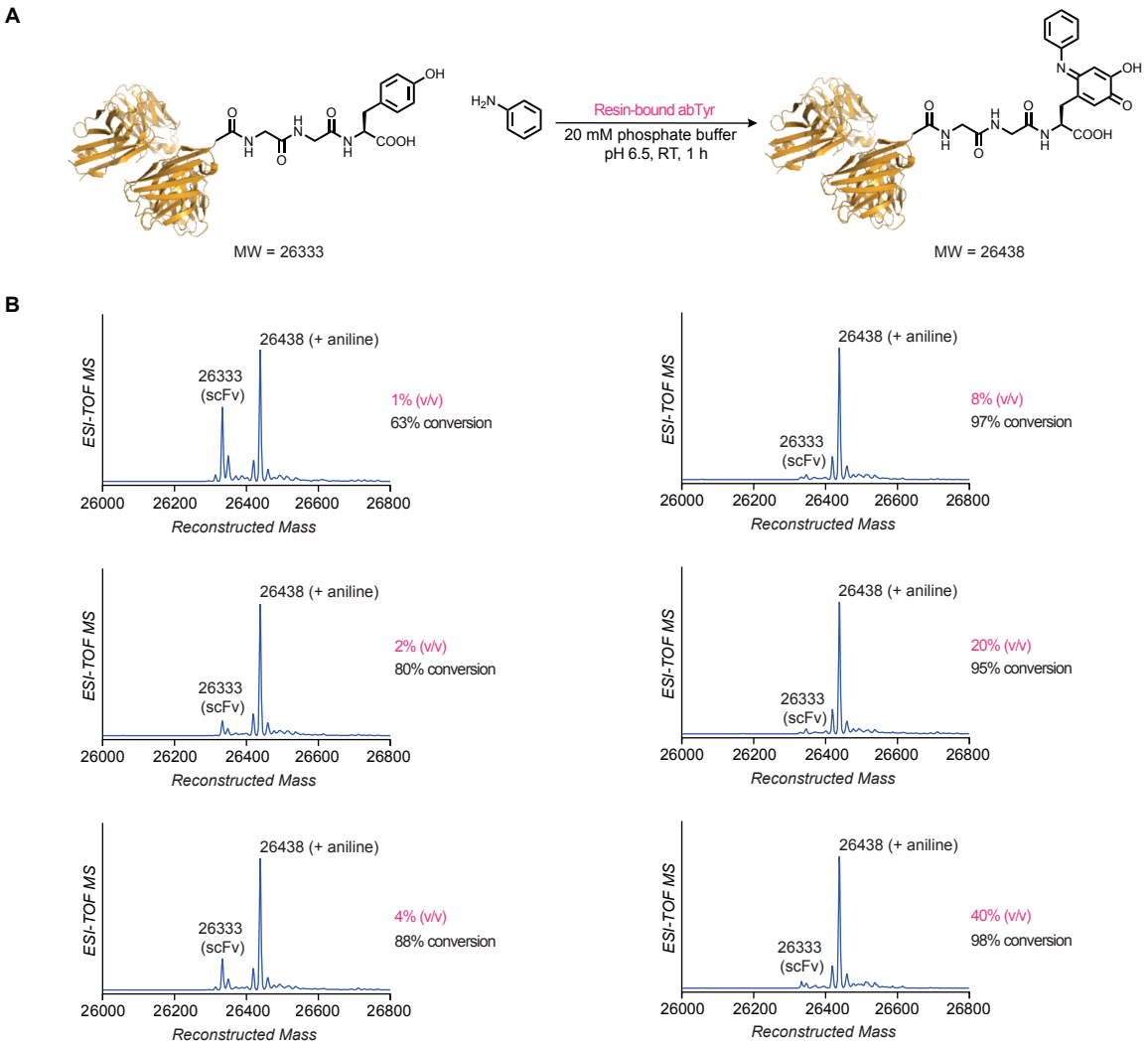

Figure 7. Resin-bound abTyr-mediated coupling of aniline to scFv-GGY. (A) scFv with a -GGY C-terminal tag (3.8 μM) was oxidized by resin-bound abTyr (at various concentrations) and coupled to aniline (150 μM). (B) Conversion depended on the concentration of resin-bound abTyr with nearly complete conversion achieved at concentrations of 8% (v/v) and higher.

gle-chain variable fragment with a tyrosine engineered at the C-terminus (scFv-GGY[11]). This protein was combined with aniline in the presence of resin-bound abTyr and 20 mM phosphate buffer at pH 6.5 (Figure 7A). While the reaction was run for longer than comparable oxidative coupling reaction with soluble abTyr (2.5 h at room temperature for resin-bound abTyr versus 1 h at room temperature for soluble abTyr), we were pleased to find that resin-bound abTyr could mediate nearly complete conversion to the desired product when 8 % (v/v) resin-bound abTyr was used (Figure 7B).

When coupling scFv-GGY to aniline, we screened six resin-bound abTyr concentrations from 1% (v/v) to 42% (v/v) (Figure 7B). While complete conversion was observed with 8% (v/v), nearly 90% conversion was achieved with a concentration of 4% (v/v). Because less than 10% (v/v) of resin-bound abTyr is required to activate a sterically hindered phenol, it is likely that less than 10% (v/v) of resin would be adequate for activation of small molecule phenols (e.g. biotin-phenol, rhodamine-phenol, and *p*-cresol). Howev-

er, 10% (v/v) remains the suggested concentration as it is applicable to oxidation of either small molecule phenols or tyrosine residues on proteins.

2.2.5 Alex's Magic Mushroom Powder

After successful storage of resin-bound abTyr in solution at 4 °C, we were interested in developing a dry version of the immobilized enzyme that could be stored at room temperature and added to reactions as a dry "powder" or that could be reconstituted in buffer just prior to use. During the first attempt at creating mushroom powder, resin-bound abTyr was flash frozen, lyophilized, and then resuspended in buffer. When exposed to the calorimetric activity assay, product was produced but at a very slow rate. It is generally not recommended by manufacturers to freeze sepharose resin, and thus flash freezing may have caused the sepharose matrix to break down. Alternatively, the abTyr may have aggregated during the drying progress.

As an alternative drying method, the resin was spin filtered to remove excess solution and was then encased in an Eppendorf tube and left at room temperature for up to 48 h. When the dried resin was resuspended and tested with the calorimetric activity assay, product was produced with little to no loss in activity. However, when the filtered resin was not encased and was instead exposed to air, the resin turned into a clump within 24 h and did not resuspend into solution. A different type of resin or solid support may be required if Magic Mushroom Powder is further pursued.

2.3 Conclusions and Future Outlook

In this chapter, it is demonstrated that abTyr immobilized on sepharose resin is a convenient alternative to soluble abTyr and can catalyze oxidation of phenolic compounds on either small molecules or proteins for subsequent oxidative coupling. Advantages of resin-bound abTyr include (1) the ability to quickly and easily remove the enzyme from solution after reaction; (2) store the enzyme in solution at 4 °C for at least a month; (3) use the same enzyme for up to three reactions without any activity loss. Furthermore, reactions with resin-bound abTyr are quick and proceed to high conversion. Thus resin-bound abTyr can be applied in cases where excess oxidation by abTyr is to be avoided or in any case where soluble abTyr is used. While the non-site-specific immobilization strategy does not appear to impact abTyr activity, a site-specific approach could be developed for comparison. Additionally, tyrosinase variants, such as megaTyr and mutated tyrosinases, could be immobilized using the presented approach. This may catalyze expanded utility of these variants. While the approach employed in this chapter was non-site-specific, the remainder of this work explores a site-specific approach to protein immoblization.

2.4 Materials and Methods

General methods and instrumentation

Unless noted otherwise, all reagents were obtained from commercial sources and used without further purification. NHS-Activated Sepharose 4 Fast Flow resin and CL-4B resin were purchased from Cytiva. Tyrosinase isolated from A*garicus bisporus* (abTyr), L-proline methyl ester, *p*-cresol, acrylamide-PEG (PEGA) resin, and tyramine were purchased from Sigma-Aldrich. Pro-sfGFP[4] and scFv-GGY[11] were expressed and purified as previously reported. EZ-link NHS biotin and NHS-rhodamine (TAMRA) were purchased from Thermo Fisher (Waltham, MA). Spin concentrators with 10 kDa molecular weight cutoffs (MWCO) and sterile spin filters with 0.22 μm pores were purchased from Millipore (Billerica, MA). Doubly distilled water (ddH_2O) was obtained from a Millipore purification system.

Electrospray Ionization Time of Flight Liquid Chromatography Mass Spectrometry (ESI-TOF LC-MS). Acetonitrile (Optima grade, 99.9%, Fisher,Waltham, MA), formic acid (1 mL ampules, 99+%, Pierce, Rockford, IL), and water purified to a resistivity of 18.2 MΩ·cm (at 25 °C) using a Milli-Q Gradient ultra-pure water purification system (Millipore, Billerica, MA) were used to prepare mobile phase solvents for LC-MS. Electrospray ionization mass spectrometry (ESI-MS) of protein bioconjugates was performed using an Agilent 1260 series liquid chromatograph outfitted with an Agilent 6224 time-of-flight (TOF) LC-MS system (Santa Clara, CA). The LC was equipped with a Proswift RP-4H (monolithic phenyl, 1.0 mm × 50 mm, Dionex) analytical column. Solvent A was 99.9% water/0.1% formic acid and solvent B was 99.9% acetonitrile/0.1% formic acid (v/v). Each sample was prepared for analysis by desalting and spinning through an 0.22 μm cellulose acetate centrifugal filter, and then 8 μL of 10 μM protein was injected onto the column. Following sample injection, a 5–100% B elution gradient was run at a flow rate of 0.30 mL/min over 8 min. Data were collected and analyzed by deconvolution of the entire elution profile in order to provide reconstructed mass spectra that were representative of the entire sample using Agilent Mass Hunter Qualitative Analysis B.05.00. Spectra were analyzed with open source Chartograph software (www.chartograph.com).

UV-Vis spectroscopy. All UV-vis measurements were obtained with a Varian Cary 50 UV-vis spectrophotometer and a quartz microcuvette.

Experimental procedures

Preparation of resin-bound abTyr (adapted from a resin protein coupling protocol from Cytiva, formerly GE Healthcare). NHS-Activated Sepharose 4 Fast Flow resin (Cytiva) was washed ten times with 1 mM HCl, followed by two washes with 50 mM phosphate buffer at pH 8. The resin was resuspended in 2 mg/mL tyrosinase in 50 mM phosphate buffer at pH 8. The resin was rotated end-over-end overnight at 4 °C and then drained and washed two times with 50 mM phosphate buffer at pH 8. Unreacted NHS was blocked for 2 h at room temperature with ethanolamine (0.5 M ethanolamine, 0.5 M NaCl, pH 8.3). The ethanolamine solution was drained, and the resin was washed three times with 0.1 M

Tris-HCl buffer at pH 8.5 and three times with 0.1 M acetate buffer, 0.5 M NaCl at pH 4.5. This was repeated three times for a total of four wash cycles. This was followed by two washes with 20 mM phosphate buffer at pH 6.5. The resin was resuspended in 20 mM phosphate buffer at pH 6.5 and stored at 4 °C until use.

For resin-bound abTyr prepared with PEGA resin, NHS-activated PEGA resin was modified as described above. However, the ethanolamine block was followed by several washes with 50 mM phosphate buffer at pH 8 rather than altering between Tris-HCl and acetate buffer.

Coupling of pro-sfGFP to rhodamine- and biotin-phenol. Rhodamine- and biotin-phenol were synthesized according to a previously published procedure.[9] Pro-sfGFP (10 μM) was combined with rhodamine-phenol (400 μM, 40 eq) or biotin-phenol (100 μM, 10 eq) in 20 mM phosphate buffer at pH 6.5. Resin-bound abTyr was added to 10% (v/v) (e.g. 10 μL of resin for 100 μL total reaction volume), and the reactions proceeded for 1 h at room temperature. Resin-bound abTyr was removed by filtering reactions through 0.22 μm cellulose acetate spin filters. The reactions were purified by spinning repeatedly with Amicon 10 kDa MWCO spin filters into 10 mM phosphate buffer at pH 7.2. Protein conjugates were analyzed by ESI-TOF LC-MS.

Quantification of abTyr immobilized on resin. After overnight coupling of abTyr to sepharose resin (NHS-Activated Fast Flow or CL-4B), the coupling solution was drained and collected, and the resin was washed several times with 50 mM phosphate buffer at pH 8. Flow through from the washes was collected, combined with the drained coupling solution, lyophilized, and then suspended in a small volume of phosphate buffer. Using a Bradford Assay, the absorbance at 595 nm was obtained and converted to abTyr concentration based on a standard curve produced from abTyr at concentrations from 0.125 to 1.5 mg/mL (in triplicate).

Calorimetric activity assay for resin-bound abTyr. *P*-cresol (0.5, 1, 1.5, 2, or 3 mM) was reacted with 100 eq L-proline methyl ester (50, 100, 150, 200, or 300 mM) in 20 mM phosphate buffer at pH 6.5 in the presence of 10% (v/v) resin-bound abTyr at room temperature. To determine the concentration of product formed, A_{520} was obtained at time points between 1 and 17 min. Resin-bound abTyr was removed by filtering reactions through 0.22 μm cellulose acetate spin filters, and the reaction was diluted 10-fold prior to absorption measurements. The extinction coefficient for the product (ε_{520} = 3,500 $M^{-1}cm^{-1}$) was used to convert A_{520} to concentration of product, and then the reaction rate was determined by plotting product concentration versus time.

Kinetic studies of resin-bound abTyr. The procedure for the calorimetric activity assay (described above) was used with *p*-cresol concentrations of 0.5, 1, 1.5, 2, and 3 mM and resin-bound abTyr at 10% (v/v). To ensure reaction completion, time point aliquots were collected until maximum product was achieved (which occurred between 30 and 90 min). The initial rate of reaction for each *p*-cresol concentration was determined from the slope of the line between the first two time points. OriginPro (2018) was used to model

the initial velocities and corresponding substrate concentrations with a Michaelis-Menten curve, which was used to estimate V_{max} and K_m values for resin-bound abTyr. Note that an accurate K_m value could not be determined due to lack of data at *p*-cresol concentrations less than 0.5 mM.

Reusability studies for resin-bound abTyr. After carrying out a reaction rate test (described above), the resin-bound abTyr was collected (by filtering through a 0.22 µm cellulose acetate spin filter) and washed four times with 50 mM phosphate buffer at pH 8. The washed resin was resuspended in phosphate buffer and then used to catalyze the next reaction rate test. This was repeated until the resin-bound abTyr had been used for six reaction rate tests.

Stability studies for resin-bound abTyr. The reaction rate test (described above) was carried out multiple times over the course of 25 days. Fresh resin was used during each test, but all resin originated from a single batch prepared on “day 1” and stored at 4 °C over the course of the study.

Coupling of scFv-GGY to aniline. scFv-GGY (3.8 µM) was added to aniline (150 µM) in 20 µM phosphate buffer at pH 6.5. Resin-bound abTyr was added (0.625, 1.25, 2.5, 5, 12.5, or 25 µL for a 60 µL reaction, corresponding to 1, 2, 4, 8, 20, and 40% (v/v)) and the reactions proceeded end-over-end for 2.5 hours at room temperature. Resin was removed by filtering reactions through 0.22 µm cellulose acetate spin filters. Reactions were purified by spinning repeatedly through Amicon 10 kDa MWCO spin filters into 10 mM phosphate buffer at pH 7.2. Protein conjugates were analyzed by ESI-TOF LC-MS.

2.5 References

(1) ElSohly, A. M.; Francis, M. B. Development of Oxidative Coupling Strategies for Site-Selective Protein Modification. *Acc. Chem. Res.* **2015**, *48* (7), 1971–1978.

(2) Hooker, J. M.; Esser-Kahn, A. P.; Francis, M. B. Modification of Aniline Containing Proteins Using an Oxidative Coupling Strategy. *J. Am. Chem. Soc.* **2006**, *128* (49), 15558–15559.

(3) Behrens, C. R.; Hooker, J. M.; Obermeyer, A. C.; Romanini, D. W.; Katz, E. M.; Francis, M. B. Rapid Chemoselective Bioconjugation through Oxidative Coupling of Anilines and Aminophenols. *J. Am. Chem. Soc*. **2011**, *133* (41), 16398–16401.

(4) Obermeyer, A. C.; Jarman, J. B.; Netirojjanakul, C.; El Muslemany, K.; Francis, M. B. Mild Bioconjugation Through the Oxidative Coupling of *Ortho*-Aminophenols and Anilines with Ferricyanide. *Angew. Chem. Int. Ed.* **2014**, *53* (4), 1057–1061.

(5) Obermeyer, A. C.; Jarman, J. B.; Francis, M. B. N-Terminal Modification of Proteins with *o*-Aminophenols. *J. Am. Chem. Soc.* **2014**, *136* (27), 9572–9579.

(6) ElSohly, A. M.; MacDonald, J. I.; Hentzen, N. B.; Aanei, I. L.; El Muslemany, K. M.; Francis, M. B. *Ortho*-Methoxyphenols as Convenient Oxidative Bioconjugation Reagents with Application to Site-Selective Heterobifunctional Cross-Linkers. *J. Am. Chem. Soc.* **2017**, *139* (10), 3767–3773.

(7) Palla, K. S.; Hurlburt, T. J.; Buyanin, A. M.; Somorjai, G. A.; Francis, M. B. Site-Se-

lective Oxidative Coupling Reactions for the Attachment of Enzymes to Glass Surfaces through DNA-Directed Immobilization. *J. Am. Chem. Soc.* **2017**, *139* (5), 1967–1974.
(8) Furst, A. L.; Smith, M. J.; Lee, M. C.; Francis, M. B. DNA Hybridization to Interface Current-Producing Cells with Electrode Surfaces. *ACS Cent. Sci*. **2018**, *4* (7), 880–884.
(9) Maza, J. C.; Bader, D. L. V.; Xiao, L.; Marmelstein, A. M.; Brauer, D. D.; ElSohly, A. M.; Smith, M. J.; Krska, S. W.; Parish, C. A.; Francis, M. B. Enzymatic Modification of N-Terminal Proline Residues Using Phenol Derivatives. J*. Am. Chem. Soc.* **2019**, *141* (9), 3885–3892.
(10) Lobba, M. J.; Fellmann, C.; Marmelstein, A. M.; Maza, J. C.; Kissman, E. N.; Robinson, S. A.; Staahl, B. T.; Urnes, C.; Lew, R. J.; Mogilevsky, C. S.; Doudna, J. A.; Francis, M. B. Site-Specific Bioconjugation through Enzyme-Catalyzed Tyrosine–Cysteine Bond Formation. *ACS Cent. Sci*. **2020**, *6* (9), 1564–1571.
(11) Marmelstein, A. M.; Lobba, M. J.; Mogilevsky, C. S.; Maza, J. C.; Brauer, D. D.; Francis, M. B. Tyrosinase-Mediated Oxidative Coupling of Tyrosine Tags on Peptides and Proteins. *J. Am. Chem. Soc*. **2020**, *142* (11), 5078–5086.
(12) Zdarta, J.; Meyer, A. S.; Jesionowski, T.; Pinelo, M. A General Overview of Support Materials for Enzyme Immobilization: Characteristics, Properties, Practical Utility. *Catalysts* **2018**, *8* (2), 92.
(13) Fang, S. M.; Want, N. H.; Zhao, Z. S.; Wang, W. H. Immobilized Enzyme Reactors in HPLC and its Application in Inhibitor Screening: A Review. *J. Pharm. Anal.* **2012**, *2* (2), 83–89.
(14) Girelli, A. M.; Mattei, E.; Messina, A. Phenols Removal by Immobilized Tyrosinase Reactor in On-Line High Performance Liquid Chromatography. *Anal. Chim. Acta* **2006**, *580* (2), 271–277.
(15) Lasmi, K.; Derder, H.; Kermad, A.; Sam, S.; Boukhalfa-Abib, H.; Belhousse, S.; Tighilt, F. Z.; Hamdani, K.; Gabouze, N. Tyrosinase Immobilization on Functionalized Porous Silicon Surface for Optical Monitoring of Pyrocatechol. *Appl. Surf. Sci.* **2018**, *446*, 3–9.
(16) de Oliveira, K. B.; Mischiatti, K. L.; Fontana, J. D.; de Oliveira, B. H. Tyrosinase Immobilized Enzyme Reactor: Development and Evaluation. *J. Chromatogr. B* **2014**, *945–946*, 10–16.
(17) Hlady, V.; Buijs, J.; Jennissen, H. P. Methods for Studying Protein Adsorption. *Methods Enzymol.* **1999**, *309*, 402–429.
(18) Pédelacq, J.-D.; Cabantous, S.; Tran, T.; Terwilliger, T. C.; Waldo, G. S. Engineering and Characterization of a Super-folder Green Fluorescent Protein. *Nature Biotech.* **2006**, *24* (1), 79–88.
(19) Männel, M. J.; Kreuzer, L. P.; Goldhahn, C.; Schubert, J.; Hartl, M. J.; Chanana, M. Catalytically Active Protein Coatings: Toward Enzymatic Cascade Reactions at the Intercolloidal Level. *ACS Catal.* **2017**, *7* (3), 1664–1672.
(20) Petkova, G. A.; Záruba, K.; Žvátora, P.; Král, V. Gold and Silver Nanoparticles for Biomolecule Immobilization and Enzymatic Catalysis. *Nanoscale Res. Lett*. **2012**, *7* (1), 287.
(21) Kampmann, M.; Boll, S.; Kossuch, J.; Bielecki, J.; Uhl, S.; Kleiner, B.; Wichmann,

R. Efficient Immobilization of Mushroom Tyrosinase Utilizing Whole Cells from Agaricus Bisporus and Its Application for Degradation of Bisphenol A. *Water Research* **2014**, *57*, 295–303.
(22) Peniche, H.; Osorio, A.; Acosta, N.; Campa, A. de la; Peniche, C. Preparation and Characterization of Superparamagnetic Chitosan Microspheres: Application as a Support for the Immobilization of Tyrosinase. *J. Appl. Polym. Sci*. **2005**, *98* (2), 651–657.
(23) Wada, S.; Ichikawa, H.; Tastsumi, K. Removal of Phenols and Aromatic Amines from Wastewater by a Combination Treatment with Tyrosinase and a Coagulant. *Biotechnol. Bioeng*. **1995**, *45* (4), 304–309.

Chapter 3

Enzyme Activated Gold Nanoparticles for Versatile Site-Selective Bioconjugation

Abstract

A new enzymatic method is reported for constructing protein- and DNA-AuNP conjugates. The strategy relies on the initial functionalization of AuNPs with phenols, followed by activation with the enzyme tyrosinase. Using an oxidative coupling reaction, the activated phenols are coupled to proteins bearing proline, thiol, or aniline functional groups. Activated phenol-AuNPs are also conjugated to a small molecule biotin and commercially available thiol-DNA. Advantages of this approach for AuNP bioconjugation include: (1) initial formation of highly stable AuNPs that can be selectively activated with an enzyme, (2) the ability to conjugate either proteins or DNA through a diverse set of functional handles, (3) site-specific immobilization, and (4) facile conjugation that is complete within 2 h at room temperature under aqueous conditions. The enzymatic oxidative coupling on AuNPs is applied to the construction of tobacco mosaic virus (TMV)-AuNP conjugates, and energy transfer between the AuNPs and fluorophores on TMV is demonstrated.

This chapter is based on the following publication:

Ramsey, A. V.; Bischoff, A. J.; Francis, M. B. Enzyme Activated Gold Nanoparticles for Versatile Site-Selective Bioconjugation. *J. Am. Chem. Soc.* **2021**, accepted.

3.1 Introduction

Gold nanoparticles (AuNPs) exhibit unique chemical and optical properties that can be exploited in many biological applications.[1] Proteins, peptides, and nucleic acids are frequently tethered to AuNPs for use in therapeutics, diagnostics, and biosensors.[1] For example, antibody-AuNP conjugates are being investigated as a novel therapy for colorectal cancer via targeted drug delivery[2] and the photothermal destruction of tumor cells.[3] Additionally, protein- and DNA-AuNP conjugates are widely used for signal amplification in lateral flow immunoassays that rely on either antibodies[4,5,6] or nucleic acids[7,8] as the detection element. The localized surface plasmon resonance (LSPR) produced by AuNPs also allows proximity-based enhancement or quenching of fluorescence from both synthetic fluorophores[9] and natural light harvesting complexes, such as Light Harvesting Complex 2 (LH2)[10]. This unique property of AuNPs has found utility in biosensing devices[11,12] and could also lead to the development of enhanced light harvesting materials. Central to all of these applications is a bioconjugation strategy that immobilizes biomolecules on AuNP surfaces. Currently, each type of biomolecule requires a different strategy that is highly dependent on the type of functional handle present on the biomolecule, thus necessitating more general conjugation strategies.

The most common method for generating protein-AuNP conjugates is physical adsorption, but the strength of this interaction depends heavily on the surface charge of the protein[13] and is reversible in many cases. Furthermore, it results in uncontrolled protein orientations, which can lead to a loss of native function.[14] A common covalent method for protein immobilization is amide bond formation between native lysine residues on proteins and carboxylic acid monolayers on AuNPs.[14,15] While widely applicable, this leads to non-homogenous protein modification and random orientation. Affinity-based strategies such as biotin/streptavidin binding[16] require the extra steps of coupling streptavidin to the particles and biotin to the biomolecule partner, which can be cumbersome. Cysteine-tagged proteins or proteins with solvent-exposed native cysteine residues can be directly conjugated to AuNPs through gold-thiol interactions.[14] However, the lack of a preformed monolayer can result in non-specific protein binding and can limit AuNP stability.[14]

The construction of DNA-AuNP conjugates has been incredibly successful owing to the direct attachment of thiol-DNA through the “salt-aging” method.[17,18] This strategy is simple, relatively inexpensive, and allows the use of commercially available thiol-DNA. Additionally, a variety of DNA surface densities can be achieved. However, the process can take several days, and AuNPs are prone to aggregation if salt is added too quickly.[12] More efficient variations of direct DNA attachment rely on low pH[19] or freezing temperatures.[11,20] To gain additional control over DNA-AuNP assembly, some research groups have taken advantage of poly-adenine adsorption to gold rather than utilizing gold-thiol chemistry.[21] Additionally, the enhanced stability of polydentate ligands has led to the development of DNA with bi- or even tri-thiol anchoring groups.[22] However, these techniques require that commercial DNA is modified prior to conjugation to AuNPs. In addition, techniques used for DNA conjugation may not be feasible for protein conjugation due to the greater sensitivity of proteins to temperature and pH. Another limitation of current DNA-

AuNP conjugation methods is that relatively dense layers of DNA are often required to maintain colloidal stability, making low density DNA-AuNP conjugates difficult to produce. Thus, while many successful strategies exist for generating DNA-AuNP conjugates, there is a need for methods that are compatible with both proteins and DNA and allow the production of low-density DNA-AuNPs.

Enzymes could offer a unique addition to the AuNP conjugation toolbox by allowing timely and efficient activation of stable, pre-functionalized AuNPs. The use of enzymes in some aspects of metal surface modification has been reported. For example, aggregates of β-agarase were tethered to magnetic particles via the initial oxidation of engineered tyrosine residues on the surface of the protein aggregates.[23] In another instance, AuNPs of two different sizes were functionalized with DNA, which was then activated with a restriction endonuclease. The activated AuNPs were subsequently ligated to form nanoparticle-based structures.[24] However, direct enzymatic activation of AuNP surfaces for subsequent bioconjugation has not been reported.

Over the years, our lab has developed a rapid and efficient oxidative coupling approach for biomolecules through the reactions of reactive *ortho*-quinoid intermediates with specific nucleophiles of interest (Figure 1).[25] The *ortho*-quinoids can be accessed by potassium ferricyanide ($K_3Fe(CN)_6$) or sodium periodate oxidation of *ortho*-phenolic compounds, such as catechols, aminophenols, and methoxyphenols.[26–30] This versatile chemistry has enabled the construction of various bioconjugates that tether proteins, peptides, and nucleic acids to small molecules, other biomolecules, and even surfaces, such as glass[31] and gold electrodes.[32] More recently, we have developed an enzymatic version of the oxidative coupling reaction that allows *ortho*-quinones to be accessed from water soluble and highly stable phenols.[33] The enzyme, tyrosinase (abTyr), features a binuclear copper active site and is responsible for the formation of melanin. abTyr is isolated from the common button mushroom, *Agaricus bisporus*, and is commercially available in its active form. Past work has demonstrated that abTyr can oxidize phenols on a variety of substrates, including small molecules, peptides, and proteins. Importantly, the enzymatic version of this reaction allows thiols to be used as a nucleophile without competing side reaction pathways.[34] Our lab has also demonstrated successful oxidative couplings with a smaller tyrosinase (35.5 kDa versus ~120 kDa for abTyr) from *Bacillus megaterium*.[35]

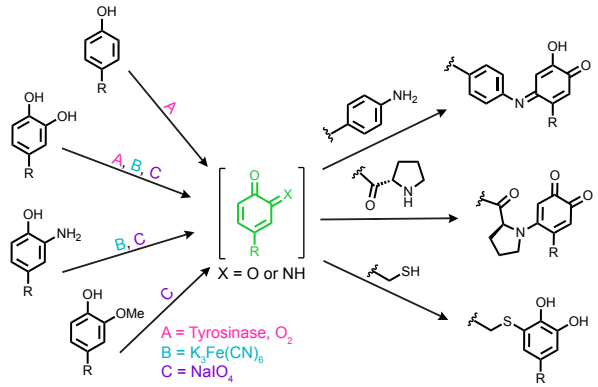

Figure 1. Oxidative coupling reactions. A variety of oxidants can be used to oxidize phenol based moieties to *ortho*-quinoid intermediates (green). These intermediates can undergo subsequent reactions with both amine- and thiol-based nucleophiles.

There are a number of features of the oxidative coupling strategy that are particularly attractive for AuNP modification. Chief among them is the ability to use a non-reac-

tive phenol functional group as a surface coating that does not decompose or otherwise react until the desired reaction takes place. In addition, the oxidative coupling reaction can proceed at the low concentrations that are frequently encountered in the context of metal nanoparticle modification. To demonstrate the utility of this approach, AuNPs are first functionalized with a monolayer of phenols that, upon enzymatic activation with abTyr, can be coupled to a variety of proteins bearing thiol, proline, or aniline functional groups. This highlights how a single type of functional AuNP is compatible with multiple functional handles and can easily be applied for versatile protein conjugation. We also demonstrate the effective coupling of thiol-DNA by producing DNA-AuNP conjugates with varying DNA densities. Finally, to highlight the utility of protein-AuNP constructs, we use this enzymatic bioconjugation technique to conjugate dye-labeled and aniline-containing circular permutant tobacco mosaic virus (cpTMV) protein disks to AuNPs and demonstrate energy transfer between the dyes and the AuNPs. The novelty of this approach is the direct enzymatic activation of AuNP surfaces with a view towards subsequent bioconjugation, which has not been reported to date.

3.2 Results and Discussion

3.2.1 Generating Phenol Monolayers on 5 nm AuNPs

Previous work in our lab has demonstrated oxidative coupling on AuNPs by decorating the particles with anilines and conjugating the functionalized AuNPs to aminophenol-containing proteins and DNA.[36] However, we were also interested in immobilizing the phenolic coupling partner on AuNPs to allow oxidative coupling with native nucleophiles on proteins, such as cysteines and N-terminal prolines (Figure 1). This would negate the need for prior functionalization with aminophenols and would also allow the coupling of commercially available thiol-DNA. In the previous iteration of the oxidative coupling reaction (involving $K_3Fe(CN)_6$ and catechols), it was necessary to immobilize the aniline partners because catechols are not stable in solution due to oxidation by air, leading to self-coupling and subsequent polymerization. However, we reasoned that the ability to oxidize phenols enzymatically would allow us to generate stable AuNPs that could be activated only when desired.

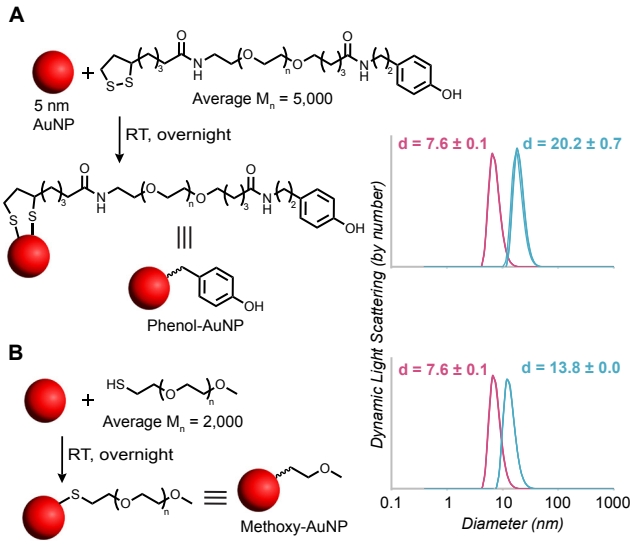

Figure 2. Monolayer formation on AuNPs. Gold nanoparticles (5 nm) were functionalized with (A) a thiol-PEG5k-phenol or (B) a thiol-PEG2k-methoxy monolayer. Monolayer formation was confirmed by DLS, where pink traces correspond to 5 nm AuNPs stabilized by BSPP and blue traces correspond to AuNPs with either phenol (top trace) or methoxy (bottom trace) monolayers.

To this end, we designed a thiol-PEG5k-phenol ligand for AuNP functionalization. The long PEG linker was chosen to shield the AuNP surfaces and prevent aggregation, and the 5k length

aided in quick purification with 3k MWCO spin filters during the synthetic manipulations. Synthesis of the phenol ligand was based on an analogous aniline ligand previously reported by our lab.[36] Briefly, DCC/NHS was used to functionalize amine-PEG5k-valeric acid with lipoic acid on one end and tyramine on the other end. To generate phenol-AuNPs, the bifunctional ligand was incubated overnight with 5 nm AuNPs (Figure 2A) that were previously stabilized with bis(p-sulfonatophenyl)phenylphosphine (BSPP).[37] BSPP-stabilized AuNPs were also incubated with a commercially available thiol-PEG2k-methoxy ligand (Figure 2B). The methoxy-AuNPs served as one of several controls in subsequent oxidative coupling reactions. Monolayer formation was confirmed with Dynamic Light Scattering (DLS, Figure 2) and a salt stability test (Figure S1A). The phenol- and methoxy-AuNPs also exhibited significant differences in electrophoretic mobility relative to BSPP-stabilized AuNPs (Figure S1B).

3.2.2 Oxidative Coupling of Proteins and a Small Molecule to Phenol-AuNPs

Our previous studies of phenol activation on proteins revealed that only highly exposed phenol compounds can reach into the active site of abTyr. It was therefore unclear whether surface phenols on metal particles would be amenable to oxidation by abTyr. In preliminary studies without added nucleophiles, phenol-AuNPs exposed to abTyr did indeed undergo a significant reduction in electrophoretic mobility when analyzed by native agarose gel electrophoresis. This indicated that a change in surface chemistry had occurred. It is important to note that because phenol- and methoxy-AuNPs exhibit low net charge relative to citrate- or BSPP-stabilized AuNPs, running the gels for longer periods of time had little effect on the extent of electrophoretic mobility.

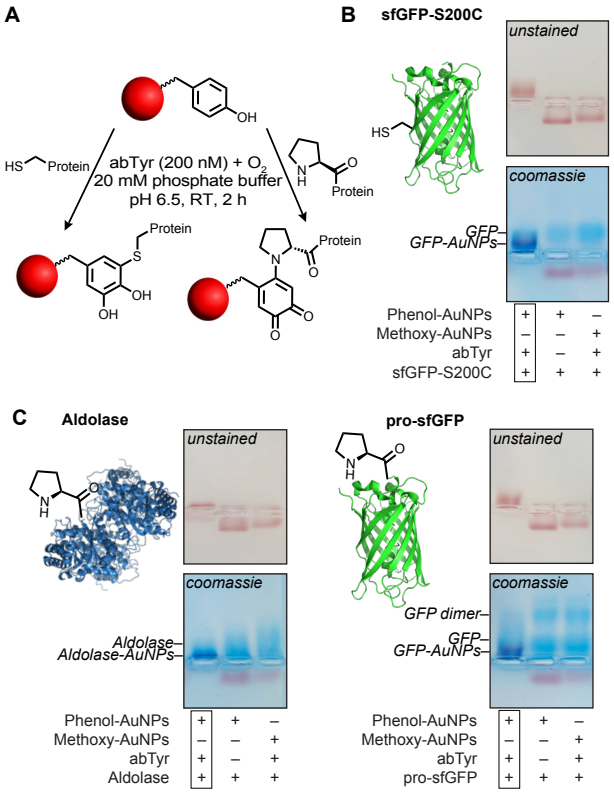

Figure 3. Conjugation of proteins to phenol-AuNPs. (A) Phenol-AuNPs were functionalized with proteins bearing either an accessible (B) cysteine residue or (C) proline N-terminus. In all cases, the protein only coupled to the AuNPs when phenol-AuNPs were used in the presence of tyrosinase (abTyr, 200 nM), as confirmed by native agarose gel electrophoresis. All conjugations were run with 400 nM AuNPs and 5 μM protein.

We next added biomolecules as nucleophilic coupling partners. A small panel of proteins that included both thiol- and proline-containing proteins was explored (Figure 3A). The thiol-containing protein was an engineered superfolder green fluorescent protein (sfGFP)[38] with a point mutation at position 200 (sfGFP-S200C, Figure 3B). The proline-containing proteins (Figure 3C) were aldolase, which contains a native proline N-terminus, and sfGFP with an engineered proline N-terminus (pro-sfGFP). The reactions were

carried out with 5 μM protein, 400 nM phenol-AuNPs, and 200 nM abTyr and were analyzed with native agarose gel electrophoresis. AuNPs moved toward the negative electrode in samples that excluded abTyr or replaced phenol-AuNPs with methoxy-AuNPs (the second and third lanes of each gel in Figure 3). In the presence of abTyr, however, phenol-AuNPs moved towards the positive electrode (the first lane of each gel in Figure 3). Upon Coomassie staining, AuNPs only stained blue when both phenol-AuNPs and abTyr were included in the coupling reaction, indicating successful protein conjugation. We also observed that the mobility of protein-AuNP conjugates was affected by the identity of the protein. Proteins with greater electrophoretic mobility resulted in greater movement of phenol-AuNPs. In contrast, there were no changes in electrophoretic mobility for controls with added protein but lacking abTyr. The lack of staining in negative controls confirmed that no proteins were adsorbed non-specifically to the phenol-AuNPs. We also characterized the conjugated AuNPs via UV-vis spectroscopy but did not observe strong shifts in the absorption wavelength. This is likely due to the 5k ligand shielding the AuNP surfaces and preventing significant changes in the refractive index upon conjugation of proteins.

The oxidative coupling reactions for the protein screen and following experiments were carried out for 2 h to ensure completion, but a more detailed study with pro-sfGFP revealed that the reactions were complete in as little as 30 min (Figure S2). We also found that the extent of phenol oxidation can be tuned by the concentration of abTyr. While the majority of these reactions were carried out with 200 nM abTyr, we also tried 20 nM and 5 μM abTyr. Higher concentrations of abTyr resulted in an increase in AuNP electrophoretic mobility and a less pronounced band of uncoupled protein, indicating a greater extent of protein conjugation (Figure S2). As an additional advantage of this approach for AuNP bioconjugation, we have found that phenol-AuNPs can be stored for at least several months at 4 °C and still be enzymatically activated to form biomolecule conjugates. This highlights how the phenol-AuNPs are stable in solution for long periods of time, allowing convenient coupling when desired.

To verify that protein structure is maintained upon immobilization, we carried out an activity assay of immobilized aldolase versus aldolase in solution (Figure 4). Final aldolase concentrations were reduced to 500 nM (1.25 eq compared to AuNPs) to ensure that all aldolase was coupled to phenol-AuNPs in the presence of abTyr. Immobilized aldolase remained active, but activity was reduced compared to soluble aldolase. While enzymes immobilized on AuNPs can exhibit retained or even enhanced activity,[39,40] it is not uncommon to observe reduced activity. For example, 40–50% activity loss has been reported for alcohol dehydrogenase

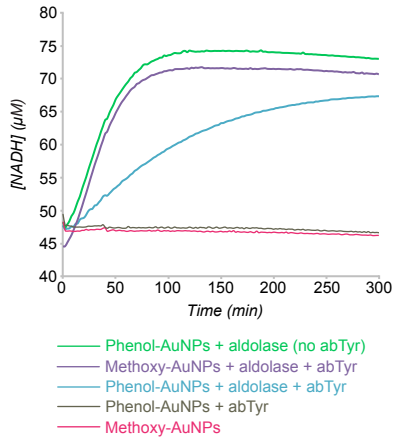

Figure 4. Activity assay of immobilized aldolase. Immobilized aldolase (blue) displayed reduced activity as compared to aldolase in solution with phenol-AuNPs but no tyrosinase (abTyr) (green) and aldolase in solution with methoxy-AuNPs and abTyr (purple). Reduced activity is likely due to active site obstruction from immobilization rather than mis-folding. Oxidative coupling reactions were carried out with 400 nM AuNPs, 500 nM aldolase, and 200 nM abTyr.

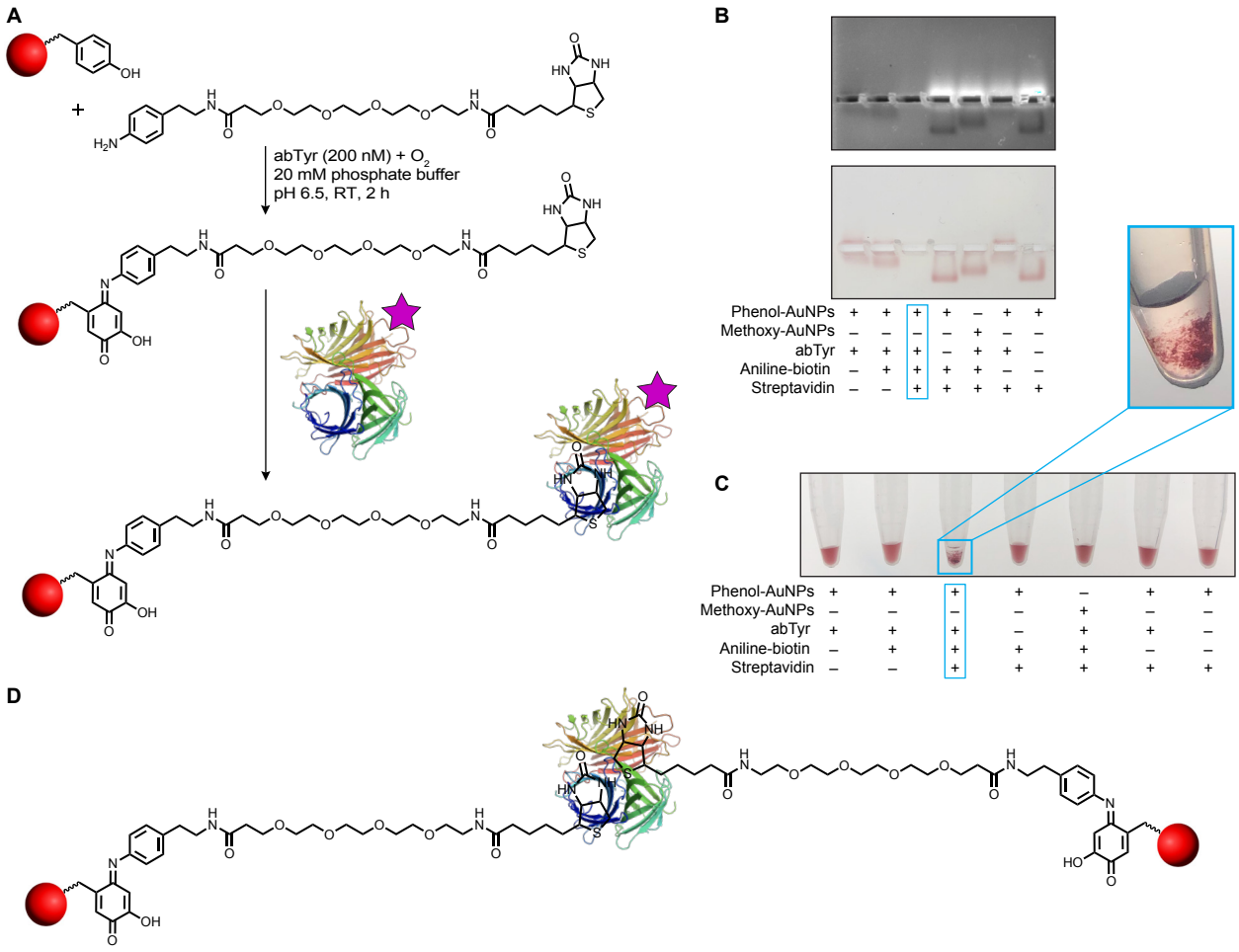

Figure 5. Coupling of aniline-biotin to phenol-AuNPs. (A) Aniline-biotin was synthesized and oxidatively coupled to phenol-AuNPs, followed by incubation with Texas red-labeled streptavidin to verify success of oxidative coupling. Reactions were carried out with 400 nM AuNPs, 200 nM tyosinase (abTyr), 10 μM biotin, and 5 μM streptavidin. (B) Agarose gel electrophoresis revealed quenching of Texas red when streptavidin was incubated with phenol-AuNPs that were exposed to abTyr during the biotin oxidative coupling reactions. This is likely from proximity-based quenching, present only when streptavidin is binding immobilized biotin. Lack of AuNP mobility is likely the result of large assembly formations, as discussed in part C. (C) After overnight incubation, large assemblies of AuNPs were observed only when both phenol-AuNPs and abTyr were present in the biotin oxidative coupling reactions, followed by streptavidin addition. (D) Large assembly formation is presumably due to streptavidin binding immobilized biotin on adjacent AuNPs. While this cartoon shows binding of only two AuNPs, a single streptavidin protein could bind up to four AuNPs.

immobilized on metal nanoparticles,[41] and the activity of immobilized glucose oxidase can be reduced by two to three orders of magnitude, possibly due to hindered active sites.[39] Because aldolase immobilized through oxidative coupling remained active, the reduction in activity is likely due to obstruction of one or more of the four active sites rather than destruction of protein secondary structure.

We were also interested in exploring small molecule functionalization of phenol-AuNPs. To this end, we functionalized biotin with an aniline moiety and oxidatively coupled it to phenol-AuNPs (Figure 5). To verify conjugation, we incubated the biotin-AuNPs with streptavidin. When allowed to settle overnight, the AuNPs formed large assemblies (visible by eye, Figure 5C) only when both abTyr and phenol-AuNPs were

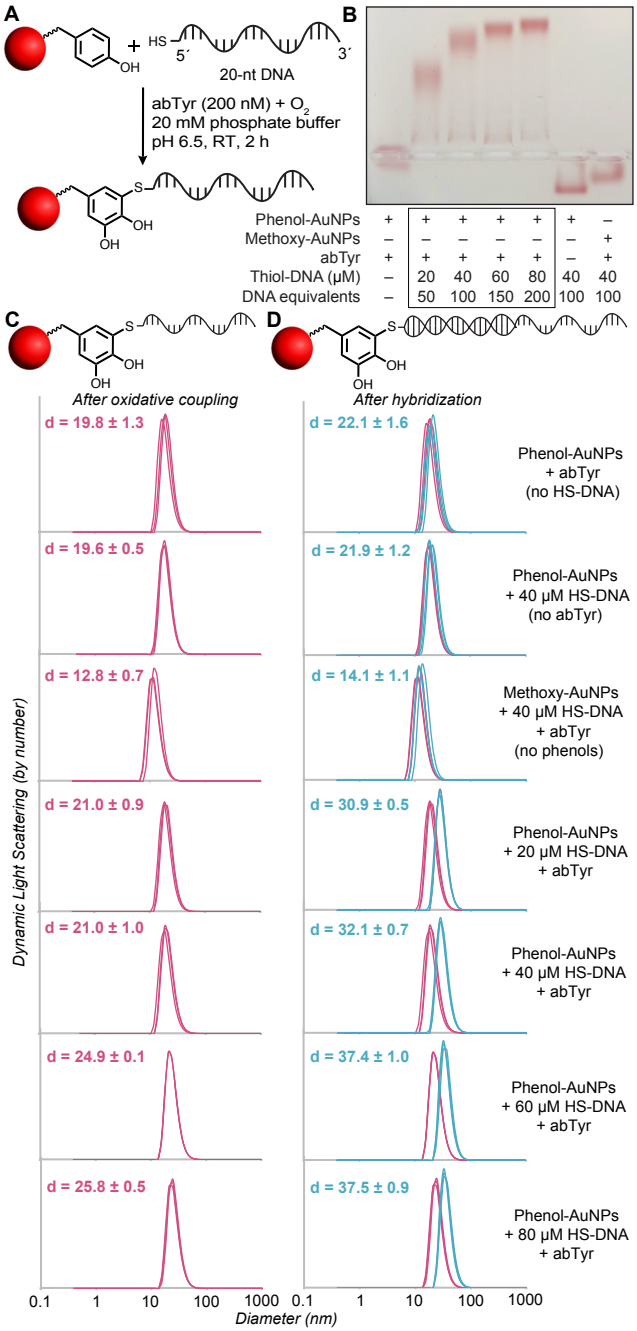

Figure 6. DNA conjugation to phenol-AuNPs and characterization by gel electrophoresis and DLS. (A) Commercially available thiol-DNA was conjugated to phenol-AuNPs. (B) Native agarose gel electrophoresis demonstrated that conjugation was successful over a range of thiol-DNA concentrations. The AuNP concentration was 400 nM. (C) DLS of DNA-AuNP conjugates revealed that oxidative coupling caused an increase in AuNP diameter only when phenol AuNPs were used in the presence of thiol-DNA and tyrosinase (abTyr, 200 nM). Lower concentrations of DNA exhibited a less dramatic shift in size. (D) Success of oxidative coupling was further confirmed by subsequent hybridization to 40-nt complementary DNA. Significant increases in size were only observed when the initial oxidative coupling reaction included both coupling partners and abTyr.

present during the initial biotin oxidative coupling reaction. These assemblies were formed through streptavidin binding of biotin on adjacent AuNPs (Figure 5D) and verify success of small molecule oxidative coupling.

While these experiments were carried out with 10 μM aniline-biotin during the oxidative coupling reaction, we also explored lower concentrations of biotin (0.5, 1, and 5 μM). In these studies, the streptavidin concentration was increased from 5 μM to 20 μM to ensure dependence of assembly formation on biotin concentration. Assembly formation was only observed at 5 and 10 μM, with a higher degree of assembly formation occurring at 10 μM aniline-biotin (based on visual observation). It is likely that streptavidin binding still occurred at the lower biotin concentrations, but larger assemblies were prevented from forming due to low density of biotin on the AuNP surfaces.

3.2.3 Oxidative Coupling of DNA to Phenol-AuNPs

DNA-AuNP conjugates have a wide variety of applications ranging from use in nanomechanical devices and computing systems to biosensing and calorimetric detection.[42] Because of this, DNA attachment to AuNPs has been the focus of many research groups over the years.[43–48] Thus, we were interested in applying the enzymatic oxidative coupling method to construction of DNA-AuNP conjugates (Figure 6A). For proof-of-concept studies, we purchased a 20-nt thiol-DNA strand with a sequence that our lab previously used to immobilize cells on gold electrodes.[32] Reactions were run with 400 nM AuNPs and 20 to 80 μM DNA and were monitored with native gel electrophoresis,

which demonstrated that DNA conjugation was successful over the entire range of tested DNA concentrations. We also observed a concentration dependent effect on the electrophoretic mobility of DNA-AuNP conjugates (Figure 6B), which could be useful for tuning the surface density of DNA on the AuNPs. As previously noted, phenol-AuNPs undergo a change in electrophoretic mobility when exposed to abTyr (Figure 6B, lane 1), which does not occur when phenol-AuNPs are exposed to DNA in the absence of abTyr (Figure 6B, lane 6). This change upon exposure to abTyr is presumably due to a change in surface chemistry from phenols to *ortho*-quinones upon oxidation by abTyr.

When analyzing the conjugates by DLS, a significant size increase was observed for the two highest DNA concentrations of 60 and 80 μM (Figure 6C). DLS did not reveal a significant size increase for the 20 and 40 μM concentrations of DNA. However, subsequent hybridization of a 40-nt palindromic complementary DNA strand revealed a ~10 nm increase in size for all phenol-AuNPs that were previously exposed to both abTyr and thiol-DNA; all negative controls exhibited no size increases (Figure 6D). This both confirmed DNA conjugation under oxidative coupling conditions and verified that the conjugated DNA remained functional.

In many direct DNA attachment methods, DNA is added at 300 eq relative to ~13 nm AuNPs (at 10 nM), yielding AuNPs with roughly 120 DNA strands per AuNP.[11,49] This dense functionalization is critical for stabilizing AuNPs in the presence of high salt concentrations. In our studies, 50 eq of DNA (20 μM) was enough to produce clearly functionalized AuNPs (Figure 6). Equivalents as low as 15 also demonstrated functionalization, as determined by gel electrophoresis (Figure S3). Because phenol-AuNPs are already stable in salt concentrations up to 1 M (Figure S1), our functionalization method allows stable DNA-AuNPs to be formed with fewer strands of DNA.

To quantify the number of DNA strands per AuNP, we dissolved purified

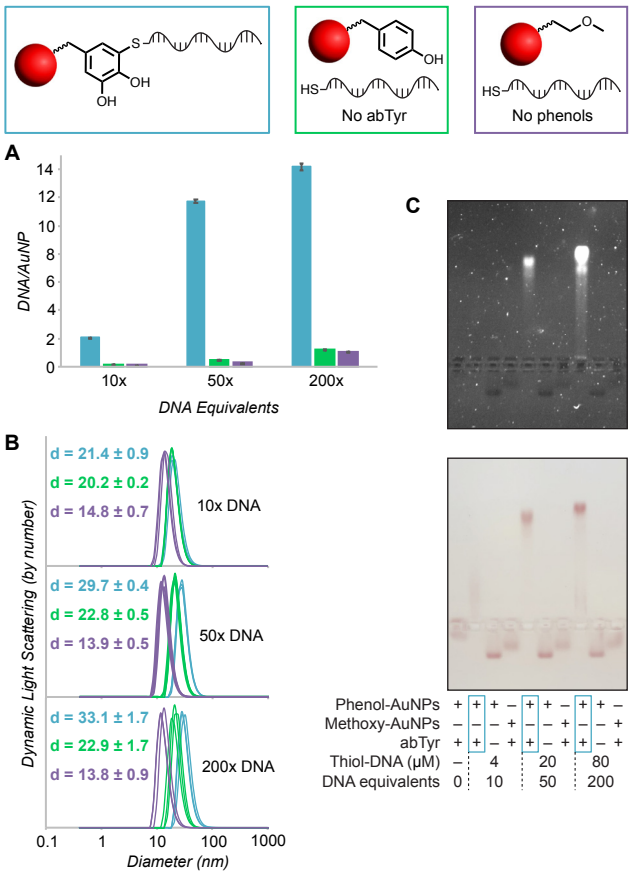

Figure 7. Quantification of DNA conjugated to phenol-AuNPs (400 nM). (A) DNA quantification revealed that up to 14 strands of DNA can be oxidatively coupled to phenol-AuNPs in the presence of tyrosinase (abTyr) (blue) and that the number of conjugated DNA strands can be tuned by changing DNA concentration during oxidative coupling. Minimal background adsorption was observed in the absence of abTyr (green) and the absence of phenols (purple). All oxidative coupling reactions were carried out with 400 nM AuNPs and 200 nM abTyr. Error bars are from triplicate measurements of a single experiment. (B) The samples used for quantifying DNA per AuNP were also analyzed by DLS. The diameter of DNA-AuNPs increased as the number of DNA strands per AuNP increased. (C) Analysis by gel electrophoresis with an agarose gel containing SYBR Safe stain revealed fluorescent bands for DNA-AuNP samples with relatively high numbers of conjugated DNA strand.

DNA-AuNPs in potassium cyanide and then quantified the resulting DNA with an Oli-Green ssDNA stain. In oxidative coupling reactions carried out with 10, 50, or 200 eq of thiol-DNA, we found that phenol-AuNPs can be functionalized with 2 to 14 strands of DNA per AuNP (Figure 7A). This is comparable to the literature, which reports ~13 strands of DNA per AuNP (5 nm) when generating DNA-AuNPs through direct attachment of 8-nt thiol-DNA.[50] We also found that a brief incubation in 300 mM sodium chloride (NaCl), followed by several washes with 150 mM NaCl, helped reduce nonspecific adsorption of DNA, although some background adsorption was still observed during quantification (Figure 7A). Incubation and washing with NaCl also helped facilitate extended radial orientation of the conjugated strands, which allowed lower DNA eq to be detected by DLS without the need for secondary hybridization (Figure 7B). Higher DNA concentrations during oxidative coupling yielded AuNPs with a larger diameter. We also found that adding SYBR Safe stain to agarose gels used for electrophoretic characterization allowed for visualization of DNA-AuNPs under UV light (Figure 7C).

Many literature methods use 13 nm AuNPs at a concentration of 10 nM, and thus we wanted to test if the enzymatic method was still effective at low AuNP concentrations. We found that the approach still produced DNA-AuNP conjugates at AuNP concentrations of 40 nM and DNA eq of 10, 50, and 200 (Figure S4). However, DNA loading capacity was reduced compared to reactions with 400 nM AuNPs, and lower concentrations were more difficult to analyze by electrophoresis and DLS. To maximize efficiency, we recommend running AuNP oxidative coupling reactions with 400 nM phenol-AuNPs (5 nm) and 50 to 200 eq thiol-DNA. For larger AuNPs, efficient coupling can likely be achieved with lower AuNP concentrations, although DNA eq may need to be increased due to higher surface area.

The salt-aging method pioneered by Mirkin and co-workers relies on high concentrations of NaCl to shield negatively charged DNA strands and overcome charge repulsion that can minimize the number of strands immobilized. Thus we were curious if including NaCl during the oxidative coupling reaction would increase the number of DNA strands per AuNP. We tested NaCl concentrations of 100 and 300 mM but did not observe an effect on final DNA density. This is consistent with the ability of oxidative coupling to produce DNA-AuNP conjugates with relatively low DNA densities. These lower densities likely reduce the effect of charge repulsion between neighboring DNA strands.

While already established methods for generating DNA-AuNPs are highly effective, our enzymatic approach is an important addition to this toolbox due to the quick reaction times, enzymatic control, and ability to produce low density yet stable DNA-AuNP conjugates.

3.2.4 Oxidative Coupling of an Aniline-Containing Multivalent Protein Assembly

One key feature of the solution-based oxidative coupling reaction is its efficacy with both natural and artificial amino acids. Thus, we next explored AuNP conjugation to a modified tobacco mosaic viral capsid protein (TMV) with an engineered aniline residue

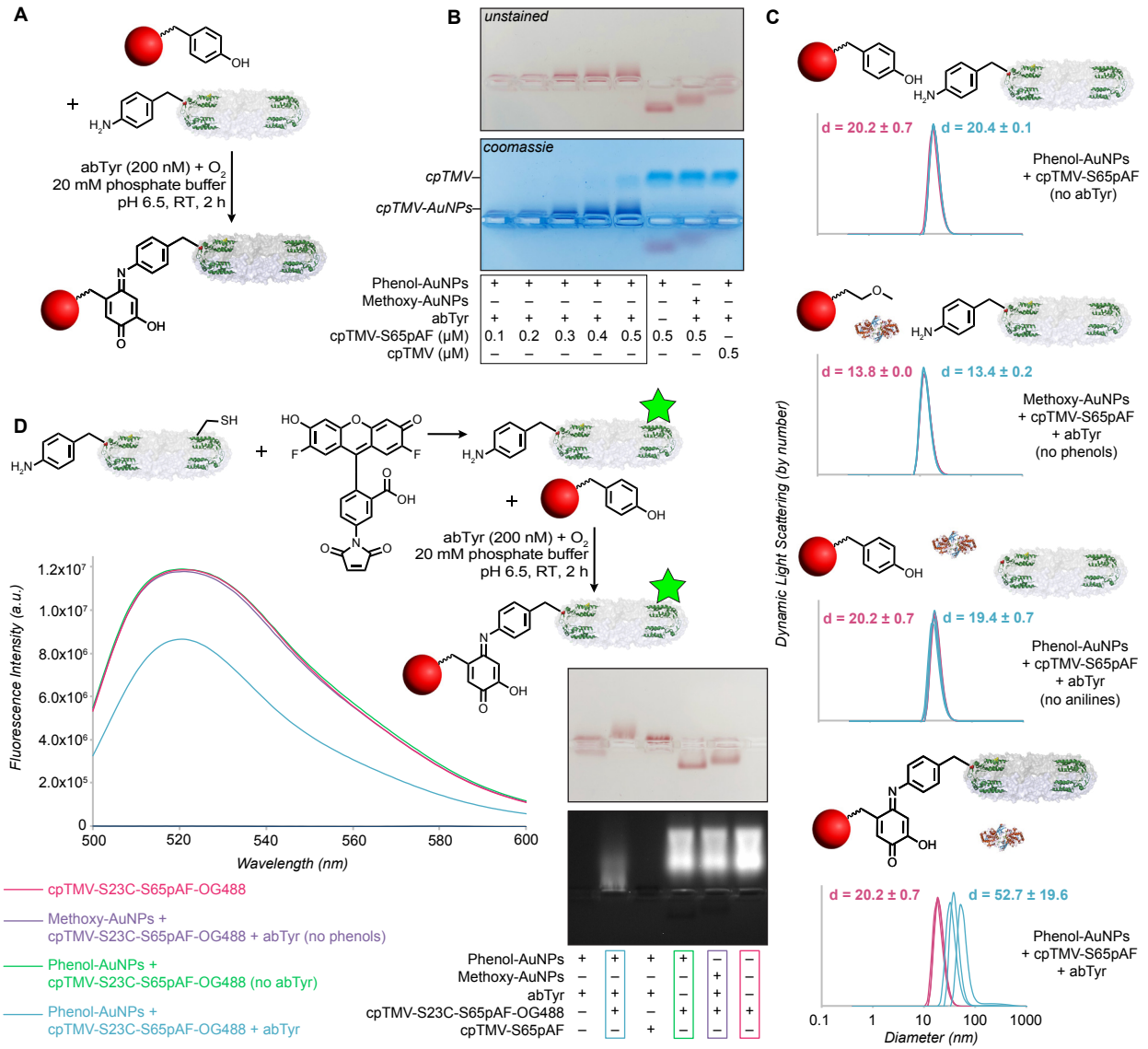

Figure 8. TMV conjugation to phenol-AuNPs. (A) TMV with an engineered aniline residue (cpTMV-S65pAF) was conjugated to phenol-AuNPs. (B) Native agarose gel electrophoresis demonstrated that conjugation was successful over a range of cpTMV-S65pAF concentrations. TMV with no engineered aniline residue (cpTMV) did not couple (far right lane of gel). Reactions were carried out with 400 nM AuNPs. (C) DLS confirmed that no conjugation occurred in the absence of tyrosinase (abTyr), absence of phenol-AuNPs, or absence of aniline-containing cpTMV. cpTMV-AuNP conjugates were only formed when phenol-AuNPs, cpTMV-S65pAF, and abTyr were present, and the conjugates could produce large arrays through multiple couplings to a single cpTMV-S65pAF assembly. (D) Oregon Green 488 (OG488) maleimide was conjugated to cpTMV-S65pAF with an engineered cysteine residue at a position on the external surface of the cpTMV disks (cpTMV-S23C-S65pAF; see Figures S5, S6A, and S6B). The resulting cpTMV-S23C-S65pAF-OG488 proteins were coupled to phenol-AuNPs and analyzed by native gel electrophoresis and fluorometry. Both characterization techniques revealed quenching of OG488 when cpTMV-S23C-S65pAF-OG488 was conjugated to AuNPs. Note that each cpTMV-S23C-S65pAF-OG488 assembly exhibited 34 aniline moieties and 34 OG488 dye molecules. Oxidative couplings were carried out with 0.2 μM (in capsid) TMV for both (C) and (D).

(Figure 8A). The choice of this coupling partner was two-fold. First, it allowed us to investigate noncanonical amino acid oxidative coupling in the context of AuNP bioconjugation. Second, it confirmed the compatibility of the AuNP oxidative coupling reaction with multivalent protein assemblies.

The coat protein of TMV is composed of 34 monomers and, once assembled, forms a disk-like structure (Figure S5) that mimics the morphology of some natural light harvesting complexes (LHCs).[51,52] Our lab has worked extensively with a circular permutant of TMV (cpTMV), which is stable under a wide variety of conditions and tolerant to mutations, unlike most naturally occurring LHCs.[52–54] In the past, we have installed chromophores at specific locations on genetically modified cpTMV coat proteins and used the resulting assemblies to explore how energy transfer efficiency is achieved in LHCs on a molecular level.[51] The overall goal of this work is to develop elements that can increase the efficiency of artificial light-harvesting systems. The tunability of the cpTMV-chromophore scaffold allows us to study the effects of small changes in the protein or chromophore on light harvesting and also allows site-specific, covalent attachment of energy donors or acceptors, such as AuNPs.

To enable participation in oxidative coupling, we used a variant of cpTMV (cpTMV-S65pAF) that exhibits an engineered p-amino-L-phenylalanine (pAF) residue on each of the 34 monomer proteins. The pAF residue was introduced using amber codon suppression.[53,55] We began with a protein concentration screen to determine the average number of cpTMV-S65pAF capsids that could be immobilized on each AuNP (Figure 8B). Reactions included 400 nM phenol-AuNPs and 0.1 to 0.5 μM cpTMV-S65pAF (based on protein disk concentration; 3.4 to 17 μM in monomer). Complete conjugation was observed at concentrations of 0.1 and 0.2 μM cpTMV-S65pAF. At higher concentrations, a small amount of cpTMV-S65pAF remained unconjugated. Complete conjugation of 0.2 μM cpTMV-S65pAF corresponded to an average loading of 0.5 cpTMV-S65pAF assemblies per AuNP. No cpTMV-S65pAF was conjugated in the absence of abTyr, absence of phenols, or when cpTMV lacked the engineered aniline residue (last lane in Figure 8B).

Because 0.2 μM cpTMV-S65pAF gave complete conjugation by agarose gel electrophoresis analysis, we used this sample for additional spectroscopic characterization. DLS again confirmed that coupling occurred only when abTyr and both coupling partners were included (Figure 8C). DLS also revealed an inconsistent increase in size when cpTMV-S65pAF was conjugated to phenol-AuNPs (bottom trace, Figure 8C). This variation in size was confirmed with TEM, which showed instances of both single phenol-AuNPs conjugated to cpTMV-S65pAF capsids and AuNP assemblies in which multiple AuNPs were linked together with cpTMV-S65pAF capsids (Figure 9). Because there are 34 aniline residues on each cpTMV-S65pAF capsid, multiple couplings on a single capsid are possible. The ability to make larger assemblies of cpTMV disks opens avenues for studying energy transfer between individual assemblies, which could lead to a better understanding of energy transfer between LHCs in nature.

Previously, our lab encapsulated AuNPs in spherical viral capsids and observed fluorescent enhancement of dyes immobilized on the surfaces of the capsids.[56] Building on this work, we next explored energy transfer interactions between AuNPs and dyes conjugated to the surface of cpTMV. Evidence of energy transfer (either via enhancement or quenching) in our cpTMV-AuNP system could lay the groundwork for developing hybrid systems with natural or synthetic chromophores that exhibit enhanced light harvesting.

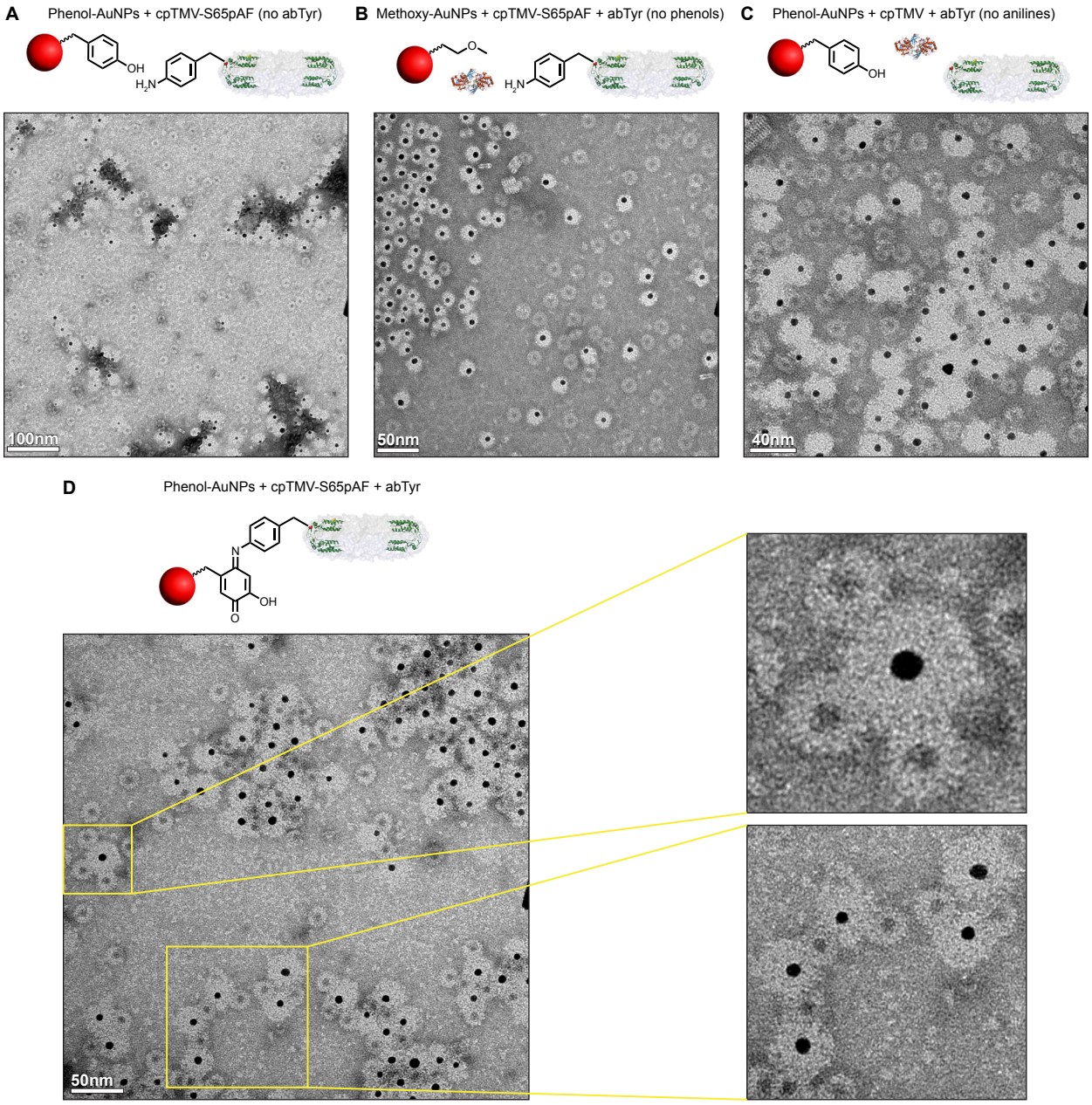

Figure 9. TEM analysis of cpTMV-AuNP conjugates. TEM suggested that no conjugation occurred in (A) the absence of tyrosinase (abTyr), (B) the absence of phenol groups, or (C) the absence of aniline-containing cpTMV. (D) cpTMV-AuNP conjugates were only formed when phenol-AuNPs, cpTMV-S65pAF, and tyrosinase were all present. Large arrays could be produced through multiple oxidative coupling reactions on a single cpTMV-S65pAF assembly.

Dye conjugation was enabled by employing a variant of cpTMV-S65pAF that exhibits a point mutation from serine to cysteine at position 23 (cpTMV-S23C-S65pAF), which is on the external surface of the disk (Figure S5). This cysteine was used to attach Oregon Green 488 maleimide to the TMV capsids (Figure S6A and S6B). The cpTMV-S23C-S65pAF-OG488 conjugate was then exposed to abTyr and phenol-AuNPs. Native agarose gel electrophoresis demonstrated successful conjugation and a possible quenching of the fluorophore relative to a negative control in which cpTMV-S23C-S65pAF was not conjugated to the AuNPs (Figure 8D). Quenching was confirmed by fluorescence

spectroscopy, which revealed a 33% decrease in fluorescence intensity. A similar result was obtained with a cpTMV-S65pAF variant exhibiting a point mutation from glutamine to cysteine at position 101 (cpTMV-S65pAF-Q101C, Figures S6C, S6D, and S7), which is within the internal cavity between the disks. These results confirm energy transfer between AuNPs and the fluorophores on cpTMV-S65pAF. We suspect that the extent of quenching or even enhancement of fluorescence can be tuned by adjusting the distance between AuNPs and cpTMV-S23C-S65pAF-OG488 (or cpTMV-S65pAF-Q101C-OG488). For LH2, maximum fluorescence enhancement from 5 nm AuNPs is observed at a distance of roughly 12.5 nm between LH2 and AuNPs.[10] By DLS, the PEG5k ligand increases the AuNP radius by ~6 nm. Thus, a longer linker for the phenol ligand may be required to observe a fluorescence enhancement or a reduction in quenching. In future studies, we will investigate the impact of linker length on energy transfer in our cpTMV-AuNP systems.

To begin exploring linker length, we synthesized a thiol-PEG10k-phenol ligand in a manner analogous to the thiol-PEG5K-phenol ligand. We then used the PEG10k ligand to generate phenol monolayer on AuNPs. DLS and gel electrophoresis confirmed monolayer formation, although, interestingly, the size and electrophoretic mobility were nearly identical to what was observed with the PEG5k ligand. The phenol-10k-AuNPs were then exposed to the oxidative coupling reaction with cpTMV-S65pAF and abTyr and were analyzed by gel electrophoresis (Figure S8). Conjugation was observed, but the extent of coupling was lower than observed for the phenol-5k-AuNPs. While we are unsure of the cause, it is possible that the longer linker caused the phenols to “sink” into the PEG layer, rendering the phenols less exposed and less amenable to oxidation by abTyr. Additionally characterization of the PEG10k ligand by NMR (Figure S13) suggested that coupling of tyramine to the PEG ligand did not proceed to completion, which may have also limited coupling efficiency during the oxidative coupling reaction.

3.3 Conclusion and Future Outlook

Herein we present, to our knowledge, the first method for constructing biomolecule-AuNP conjugates via direct enzymatic activation of AuNP surfaces. AuNPs are first functionalized with phenol monolayers, which stabilize the particles by preventing aggregation and blocking non-specific adsorption of biomolecules. Once desired, the functionalized AuNPs can be enzymatically activated, and a biomolecule or small molecule of choice can be tethered to the AuNPs within 2 h. The site-specific oxidative coupling strategy described here is compatible with both DNA and proteins containing a wide variety of functional handles, including accessible N-terminal proline, aniline, and thiol residues. This makes the approach a versatile, one-stop method for the quick and efficient construction of biomolecule-AuNP conjugates. Given the increasingly important role of biomolecule-AuNP conjugates in lateral flow assays, photothermal therapy, and drug delivery, this enzymatic oxidative coupling approach has the capacity to improve biomolecule-AuNP synthesis across a wide range of applications.

3.4 Materials and Methods

General methods and instrumentation

Unless noted otherwise, all reagents were obtained from commercial sources and used without further purification. Amine-PEG5k-valeric acid was purchased from Laysan Bio (Arab, AL). Amine-PEG10k-valeric acid was purchased from Creative Pegworks (Durham County, NC). Tyrosinase isolated from *Agaricus bisporus* (abTyr), aldolase isolated from rabbit muscle, glyceraldehyde-3-phosphate dehydrogenase from rabbit muscle (GAPDH), fructose 1,6-bisphosphate (FBP), all DNA sequences, bis(p-sulfonatophenyl)phenylphosphine dihydrate dipotassium salt (BSPP), poly(ethylene glycol) methyl ether thiol (average M_n = 2,000, thiol-PEG2k-methoxy), potassium cyanide (KCN), lipoic acid, aniline, tropolone, tyramine, and 4-(2-aminoethyl)aniline were purchased from Sigma-Aldrich (St. Louis, MO). Texas Red streptavidin conjugate, EZ-Link NHS-PEG4-biotin, Oregon Green 488 maleimide, and Quant-iT OliGreen ssDNA Assay Kit were purchased from Thermo Fisher (Waltham, MA). Unconjugated gold colloids (AuNPs, 5 nm) were purchased from Ted Pella, Inc. (Redding, CA). Pro-sfGFP[28] and sfGFP-Y200C[34] were expressed and purified as previously reported. NAD^+ and spin concentrators with 10 and 100 kDa molecular weight cutoffs (MWCO) were purchased from EMD Millipore (Billerica, MA). Doubly distilled water (ddH_2O) was obtained from a Millipore purification system.

UV-vis Spectroscopy. Concentrations of AuNP solutions were determined with a Thermo Scientific Nanodrop 1000.

Gel Analyses. Native agarose gel electrophoresis was carried out with 1% agarose gels and 1x TBE buffer. Prior to loading, samples were mixed with 50% glycerol in a ratio of 2:1 sample:50% glycerol. Gels were run at 60 V for either 60 or 90 min. Protein gels were stained with Coomassie Brilliant Blue. For imaging (both with and without stain), gels were placed on a white gel tray and imaged in a light box with an iPhone 8. Gels containing SYBR Safe stain (6 µL added to 60 mL gels) were imaged under UV light in a Bio-Rad Gel Doc EZ System.

Dynamic Light Scattering. DLS measurements were carried out with a Malvern Panalytical Zetasizer Nano ZS. Measurements were taken in triplicate at AuNP concentrations of 5–10 nM in ddH_2O or protein concentrations of 0.2–1.0 mg/mL in 10 mM sodium phosphate buffer, pH 7.2, at 25 °C.

Transmission Electron Microscopy. TEM analysis of cpTMV-AuNP conjugates and cpTMV mutants was carried out at the Berkeley Electron Microscopy Lab with an FEI Tecnai 12 transmission electron microscope with 100 kV accelerating voltage. Samples were prepared for analysis by applying analyte solution (5 µL of 150 nM cpTMV-AuNPs in 20 mM sodium phosphate buffer at pH 6.5 or 5 µL of 0.2–1 mg/mL cpTMV in 10 mM sodium phosphate buffer at pH 7.2) to carbon-coated copper grids for 2 min. For cpTMV-AuNPs, sample application was followed by rinsing in 3x10 µL of ddH_2O and then staining with 5 µL 1% aqueous uranyl acetate; samples were left in the stain for 1 min. For characteriza-

tion of cpTMV mutants, sample application was followed by rinsing in 4x10 µL droplets of 1% aqueous uranyl acetate; samples were left in the final droplet for 1 min.

Fluorometry. Fluorescence measurements were obtained with a Fluoromax-4 Spectrofluorometer (HORIBA Scientific). Samples were excited at 485 nm with a 5 nm window and emission was monitored from 500 to 700 nm.

NMR. ^{1}H spectra were recorded on either a Bruker AV-300 (300 MHz) or a Bruker AV-600 (600 MHz) spectrometer.

Electrospray Ionization Time of Flight Liquid Chromatography Mass Spectrometry (ESI-TOF LC-MS). Acetonitrile (Optima grade, 99.9%, Fisher, Waltham, MA), formic acid (1 mL ampules, 99+%, Pierce, Rockford, IL), and water purified to a resistivity of 18.2 MΩ·cm (at 25 °C) using a Milli-Q Gradient ultrapure water purification system (Millipore, Billerica, MA) were used to prepare mobile phase solvents for LC-MS. Electrospray ionization mass spectrometry (ESI-MS) of protein bioconjugates was performed using an Agilent 1260 series liquid chromatograph outfitted with an Agilent 6224 time-of-flight (TOF) LC-MS system (Santa Clara, CA). The LC was equipped with a Proswift RP-4H (monolithic phenyl, 1.0 mm × 50 mm, Dionex) analytical column. Solvent A was 99.9% water/0.1% formic acid and solvent B was 99.9% acetonitrile/0.1% formic acid (v/v). Each sample was prepared for analysis by desalting and spinning through an 0.22 µm cellulose acetate centrifugal spin filter, and then 8 µL of 10 µM protein was injected onto the column. Following sample injection, a 5–100% B elution gradient was run at a flow rate of 0.30 mL/min over 8 min. Data were collected and analyzed by deconvolution of the entire elution profile (using Agilent Mass Hunter Qualitative Analysis B.05.00) in order to provide reconstructed mass spectra that were representative of the entire sample. Spectra were analyzed with open source Chartograph software (www.chartograph.com).

High Performance Liquid Chromatography (HPLC). HPLC was performed on an Agilent 1100 Series HPLC System (Agilent, USA). Sample analysis for all HPLC experiments was achieved with an in-line diode array detector (DAD) and in-line fluorescence detector (FLD). Size exclusion chromatography (SEC) was performed using a Polysep-GFC-P-5000 column (4.6 x 250 mm) (Phenomenex, USA) at 1 mL/min using a mobile phase of 10 mM sodium phosphate buffer at pH 7.2.

Experimental procedures

Preparation of 5 nm BSPP-stabilized AuNPs.[37] Bis(p-sulfonatophenyl)phenylphosphine (BSPP) was dissolved to 4 mg/mL in ddH_2O. To every 1 mL of citrate-stabilized 5 nm AuNPs was added 100 µL of the BSPP solution. The solution was rotated end-over-end overnight at room temperature. The AuNPs were washed repeatedly with 1 mM aqueous BSPP in 30 kDa MWCO spin filters and concentrated 10-fold.

Preparation of phenol- and methoxy-AuNPs. A solution of concentrated 5 nm BSPP-stabilized AuNPs was diluted 10-fold with an aqueous solution of the phenol- or methoxy-PEG5k

ligand (see synthetic procedures and general methods) and ddH_2O, such that the final concentration of ligand was 1 mg/mL. The solution was rotated end-over-end overnight at room temperature. The AuNPs were washed with ddH_2O in 100 kDa MWCO spin filters, concentrated 10-fold, and stored at 4 °C until use.

DTNB capping of aldolase. 5,5-dithio-bis-(2-nitrobenzoic acid) (DTNB, 2 mM final concentration) was combined with aldolase (100 μM) in 50 mM phosphate buffer at pH 8. The reaction was incubated at room temperature for 15 min (a bright yellow color was observed). The solution was spin concentrated with 10 kDa MWCO spin filters and 10 mM phosphate buffer at pH 7.2 (4 spins total at 14,500 xg).

Oxidative coupling to prepare protein-AuNP conjugates. Phenol- or methoxy-AuNPs (400 nM final concentration, $\epsilon = 9.3x10^6\ M^{-1}cm^{-1}$) were combined with sfGFP-S200C, DTNB-capped aldolase, or pro-sfGFP (5 μM final concentration) and abTyr (200 nM final concentration) in 20 mM phosphate buffer at pH 6.5. The reaction was inverted end-over-end at room temperature for 2 h and then quenched with aniline and tropolone (5 mM and 1 mM final concentrations, respectively). Samples with sfGFP were spin concentrated with 100 kDa MWCO spin filters and ddH_2O (two spins total at 7,000 xg). For native agarose gel electrophoresis, gels were run for 60 min.

Immobilized aldolase activity assay. Phenol- or methoxy-AuNPs (400 nM final concentration, $\epsilon = 9.3x10^6\ M^{-1}cm^{-1}$) were combined with DTNB-capped aldolase (500 nM final concentration) and abTyr (200 nM final concentration) in 20 mM phosphate buffer at pH 6.5. The reactions were inverted end-over-end at room temperature for 2 h and then quenched with aniline and tropolone (5 mM and 1 mM final concentrations, respectively). The activity of immobilized aldolase versus soluble aldolase was based on a protocol previously published.[31] Briefly, aldolase-AuNPs (positive condition with phenol-AuNPs, DTNB-capped aldolase, and abTyr), phenol-AuNPs + DTNB-capped aldolase (negative control with no abTyr), methoxy-AuNPs + DTNB-capped aldolase + abTyr (negative control with no phenols), phenol-AuNPs + abTyr (negative control with no DTNB-capped aldolase), and methoxy-AuNPs (negative control with no phenols, DTNB-capped aldolase, or abTyr) were diluted (20 nM final concentration of aldolase for a 200 μL final volume) in assay buffer (20 mM phosphate buffer at pH 8.5). To this solution was added NAD^+ (1 mM final concentration for a 200 μL final volume) and GAPDH (1.35 μM final concentration for a 200 μL final volume). Just before absorbance measurements, FBP was added to a final concentration of 100 μM, bringing the total volume of each sample to 200 μL in a 96-well plate. Immediately after adding FBP, the absorbance at 340 nm was measured every 2 min for 5 h at 37 °C in a Tecan microplate reader. All samples were run in triplicate.

Preparation of streptavidin-biotin-AuNPs. Phenol- or methoxy-AuNPs (400 nM final concentration, $\epsilon = 9.3x10^6\ M^{-1}cm^{-1}$) were combined with biotin-PEG4-aniline (0.5, 1, 5, or 10 μM final concentration), and abTyr (200 nM final concentration) in 20 mM phosphate buffer at pH 6.5. The reaction was inverted end-over-end at room temperature for 2 h and then quenched with aniline and tropolone (5 mM and 1 mM final concentrations, respectively). Samples were spin concentrated with 100 kDa MWCO spin filters and ddH_2O

(two spins total at 14,500 xg). Streptavidin (5 μM final concentration) was added, and the mixture was shaken at 37 °C for 1 h and then incubated at 4 °C overnight.

Reduction of thiol-DNA for conjugation to AuNPs. Thiol-DNA of the following sequence was used for all primary conjugation of DNA to AuNPs: [ThiC6]CCCTAGAGTGAGTCG-TATGA. Before use, the DNA was reduced in ddH_2O with TCEP (2 eq) for 2.5 h at room temperature. The reduced DNA was purified with a NAP-5 column and then lyophilized overnight.

Oxidative coupling to prepare DNA-AuNP conjugates. Phenol- or methoxy-AuNPs (400 nM final concentration, $\epsilon = 9.3x10^6\ M^{-1}cm^{-1}$) were combined with reduced thiol-DNA (4, 20, 40, 60, or 80 μM final concentration), and abTyr (200 nM final concentration) in 20 mM phosphate buffer at pH 6.5. The reaction was inverted end-over-end at room temperature for 2 h and then quenched with aniline and tropolone (5 mM and 1 mM final concentrations, respectively). For native agarose gel electrophoresis, gels were run for 90 min. For DLS analysis, samples were first spin concentrated with 100 kDa MWCO spin filters and ddH_2O (two spins total at 14,500 xg). For experiments with 40 nM AuNPs, final thiol-DNA concentrations were 0.4, 2, or 8 μM. These lower concentration experiments were concentrated with spin filters prior to analysis. For samples (both 40 nM and 400 nM) prepared for DNA quantification: After quenching, NaCl was added to a final concentration of 300 mM and samples were incubated end-over-end at room temperature for 30 min (to minimize background adsorption of DNA). Samples were then spin concentrated with 100 kDa MWCO spin filters and ddH_2O x1, 5 mM HEPES at pH 7.7 with 150 mM NaCl x2, and ddH_2O x1 (all at 14,500 xg).

DNA hybridization. DNA of the following palindromic complementary sequence was used for hybridization to DNA-AuNPs: GGGATCTCACTCAGCATACTTCATACGACT-CACTCTAGGG
The above complementary DNA sequence was added to DNA-AuNPs at 10x the concentration of thiol-DNA used for preparation of the DNA-AuNPs (e.g. 200 μM of the complementary stand was used for DNA-AuNPs that were prepared with 20 μM DNA). The samples were heated to 70 °C for 10 min and then allowed to sit at room temperature overnight before analysis by DLS.

DNA quantification. After preparing samples as described above, KCN (35 mM final concentration) was added to an aliquot of each sample and incubated overnight to dissolve the AuNPs. DNA released into solution was quantified with an OliGreen ssDNA Assay Kit (carried out in a 96-well plate format with triplicate measurements). The following DNA sequence was used to prepare the standard curve: CCCTAGAGTGAGTCGTATGA
To obtain the DNA/AuNP ratio, the concentration of DNA determined by the quantification kit was divided by the concentration (as determined by UV-vis) of the purified DNA-AuNPs.

Oxidative coupling to prepare cpTMV-AuNP conjugates. Phenol- or methoxy-AuNPs (400 nM final concentration, $\epsilon = 9.3x10^6\ M^{-1}cm^{-1}$) were combined with cpTMV-S23C-S65pAF,

cpTMV, or cpTMV-S23C-S65pAF-OG488 (0.1, 0.2, 0.3, 0.4, or 0.5 μM final capsid concentration), and abTyr (200 nM final concentration) in 20 mM phosphate buffer at pH 6.5. The reaction proceeded end-over-end at room temperature for 2 h and then was quenched with aniline and tropolone (5 mM and 1 mM final concentrations, respectively). For native agarose gel electrophoresis, gels were run for 60 min. cpTMV-AuNP conjugates were not purified prior to analysis by gel electrophoresis, DLS, or TEM.

Preparation of cpTMV-S23C-S65pAF-OG488 and cpTMV-S65pAF-Q101C-OG488. cpTMV-S23C-S65pAF (25 μM monomer) was combined with Oregon Green 488 maleimide (250 μM, 10 eq) in 40 mM phosphate buffer at pH 7. The reaction proceeded at 4 °C overnight. Excess dye was removed through spin concentration with 10 kDa MWCO spin filters. Successful conjugation was confirmed with ESI-TOF LC-MS. This procedure was repeated with cpTMV-S65pAF-Q101C.

Preparation of cpTMV-AuNP conjugates for TEM. cpTMV-AuNP conjugates for TEM analysis were generated with 1.5 μM phenol- or methoxy-AuNPs and 0.75 μM cpTMV-S65pAF or cpTMV. All other conditions were the same as previously described.

Expression and purification of cpTMV mutants

Construction of cpTMV expression plasmids

pDule-para-aminoPhe (Addgene #85502)[53] and pBad-sfGFP 150TAG (Addgene #85483)[54] plasmids were gifts from Ryan Mehl.

The gene of the circular permutant of TMV (cpTMV) was produced using standard molecular biology techniques based on a gene for the coat protein of the TMV U1 strain optimized for the codon usage of *E. coli* (Genscript, Piscataway, NJ) as reported by Dedeo *et al*.[52] The S23C and Q101C mutations were made as previously reported.[53] The cpTMV gene was inserted into a pBad/myc-His A vector (pBad-sfGFP 150TAG) using a Gibson Assembly kit (New England Biotechnology, Ipswich, MA). Site-directed mutagenesis was performed using a PfuUltra II Fusion HS DNA Polymerase kit (Agilent, Santa Clara, CA). The following sets of primers were used for these mutations, where * represents the amber codon TAG:

Excision of pBad/myc-His A entry vector from pBad-sfGFP 150TAG:
Sense: 5’ TAAAGCTCGAGATCTGCAGCT 3’
Antisense: 5’ CATGGTTAATTCCTCCTGTTAGC 3’

Insertion of cpTMV into pBad/myc-His A entry vector:
Sense: 5’ GCTAACAGGAGGAATTAACCATGGGCGCCAATCCGACCA 3’
Antisense: 5’ AGCTGCAGATCTCGAGCTTTACTGGTTTTCCACTTCAATGATAC 3’

S65*:
Sense: 5’ GGGCGAAGGCAGCTATTAGATTACCACCCCGAGCC 3’

Antisense: 5’ GGGGTGGTAATCTAATAGCTGCCTTCGCCCGCC 3’

Protein expression and purification

The following conditions and general procedure for the production of p-amino-L-phenylalanine (pAF)-containing proteins are adapted from a previously published protocol,[55] with minimal modifications. The pBAD-cpTMV-S65*, pBAD-cpTMV-S23C-S65* or pBAD-cpTMV-S65*-Q101C vectors with pDule-pAF were co-transformed into DH10B *E. coli* cells and plated on LB agar plates containing 50 µg/mL ampicillin and 12.5 µg/mL tetracycline. The resulting colonies were grown overnight in 10 mL of LB containing 50 µg/mL ampicillin and 12.5 µg/mL tetracycline at 37 °C and then added to 1 L of arabinose media (recipe below). The 1 L culture was allowed to shake at 37 °C, 220 rpm, until it reached an OD_{600} of 0.6–0.8. Then, 10 mL of a 100 mM solution of pAF in ddH_2O was added to the growth medium to a final concentration of 1 mM (instructions for preparation of this solution are below). The culture was incubated at 37 °C, 220 rpm, for an additional 18 h. Cell pellets were collected at 8,000 rpm for 30 min, after which the supernatant was discarded, and the cell pellets were frozen at -20 °C until purification.

The purification of cpTMV proteins is based on a previously reported procedure[55] with minimal modifications. After freezing, cell pellets were partially thawed and resuspended in 10 mL lysis buffer with 20 mM triethanolamine (TEA) at pH 7.2. Cells were lysed by sonication with a 2 s on, 4 s off cycle for a total of 10 min using a standard disruptor horn at 60% amplitude (Branson Ultrasonics, Danbury, CT). The resulting lysate was cleared at 14,000 rpm for 30 min. The supernatant was treated with 30 to 40% volume (3 to 4 mL) of saturated ammonium sulfate and allowed to rotate for 10 min at 4 °C to allow for complete protein precipitation. The precipitated protein was collected at 11,000 rpm for 30 min and resuspended in 10 mL of lysis buffer. Complete dissolution of the protein and removal of the residual ammonium sulfate was accomplished by performing dialysis in 1 L of lysis buffer overnight with at least one buffer exchange. The resulting protein solution was treated with 5 µL benzonase nuclease (Millipore, Madison, WI) and 4 mg $MgCl_2$ at room temperature for 30 min before the solution was centrifuged at 10,000 rpm for 10 min. The resulting supernatant was filtered through a 0.22 µm filter and purified using a diethylaminoethanol (DEAE) Sepharose column with a 0 to 300 mM NaCl gradient elution in 20 mM TEA buffer at pH 7.2. The fractions containing cpTMV were further purified using a Sephacryl S-500 column in 10 mM sodium phosphate at pH 7.2 elution buffer. Pure fractions were collected and concentrated using Amicon Ultra 100 kDa MWCO centrifugal concentrators. Purity was confirmed by SDS-PAGE and ESI-TOF LC-MS (Figure S9). The assembly state was confirmed by HPLC-SEC, DLS, and TEM (Figure S10). The assembly state was compared to a protein of known structure, cpTMV-S23C.[52] Protein was flash frozen and stored indefinitely at -80 °C or stored for no longer than 2 weeks at 4 °C without observed decomposition or change in assembly state.

<u>Arabinose media (1 L, H_2O)</u>
40 mL 25x M salts (1.25 M Na_2HPO_4, 1.25 M KH_2PO_4, 2.5 M NH_4Cl, 0.25 M Na_2SO_4; autoclaved)

2 mL 1 M $MgSO_4$ (autoclaved)
40 mL 5% (w/v) L-aspartate pH 7.5 (autoclaved)
20 ml 4 mg/mL L-leucine pH 7.5 (autoclaved)
2.4 mL 20% glucose (autoclaved)
853 mL ddH_2O (autoclaved)
40 mL 18 amino acid solution at pH 7 (5 mg/mL of every natural L-amino acid, excluding tyrosine and cysteine; sterile filtered)
1 mL 1,000x heavy metal stock solution (sterile filtered)
1.25 mL 20% arabinose (sterile filtered)
12.5 mg tetracycline
50 mg ampicillin

1,000x heavy metal stock solution (1 L, 1 M HCl)
500 mg $MoNa_2O_2 \cdot 2H_2O$
250 mg $CoCl_2$
175 mg $CuSO_4 \cdot 5H_2O$
1 g $MnSO_4 \cdot H_2O$
8.75 g $MgSO_4 \cdot 7H_2O$
1.25 g $ZnSO_4 \cdot 7H_2O$
1.25 g $FeCl_2 \cdot 4H_2O$
2.5 g $CaCl_2 \cdot 2H_2O$
1 g H_3BO_3

Solutions containing noncanonical amino acids were prepared no more than 1 h prior to addition to cell culture. pAF was dissolved in 8 mL ddH_2O and adjusted to pH 7 using 2 M NaOH before the final solution volume was brought to 10 mL using ddH_2O. The solution was then stored at 4 °C until use.

DLS-determined particle diameters of cpTMV mutants (see Figure S9 and Figure S10 for additional characterization)

Sample Name	Intensity Mean (nm)	PDI Mean
cpTMV-S23C	20.7 ± 0.3	0.17 ± 0.02
cpTMV-S65pAF	19.0 ± 0.4	0.12 ± 0.01
cpTMV-S23C-S65pAF	20.4 ± 0.3	0.15 ± 0.01
cpTMV-S65pAF-Q101C	20.3 ± 0.3	0.22 ± 0.01

Synthetic procedures

Synthesis of lipoic acid-NHS (based on a previously reported procedure[35]). Lipoic acid (406 mg, 1 eq) and *N*-hydroxysuccinimide (NHS) (230 mg, 1 eq) were dissolved in 4 mL of dry DCM. Separately, *N,N'*-dicyclohexylcarbodiimide (DCC) (413 mg, 0.94 eq) was dissolved in 3 mL of dry DCM. The lipoic acid solution was added dropwise to the DCC solution, and the mixture was stirred on ice for 1 h. The reaction was then stirred at 4 °C

for 1 h, after which the stirring was stopped, and the mixture was left overnight at 4 °C. The next morning, the mixture was placed in a -20 °C freezer for 30 min. The solution was then filtered with a Buchner funnel, and the collected solid was washed with two 3 mL portions of DCM that were pre-cooled to -20 °C. The filtrate was collected and subjected to rotary evaporation. The resulting pale-yellow solid was confirmed by ^{1}H NMR in $CDCl_3$ (see Figure S11).

Synthesis of lipoamide-PEG5k-valeric acid (based on a previously reported procedure[35]). Amine-PEG5k-valeric acid (100 mg, 1 eq) and lipoic acid-NHS (30 mg, 5 eq) were dissolved in 0.5 mL of dry DCM in a 4 mL vial. Triethylamine (27 µL, 10 eq) was added, and the reaction was stirred overnight at room temperature. The next morning, the reaction was concentrated under a gentle stream of nitrogen, and then 1 mL of ddH_2O was added. The mixture was filtered through a 0.22 µm cellulose-acetate spin filter. To remove small molecules, the filtrate was repeatedly spin concentrated with ddH_2O in a 3 kDa MWCO spin filter. The resulting product was lyophilized to afford a white solid product.

Synthesis of thiol-PEG5k-phenol. Lipoamide-PEG5k-valeric acid (30 mg, 1 eq), DCC (12.3 mg, 10 eq), and NHS (6.9 mg, 10 eq) were dissolved in 1 mL of dry DCM in a 4 mL vial and stirred for 1 h at room temperature. Tyramine (8.25 mg, 10 eq) was added, and the reaction was stirred overnight at room temperature. The next morning, the reaction was concentrated under a gentle stream of nitrogen, and then 1 mL of ddH_2O was added. The mixture was filtered through a 0.22 µm cellulose-acetate spin filter. To remove small molecules, the filtrate was repeatedly spin concentrated with ddH_2O in a 3 kDa MWCO spin filter. The resulting product was lyophilized to afford a white solid product that was confirmed by ^{1}H NMR in $CDCl_3$ (see Figure S12).

Synthesis of lipoamide-PEG10k-valeric acid and thiol-PEG10k-phenol. Synthesis was carried out analogous as to what is described above for the 5k ligand. However, amine-PEG10k-valeric acid was used instead of amine-PEG5k-valeric acid during synthesis of lipoamide-PEG10k-valeric acid. Additionally, DIPEA (10 eq) was included when reacting NHS-activated valeric acid-PEG10k-lipoamide and tyramine. The final product was confirmed by ^{1}H NMR in $CDCl_3$ (see Figure S13).

Synthesis of biotin-PEG4-aniline. EZ-Link NHS-PEG4-biotin (44 mM, 1.1 eq) was combined with 4-(2-aminoethyl)aniline (1 eq) in DMF. The mixture was rotated end-over-end overnight at room temperature. Formation of the product was confirmed with LC-MS. The solution was diluted to a concentration of 4.5 mM prior to use. QTOF-MS: m/z for $C_{28}H_{47}N_5O_7S$ $[M+H]^+$ 610.3, observed 610.3.

3.5 References

1) Graczyk, A.; Pawlowska, R.; Jedrzejczyk, D.; Chworos, A. Gold Nanoparticles in Conjunction with Nucleic Acids as a Modern Molecular System for Cellular Delivery. *Molecules* **2020**, *25* (1), 204.

(2) Haniti Mohd-Zahid, M.; Mohamud, R.; Abdullah, C. A. C.; Lim, J.; Alem, H.; Hanaffi,

W. N. W.; A, I. Z. Colorectal Cancer Stem Cells: A Review of Targeted Drug Delivery by Gold Nanoparticles. *RSC Adv*. **2020**, *10* (2), 973–985.
(3) Emami, F.; Banstola, A.; Vatanara, A.; Lee, S.; Kim, J. O.; Jeong, J.-H.; Yook, S. Doxorubicin and Anti-PD-L1 Antibody Conjugated Gold Nanoparticles for Colorectal Cancer Photochemotherapy. *Mol. Pharm*. **2019**, *16* (3), 1184–1199.
(4) Wang, R.; Kim, K.; Choi, N.; Wang, X.; Lee, J.; Jeon, J. H.; Rhie, G.; Choo, J. Highly Sensitive Detection of High-Risk Bacterial Pathogens Using SERS-Based Lateral Flow Assay Strips. *Sens. Actuators B Chem.* **2018**, *270*, 72–79.
(5) Kim, D. S.; Kim, Y. T.; Hong, S. B.; Kim, J.; Heo, N. S.; Lee, M.-K.; Lee, S. J.; Kim, B. I.; Kim, I. S.; Huh, Y. S.; Choi, B. G. Development of Lateral Flow Assay Based on Size-Controlled Gold Nanoparticles for Detection of Hepatitis B Surface Antigen. *Sensors (Basel)* **2016**, *16* (12), 2154.
(6) Wang, W.; Liu, L.; Song, S.; Xu, L.; Kuang, H.; Zhu, J.; Xu, C. Identification and Quantification of Eight Listeria Monocytogene Serotypes from Listeria Spp. Using a Gold Nanoparticle-Based Lateral Flow Assay. *Microchim. Acta* **2017**, *184* (3), 715–724.
(7) Jauset-Rubio, M.; Svobodová, M.; Mairal, T.; McNeil, C.; Keegan, N.; Saeed, A.; Abbas, M. N.; El-Shahawi, M. S.; Bashammakh, A. S.; Alyoubi, A. O.; O´Sullivan, C. K. Ultra-sensitive, Rapid and Inexpensive Detection of DNA Using Paper Based Lateral Flow Assay. *Sci. Rep.* **2016**, *6* (1), 37732.
(8) Javani, A.; Javadi-Zarnaghi, F.; Rasaee, M. J. Development of a Colorimetric Nucleic Acid-Based Lateral Flow Assay with Non-Biotinylated Capture DNA. *Appl. Biol. Chem*. **2017**, *60* (6), 637–645.
(9) Acuna, G. P.; Bucher, M.; Stein, I. H.; Steinhauer, C.; Kuzyk, A.; Holzmeister, P.; Schreiber, R.; Moroz, A.; Stefani, F. D.; Liedl, T.; Simmel, F. C.; Tinnefeld, P. Distance Dependence of Single-Fluorophore Quenching by Gold Nanoparticles Studied on DNA Origami. *ACS Nano* **2012**, *6* (4), 3189–3195.
(10) Bujak, L.; Brotosudarmo, T. H. P.; Czechowski, N.; Olejnik, M.; Ciszak, K.; Litvin, R.; Cogdell, R. J.; Heiss, W.; Mackowski, S. Spectral Dependence of Fluorescence Enhancement in LH2-Au Nanoparticle Hybrid Nanostructures. *Acta Phys. Pol. A* **2012**, *122* (2), 252–254.
(11) Liu, B.; Liu, J. Freezing Directed Construction of Bio/Nano Interfaces: Reagentless Conjugation, Denser Spherical Nucleic Acids, and Better Nanoflares. *J. Am. Chem. Soc.* **2017**, *139* (28), 9471–9474.
(12) Petryayeva, E.; Krull, U. Localized Surface Plasmon Resonance: Nanostructures, Bioassays, and Biosensing–A Review. *Anal. Chim. Acta* **2011**, *706* (1), 8–24.
(13) Kozlowski, R.; Ragupathi, A.; Dyer, R. B. Characterizing the Surface Coverage of Protein-Gold Nanoparticle Bioconjugates. *Bioconjugate Chem*. **2018**, *29* (8), 2691–2700.
(14) Liu, S.; Lämmerhofer, M. Functionalized Gold Nanopar-ticles for Sample Preparation: A Review. *Electrophoresis* **2019**, *40*, 2438–2461.
(15) Busch, R. T.; Karim, F.; Weis, J.; Sun, Y.; Zhao, C.; Vasquez, E. S. Optimization and Structural Stability of Gold Nanoparticle–Antibody Bioconjugates. *ACS Omega* **2019**, *4* (12), 15269–15279.
(16) Chirra, H. D.; Sexton, T.; Biswal, D.; Hersh, L. B.; Hilt, J. Z. Catalase Coupled Gold

Nanoparticles: Comparison between Carbodiimide and Biotin-Streptavidin Methods. *Acta Biomater.* **2011**, *7* (7), 2865–2872.
(17) Hurst, S. J.; Lytton-Jean, A. K. R.; Mirkin, C. A. Maximizing DNA Loading on a Range of Gold Nanoparticle Sizes. *Anal. Chem*. **2006**, *78* (24), 8313–8318.
(18) Park, S. Y.; Lytton-Jean, A. K. R.; Lee, B.; Weigand, S.; Schatz, G. C.; Mirkin, C. A. DNA-Programmable Nanoparticle Crystallization. *Nature* **2008**, *451* (7178), 553–556.
(19) Zhang, X.; Servos, M. R.; Liu, J. Instantaneous and Quantitative Functionalization of Gold Nanoparticles with Thiolated DNA Using a pH-Assisted and Surfactant-Free Route. *J. Am. Chem. Soc.* **2012**, *134* (17), 7266–7269.
(20) Liu, B.; Liu, J. Freezing-Driven DNA Adsorption on Gold Nanoparticles: Tolerating Extremely Low Salt Concentration but Requiring High DNA Concentration. *Langmuir* **2019**, *35* (19), 6476–6482.
(21) Yao, G.; Pei, H.; Li, J.; Zhao, Y.; Zhu, D.; Zhang, Y.; Lin, Y.; Huang, Q.; Fan, C. Clicking DNA to Gold Nanoparticles: Poly-Adenine-Mediated Formation of Monovalent DNA-Gold Nanoparticle Conjugates with Nearly Quantitative Yield. *NPG Asia Mater.* **2015**, *7* (1), e159–e159.
(22) Li, Z.; Jin, R.; Mirkin, C. A.; Letsinger, R. L. Multiple Thiol-Anchor Capped DNA–Gold Nanoparticle Conjugates. *Nucleic Acids Res*. **2002**, *30* (7), 1558–1562.
(23) Kanaras, A. G.; Wang, Z.; Hussain, I.; Brust, M.; Cosstick, R.; Bates, A. D. Site-Specific Ligation of DNA-Modified Gold Nanoparticles Activated by the Restriction Enzyme StyI. *Small* **2007**, *3* (1), 67–70.
(24) Weldemhret, T. G.; Nisola, G. M.; Ramos, K. R. M.; Ba-ñares, A. B.; Valdehuesa, K. N. G.; Lee, W.-K.; Chung, W.-J. Tyrosinase-Catalyzed Phenol-Mediated Immobilization of β-Agarase on l-Lysine-Coated Magnetic Particles for the Production of Neoagarooligosaccharides from Gelidium Amansii. *ACS Sustain*. *Chem. Eng*. **2020**, *8* (9), 3573–3582.
(25) ElSohly, A. M.; Francis, M. B. Development of Oxidative Coupling Strategies for Site-Selective Protein Modification. *Acc. Chem. Res*. **2015**, *48* (7), 1971–1978.
(26) Hooker, J. M.; Esser-Kahn, A. P.; Francis, M. B. Modification of Aniline Containing Proteins Using an Oxidative Coupling Strategy. *J. Am. Chem. Soc*. **2006**, *128* (49), 15558–15559.
(27) Behrens, C. R.; Hooker, J. M.; Obermeyer, A. C.; Romanini, D. W.; Katz, E. M.; Francis, M. B. Rapid Chemoselective Bioconjugation through Oxidative Coupling of Anilines and Aminophenols. *J. Am. Chem. Soc*. **2011**, *133* (41), 16398–16401.
(28) Obermeyer, A. C.; Jarman, J. B.; Netirojjanakul, C.; El Muslemany, K.; Francis, M. B. Mild Bioconjugation Through the Oxidative Coupling of *Ortho*-Aminophenols and Anilines with Ferricyanide. *Angew. Chem. Int. Ed*. **2014**, *53* (4), 1057–1061.
(29) Obermeyer, A. C.; Jarman, J. B.; Francis, M. B. N-Terminal Modification of Proteins with *o*-Aminophenols. *J. Am. Chem. Soc*. **2014**, *136* (27), 9572–9579.
(30) ElSohly, A. M.; MacDonald, J. I.; Hentzen, N. B.; Aanei, I. L.; El Muslemany, K. M.; Francis, M. B. *Ortho*-Methoxyphenols as Convenient Oxidative Bioconjugation Reagents with Application to Site-Selective Heterobifunctional Cross-Linkers. *J. Am. Chem. Soc*. **2017**, *139* (10), 3767–3773.
(31) Palla, K. S.; Hurlburt, T. J.; Buyanin, A. M.; Somorjai, G. A.; Francis, M. B. Site-Se-

lective Oxidative Coupling Reactions for the Attachment of Enzymes to Glass Surfaces through DNA-Directed Immobilization. *J. Am. Chem. Soc*. **2017**, *139* (5), 1967–1974.
(32) Furst, A. L.; Smith, M. J.; Lee, M. C.; Francis, M. B. DNA Hybridization to Interface Current-Producing Cells with Electrode Surfaces. *ACS Cent. Sci*. **2018**, *4* (7), 880–884.
(33) Maza, J. C.; Bader, D. L. V.; Xiao, L.; Marmelstein, A. M.; Brauer, D. D.; ElSohly, A. M.; Smith, M. J.; Krska, S. W.; Parish, C. A.; Francis, M. B. Enzymatic Modification of N-Terminal Proline Residues Using Phenol Derivatives. *J. Am. Chem. Soc*. **2019**, *141* (9), 3885–3892.
(34) Lobba, M. J.; Fellmann, C.; Marmelstein, A. M.; Maza, J. C.; Kissman, E. N.; Robinson, S. A.; Staahl, B. T.; Urnes, C.; Lew, R. J.; Mogilevsky, C. S.; Doudna, J. A.; Francis, M. B. Site-Specific Bioconjugation through Enzyme-Catalyzed Tyrosine–Cysteine Bond Formation. *ACS Cent. Sci.* **2020**, *6* (9), 1564–1571.
(35) Marmelstein, A. M.; Lobba, M. J.; Mogilevsky, C. S.; Maza, J. C.; Brauer, D. D.; Francis, M. B. Tyrosinase-Mediated Oxidative Coupling of Tyrosine Tags on Peptides and Proteins. *J. Am. Chem. Soc.* **2020**, *142* (11), 5078–5086.
(36) Capehart, S. L.; ElSohly, A. M.; Obermeyer, A. C.; Francis, M. B. Bioconjugation of Gold Nanoparticles through the Oxidative Coupling of *Ortho*-Aminophenols and Anilines. *Bioconjugate Chem.* **2014**, *25* (10), 1888–1892.
(37) Liu, A.; Verwegen, M.; de Ruiter, M. V.; Maassen, S. J.; Traulsen, C. H.-H.; Cornelissen, J. J. L. M. Protein Cages as Containers for Gold Nanoparticles. *J. Phys. Chem. B* **2016**, *120* (26), 6352–6357.
(38) Pédelacq, J.-D.; Cabantous, S.; Tran, T.; Terwilliger, T. C.; Waldo, G. S. Engineering and Characterization of a Superfolder Green Fluorescent Protein. *Nature Biotech.* **2006**, *24* (1), 79–88.
(39) Männel, M. J.; Kreuzer, L. P.; Goldhahn, C.; Schubert, J.; Hartl, M. J.; Chanana, M. Catalytically Active Protein Coatings: Toward Enzymatic Cascade Reactions at the Intercolloidal Level. *ACS Catal.* **2017**, *7* (3), 1664–1672.
(40) Pandey, P.; Singh, S. P.; Arya, S. K.; Gupta, V.; Datta, M.; Singh, S.; Malhotra, B. D. Application of Thiolated Gold Nanoparticles for the Enhancement of Glucose Oxidase Activity. *Langmuir* **2007**, *23* (6), 3333–3337.
(41) Petkova, G. A.; Záruba, K.; Žvátora, P.; Král, V. Gold and Silver Nanoparticles for Biomolecule Immobilization and Enzymatic Catalysis. *Nanoscale Res. Lett.* **2012**, *7* (1), 287.
(42) Graczyk, A.; Pawlowska, R.; Jedrzejczyk, D.; Chworos, A. Gold Nanoparticles in Conjunction with Nucleic Acids as a Modern Molecular System for Cellular Delivery. *Molecules* **2020**, *25* (1), 204.
(43) Xu, X.; Rosi, N. L.; Wang, Y.; Huo, F.; Mirkin, C. A. Asymmetric Functionalization of Gold Nanoparticles with Oligonucleotides. *J. Am. Chem. Soc*. **2006**, *128* (29), 9286–9287.
(44) Hill, H. D.; Millstone, J. E.; Banholzer, M. J.; Mirkin, C. A. The Role Radius of Curvature Plays in Thiolated Oligonucleotide Loading on Gold Nanoparticles. *ACS Nano* **2009**, *3* (2), 418–424.
(45) Cutler, J. I.; Auyeung, E.; Mirkin, C. A. Spherical Nucleic Acids. *J. Am. Chem. Soc.*

2012, *134* (3), 1376–1391.
(46) Li, H.; Zhang, B.; Lu, X.; Tan, X.; Jia, F.; Xiao, Y.; Cheng, Z.; Li, Y.; Silva, D. O.; Schrekker, H. S.; Zhang, K.; Mirkin, C. A. Molecular Spherical Nucleic Acids. *PNAS* **2018**, *115* (17), 4340–4344.
(47) Claridge, S. A.; Liang, H. W.; Basu, S. R.; Fréchet, J. M. J.; Alivisatos, A. P. Isolation of Discrete Nanoparticle−DNA Conjugates for Plasmonic Applications. *Nano Lett*. **2008**, *8* (4), 1202–1206.
(48) Goodman, C. M.; Chari, N. S.; Han, G.; Hong, R.; Ghosh, P.; Rotello, V. M. DNA-Binding by Functionalized Gold Nanoparticles: Mechanism and Structural Requirements. *Chem. Biol. Drug Des.* **2006**, *67*, 297–304.
(49) Liu, B.; Liu, J. Methods for Preparing DNA-Functionalized Gold Nanoparticles, a Key Reagent of Bioanalytical Chemistry. *Anal. Methods* **2017**, *9* (18), 2633–2643.
(50) Pellegrino, T.; Sperling, R. A.; Alivisatos, A. P.; Parak, W. J. Gel Electrophoresis of Gold-DNA Nanoconjugates. *J. Biomed. Biotechnol.* (Hindawi Publishing Corporation). **2007**, Article ID 26796.
(51) Delor, M.; Dai, J.; Roberts, T. D.; Rogers, J. R.; Hamed, S. M.; Neaton, J. B.; Geissler, P. L.; Francis, M. B.; Ginsberg, N. S. Exploiting Chromophore–Protein Interactions through Linker Engineering to Tune Photoinduced Dynamics in a Biomimetic Light-Harvesting Platform. *J. Am. Chem. Soc*. **2018**, *140* (20), 6278–6287.
(52) Dedeo, M. T.; Duderstadt, K. E.; Berger, J. M.; Francis, M. B. Nanoscale Protein Assemblies from a Circular Permutant of the Tobacco Mosaic Virus. *Nano Lett*. **2010**, *10* (1), 181–186.
(53) Mehl, R. A.; Anderson, J. C.; Santoro, S. W.; Wang, L.; Martin, A. B.; King, D. S.; Horn, D. M.; Schultz, P. G. Generation of a Bacterium with a 21 Amino Acid Genetic Code. *J. Am. Chem. Soc*. **2003**, *125*, 935–939.
(54) Miyake-Stoner, S. J.; Refakis, C. A.; Hammill, J. T.; Lusic, H.; Hazen, J. L.; Deiters, A.; Mehl, R. A. Generating permissive site-specific unnatural aminoacyl-tRNA synthetases. *Biochemistr*y **2010**, *49*, 1667–1677.
(55) Hammill, J. T.; Miyake-Stoner, S.; Hazen, J. L.; Jackson, J. C.; Mehl, R. A. Preparation of site-specifically labeled fluorinated proteins for ^{19}F-NMR structural characterization. *Nat. Protoc*. **2007**, *2*, 2601–2607.
(56) Capehart, S. L.; Coyle, M. P.; Glasgow, J. E.; Francis, M. B. Controlled Integration of Gold Nanoparticles and Organic Fluorophores Using Synthetically Modified MS2 Viral Capsids. *J. Am. Chem. Soc*. **2013**, *135* (8), 3011–3016.

3.6 Supplementary Figures

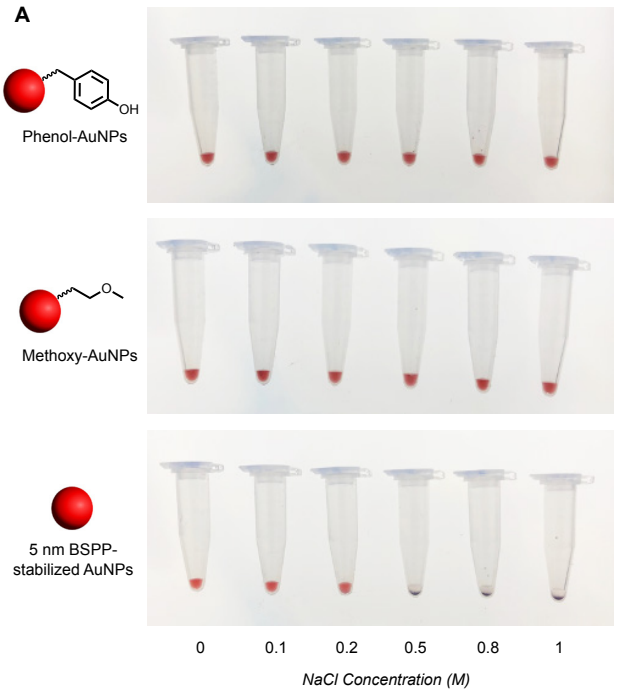

Figure S1. Characterization of phenol- and methoxy-AuNPs via a salt stability screen and electrophoresis. (A) Overnight incubation of AuNPs with various salt concentrations demonstrated that both methoxy and phenol monolayers prevented AuNPs from aggregating in the presence of high salt concentrations. In contrast, AuNPs that were stabilized only with BSPP aggregated as salt concentrations approached 0.5 M. (B) Native agarose gel elecetrophoresis demonstrated significant changes in electrophoretic mobility upon monolayer formation.

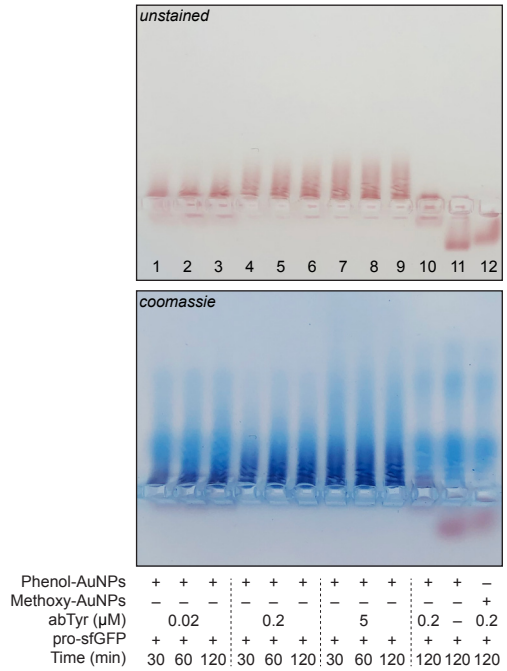

Figure S2. Screen of oxidative coupling reaction times and tyrosinase concentrations. Oxidative coupling reactions were used to conjugate pro-sfGFP to phenol-AuNPs with different reaction times and concentrations of tyrosinase (abTyr). Reactions were run with 5 μM pro-sfGFP and 400 nM phenol- or methoxy-AuNPs and were quenched with 5 mM aniline and 1 mM troplone. The sample in lane 10 was a negative control in which aniline was added at the same time as pro-sfGFP. As expected, the aniline reacted faster than pro-sfGFP, and no protein coupling was observed. The shift in AuNP mobility for this sample was due to oxidation of the surface phenols.

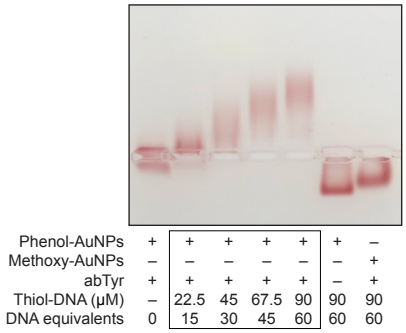

Figure S3. Concentration screen with lower concentrations of DNA. Thiol-DNA of various concentrations was reacted with phenol-AuNPs (1.5 μM) and tyrosinase (abTyr, 200 nM). Despite shifts in mobility, DLS revealed no changes in size, likely due to conjugated DNA folding around the surface of AuNPs rather than being oriented radially.

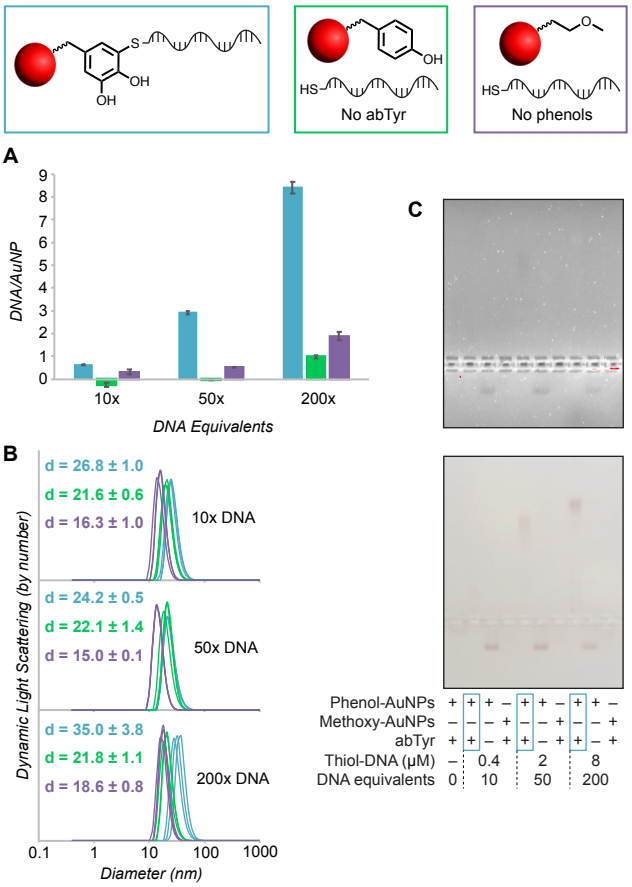

Figure S4. Quantification of DNA conjugated to phenol-AuNPs (40 nM). (A) DNA quantification revealed that up to 8 strands of DNA can be oxidatively coupled to phenol-AuNPs in the presence of tyrosinase (abTyr) (blue) and that the number of conjugated DNA strands can be tuned by changing DNA concentration during oxidative coupling. Some background adsorption was observed in the absence of abTyr (green) and the absence of phenols (purple). All oxidative coupling reactions were carried out with 40 nM AuNPs and 200 nM abTyr. Error bars are from triplicate measurements of a single experiment. (B) The samples used for quantifying DNA strands per AuNP were also analyzed by DLS. While size increased upon conjugation to DNA (blue), variable measurements were produced, which is likely due to the low concentrations of AuNPs. (C) Mobility changes from analysis by gel electrophoresis confirmed conjugation, but analysis of the SYBR Safe stained gel under UV was inconclusive, presumably due to low AuNP concentrations.

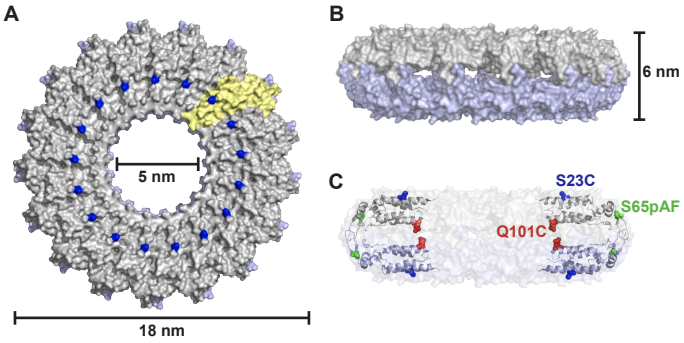

Figure S5. The double disk structure of cpTMV. cpTMV assembles into two disks, each comprising 17 monomers, and displays C2 symmetry. (A) The top-down view of cpTMV reveals the disk-like structure. A single monomer is shown in yellow. The surface S23C mutation site is highlighted in blue. (B) The side view of cpTMV shows the height of the double disk structure. (C) A cross-section of cpTMV highlights the mutation sites. The surface S23C mutation site is shown in blue, the inner cavity Q101C mutation site is shown in red, and the S65pAF mutation site is shown in green.

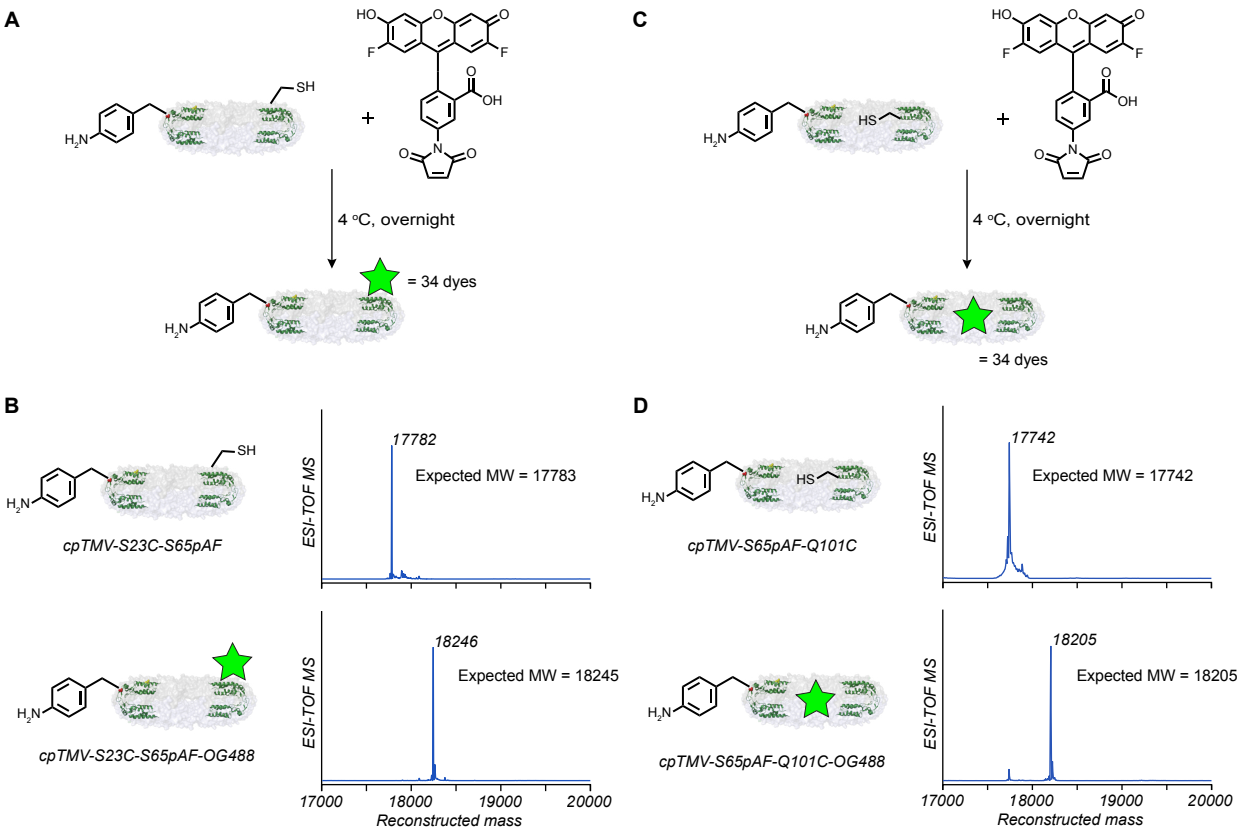

Figure S6. cpTMV-S23C-S65pAF-OG488 and cpTMV-S65pAF-Q101C-OG488 characterization by ESI-TOF LC-MS. (A) Maleimide-thiol chemistry was used to label cpTMV-S23C-S65pAF with Oregon Green 488 (OG488). (B) Full conversion of cpTMV-S23C-S65pAF to cpTMV-S23C-S65pAF-OG488 was observed. (C) Maleimide-thiol chemistry was also used to label cpTMV-S65pAF-Q101C with OG488. (D) Almost full conversion of cpTMV-S65pAF-Q101C to cpTMV-S65pAF-Q101C-OG488 was observed.

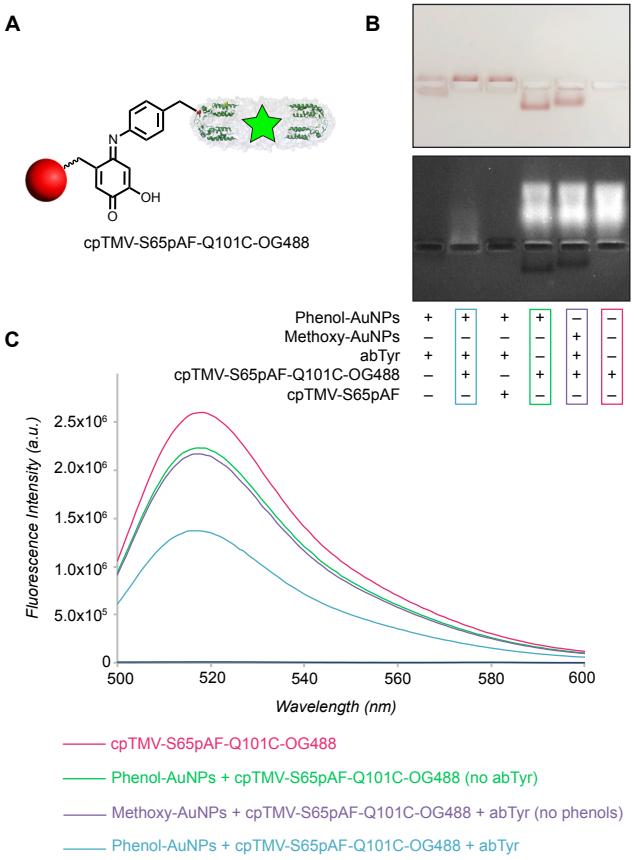

Figure S7. Fluorescent measurements of cpTMV-S65pAF-Q101C-OG488 conjugated to phenol-AuNPs. (A) Oregon Green 488 (OG488) maleimide was conjugated to cpTMV-S65pAF-Q101C (cpTMV-S65pAF with an engineered cysteine residue on the internal surface of the disks; see Figures S8, S10C, and S10D). The resulting cpTMV-S65pAF-Q101C-OG488 proteins were oxidatively coupled to phenol-AuNPs in the presence of tyrosinase (abTyr) and analyzed by (B) native gel electrophoresis and (C) fluorometry. Both characterization techniques revealed quenching of OG488 when cpTMV-S65pAF-Q101C-OG488 was conjugated to the AuNPs. Slight quenching in the presence of methoxy-AuNPs and phenol-AuNPs with no abTyr was attributed to light scattering from AuNPs in solution. Each cpTMV-S65pAF-Q101C-OG488 assembly exhibited 34 aniline moieties and 34 OG488 dye molecules. Oxidative coupling was carried out with 400 nM AuNPs and 0.2 μM (in capsid) TMV.

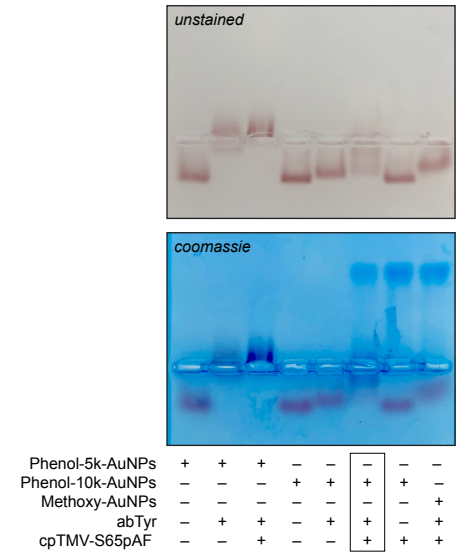

Figure S8. Electrophoretic analysis of oxidative coupling between phenol-10k-AuNPs and cpTMV-S65pAF. Phenol-AuNPs (400 nM) functionalized with a PEG10k monolayer were exposed to the oxidative coupling reaction with cpTMV-S65pAF (0.2 μM in capsid) and tyrosinase (abTyr, 200 nM). While conjugation was observed (lane 6), coupling efficiency was lower than when phenol-AuNPs were functionalized with a PEG5k monolayer (lane 3).

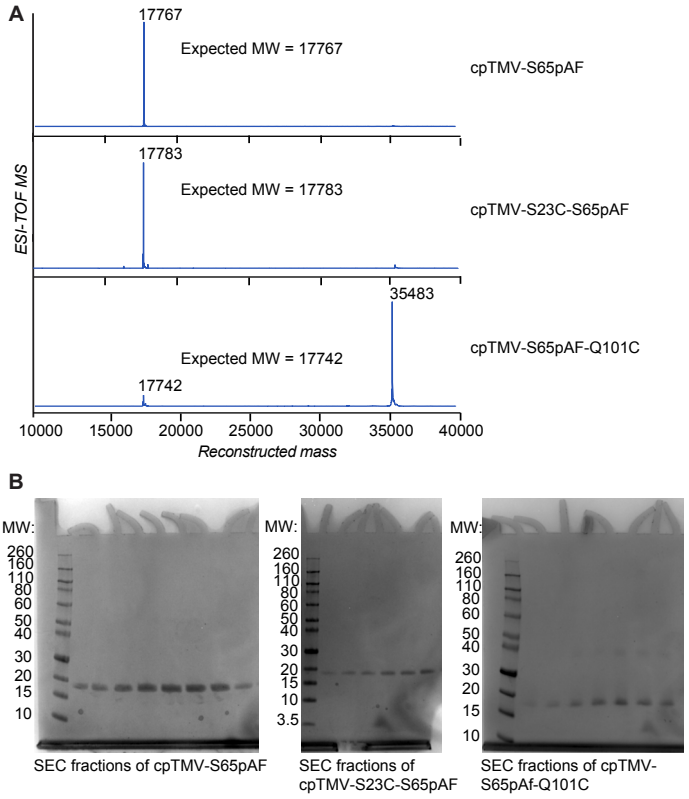

Figure S9. Characterization of purified cpTMV-S65pAF, cpTMV-S23C-S65pAF, and cpTMV-S65pAF-Q101C. (A) Mass spectra for the purified proteins confirmed the expected masses. The Q101C mutant was predominantly present as a dimer due to disulfide formation between cysteines on neighboring monomers. (B) Gel electrophoresis of the purified proteins revealed successful purification.

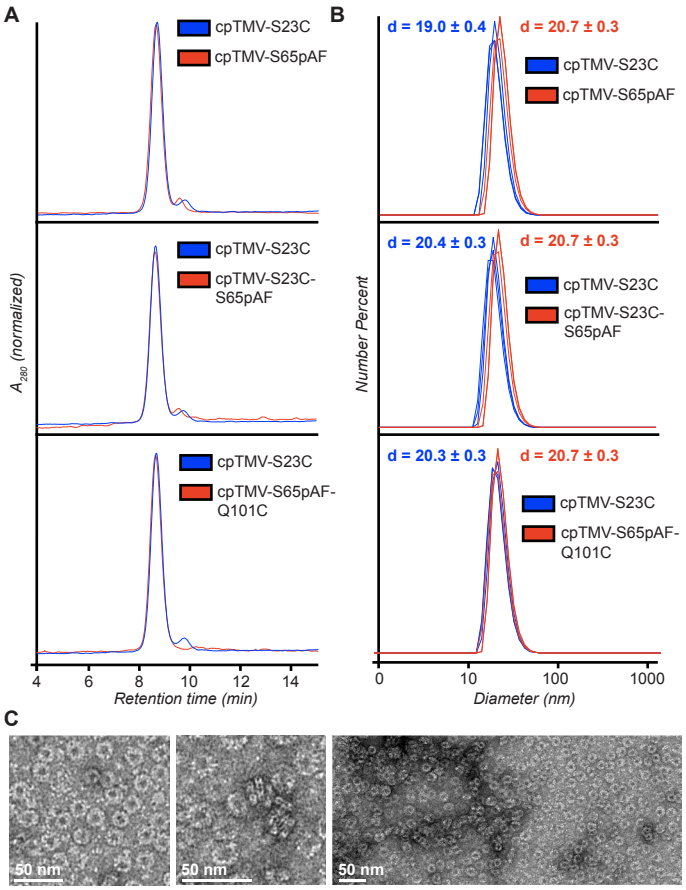

Figure S10. Characterization of TMV protein assembly states. A) HPLC data of cpTMV-S65pAF, cpTMV-S23C-S65pAF, and cpTMV-S65pAF-Q101C revealed disk structures similar to those of cpTMV-S23C, a protein of known structure. A retention time of 8.5 min indicated a double disk assembly state; the small peaks at 9.5 min indicated a small population of monomers. (B) Dynamic light scattering number percent data demonstrated consistent sizes between each cpTMV mutant and cpTMV-S23C, a protein of known double disk structure. The average diameter was calculated from intensity percent data from three replicates. (c) TEM images of cpTMV-S65pAF confirmed the double disk structure via top-down and side views of the disks.

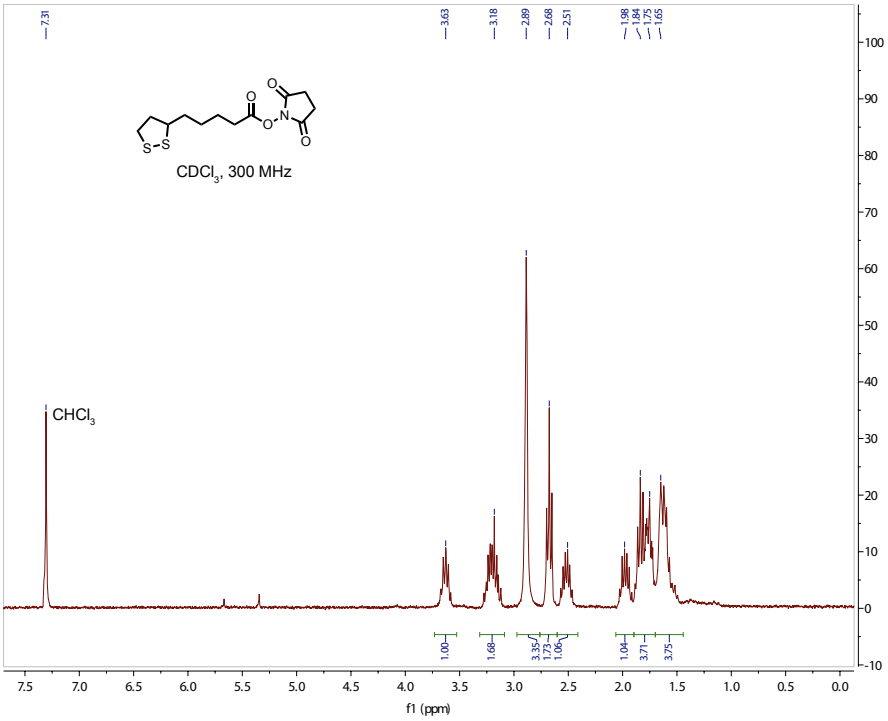

Figure S11. Characterization of lipoic acid-NHS via ^{1}H NMR.

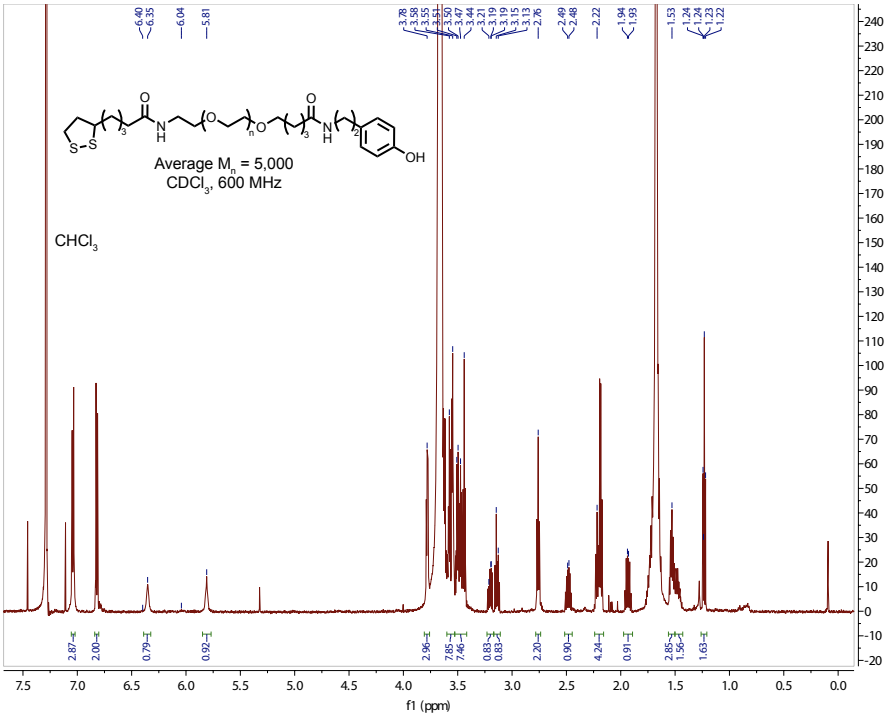

Figure S12. Characterization of thiol-PEG5k-phenol via ^{1}H NMR.

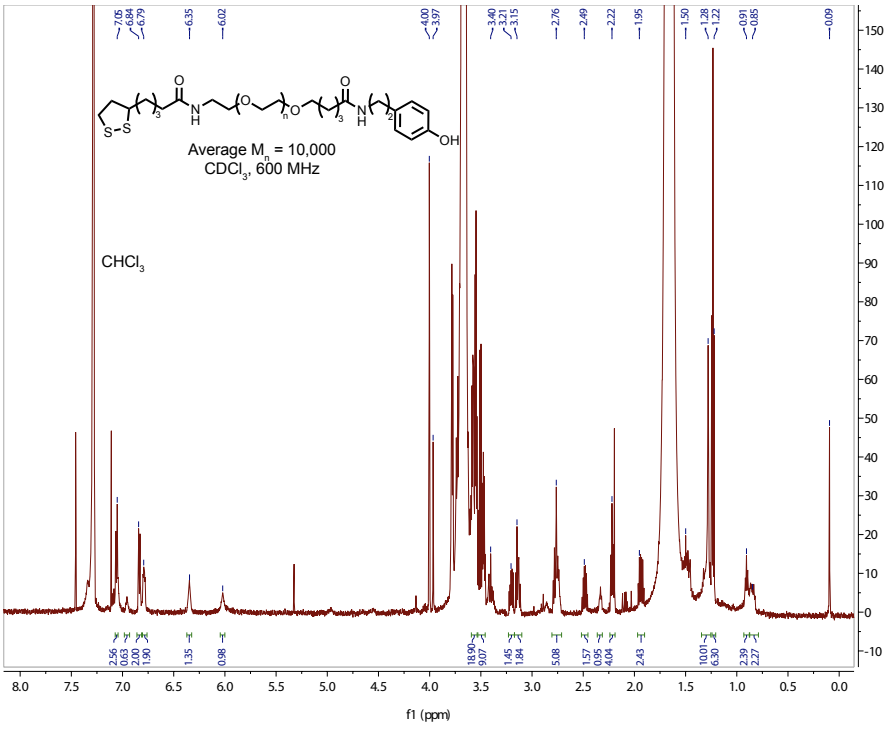

Figure S13. Characterization of thiol-PEG10k-phenol via ^{1}H NMR.

Chapter 4

Oxidative Coupling as a New Method for Conjugating Small Molecules and Biomolecules to Cellulose

Abstract

Inexpensive and biodegradable biosensors are of high importance. Cellulose is a durable and readily available material that can enable development of such devices, but this necessitates effective strategies to immobilize biomolecules on cellulose-based platforms. In this chapter, several new methods are reported for functionalizing cellulose-based filter paper with aniline, catechol, and phenol functional groups. The functionalized cellulose was exposed to a variety of oxidative coupling reactions, including those mediated by an enzyme, to immobilize small molecules, fluorophores, proteins, and DNA. Depending on the type of functional cellulose employed, this reaction was compatible with catechol, aminophenol, phenol, proline, or aniline functional groups on the non-cellulose coupling partner. Oxidative coupling with small molecules was successfully demonstrated based on the formation of colored product. While further optimization is required, the oxidative coupling strategy has potential to also facilitate site-specific immobilization of proteins, which is an unmet need across a broad range of applications.

4.1 Introduction

The Global Disposable Medical Sensors Market (GDMSM) has recently experienced tremendous growth and is expected to continue growing over the next decade. In 2016, the GDMSM was valued at roughly $5 billion and is predicted to reach over $12 billion by 2025.[1] This push towards the development of disposable sensors is driven, in large part, by the high demand for point-of-care diagnostics in the developing world and other resource-limited environments[2] where there is a need for low-cost and easy-to-use alternatives to expensive diagnostic tests that require technical expertise. Disposable biosensors often utilize solid platforms for immobilization of antibodies or other biomolecules that act as specific analyte recognition units. Common examples include pregnancy strip tests, which rely on lateral flow technology, and electrochemical blood glucose monitors.[2] A routine laboratory diagnostic that is based on biomolecule surface immobilization is the enzyme-linked immunosorbent assay (ELISA).

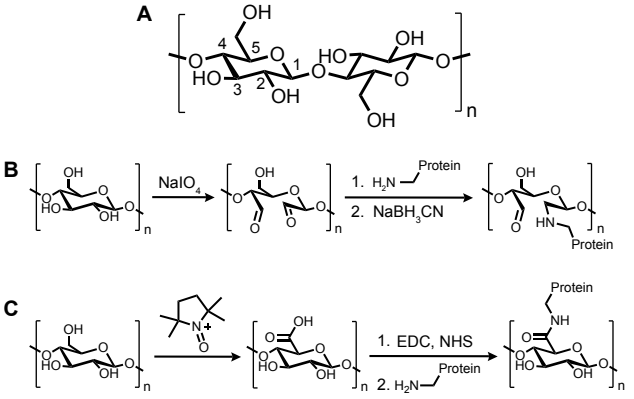

Figure 1. Cellulose structure and common functionalization strategies. (A) Cellulose is composed of glucose monomers that are linked through β-1,4-glycosidic bonds. (B) Cellulose is frequently exposed to sodium periodate to cleave 2,3-diol bonds and generate aldehydes. These aldehydes can undergo reductive alkylation with native lysine residues on proteins. (C) Upon exposure to TEMPO, alcohols at the 5 position of the glucose ring are oxidized to carboxylic acids, which can then be activated with EDC and NHS and reacted with native lysine residues to generate amide bond linkages.

One promising platform for biosensors is cellulose, a material that is highly abundant in a variety of purities and is inexpensive, biodegradable, and readily functionalized. Immobilization of biomolecules on cellulose-based materials has already found applications in microfluidic diagnostic devices,[3,4] lateral flow assays,[5] and paper-based ELISA for detection of *E. coli*.[6] Cellulose, which compromises the structure of plant cell walls, is composed of D-glucose molecules linked through β-1,4-glycosidic bonds. (Figure 1A) The resulting chains of glucose are long and linear and interact through hydrogen bonds. This gives pure cellulose a crystalline structure, yielding a very durable substance that is not readily broken down. In the human body, cellulose is considered an insoluble fiber because humans do not produce cellulase, an enzyme that hydrolyzes the β-1,4-glycosidic bonds, which is necessary to digest cellulose. In cows, horses, and other similar mammals, symbiotic bacteria produce cellulases, allowing many herbivores to break down the cellulose chains and digest green vegetation.

A variety of functionalization strategies are currently employed to immobilize biomolecules on cellulose. The glucose structure leads to a vast number of surface hydroxyl groups that are capable of being modified. Hydroxyl groups at position 5 on the glucose rings are most susceptible to chemical modification, although the 2,3-diol bond can also be oxidized to generate two aldehydes for subsequent modification. One of the most common methods for functionalizing cellulose with proteins is physical adsorption, which re-

lies on electrostatic interactions between biomolecules (typically negatively charged) and the cellulose surface. While convenient and easy to carry out, this method suffers from reversibility. Up to 40% of antibodies can be desorbed from the cellulose surface,[7] which limits efficiency and leads to non-reproducible results.[8] Furthermore, adsorption can lead to surface aggregation of proteins and corresponding activity loss. A common covalent functionalization method is sodium periodate-mediated cleavage of 2,3-diol bonds, followed by reductive alkylation with native lysine residues on proteins (Figure 1B).[9] Another covalent strategy is TEMPO-mediated oxidation of surface hydroxyl groups to carboxylic acids, followed by EDC/NHS activation and coupling to native lysine residues (Figure 1C).[10] While reductive alkylation and EDC/NHS chemistries allow for covalent modification of cellulose, they are not site-selective, which can lead to random orientation and reduction in native function. Thus there is a need for site-selective methods for functionalizing cellulose with biomolecules. Such strategies are critical for the development of sensitive and accurate paper-based biosensors and diagnostics.

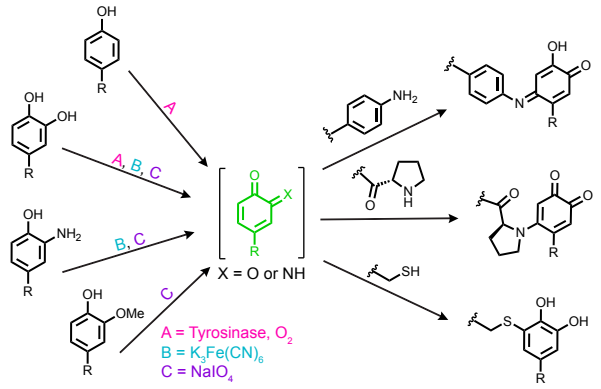

Figure 2. Oxidative coupling reactions. A variety of oxidants can be used to oxidize phenol based moieties to *ortho*-quinoid intermediates (green). These intermediates can undergo subsequent reactions with both amine- and thiol-based nucleophiles.

In this chapter, we highlight an oxidative coupling strategy (Figure 2) as a new method for modification of cellulose with a view towards covalent immobilization of proteins and DNA. In the oxidative coupling reaction, a phenol- or catechol-based electrophilic coupling partner is oxidized to an *ortho*-quinoid intermediate that can undergo subsequent reaction with an amine-[11-16] or thiol-based[17] nucleophile. The reactive *o*-quinoid intermediate can be accessed by one of a variety of oxidants, depending on the identity of the electrophilic coupling partner. This versatile chemistry has enabled the construction of various bioconjugates that tether proteins, peptides, or nucleic acids to small molecules, other biomolecules, and even surfaces, such as glass[18] and gold electrodes.[19] More recently, our lab has developed an enzymatic version of the oxidative coupling reaction that allows *o*-quinones to be accessed from water soluble and highly stable phenols.[20] The enzyme, tyrosinase (abTyr), features a binuclear copper active site and is responsible for the formation of melanin. abTyr is isolated from the common button mushroom, *Agaricus bisporus*, and is commercially available in its active form. Past work has demonstrated that abTyr can oxidize phenols on a variety of substrates, including small molecules, peptides, and proteins. Importantly, the enzymatic version of this reaction allows thiols to be used without competing side reaction pathways.[17] Our lab has also demonstrated successful oxidative couplings with a smaller tyrosinase (35.5 kDa versus ~120 kDa for abTyr) from *Bacillus megaterium*.[21]

To enable oxidative coupling on cellulose surfaces, cellulose is first functionalized with aniline, which can undergo reaction with a variety of substrates bearing catechol,

aminophenol, or phenol functional groups. We demonstrate the successful attachment of small molecules and show preliminary results for conjugation of proteins and DNA. Several different methods for aniline functionalization are described, and in many cases, further optimization is needed to prevent background adsorption of biomolecules. In other cases, background adsorption is minimized, but effective coupling of biomolecules is not observed. Cellulose is also functionalized with catechols and phenols to enable oxidative coupling of substrates with aniline and proline functional groups. Small molecule oxidative coupling is demonstrated, but conjugation of biomolecules to catechol- or phenol-coated cellulose requires further optimization.

4.2 Results and Discussion

4.2.1 Cellulose Activation with Tosyl Chloride

There are a variety of cellulose substrates available for functionalization, including both bulk materials and nanocrystals. However, we focused on paper as the cellulose substrate due to the relevance in paper-based diagnostics and microfluidic devices.[4] Whatman No. 1 filter paper is a very durable paper that, being composed of almost pure cellulose (98%), contains little lignin and other impurities that could interfere with the oxidative coupling reaction. Additionally, this filter paper exhibits uniform thickness and wicking characteristics that make it highly amenable to functionalization.[4]

As noted in the introduction, previous work in the lab has demonstrated effective oxidative coupling on glass surfaces and gold electrodes. In the case of glass, azides were immobilized and then reduced to anilines, followed by potassium ferricyanide ($K_3Fe(CN)_6$)-mediated oxidative coupling to DNA functionalized with aminophenol groups.[18] In the case of gold electrodes, catechols were immobilized and then electrochemically oxidized and coupled to aniline-functionalized DNA.[19] The precise control over oxidation events allowed surface catechols to be oxidized concurrently. However, in solution, catechols exhibit limited stability due to air-induced oxidation, which can lead to self-reaction and subsequent polymerization if catechols are oxidized sequentially rather than simultaneously. This can cause significant complications in solution and also limits the feasibility of immobilizing catechols on surfaces. To avoid the inherent stability issues associated with catechols, we initially chose to functionalize cellulose with the nucleophilic coupling partner.

We drew inspiration from a method for cellulose-based solid-phase peptide synthesis that relies on activation of surface hydroxyls with tosyl chloride, followed by displacement of the tosylates with aliphatic amine compounds.[22] We chose to carry out a variation of this functionalization method by displacing surface tosylates with the aliphatic amine of 4-(2-aminoethyl)aniline to generate aniline(TsCl)-cellulose (Figure 3A). The functionalized cellulose was characterized by FTIR spectroscopy, X-ray photo-electron spectroscopy (XPS), and elemental analysis (EA). In FTIR, N-H stretches are observed in the 3500 to 3300 cm^{-1} range while aromatic C=C stretches, N-H bends, and C-N stretches are found in the 1700 to 1280 cm^{-1} range. However, the FTIR spectra for aniline(TsCl)-cel-

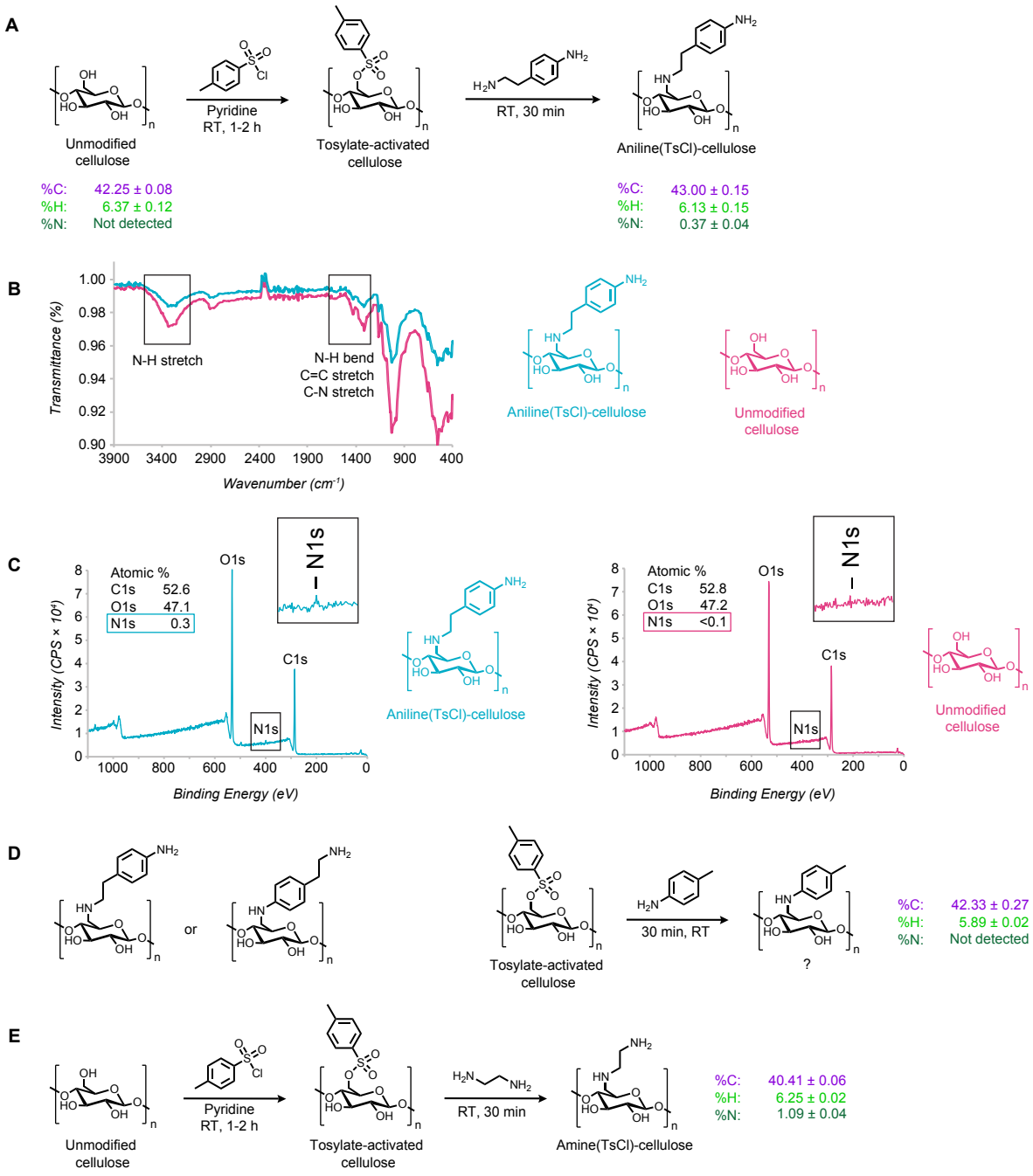

Figure 3. Generation and characterization of aniline(TsCl)-cellulose and amine(TsCl)-cellulose. (A) Cellulose was activated with tosyl chloride in pyridine, followed by displacement of tosylates with 4-(2-aminoethyl)aniline to generate aniline(TsCl)-cellulose. Both unmodified and aniline(TsCl)-cellulose were characterized by elemental analysis. While no nitrogen was detected in unmodified cellulose, a significant quantity of nitrogen was detected in aniline(TsCl)-cellulose. (B) Aniline(TsCl)-cellulose (blue) was characterized by FTIR, which revealed no new peaks (relative to unmodified cellulose, pink) in regions where stretches and bends from the aniline moiety and secondary amine linkage would be expected. (C) Aniline(TsCl)-cellulose (blue) was characterized by X-ray photo-electron spectroscopy, which revealed an increase in nitrogen content relative to unmodified cellulose (pink). (D) Theoretically, two different orientations of 4-(2-aminoethyl)aniline are possible. However, reaction of tosylate-activated cellulose with *p*-toluidine produced cellulose with no detectable nitrogen (as confirmed by elemental analysis), thus verifying that the aniline nitrogen is not nucleophilic enough to displace tosylates on activated cellulose. (E) Cellulose was activated with tosyl chloride in pyridine, followed by displacement of tosylates with ethylenediamine to generate amine(TsCl)-cellulose. Elemental analysis confirmed success of functionalization.

lulose revealed no new peaks in these regions when compared to unmodified cellulose (Figure 3B). This did not necessarily negate functionalization as IR radiation penetrates through the material rather than reflecting off the surface (unless carrying out analysis with attenuated total reflection FTIR). Thus the vast number of O-H bonds in the cellulose structure likely dampen the signal that would be observed from N-H and C=C bonds on the surface. Confirmation of functionalization was achieved through XPS and EA characterization, which revealed nitrogen content of 0.3 to 0.4% for aniline(TsCl)-cellulose and <0.1% nitrogen (or undetected) for unmodified cellulose (Figure 3A and 3C). Similar to IR, the seemingly low percentage of nitrogen in aniline(TsCl)-cellulose is likely due to the high quantity of carbon, oxygen, and hydrogen in the cellulose structure.

Having established the presence of nitrogen, we next sought to verify the orientation of the aniline for samples treated with 4-(2-aminoethyl)aniline. In theory, 4-(2-aminoethyl)aniline could be immobilized through either the aromatic or the aliphatic amine (Figure 3D), although it was expected that the aliphatic amine would be more nucleophilic since the aromatic amine is in conjugation with the ring. To verify this hypothesis, tosylate-activated cellulose was reacted with *p*-toluidine, and the resulting cellulose was characterized by EA. No nitrogen was detected, confirming that aromatic nitrogens are not nucleophilic enough to displace tosylates on cellulose. Furthermore, no product was observed when carrying out small molecule oxidative coupling (described in section 4.2.2) on this cellulose sample.

While aniline, proline, and thiol groups are most reactive in the oxidative coupling reaction, we have also observed participation from native lysine residues. Thus for comparison to aniline(TsCl)-cellulose, we also generated amine(TsCl)-cellulose by reacting tosylate-activated cellulose with ethylenediamine (Figure 3E). By EA, the nitrogen content of amine(TsCl)-cellulose was significantly higher than aniline(TsCl)-cellulose (1.09% vs. 0.37%, respectively). The increase in nitrogen content in amine(TsCl)-cellulose relative to aniline(TsCl)-cellulose can be explained by the increased ratio of nitrogen in ethylenediamine versus 4-(2-aminoethyl)aniline. Ethylenediamine contains ~47% nitrogen while 4-(2-aminoethyl)aniline contains ~21% nitrogen. Thus for equivalent functionalization, the nitrogen content of amine(TsCl)-cellulose would be expected to be 2.3x that of aniline(TsCl)-cellulose. Instead, amine(TsCl)-cellulose exhibited a nitrogen content of 2.8x that of aniline(TsCl)-cellulose. The slight increase in functionalization for amine(TsCl)-cellulose can be attributed to the reduced steric bulk of ethylenediamine compared to 4-(2-aminoethyl)aniline.

4.2.2 Small Molecule Oxidative Coupling on Aniline(TsCl)-Cellulose

To test reactivity of the surface anilines, an oxidative coupling reaction was carried out between the surface aniline (or aliphatic amine) and 4-methyl catechol in the presence of $K_3Fe(CN)_6$ as oxidant (Figure 4A and 4B). It has previously been observed that the oxidative coupling product with amine nucleophiles absorbs between 505 and 525 nm, with the exact wavelength depending on the identity of the amine.[15] Thus the oxidative coupling reaction between the surface anilines and 4-methyl catechol was char-

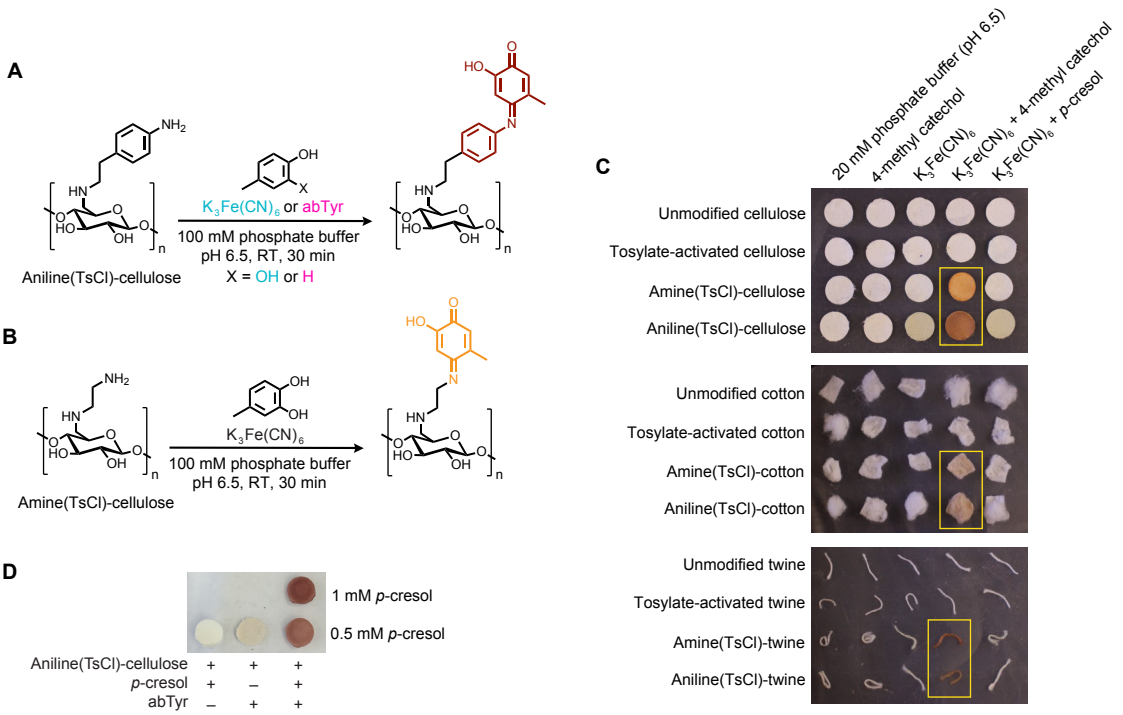

Figure 4. Small molecule oxidative coupling on aniline(TsCl)-cellulose and amine(TsCl)-cellulose. (A) Aniline(TsCl)-cellulose was reacted with 4-methy catechol and $K_3Fe(CN)_6$ (blue) or *p*-cresol and abTyr (pink) to produce a deep red/brown product. (B) Amine(TsCl)-cellulose was reacted with 4-methy catechol and $K_3Fe(CN)_6$ to produce an orange product. (C) Significant product was observed only when both $K_3Fe(CN)_6$ and 4-methyl catechol were reacted with aniline(TsCl)-cellulose, amine(TsCl)-cellulose, or corresponding cotton and twine substrates. In the absence of 4-methyl catechol, $K_3Fe(CN)_6$ adsorbed electrostatically to aniline(TsCl)-cellulose, evidenced by a light yellow color. (D) In the presence of *p*-cresol, abTyr can mediate oxidative coupling on aniline(TsCl)-cellulose. Higher concentrations of *p*-cresol yielded a higher concentration of product (based on the formation of a darker color).

acterized visually by monitoring the formation of colored product. In initial tests, aqueous 4-methyl catechol and $K_3Fe(CN)_6$ were spotted with a pipet onto aniline(TsCl)-cellulose, and a light, pale pink product was observed. However, when the functionalized cellulose was incubated with 1 mM 4-methyl catechol and 6 mM $K_3Fe(CN)_6$ for 30 min, the product was deep red/brown (Figure 4C, top picture, fourth row). The darker color was associated with a higher density of product. Additionally, the color appeared within the first 1 to 2 min, indicating that the reaction proceeded very rapidly. No product was observed when 4-methyl catechol was applied in the absence of $K_3Fe(CN)_6$, confirming the importance of oxidation in facilitating the reaction. Application of 4-methyl catechol and $K_3Fe(CN)_6$ to primary amine(TsCl)-cellulose (Figure 4B) also produced product, but the color was orange rather than dark red/brown (Figure 4C, top picture, third row). Aniline nucleophiles produce a highly conjugated product, and this increase in conjugation relative to the product from aliphatic amine nucleophiles explains the color difference between the two products.

It should be noted that aniline(TsCl)-cellulose exposed only to $K_3Fe(CN)_6$ resulted in a light yellow color, even after extensive washing with water and buffers. The secondary amine linkage produced through tosylate displacement can become protonated at low pH, leading to a cationic surface that can electrostatically adsorb compounds. Additionally, the aromatic ring of the aniline can result in pi-charge interactions. Both phe-

nomena could lead to $K_3Fe(CN)_6$ adsorption, but pi-charge interactions likely contribute more strongly since background adsorption of $K_3Fe(CN)_6$ on amine(TsCl)-cellulose was minimal. In the case of aniline(TsCl)-cellulose, adsorption of $K_3Fe(CN)_6$ could be reversed by washing with 1 M NaOH, confirming electrostatic interactions.

Small molecule oxidative coupling on aniline(TsCl)-cellulose was also successful when mediated by abTyr (4 mol% or 200 nM, with comparable results for both) and 1 mM *p*-cresol (Figure 4D). By visual characterization, abTyr-mediated oxidative coupling produced a similar quantity of product as when mediated by $K_3Fe(CN)_6$. The product was also slightly more brown than red, possibly due to lack of $K_3Fe(CN)_6$ adsorption. Interestingly, the cellulose turned gray upon exposure to only abTyr (middle column). In addition to phenols, abTy can accept aniline moieties as substrates. Thus this result suggests that abTyr can oxidize surface anilines, which is non-trivial owing to the sterically hindered abTyr active site and short linker length between the aniline moieties and the cellulose surface. This exciting result paved the way for immobilization of phenols, as discussed in section 4.2.7.

In addition to filter paper, both cotton balls and cotton twine are composed of high quantities of cellulose, and thus we also applied small molecule oxidative coupling to these materials. Like with filter paper, the cotton and twine substrates were activated with TsCl, and subsequent tosylate displacement was carried out with either 4-(2-aminoethyl)aniline or ethylenediamine. Oxidative coupling on both aniline(TsCl)- and amine(TsCl)-cotton yielded a beige product only when in the presence of both 4-methyl catechol and $K_3Fe(CN)_6$ (Figure 4C, middle picture). The lighter color of product was attributed to the diffuse nature of the cotton ball structure. Oxidative coupling on aniline(TsCl)- and amine(TsCl)-twine generated a much denser product, likely because the cellulose strands are more tightly intertwined than in cotton balls. Interestingly, amine(TsCl)-cotton produced a red color that was distinct from the orange color observed with amine(TsCl)-cellulose. This could be the result of impurities present in the twine. For example, lignin, a common impurity, is composed of methoxy phenols and other phenol-based residues that could participate in the oxidative coupling reaction.

With success of small molecule oxidative coupling, we envisioned the ability to print patterns on functionalized cellulose by localizing the oxidative coupling to specific locations on the surface. This could be particularly useful in the context of using aniline-cellulose to develop a biosensor or immunoassay. To this end, we developed a method for blocking the oxidative coupling reaction in discrete places on the cellulose. Aniline(TsCl)-functionalized cellulose was spotted with acetic anhydride in 10% pyridine (Figure S1A), allowed to sit at RT for 1 min, and then washed. Upon exposing the same cellulose sample to the small molecule oxidative coupling reaction, product was produced only in locations that were not exposed to acetic anhydride (Figure S1B). This allows the potential to generate discrete zones on cellulose and immobilize different biomolecules in specific locations on a single strip of cellulose.

We also wanted to explore the coupling of a fluorophore to aniline(TsCl)-cellulose.

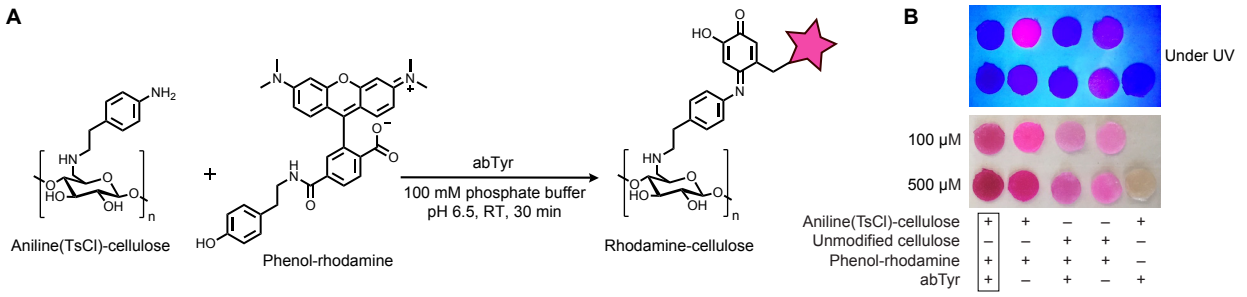

Figure 5. Oxidative coupling of rhodamine to aniline(TsCl)-cellulose. (A) Phenol-rhodamine was conjugated to aniline(TsCl)-cellulose in the presence of abTyr. (B) The resulting cellulose was observed both by eye (bottom picture) and under UV light (top picture). While there was a visual difference between samples with and without abTyr and between aniline(TsCl)-cellulose and unmodified cellulose, there was significant adsorption of the fluorophore in all samples that contained phenol-rhodamine. Based on UV characterization, fluorescent quenching was observed in most cases, except for when phenol-rhodamine at 100 µM was reacted with aniline(TsCl)-cellulose in the absence of abTyr (second column, top row).

To facilitate this, we synthesized phenol-rhodamine by reacting tyramine with a commercially available NHS version of the fluorophore. This phenol dye was then oxidatively coupled to aniline(TsCl)-cellulose in the presence of abTyr to generate rhodamine-cellulose (Figure 5A), which was characterized by visual observation and UV light. While there were distinct color differences for immobilized phenol-rhodamine when in the presence versus absence of abTyr, significant adsorption was observed in all samples that included rhodamine, even when unmodified cellulose was used (Figure 5B). This is not surprising as dye adsorption to cellulose is commonly reported in the literature as a method for removing dye contaminants from solution. In fact, cellulose is often first functionalized with aliphatic amines to increase electrostatic interactions and enhance dye adsorption.[23,24] Thus it was difficult to attribute dye immobilization to oxidative coupling.

4.2.3 Oxidative Coupling of Biomolecules to Aniline(TsCl)-Cellulose

Having confirmed small molecule reactions, we next tested protein immobilization using a superfolder GFP (sfGFP)[25] variant that exhibited an engineered tyrosine residue at position 64 and an engineered cysteine residue at position 208 (sfGFP-S64Y-S208C). Because thiols can participate as nucleophiles in the oxidative coupling reaction, the cysteine residue was capped with 5,5-dithio-bis-(2-nitrobenzoic acid) (DTNB) prior to oxidative coupling. DTNB-capped sfGFP-S64Y-S208C (10 to 50 µM) was combined with abTyr in phosphate buffer at pH 6.5 and incubated with aniline(TsCl)-cellulose (Figure 6A), in addition to unmodified cellulose. After reaction and washing, the cellulose was visualized under UV light. Unfortunately, sfGFP was immobilized on aniline(TsCl)-cellulose even in the absence of abTyr (as evidenced by a strong fluorescent signal in both cases, Figure 6B), and thus immobilization via oxidative coupling could not be confirmed. If tosylates were not completely displaced during initial cellulose functionalization, remaining tosylates could be displaced by native lysine residues on sfGFP, leading to covalent immobilization. Indeed, we later found that incubation of pro-sfGFP (sfGFP with an engineered proline N-terminus) with tosylate-activated cellulose resulted in strong surface fluorescence (see section 4.2.5).

To characterize the extent of tosylate displacement, we evaluated the sulfur con-

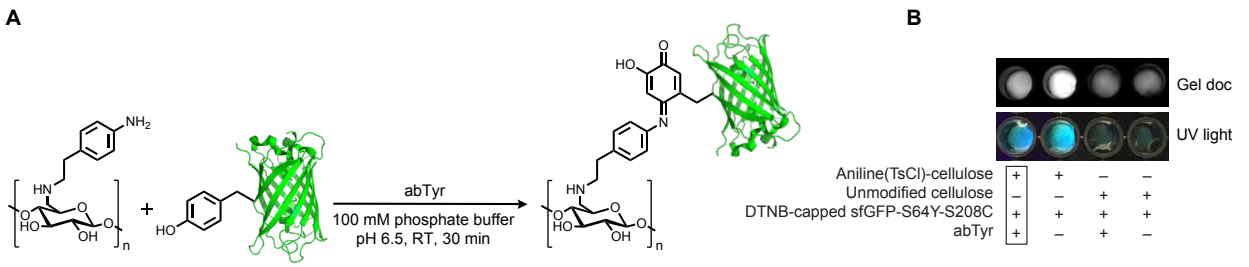

Figure 6. Oxidative coupling of tyrosine-tagged sfGFP to aniline(TsCl)-celluose. (A) Aniline(TsCl)-cellulose was exposed to DTNB-capped sfGFP-S64Y-S208C and abTyr to immobilize sfGFP. (B) Analysis by UV light revealed that sfGFP is immobilized on aniline(TsCl)-cellulose even in the absence of abTyr.

tent of aniline(TsCl)-cellulose and tosylate-activated cellulose through EA. As expected, aniline(TsCl)-cellulose exhibited significantly less sulfur than tosylate-activated cellulose (0.84% sulfur versus 1.7%, respectively). However, the significant sulfur content of aniline(TsCl)-cellulose confirmed incomplete tosylate displacement. We also found that the nitrogen content of tosylate-activated cellulose (0.43%) was similar to the nitrogen content for aniline(TsCl)-cellulose (0.37%). While the source of nitrogen in tosylate-activated cellulose is likely pyridine, we were initially concerned that the nitrogen content for aniline(TsCl)-cellulose could result from pyridine rather than aniline. However, tosylate-activated cellulose reacted with *p*-toluidine produced a sample with no detectable nitrogen (see section 4.2.1 and Figure 3D), and thus excess pyridine is removed when tosylate-activated cellulose is exposed to subsequent functionalization. As an additional verification, no product was observed with negative controls in which tosylate-activated cellulose was exposed to the oxidative coupling reaction (Figure 4C). This confirms that nitrogen on tosylate-activated cellulose is distinct from nitrogen on aniline(TsCl)-cellulose.

Because native lysine residues can displace tosylates, we reasoned that we could backfill aniline(TsCl)-cellulose with a small aliphatic amine to displace any tosylates that remain after aniline functionalization. Thus we incubated aniline(TsCl)-cellulose with butylamine. Tosylates feature an aromatic moiety that allowed us to use UV-vis analysis of the incubation solution to characterize the success of tosylate displacement with butylamine. When exposing aniline(TsCl)-cellulose with no butylamine backfill to 1 M NaOH for 1 h, we observed an absorbance of ~0.3 at 260 nm. We attributed this peak to tosylates that were displaced by NaOH. In contrast, no absorbance at 260 nm was observed when aniline(TsCl)-cellulose with butylamine was exposed to NaOH. Encouraged by this result, we repeated oxidative coupling to tyrosine-tagged sfGFP in the presence of abTyr. However, we still observed significant adsorption of sfGFP in the absence of abTyr. Subsequent washings with up to 500 mM NaCl had little effect. As previously mentioned, protonation of the secondary amine in the aniline linkage could lead to surface electrostatic interactions. This is likely the source of background adsorption, and thus for further protein immobilization, we investigated different methods for generating aniline-cellulose.

Our interest in protein immobilization was driven by the fact that many paper-based diagnostic devices employ antibodies as the detection element. However, aptamers are becoming increasingly common for analyte detection due to high target sensitivity, ease

of construction (especially compared to antibodies), and the enhanced stability of DNA relative to proteins.[26] Thus we wanted to test oxidative coupling in the context of DNA immobilization on cellulose. DNA with a 5' amine modification was purchased and reacted with an NHS-activated nitrophenol compound to generate aminophenol-DNA (AP-DNA).[14] Sodium dithionite was then used to reduce the nitrophenol to the desired aminophenol (Figure S2A). Successful functionalization and reduction was confirmed with MALDI.

In initial tests, we noted significant absorbance of AP-DNA to aniline(TsCl)-cellulose in the absence $K_3Fe(CN)_6$. We reasoned that this could be due to electrostatic interactions, pi-stacking interactions, or both. To further explore the cause of adsorption, we carried out oxidative coupling on aniline(TsCl)-cellulose or amine(TsCl)-cellulose with 50 μM AP-DNA and 1 mM $K_3Fe(CN)_6$ at various pH (100 mM phosphate buffer at pH 6.4, pure water, or 100 mM phosphate buffer at pH 8.1) (Figure S2B). After oxidative coupling and washing, the paper was incubated with 50 μM ssDNA that was non-complementary to the AP-DNA sequence. Subsequent exposure to 1 M NaOH disrupted any surface interaction, allowing quantification of adsorbed ssDNA through UV-vis analysis of the resulting solution. In the case of aniline(TsCl)-cellulose, a significant amount of ssDNA was adsorbed regardless of the pH employed during the oxidative coupling reaction (Figure S2B). This suggested that ssDNA adsorption to aniline(TsCl)-cellulose was primarily facilitated by pi-stacking interactions. In contrast, ssDNA adsorption to amine(TsCl)-cellulose was significantly lower that adsorption to aniline(TsCl)-cellulose, and a pH dependent effect was observed. While water and pH 8.1 buffer did not lead to ssDNA adsorption, pH 6.4 resulted in a relatively high amount of adsorption. This suggests that adsorption to amine(TsCl)-cellulose is driven primarily by electrostatic interactions between cationic cellulose and negatively charged DNA. Because of the strong background adsorption of ssDNA in the case of aniline(TsCl)-cellulose, oxidative coupling of AP-DNA to aniline(TsCl)-cellulose was not investigated further.

4.2.4 Aniline-Functionalization of Cellulose with Isatoic Anhydride

Previous work in the lab has demonstrated that native lysine residues on proteins can react with isatoic anhydride under slightly basic conditions to generate aniline functional moieties for subsequent oxidative coupling.[27] Thus we hypothesized that when reacted with a strong enough base, surface hydroxyl groups on cellulose could become effective nucleophiles and produce aniline-functionalized paper when reacted with isatoic anhydride (Figure 7A). We tested both 10% pyridine and 200 mM DMAP as the base, and in both cases, product was observed upon the addition of 4-methyl catechol and $K_3Fe(CN)_6$. However, a darker color was produced for the aniline(IA)-cellulose prepared with DMAP, and thus this sample was characterized by FTIR spectroscopy and EA (Figure 7A and 7B). Carbonyl ester stretches typically appear at 1750 to 1735 cm^{-1} in FTIR spectra while N-H bends are characteristic between 1650 and 1580 cm^{-1}. The aniline(IA)-cellulose sample revealed new peaks at 1725 and 1660 cm^{-1}, confirming modification. EA verified functionalization with a nitrogen content of 0.48%, higher than that observed for aniline(TsCl)-cellulose. The nitrogen content of the added functional group in aniline(IA)-cellulose is ~12% (versus 21% for 4-(2-aminoethyl)aniline), and thus

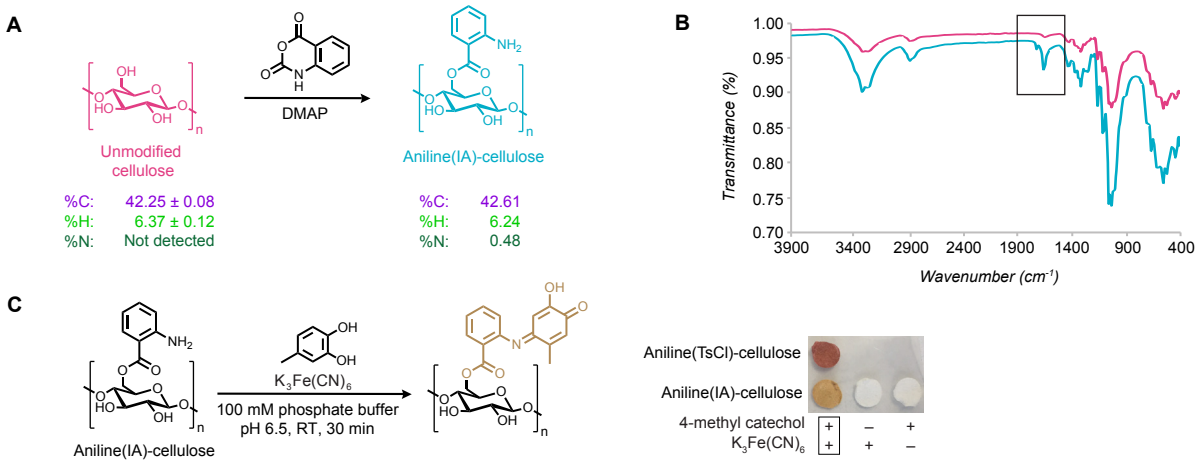

Figure 7. Functionalization and characterization of aniline-cellulose generated from reaction with isatoic anhydride. (A) Unmodified cellulose was reacted with isatoic anhydride in the presence of DMAP to generate aniline(IA)-cellulose. Elemental analysis confirmed conjugation based on increased nitrogen content after reaction with isatoic anhydride. (B) FTIR spectroscopy revealed new peaks at 1725 and 1660 cm^{-1}, further confirming successful modification. (C) Small molecule oxidative coupling with 4-methyl catechol produced product only in the presence of $K_3Fe(CN)_6$ (first column). Although the color was lighter than small molecule oxidative coupling with aniline(TsCl)-cellulose, this could be the result of increased conjugation in the aniline(IA)-cellulose oxidative coupling product.

to achieve equivalent functionalization, we would expect a nitrogen content of 0.5x that of aniline(TsCl)-cellulose. Because we instead observed a higher nitrogen content, reaction with isatoic anhydride leads to elevated aniline modification. Additionally, we found that the aniline(IA)-cellulose was fluorescent under UV light. This is in line with previous results in the lab that showed proteins reacted with isatoic anhydride are fluorescent under UV.[27] The color of product produced from oxidative coupling on aniline(IA)-cellulose was lighter than product produced by oxidative coupling on aniline(TsCl)-cellulose (Figure 7C), which is likely due to differing conjugation between the two products. We also observed that $K_3Fe(CN)_6$ did not adsorb to aniline(IA)-cellulose, supporting the hypothesis that adsorption of $K_3Fe(CN)_6$ to aniline(TsCl)-cellulose was mediated by protonation of the secondary amine linkage.

While reaction with isatoic anhydride was an effective method for generating aniline-cellulose, we were concerned about hydrolysis of the ester linkage when exposed to aqueous conditions for extended periods of time. Because aniline compounds absorb at 230 and 280 nm, we used UV-vis spectroscopy to monitor hydrolysis. Aniline(IA)-cellulose was incubated overnight at 60 °C in buffers at various pH (5, 6, 7, 8, or 9). As expected, significant absorbance was observed in a pH-dependent manner. pH levels of 7, 8, or 9 led to significantly higher aniline in solution as compared to pH 5 and 6, which is consistent with a hydrolytic mechanism facilitated by basic conditions.

While hydrolysis was observed at higher pH levels, we wanted to test our hypothesis that an ester linkage would lead to less surface adsorption than a secondary amine linkage. To do this, we took advantage of the natural hydrolytic ability of the ester linkage to quantify the extent of biomolecule conjugation or adsorption to aniline(IA)-cellulose. Oxidative coupling was carried out with 50 μM AP-DNA in 100 mM phosphate buffer at pH

9 since higher pH tended to reduce DNA adsorption to cellulose. After oxidative coupling with AP-DNA and $K_3Fe(CN)_6$, the ester linker was hydrolyzed with 50 mM NaOH. Unreacted anilines were removed from solution by spin concentrating the hydrolyzed reaction solution with 3k MWCO spin filters. The resulting DNA concentration was determined by A_{260} absorbance. However, hydrolyzed solutions yielded similar DNA concentrations both in the presence and absence of $K_3Fe(CN)_6$ (Figure 8). Subsequent MALDI characterization of the AP-DNA revealed that the aminophenol moiety of AP-DNA had undergone oxidation in air, and thus it is possible that oxidative coupling occurred even in the absence of $K_3Fe(CN)_6$. Adsorption of ssDNA with no aminophenol group was less than AP-DNA but still significant compared to the negative control with no DNA added. Additionally, the hydrolytic instability of the ester linkage was still a concern, and thus aniline(IA)-cellulose was not explored further.

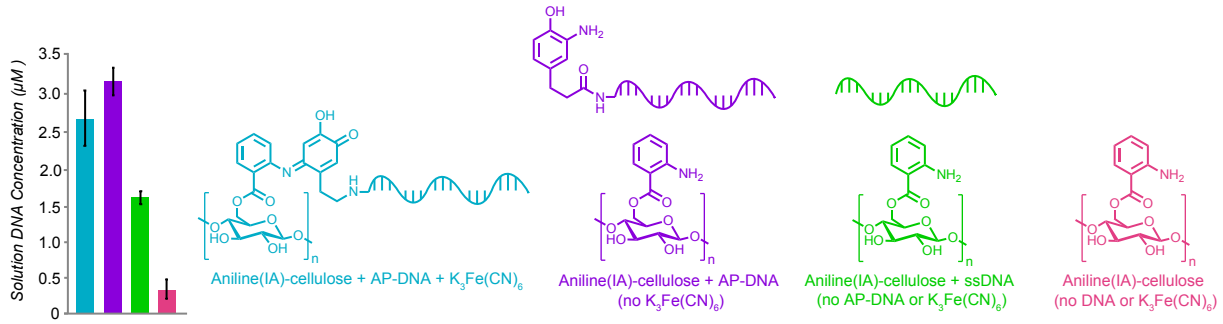

Figure 8. Oxidative coupling of DNA to aniline(IA)-cellulose. Aminophenol-DNA (AP-DNA) was coupled to aniline(IA)-cellulose at pH 9, followed by hydrolysis of the ester linkage and subsequent quantification of DNA in solution. Significant background adsorption of DNA (both AP-DNA and ssDNA) was observed.

To both enhance the extent of functionalization and replace the ester linkage with a more hydrolytically stable amide linkage, we generated primary amine cellulose by functionalizing unmodified cellulose with (3-aminopropyl)triethoxysilane. Silanation is a common method for functionalizing cellulose and was chosen over tosylate activation because of previous concerns with incomplete tosylate displacement. Once silanated and reacted with isatoic anhydride, characterization was carried out by EA and FTIR spectroscopy (Figure 9A and 9B). EA revealed a nitrogen content of 1.94% prior to reaction with isatoic anhydride, which corresponded to even greater amine functionalization compared to aniline(TsCl)-cellulose and aniline(IA)-cellulose. After reaction with isatoic anhydride, the nitrogen content was 1.75%. When compared to silanated-cellulose, few conclusions could be drawn on the basis of EA alone, but unlike unmodified and silanated cellulose, aniline(SiIA)-cellulose exhibited peaks at ~1640 and 1520 cm^{-1} in the FTIR spectrum. Thus the carbonyl peaks in the FTIR spectrum verified formation of an amide bond and functionalization with aniline. Small molecule oxidative coupling produced product to a similar extent as aniline(TsCl)-cellulose (Figure 9C). While encouraging, surface aliphatic amines unreacted with isatoic anhydride could still lead to unwanted electrostatic interactions (although $K_3Fe(CN)_6$ did not adsorb). As previously mentioned, aliphatic amine paper is often generated to enhance adsorption to cellulose.[23,24] Additionally, similar to the ester linkage, the hydrolytic instability of the Si-O bond was a concern. Thus we next chose to pursue cellulose functionalization via carbamate linkages.

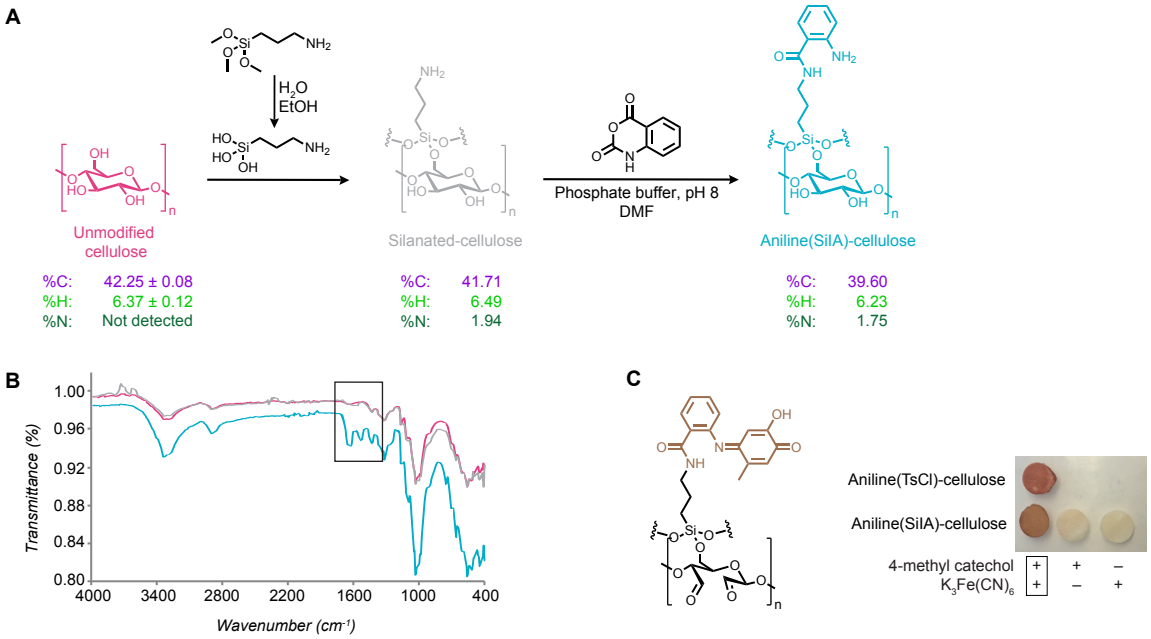

Figure 9. Functionalization and characterization of aniline-cellulose generated from reaction of isatoic anhydride and silanated-cellulose. (A) Unmodified cellulose was silanated with (3-aminopropyl)triethoxysilane to generate a primary amine surface, which was then reacted with isatoic anhydride at pH 8 to generate aniline(SiIA)-cellulose. Elemental analysis confirmed silanation based on increased nitrogen content after reaction with the silane. Elemental analysis after subsequent reaction with isatoic anhydride was inconclusive due to comparable levels of nitrogen. (B) Compared to unmodified cellulose (pink) and silanated cellulose (silver), FTIR spectroscopy revealed new peaks at 1640 and 1520 cm^{-1} for aniline(SiIA)-cellulose (blue), suggesting successful modification. (C) Small molecule oxidative coupling with 4-methyl catechol produced product only in the presence of $K_3Fe(CN)_6$ (first column).

4.2.5 Cellulose Activation with 4-Nitrophenyl Chloroformate and Carbonyldiimidazole

Because of the electrostatic issues and hydrolytic instability associated with previously discussed functionalization methods, we next pursued other approaches for hydroxyl activation. Two activation agents were explored: 4-nitrophenyl chloroformate (4-NPC) and carbonyldiimidazole (CDI). Both activation reagents, once reacted with 4-(2-aminoethyl)aniline, yield stable carbamate linkages that do not feature a protonizable secondary amine. However, similar to tosylate activation (see section 4.2.1), we anticipated that it would be necessary to backfill the samples with a small amine compound to ensure that all 4-NPC or CDI was displaced.

An attractive characteristic of 4-NPC is that once cleaved from the surface, it can be quantified with UV-vis spectroscopy due to a characteristic wavelength at 410 nm.[28] This allowed convenient screening of reaction conditions to maximize initial cellulose activation with 4-NPC. Triethylamine (TEA), *N,N*-diisopropylethylamine (DIPEA), and pyridine were screened as bases, while DMF, DCM, and THF were screened as solvents. Pyridine in the presence of DCM led to the greatest extent of surface activation, with TEA also leading to relatively high activation. Once activation conditions were optimized, we carried out subsequent displacement with 4-(2-aminoethyl)aniline (Figure 10A) and exposed aniline(NPC)-cellulose to the small molecule oxidative coupling reaction with 4-methyl catechol and $K_3Fe(CN)_6$ (Figure 10B). Initially, the reaction appeared to produce

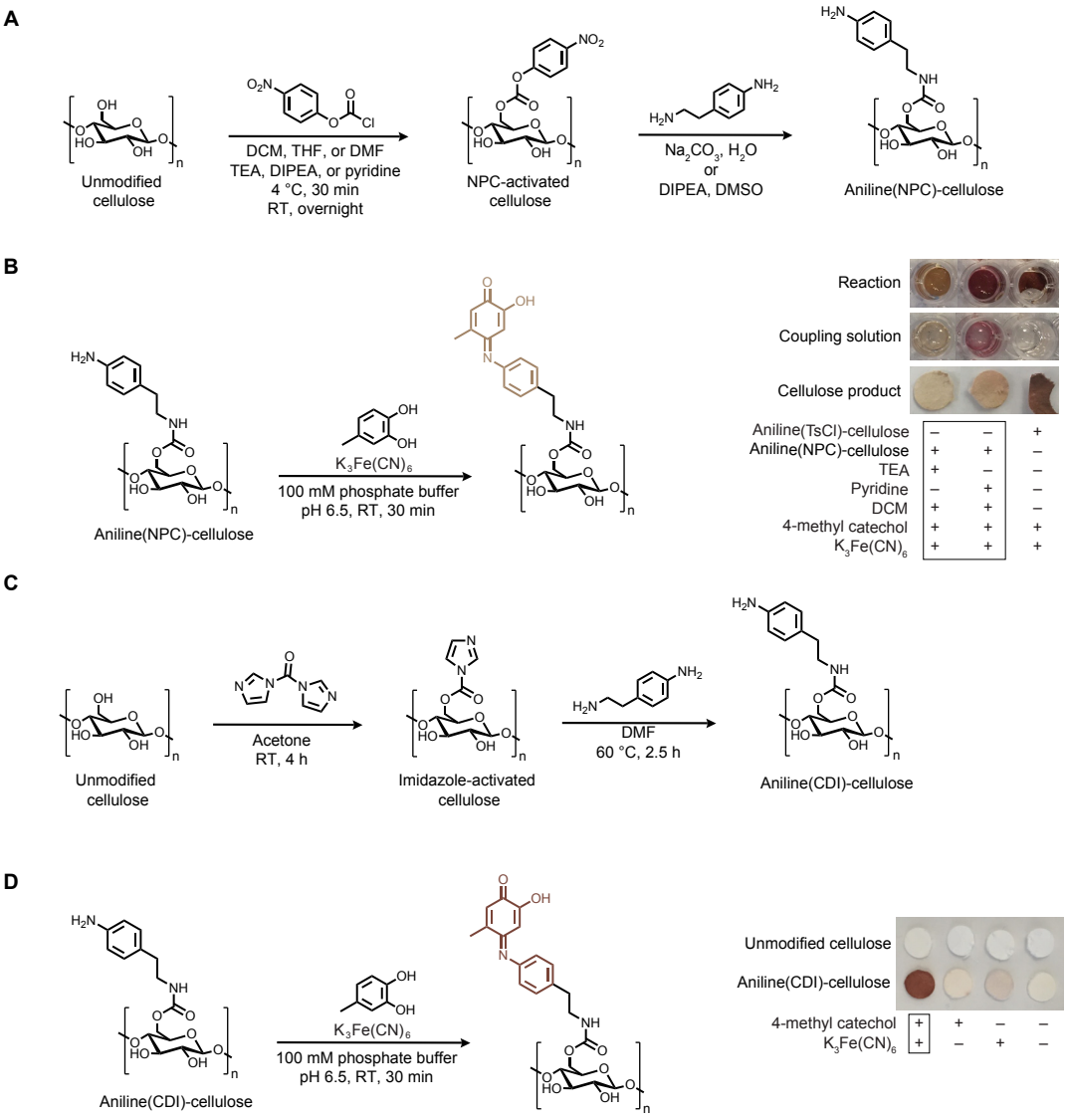

Figure 10. Activation of cellulose with 4-nitrophenyl chloroformate (4-NPC) and carbonyldiimidazole (CDI). (A) Unmodified cellulose was reacted with 4-NPC in one of various solvents and TEA, DIPEA, or pyridine to generate NPC-activated cellulose. The nitrophenyl was displaced by 4-(2-aminoethyl)aniline in the presence of either Na_2CO_3 or DIPEA as base to generate aniline(NPC)-cellulose. (B) Aniline(NPC)-cellulose was oxidatively coupled to 4-methyl catechol in the presence of $K_3Fe(CN)_6$. The color of product and coupling solution depended on the solvent and base used during 4-NPC activation, but in general, little oxidative coupling product was formed on the cellulose surface, regardless of the activation conditions employed. (C) Unmodified cellulose was reacted with CDI to generate imidazole-activated cellulose. The imidazole was displaced by 4-(2-aminoethyl)aniline to generate aniline(CDI)-cellulose. (D) Aniline(CDI)-cellulose was oxidatively coupled to 4-methyl catechol in the presence of $K_3Fe(CN)_6$ to produce a deep brown product.

product, but the majority of color remained in solution when the cellulose samples were removed. We suspect that a significant amount of 4-NPC remained on aniline(NPC)-cellulose at the time of coupling. The 4-NPC then reacted with *o*-quinones produced from oxidation of 4-methyl catechol, which quenched the *o*-quinones in solution, leading to minimal product on the cellulose surface. Despite screening various activation conditions, this issue continued, and so we chose to instead explore CDI activation.

CDI activation of cellulose is reported in the literature as a strategy for immobilizing

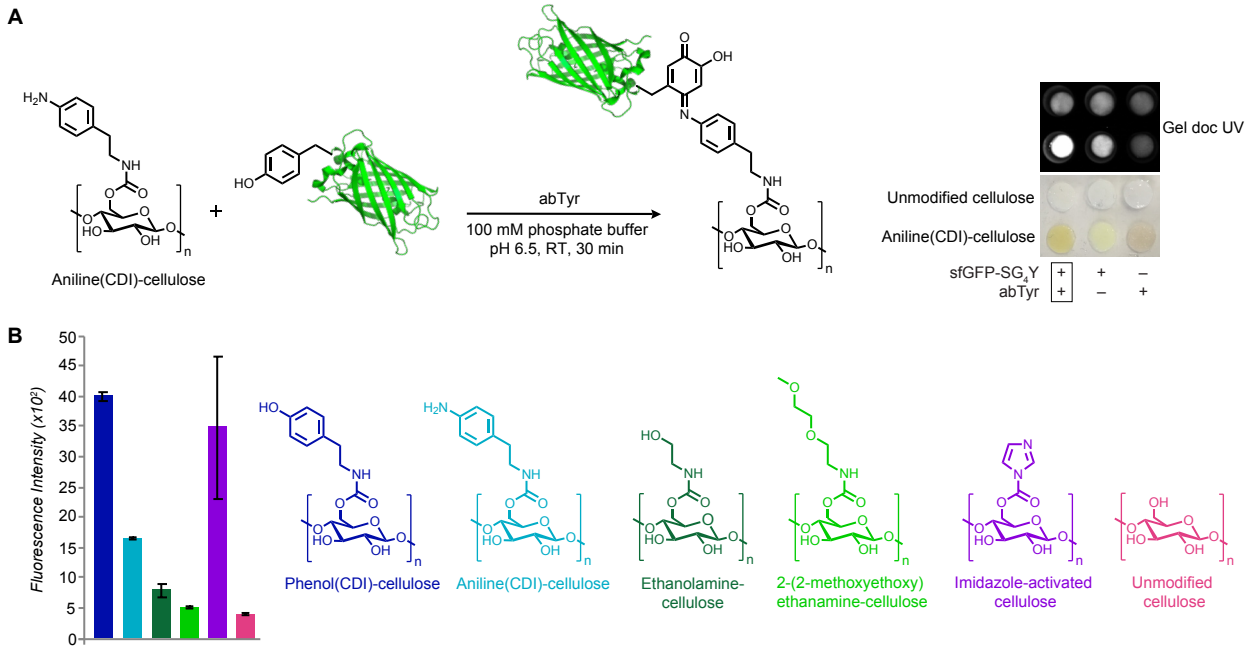

Figure 11. sfGFP-SG_4Y immobilization on cellulose functionalized via CDI activation. (A) sfGFP-SG_4Y was oxidatively coupled to aniline(CDI)-cellulose in the presence of abTyr. A higher quantity of sfGFP-SG_4Y was immobilized in the presence of abTyr (based on UV visualization), but sfGFP-SG_4Y was still adsorbed in the absence of abTyr. (B) CDI-activated cellulose was exposed to ethanolamine or 2-(2-methoxyethoxy)ethanamine to passivate the cellulose surface relative to phenol-, aniline-, and CDI-cellulose. The cellulose samples were incubated with 20 µM sfGFP-SG_4Y in 50 mM phosphate buffer at pH 6.5, and the resulting fluorescence was quantified after washing the samples with water and phosphate buffer. 2-(2-methoxyethoxy)ethanamine (light green) was the more effective surface passivation compound. Error bars represent standard deviation for n=2.

glucose oxidase through native lysine residues in order to develop an immunosensor.[29] We followed the reported activation method and carried out subsequent displacement of imidazole with 4-(2-aminoethyl)aniline (Figure 10C). Ethanolamine was then added to displace any remaining imidazole and passivate the surface. Reaction of aniline(CDI)-cellulose with 4-methyl catechol and $K_3Fe(CN)_6$ produced a significant quantity of deep brown product (Figure 10D), similar to what was observed for aniline(TsCl)-cellulose. Furthermore, the product remained on the cellulose surface, rather than staying in solution as was observed with 4-NPC activation. Encouraged by these results, we pursued oxidative coupling of sfGFP-SG_4Y in the presence of abTyr. However, while background adsorption of sfGFP was lower compared to previous tests, there was still adsorption in the absence of abTyr (Figure 11A). This adsorption could not be reversed, even with wash solutions containing up to 1 M NaCl, 2% Tween20, or 10 mM glycine at pH 2.2 (which is reported to be highly effective at removing electrostatically adsorbed antibodies[30]). Lower sfGFP concentrations were also tested but yielded similar results.

The continued adsorption of sfGFP was likely the result of pi-pi or pi-cation interactions. To examine these interactions, CDI-activated cellulose was reacted with ethylenediamine to produce amine(CDI)-cellulose that exhibited no aromatic groups. While positive test conditions with GYGGS-sfGFP and abTyr yielded slightly higher fluorescence readings, background adsorption was again observed. Pro-sfGFP with abTyr was also tested as a negative control (since no phenols or exposed tyrosine residues were

present), and while adsorption was observed, it was lower than observed for GYGGS-sfGFP. The exposed tyrosine residue at the N-terminus of GYGGS-sfGFP may have led to pi-cation interactions with positively charged primary amines on the cellulose surface. In contrast, pro-sfGFP would not exhibit these interactions.

Similar to tosylate activation, it was possible that native lysine residues on sfGFP were displacing surface imidazole groups not displaced during reaction with 4-(2-aminoethyl)aniline. To test this hypothesis, we carried out a screen of surface passivation molecules. CDI-activated cellulose was reacted with tyramine, 4-(2-aminoethyl)aniline, ethanolamine, or 2-(2-methoxyethoxy)ethanamine (Figure 11B). These samples, along with CDI-activated cellulose and unmodified cellulose, were exposed to 20 μM sfGFP-SG_4Y in 50 mM phosphate buffer at pH 6.5 in the absence of abTyr. Surface fluorescence was quantified after subsequent washes with water and phosphate buffer. Phenol(CDI)-cellulose yielded the highest sfGFP adsorption, comparable to sfGFP incubation with CDI-activated cellulose. Significant adsorbance was also observed on aniline(CDI)-cellulose. Ethanolamine and 2-(2-methoxyethoxy)ethanamine passivation led to very little sfGFP adsorption with 2-(2-methoxyethoxy)ethanamine being particularly effective. This supports the involvement of pi-interactions in mediating sfGFP adsorption and verifies that the surface can be effectively passivated with the right molecule. It is possible that a slightly longer PEG molecule would achieve complete passivation.

4.2.6 Cellulose Functionalization through Oxime Ligation

Periodate oxidation is a common method for modifying cellulose. Oxidation of the 2,3-diol bond in glucose monomers produces two aldehydes which, in the context of protein immobilization, are typically conjugated to native lysine residues through reductive alkylation.[9] However, as previously noted, this approach is not site-specific. Instead of direct protein immobilization, we chose to generate aldehydes as an activation strategy for producing aniline-cellulose. Cellulose oxidation was facilitated by sodium periodate at concentrations ranging from 1 to 30 mM. Subsequently, the oxidized cellulose was ligated to an aminoxy-aniline compound that was synthesized according to a previously reported procedure[31] (Figure 12A). When aniline($NaIO_4$)-cellulose was exposed to the oxidative coupling reaction with 4-methyl catechol and $K_3Fe(CN)_6$, we observed colored product with a dependence on periodate concentration (Figure 12B). Additionally, no product was observed when the cellulose was oxidated but not ligated to the aminoxy-aniline (Figure 12C), confirming that aniline is critical for the formation of product.

While oxidative coupling of phenol-rhodamine on aniline(TsCl)-cellulose led to significant dye adsorption (see section 4.2.2), we reasoned that aniline($NaIO_4$)-cellulose might be less susceptible to adsorption due to an aminoxy rather than secondary amine linkage. Instead of rhodamine, we used Oregon Green 488 (OG488) that we functionalized with a phenol moiety (Figure 13A). Encouragingly, the phenol-OG488 did not adsorb to unmodified paper (Figure 13B). Additionally, a deep orange color was observed when aniline($NaIO_4$)-cellulose was exposed to phenol-OG488 in the presence of abTyr while a light yellow color was observed when aniline($NaIO_4$)-cellulose was exposed to

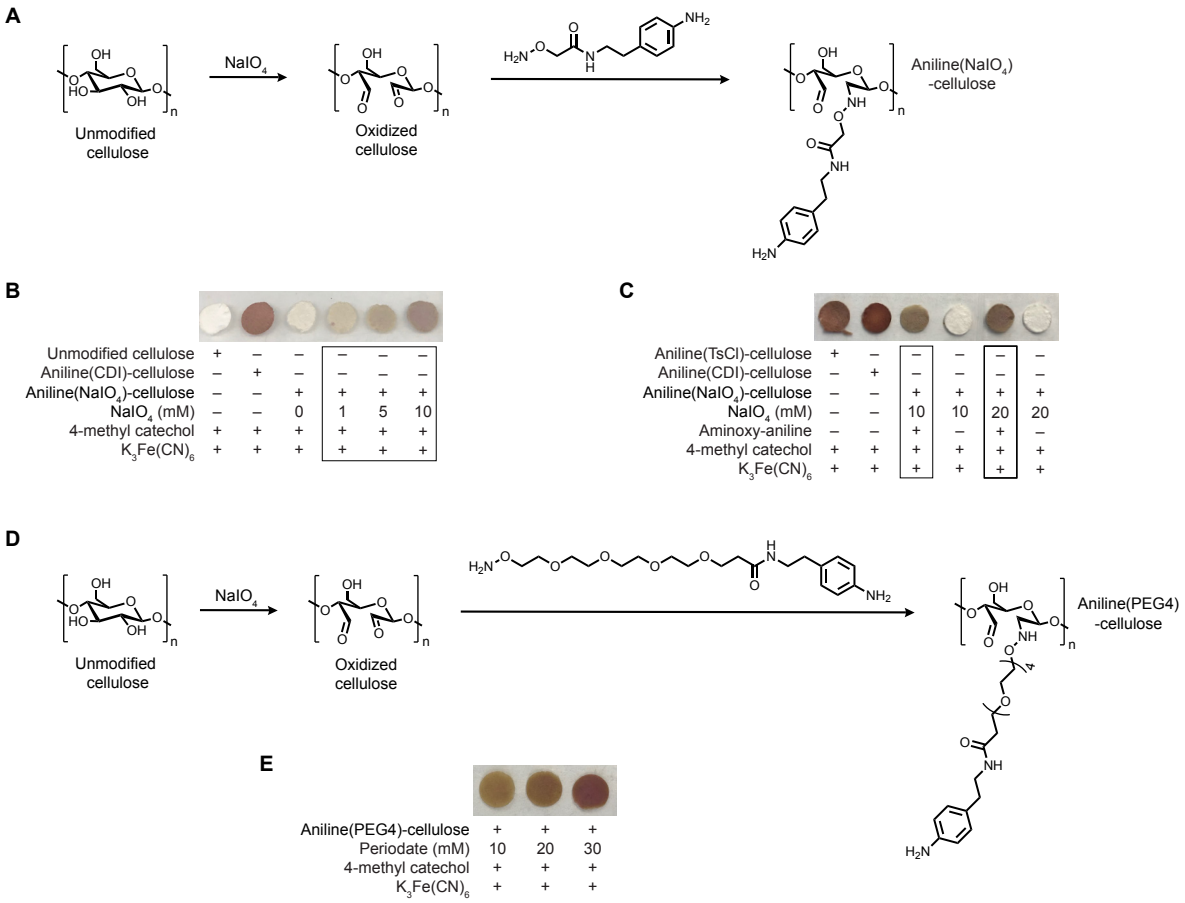

Figure 12. Aniline functionalization of cellulose through periodate oxidation. (A) Cellulose was exposed to sodium periodate ($NaIO_4$) to generate aldehydes. Subsequent ligation was carried out with a small aminoxy-aniline compound to generate aniline($NaIO_4$)-cellulose. (B) Upon oxidative coupling with 4-methyl catechol and $K_3Fe(CN)_6$, product was formed with a dependence on the concentration of $NaIO_4$ used during cellulose oxidation. (C) To verify that product is formed through reaction with anilines rather than aldehydes, oxidized cellulose was exposed to the oxidative coupling reaction (fourth and sixth columns). However, product was only formed when oxidized cellulose was ligated to aminoxy-aniline (third and fifth columns), confirming the importance of the aniline moiety. (D) To extend the distance between the cellulose surface and the aniline moiety, oxidized cellulose was ligated to an aminoxy-PEG4-aniline compound. (E) The density of product formed from subsequent oxidative coupling again depended on the concentration of $NaIO_4$ used during cellulose oxidation.

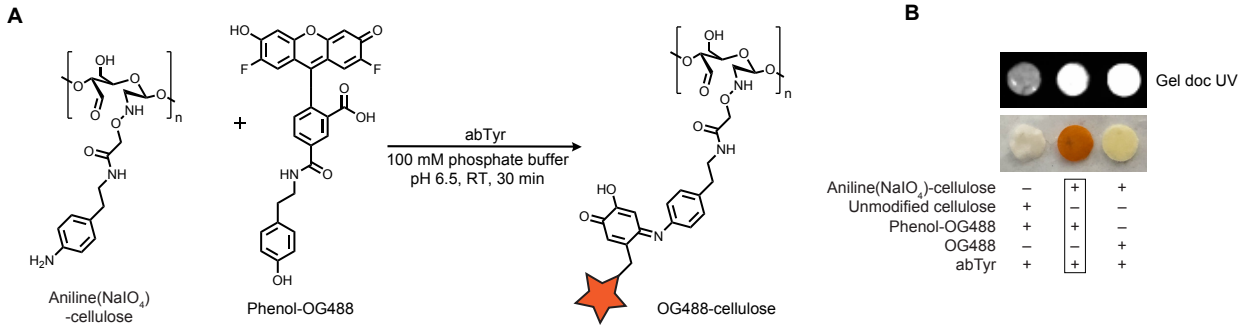

Figure 13. Oxidative coupling of Oregon Green 488 to aniline($NaIO_4$)-cellulose. (A) Oregon Green 488 (OG488) with a phenol functional moiety was conjugated to aniline(TsCl)-cellulose in the presence of abTyr. (B) Resulting product was observed both by eye and under UV light on a gel doc. Conjugation in the presence of abTyr and phenol-OG488 (middle column) was significantly darker than in the presence of abTyr and OG488 lacking a phenol group (far right column). This suggested successful oxidative coupling, although background adsorption was still observed (based on UV fluorescence).

OG488 (with no phenol) and abTyr. However, under UV light, both samples with aniline($NaIO_4$)-cellulose were fluorescently saturated, and thus it was difficult to discern how much more, if any, dye was immobilized with phenol-functionalized OG488. We also cannot rule out the possibility that phenol groups on the OG488 were oxidized by abTyr, polymerized in solution, and then deposited on the cellulose surface.

Encouraged by potentially reduced dye adsorption to aniline($NaIO_4$)-cellulose, we tested adsorption of proteins. mCherry with an engineered cysteine residue was incubated with aniline($NaIO_4$)-cellulose, along with unmodified cellulose and aniline(CDI)-cellulose. In contrast to aniline(CDI)-cellulose, which exhibited a strong fluorescence signal even after washing the cellulose samples, no mCherry was adsorbed to aniline($NaIO_4$)-cellulose. Motivated by this result, we next tested conjugation of DTNB-capped sfGFP-S64Y-S208C. Like with mCherry, no sfGFP was adsorbed in the absence of abTyr. However, there was also no coupling in the presence of abTyr, as observed by fluorescence under UV light. We reasoned that the short linkage of the aminoxy-aniline compound could make it difficult for the oxidized tyrosine residue on sfGFP-S64Y-S208C to access the nucleophilic coupling partner. To extend the distance between the cellulose surface and the aniline, we synthesized an aminoxy-aniline compound with a PEG4 linker and ligated this compound to oxidized cellulose (Figure 12D). While this yielded encouraging small molecule results (Figure 12E), the extended linker length did not increase the extent of sfGFP immobilization. It was possible that the apparent lack of sfGFP conjugation could be due to fluorescent quenching induced by immobilization of sfGFP in close proximity. However, quenching was not observed in other instances of sfGFP immobilization on cellulose. An sfGFP concentration study might yield insight into the potential of fluorescent quenching upon immobilization.

Because quenching of fluorescence was feasible, we wanted to develop a positive control for sfGFP immobilization that did not involve oxidative coupling directly on the cellulose surface. This control was facilitated by first generating aminoxy-cellulose. Cellulose was activated with CDI, followed by reaction with 1,8-diamino-2,6-dioxaoctane and subsequent addition of a small NHS-activated aminoxy (Figure S3A). We then reacted the aminoxy-cellulose with *o*-quinone-pro-sfGFP, which was produced by reaction of pro-sfGFP with *p*-cresol. *O*-quinone-pro-sfGFP features a reactive ketone at the site of oxidative coupling, and we previously demonstrated that this ketone can be ligated to a variety of aminoxy- or hydrazine-based nucleophiles.[31] As a control, aminePEG(CDI)-cellulose (the intermediate product in the synthesis of aminoxy-cellulose) was also exposed to *o*-quinone-pro-sfGFP. In comparison to unmodified cellulose, both aminePEG(CDI)-cellulose and aminoxy-cellulose became fluorescently saturating upon exposure to *o*-quinone-pro-sfGFP (Figure S3C), even after washing with 500 mM NaCl (which successfully removed *o*-quinone-pro-sfGFP from unmodified cellulose). The fluorescent saturation on aminePEG(CDI)-cellulose may have resulted from covalent conjugation of *o*-quinone-pro-sfGFP through alkylation with native lysine residues. While we were unable to verify covalent conjugation of *o*-quinone-pro-sfGFP to aminoxy-cellulose, this study further suggested that fluorescent quenching of immobilized sfGFP is unlikely.

4.2.7 Catechol and Phenol Functionalization of Cellulose

We initially chose to immobilize the nucleophilic coupling partner due to the potential of oxidation and self-coupling of catechols. However, we were also interested in immobilizing the electrophilic coupling partner. This would allow access to the wide range of nucleophiles compatible with the oxidative coupling reaction (Figure 2). As previously discussed, our lab has immobilized catechols on gold electrodes and accessed the *o*-quinone intermediate through electrochemical oxidation.[19] In this case, the immobilized catechols remained unreacted, and *o*-quinones were only accessed upon application of electrochemical potential. This uniform oxidation limited the potential for unoxidized catechols to serve as nucleophiles and react with *o*-quinone electrophiles. Encouraged by these results, we sought to immobilize catechols on cellulose. Initially, we generated catechol-cellulose through activation with tosyl chloride and subsequent tosylate displacement with the aliphatic amine of dopamine (Figure 14A). Addition of $K_3Fe(CN)_6$ and *p*-toluidine to the catechol(TsCl)-cellulose produced a brown color, which was not observed when *p*-toluidine was added in the absence of $K_3Fe(CN)_6$ (Figure 14B). Because the brown color did not occur when catechol(TsCl)-cellulose was exposed to only $K_3Fe(CN)_6$, the color can be attributed to the formation of the oxidative coupling product rather than oxidation and polymerization of surface catechols. Similar to oxidative coupling with aniline(TsCl)-cellulose, a yellow color was observed when catechol(TsCl)-cellulose was exposed to only $K_3Fe(CN)_6$. However, this adsorption could again be reversed by employing an NaOH wash after oxidative coupling.

We next tested catechol(TsCl)-cellulose in the context of protein oxidative coupling by reacting catechol(TsCl)-cellulose with pro-sfGFP (Figure S4A). However, like with protein coupling to aniline(TsCl)-cellulose, significant fluorescence was observed even in the absence of $K_3Fe(CN)_6$ (Figure S4B). This is again attributed to incomplete displacement

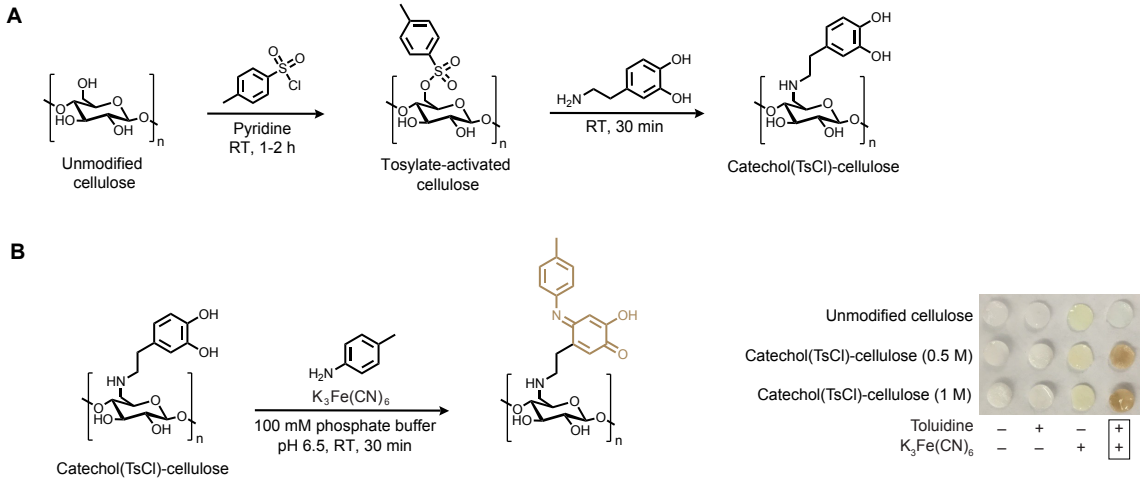

Figure 14. Phenol functionalization of cellulose through tosyl chloride activation. (A) Unmodified cellulose was reacted with tosyl chloride in the presence of pyridine to generate tosylate-activated cellulose. The tosylates were displaced by subsequent reaction with dopamine to generate catechol(TsCl)-cellulose. (B) Exposure of catechol(TsCl)-cellulose to *p*-toluidine and $K_3Fe(CN)_6$ produced a brown product that was not observed in the absence of $K_3Fe(CN)_6$ or absence of *p*-toluidine. The two different concentrations for catechol(TsCl)-cellulose represent two different concentrations of dopamine used during tosylate displacement.

of tosylates while generating catechol(TsCl)-cellulose and/or protonation of the secondary amine in the catechol linkage.

Initially, it was necessary to immobilize catechols as the electrophilic coupling partner because oxidative coupling via tyrosinase oxidation had not yet been established. However, the development of tyrosinase chemistry allowed us to immobilize phenols, which, unlike catechols, cannot be oxidized by oxygen alone and thus are less susceptible to self-coupling and polymerization. In solution, we have encountered steric- and charge-based limitations of phenol activation by abTyr as the abTyr active site is relatively small and features negatively charged residues. Thus we anticipated complications with enzymatic oxidation of surface phenols. However, we were encouraged by the finding that aniline(TsCl)-cellulose exposed to abTyr resulted in a distinct color change (see section 4.2.1). We initially generated phenol-cellulose through surface activation with tosyl chloride and then subsequent reaction with tyramine (Figure 15A). Upon exposure to abTyr, phenol(TsCl)-cellulose underwent a color change from white to gray (Figure 15B, third column), indicating that surface phenols are accessible to abTyr. Upon exposure to both abTyr and *p*-toluidine, we observed formation of an orange product (Figure 15B, first column). However, the orange color was observed both on the cellulose surface and in the coupling solution at the end of the reaction. As discussed in section 4.2.1, abTyr can also accept aniline moieties as substrates, and thus the orange color in solution was attributed to *p*-toluidine oxidation and subsequent polymerization.

The competition of aniline moieties with phenols for the abTyr active site highlights a limitation of this version of surface oxidative coupling. This limitation is further highlighted by small molecule oxidative coupling on phenol(CDI)-cellulose (Figure 15C

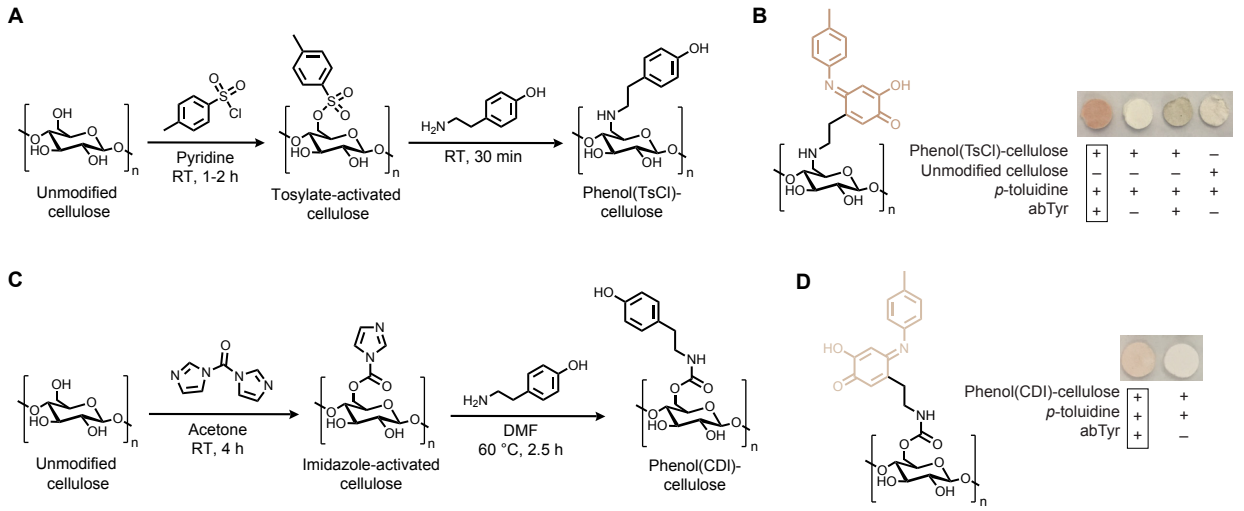

Figure 15. Phenol functionalization of cellulose through tosyl chloride or CDI activation. (A) Unmodified cellulose was reacted with tosyl chloride in the presence of pyridine to generate tosylate-activated cellulose. The tosylates were displaced by subsequent reaction with tyramine to generate phenol(TsCl)-cellulose. (B) Exposure of phenol(TsCl)-cellulose to *p*-toluidine and abTyr produced an orange product that was not observed in the absence of abTyr or when *p*-toluidine and abTyr were reacted with unmodified cellulose (although the coupling solution still turned orange). (C) Unmodified cellulose was reacted with CDI to generate imidazole-activated cellulose. Imidazole was displaced by subsequent reaction with tyramine to generate phenol(CDI)-cellulose. (C) Exposure of phenol(CDI)-cellulose to *p*-toluidine and abTyr produced a light orange product that was not observed in the absence of abTyr.

and 15D). In this case, an even lower density of orange product was observed on the cellulose surface. It is possible that the observed color on the surface was deposition of the polymerized aniline rather than oxidative coupling product. However, deposition was not observed when *p*-toluidine and abTyr were reacted with unmodified cellulose, despite the coupling solution turning orange. Thus if deposition was occurring, it was likely through an electrostatic interaction. If deposition was occurring, it may be necessary to reduce the concentration of aniline in the reaction solution and/or pre-activate the surface phenols with abTyr. However, care should be taken if employing the second approach since non-simultaneous oxidation of surface phenols could lead to polymerization. Thus it may be necessary to form a mixed monolayer on the cellulose surface that contains both phenols and aliphatic groups that cannot participate in the oxidative coupling reaction. Increasing the distance between neighboring phenol groups would help prevent surface polymerization in the case of non-uniform phenol oxidation.

For aniline-cellulose, the choice of cellulose activation strategy affected subsequent oxidative coupling reactions. We hypothesized that the same may be true for phenol-cellulose, and thus we also explored the oxime ligation method (see section 4.2.6) for generation of phenol-cellulose. We started by synthesizing an aminoxy-PEG4-phenol compound, which was subsequently ligated to oxidized cellulose (Figure S5A). To test oxidative coupling, we used L-proline methyl ester as the nucleophile rather than *p*-toluidine. The product of L-proline methyl ester coupled to small phenols is purple and absorbs at 520 nm. Thus the proline nucleophile again allowed us to monitor the oxidative coupling reaction through visual observation, but because L-proline methyl ester cannot be oxidized by abTyr, it avoided the limitations observed with *p*-toluidine. However, little to no product was formed when L-proline methyl ester was exposed to phenol(PEG4)-cellulose in the presence of abTyr. It was possible that the PEG4 linker was too short, leading to steric interactions that limited the ability of the abTyr active site to access surface phenols. Unfortunately, functionalization of oxidized cellulose with an aminoxy-PEG5k-phenol ligand (Figure S5B) also did not produce product when exposed to abTyr and L-proline methyl ester. Reaction of phenol(PEG5k)-cellulose with abTyr and *p*-toluidine again produced an orange color in solution, but very little, if any, color was observed on the cellulose surface (Figure S5C).

Overall, the most successful strategy for generating phenol-cellulose was initial activation with tosyl chloride. However, it is important to note that in the case of aniline(TsCl)-cellulose, charge interactions led to significant adsorption of $K_3Fe(CN)_6$ and biomolecules. Thus it possible that the higher quantity of product observed on phenol(TsCl)-cellulose, as compared to phenol-cellulose produced through other activation methods, could be the result of increased adsorbance of polymerized *p*-toluidine.

4.3 Conclusion and Future Outlook

In this chapter, we demonstrated several new methods for functionalizing cellulose with aniline to allow for oxidative coupling on the cellulose surface. Both $K_3Fe(CN)_6$ and abTyr are compatible oxidants, allowing conjugation to phenol, catechol, and aminophe-

nol functional groups. While small molecule oxidative coupling was successful across a range of cellulose functionalization strategies, oxidative coupling with biomolecules requires further optimization as significant background adsorption was observed. We also immobilized catechol and phenol moieties on cellulose and subsequently carried out oxidative coupling to aniline-containing small molecules. Again, further optimization is required before successful application of this method to conjugation of aniline-, proline-, or thiol-containing biomolecules. Optimization of oxidative coupling with small-molecule nucleophiles may also be required in the case of phenol-cellulose. Despite limited success of biomolecule conjugation, oxidative coupling on cellulose substrates could eventually have applications across a broad range of fields, particularly those for biosensors and point-of-care diagnostics.

4.4 Materials and Methods

General methods and instrumentation

Unless noted otherwise, all reagents were obtained from commercial sources and used without further purification. Valeric acid-PEG5k-amine was purchased from Laysan Bio (Arab, AL). Tyrosinase isolated from *Agaricus bisporus* (abTyr), Whatman No. 1 filter paper, all DNA sequences, tosyl chloride, isatoic anhydride, ethylenediamine, 4-(2-aminoethyl)aniline, sodium periodate, 4-nitrophenyl chloroformate, carbonyldiimidazole, 2-(2-methoxyethoxy)ethanamine, dopamine, and tyramine were purchased from Sigma-Aldrich (St. Louis, MO). Rhodamine-NHS, Oregon Green 488-NHS, and EZ-Link NHS-PEG4-biotin were purchased from Thermo Fisher (Waltham, MA). Spin concentrators were purchased from Millipore (Billerica, MA). Doubly distilled water (ddH_2O) was obtained from a Millipore purification system.

UV-vis Spectroscopy. UV-vis measurements were carried out with a Thermo Scientific Nanodrop 1000.

UV Analysis. UV images of cellulose samples were obtained with a Bio-Rad Gel Doc EZ System.

Elemental Analysis. Elemental analysis was carried out by the UC Berkeley Microanalytical Facility on a ThermoFisher Flash*Smart* Elemental Analyzer. One 6 mm diameter circle of cellulose was submitted for each sample.

FTIR Spectroscopy. FTIR analysis was carried out at the LBNL Catalysis Laboratory on a Bruker Vertex80 Time-resolved FTIR.

X-Ray Photo-Electron Spectroscopy. XPS was carried out at the Biomolecular Nanotechnology Center (UC Berkeley QB3) on a Physical Electronics 5600/5800 system.

NMR. ^{1}H spectra were recorded on either a Bruker AV-300 (300 MHz) or a Bruker AVB-400 (400 MHz) spectrometer.

Procedures for activating and functionalizing cellulose

Generating functionalized cellulose through tosylate activation.[22] Whatman No. 1 filter paper was cut into strips, submerged in 20% TFA in DCM, and incubated at room temperature for 10 min. The paper was transferred to DCM and incubated at room temperature for an additional 5 min. The DCM incubation step was repeated one time with fresh DCM. The paper was removed from DCM, dried under N_2, and submerged in 1 M tosyl chloride in pyridine for 1 h. The paper was washed by submerging two times in EtOH for 5 min and one time in DCM for 5 min and drying under N_2. The tosylate-activated cellulose was submerged in 1 M of primary amine compound (4-(2-aminoethyl)aniline, ethylenediamine, dopamine, or tyramine) in DMF and heated at 80 °C for 30 min. The functionalized cellulose was washed by consecutively submerging in the following solvents (5 min incubation for each): DMF, EtOH, 1 M NaOH, ddH_2O, EtOH (2x), and DCM. The cellulose was then dried under N_2 for 10 min. For samples reacted with butylamine, three 6 mm diameter circles of aniline(TsCl)-cellulose were submerged in 100 mM butylamine in DMF and incubated at room temperature for 4 h. The cellulose was then washed with DMF, EtOH, and DCM and dried under N_2. To determine the success of backfill, the samples were submerged in 1 M NaOH to release unreacted tosylates, followed by analysis of the solution by UV-vis absorbance at 260 nm.

Generating aniline(IA)-cellulose. Whatman No. 1 filter paper was cut into strips, submerged in 20% TFA in DCM, and incubated at room temperature for 10 min. The cellulose was then washed with EtOH and DCM and dried under N_2. The cellulose was washed two times with DMSO and then submerged in a solution of 0.16 M isatoic anhydride, 0.02 M DMAP, and 5% pyridine in DMSO. The reaction was gently stirred at 60 °C for 6 h under N_2. The N_2 was then removed, and the reaction was gently stirred overnight at 60 °C. The cellulose was washed with DMSO, acetone, and DCM (for each wash, the cellulose was submerged in the wash solvent and agitated for 5 min at room temperature) and dried under N_2.

Quantification of ester linkage hydrolysis. Each 6 mm diameter circle of aniline(IA)-cellulose was incubated with 200 µL of 100 mM phosphate buffer at pH 5, 6, 7, 8, or 9 for 2 h at room temperature. The UV-vis absorbance of the resulting solution was measured at 280 nm.

Generating aniline(SiIA)-cellulose.[32] (3-aminopropyl)triethoxysilane was dissolved in 80/20 (v/v) EtOH/ddH_2O at 10 mg/mL. Whatman No. 1 filter paper was cut into strips and submerged in the silane solution for 2 h. The silane/cellulose was then heated at 40 °C under N_2 for 2 h, after which the temperature was increased to 55 °C for 45 min and then increased to 65 °C for 15 min. The vial containing the cellulose was then transferred to an oven to dry completely. Once dry, the silanated paper was submerged in a 2:1 mixture of 100 mM phosphate buffer at pH 8 and 150 mM isatoic anhydride in DMF (50 mM final concentration of isatoic anhydride) and was stirred at room temperature for 1 h followed by washing with DMF, EtOH, and DCM and drying under N_2.

G*eneral procedure for generating aniline(NPC)-cellulose and 4-nitrophenol chloroformate quantification*.[28] Whatman No. 1 filter paper was cut into strips, submerged in THF, and subject to rotory evaporation under high vacuum at 70 °C to remove any excess water. Once all THF was removed, the cellulose was subject to further rotory evaporation for 30 min. Four 6 mm diameter circles of the dried cellulose were submerged in 1 mL of solvent (dry DCM, dry THF, or dry DMF) containing 150 μM 4-nitrophenol chloroformate (1 eq) and either 200 μL of triethylamine (TEA) or 120 μL of pyridine (10 eq). The mixtures were rotated at 4 °C for 30 min and then vortexed at 600 rpm overnight. The activated cellulose was washed three times with the reaction solvent and once with DCM and then dried under N_2. To quantify nitrophenyl, each 6 mm circle of activated cellulose was placed in a 96-well plate and covered with 50 μL of 0.2 M NaOH. After 25 min, the absorbance of the solution at 420 nm was determined.

Generating aniline(NPC)-cellulose with Na_2CO_3.[33] Three 6 mm circles of cellulose activated with 4-NPC (see above) were submerged in 1 mL of ddH_2O containing 150 mM 4-(2-aminoethyl)aniline (1 eq) and 600 mM Na_2CO_3 (4 eq). The mixture was heated at 50 °C for ~18 h, and then washed three times with ddH_2O, one time with EtOH, and two times with DCM and dried under N_2.

Generating aniline(NPC)-cellulose with DIPEA. Three 6 mm diameter circles of cellulose activated with 4-NPC (see above) were submerged in 1 mL of ddH_2O containing 150 mM 4-(2-aminoethyl)aniline (1 eq) and 80 μL N,N-diisopropylethylamine (3 eq). The mixture was vortexed at 600 rpm overnight and then washed two times with DMSO, one time with EtOH, and one time with DCM and dried under N_2.

Generating aniline(CDI)-cellulose and *phenol(CDI)-cellulose*.[29] Whatman No. 1 filter paper was washed sequentially with ddH_2O, 30/70 (v/v) acetone/ddH_2O, 50/50 (v/v) acetone/ddH_2O, 70/30 (v/v) acetone/ddH_2O, and acetone. The washed paper was submerged in 50 μmol/cm^2 CDI (based on total surface area of cellulose) in dry acetone. The reaction was stirred for 4 h at room temperature. The activated cellulose was washed four times with dry acetone and either stored in dry acetone at 4 °C or immediately carried forward. Final functionalization of the paper was carried out by submerging the CDI-activated cellulose in ~150 mM tyramine or 4-(2-aminoethyl)aniline in DMF and stirring at 60 °C for 2.5 h. The functionalized cellulose was washed two times with DMF, one time with DCM, one time with EtOH, and one time with DCM and then dried under N_2. To displace any remaining imidazole, the cellulose was incubated in 1 M ethanolamine in ddH_2O (adjusted to pH 7.5) for 1.5 h and then washed two times with ddH_2O, one time with 1 M NaCl, two times with ddH_2O, and one time with EtOH and then dried under N_2.

Generating aniline- or phenol-cellulose through oxidation and oxime ligation. Circles (6 mm diameter) of Whatman No. 1 filter paper were submerged in a solution containing sodium periodate (1, 5, 10, 20, or 30 mM final concentration) in 100 mM phosphate buffer with 125 mM NaCl at pH 7. The reaction was vortexed on low speed for 15 min. To quench oxidation, serine (20 mM final concentration) in ddH_2O was added, and the reaction was vortexed on low speed for another 10 min. The oxidized cellulose was carefully washed

three times with 100 mM phosphate buffer at pH 6. The cellulose was then submerged in a 4:1 solution of 100 mM phosphate buffer at pH 6 and 50 mM aminoxy compound (10 mM final concentration of aminoxy). The oxime ligation proceeded for 3 h to overnight at room temperature. Functionalized cellulose was washed two times with ddH_2O, two times with EtOH, and one time with DCM and then dried under N_2.

Generation of aminoxy-cellulose. Whatman No. 1 filter paper was activated with CDI as described above. The activated cellulose was stirred overnight at room temperature with 1 M 1,8-diamino-2,6-dioxaoctane in 1 M carbonate buffer at pH 9.5. The cellulose was washed two times with PBS containing 0.05% (v/v) tween 20, two times with PBS, one time with EtOH, and one time with DCM and then dried under N_2. The amine-modified cellulose was set aside. Meanwhile, a vial was flame-dried, and (boc-aminoxy)acetic acid (118 mg, 1 eq) was added to 8 mL of dry DCM. DCC (144 mg, 1.13 eq) and NHS (71 mg, 1 eq) were added, and the solution was stirred at room temperature for 15 min. The solution was then filtered through a 0.22 µm nylon syringe filter into a flame-dried vial. The amine-modified cellulose (ten 6 mm diameter circles) was added to the filtered solution, along with TEA (229 µL, 2.67 eq), and the reaction was stirred overnight at room temperature. The cellulose samples were washed three times with DCM and dried under N_2. Boc de-protection was facilitated by submerging the cellulose samples in 50/50 DCM/TFA for 1 h at room temperature with occasional swirling. The aminoxy-cellulose was washed three times with DCM and dried under N_2.

Generation of 2-(2-methoxyethoxy)ethanamine-cellulose. Whatman No. 1 filter paper was activated with CDI as previously described. The activated cellulose was submerged in 2-(2-methoxyethoxy)ethanamine (~330 mM in DMF) and heated at 60 °C for 2.5 h. The cellulose was washed two times with DMSO, one time with EtOH, and one time with DCM and dried under N_2.

Generation of ethanolamine-cellulose. Whatman No. 1 filter paper was activated with CDI as described above. The activated cellulose was submerged in an ethanolamine solution (aqueous 0.5 M ethanolamine with 0.5 M NaCl at pH 8) and rotated at room temperature for 2.5 h. The cellulose was washed two times with ddH_2O, one time with EtOH, and one time with DCM and dried under N_2.

Small molecule oxidative coupling

General procedure for small molecule oxidative coupling on aniline-cellulose. A 6 mm hole punch was used to cut circles out of functionalized cellulose strips. The circles were placed at the bottom of wells in a 96-well plate and covered with 50 µL of 1 mM 4-methyl catechol and 6 mM $K_3Fe(CN)_6$ in 100 mM phosphate buffer at pH 6.5. The reactions proceeded for 30-45 min at room temperature, followed by two washes with ddH_2O. For oxidative coupling with *p*-cresol, each circle of aniline-cellulose was exposed to 0.5 mM or 1 mM *p*-cresol and abTyr (200 nM to 1.3 µM) in phosphate buffer (20 to 50 mM) at pH 6.5. The reactions proceeded for 30 min to 1 h at room temperature, followed by two washes with ddH_2O.

General procedure for small molecule oxidative coupling on catechol-cellulose or phenol-cellulose. A 6 mm hole punch was used to cut circles out of functionalized cellulose strips. The circles were placed at the bottom of wells in a 96-well plate and covered with 50 µL of 1 mM *p*-toluidine and abTyr (200 nM to 1.3 µM) in phosphate buffer (20, 50, or 100 mM) at pH 6.5. The reactions proceeded for 30 min to 1 h at room temperature, followed by two washes with ddH_2O.

Blocking anilines on aniline(TsCl)-cellulose. A blocking solution was made by combining acetic anhydride and pyridine at a ratio of 9:1 acetic anhydride:pyridine. This solution was spotted onto aniline(TsCl)-cellulose with a pipet. The cellulose was washed with ddH_2O prior to subsequent oxidative coupling on unblocked regions of cellulose.

Oxidative coupling of phenol-fluorophores to aniline(TsCl)-cellulose. Phenol-rhodamine and phenol-OG488 were synthesized as previously described.[20] A 6 mm hole punch was used to cut circles out of aniline(TsCl)-cellulose strips. Each circle was exposed to 50 µL of 100 or 500 µM phenol-rhodamine (or 500 µM phenol-OG488) and 200 nM abTyr in 20 mM phosphate buffer at pH 6.5. The reactions were carried out on a shaking table for 1.25 h at room temperature. The functionalized cellulose was washed with ddH_2O and 500 mM aqueous NaCl.

Protein and DNA oxidative coupling on cellulose (and other biomolecule procedures)

DTNB capping of cysteine-exposed sfGFP. 5,5-dithio-bis-(2-nitrobenzoic acid) (DTNB, 2 mM final concentration) was combined with sfGFP-S64Y-S208C (100 µM) in 50 mM phosphate buffer at pH 8. The reaction incubated at room temperature for 15 min (a bright yellow color was observed). The solution was spin concentrated with 10 kDa MWCO spin filters and 10 mM phosphate buffer at pH 7.2 (4 spins total at 14,500 xg).

General procedure for oxidative coupling of tyrosine-containing sfGFP to aniline-cellulose. sfGFP (sfGFP-SG_4Y or DTNB-capped sfGFP-S64Y-S208C) was added at concentrations of 10, 25, or 50 µM to 6 mm diameter circles of aniline-cellulose in the presence of abTyr (either 200 nM or 4 mol% relative to sfGFP) in 10 mM phosphate buffer at pH 6.5 or 50 mM phosphate buffer at pH 8. Suggested conditions are 10 µM sfGFP with 200 mM abTyr in 20 mM phosphate buffer at pH 6.5. After reaction, cellulose samples were washed with phosphate buffer and sometimes additional buffers, including:
PBS with 2% tween 20
PBS with 2% tween 20 and 1 M NaCl
100 mM phosphate buffer at pH 7 or 9
100 mM phosphate buffer at pH 7 with 100 mM NaCl
100 mM phosphate buffer at pH 7 with 500 mM NaCl and 50 mM $MgSO_4$
10 mM glycine with 160 mM KCl at pH 2.2[30] (Note that sfGFP often unfolds below pH 6. Thus when the glycine wash was used, it was followed by incubation in 50 mM phosphate buffer at pH 8. Based on visual observation, this subsequent incubation did restore fluorescence.)

Oxidative coupling of pro-sfGFP to catechol(TsCl)-cellulose. Each 6 mm diameter circle of catechol(TsCl)-cellulose was incubated with 25 µL pro-sfGFP (50 µM) and 6 mM $K_3Fe(CN)_6$ in 20 mM phosphate buffer at pH 7. The reaction proceeded at room temperature for 1.5 h. The cellulose samples were washed with phosphate buffer.

Adsorption of mCherry to aniline($NaIO_4$)-cellulose. Cellulose (aniline($NaIO_4$)-cellulose, unmodified, or CDI-activated) was exposed to 50 µL of mCherry (containing an engineered cysteine residue, 10 µM) in 20 mM phosphate buffer at pH 6.5. The mCherry incubated with the cellulose samples for 1 h, followed my washing one time with 50 mM HEPES at pH 7 containing 300 mM $MgSO_4$ and one time with 100 mM phosphate buffer at pH 6.5 containing 1% Triton X-100.

Oxidative coupling to generate o*-quinone sfGFP.*[31] Pro-sfGFP (10 µM) was combined with *p*-cresol (100 µM) and resin-bound abTyr (10% v/v) in 20 mM phosphate buffer at pH 6.5. The reaction proceeded for 30 min at room temperature and was then filtered through a 0.22 µm cellulose acetate spin filter. TCEP was added to 1.9 mM final concentration, and the solution incubated at room temperature for 1 min, followed by centrifugation with 20 kDa MWCO spin filters and 20 mM phosphate buffer at pH 7.2. Successful oxidative coupling was confirmed with ESI-TOF MS.

Ligation of o*-quinone sfGFP to aminoxy-cellulose*. Each 6 mm circle of aminoxy-cellulose (or negative controls) was exposed to 33 µL of 10 µM *o*-quinone GFP in 50 mM phosphate buffer at pH 5. The samples were agitated overnight at room temperature and then washed one time with ddH_2O, one time with 0.5 M NaCl, and one time with ddH_2O.

Synthesis of aminophenol-DNA (AP-DNA).[14] 5' amine-DNA of the following sequence was used for all conjugation of DNA to cellulose: [AmC6]CCCTAGAGTGAGTCGTATGA. Amine-DNA (300 µM) in 50 mM phosphate buffer at pH 8 was combined at a ratio of 1:1 with 50 mM nitrophenol-NHS in DMF. The reaction was mixed and incubated at room temperature for 1.5 h. The reaction was filtered through a 0.22 µm cellulose acetate spin filter and then purified on a NAP-5 column with 10 mM phosphate buffer at pH 6.5. A 100 mM solution of $Na_2S_2O_4$ (in 100 mM phosphate buffer at pH 6.5) was added to 10% (v/v) (e.g. 50 µL was added to 500 µL of eluent from NAP column). The nitrophenol reduction was carried out at room temperature for 20 min and then purified with two NAP-5 columns (equilibrated with ddH_2O) and lyophilized.

Adsorption of ssDNA to DNA-cellulose. Each 6 mm diameter circle of aniline(TsCl)-cellulose or amine(TsCl)-cellulose was exposed to 50 µL of AP-DNA (50 µM) and $K_3Fe(CN)_6$ (1 mM) in either ddH_2O or 100 mM phosphate buffer at pH 6.5 or 8.1. The reaction proceeded for 45 min at room temperature, followed by one wash with ddH_2O, one wash with 1 M NaOH, and one wash with ddH_2O. Each sample was then exposed to 50 µL of 50 µM ssDNA (non-complementary to AP-DNA sequence) in 1x SSC buffer and incubated at room temperature for 10 min. The cellulose was washed two times with ddH_2O and then exposed to 100 µL of 1 M NaOH. After incubating at room temperature for ~10 min, the absorbance at 260 nm was measured to determine the amount of non-complementary

DNA adsorbed to DNA-aniline(TsCl)-cellulose and DNA-amine(TsCl)-cellulose.

Oxidative coupling of AP-DNA to aniline(IA)-cellulose. Each 6 mm diameter circle of aniline(IA)-cellulose was exposed to 50 µL of AP-DNA (50 µM) and $K_3Fe(CN)_6$ (300 µM) in 100 mM phosphate buffer at pH 6.5. The reaction proceeded for 30–45 min at room temperature, followed by washes with ddH_2O. Some samples were also washed with buffers at various pH levels and containing various concentrations of NaCl.

Synthetic procedures

Nitrophenol-NHS,[14] aminoxy-PEG4-aniline,[31] aminoxy-aniline,[34] phenol-rhodamine,[20] and phenol-OG488[20] were synthesized as previously described.

Synthesis of aminoxy-PEG4-phenol. (Boc-aminooxy)acetic acid (144 mg, 1 eq) was dissolved in 10 mL of dry DCM in a flame-dried vial. *N,N'*-Dicyclohexylcarbodiimide (DCC, 176 mg, 1.13 eq) and *N*-Hydroxysuccinimide (NHS, 87 mg, 1 eq) were added, and the reaction was stirred for 15 min at room temperature. The reaction was then filtered through a 0.22 µm PVDF syringe into a flame-dried vial. t-Boc-*N*-amido-PEG4-acid (200 mg, 1 eq) and triethylamine (TEA, 280 µL, 2.67 eq) were added to the filtered reaction and stirred at room temperature for 2 h. Solvent was removed by rotary evaporation, and the product was put under high vacuum for 30 min. Quantitative conversion was assumed. The vial containing the NHS-activated PEG4 compound was flushed with N_2, and then the compound was dissolved in 10 mL of dry DCM. DCC (176 mg, 1.13 eq) and NHS (87 mg, 1 eq) were added and the reaction was stirred for 15 min at room temperature. The reaction was filtered through a 0.22 µm PVDF syringe. Tyramine (124 mg, 1.2 eq) and TEA (280 µL, 2.67 eq) were added to the filtered solution, and the reaction was stirred overnight at room temperature. The reaction was filtered through celite and then a 0.22 µm PVDF syringe. Analysis by QTRAP LC-MS showed 458 as the main peak (the desired product minus the boc group). Solvent was removed by rotary evaporation, and the product was purified by flash silica column chromatography with a solvent system of 8% MeOH in DCM. After collecting the product, solvent was removed by rotary evaporation. Deprotection was carried out by dissolving the product in 1:1 DCM/TFA and allowing the reaction to proceed for 30 min at room temperature. Solvent was removed under N_2. The product was dissolved in 1 M NaOH in brine and then neutralized with 1 M HCl and lyophilized. The dried product was suspended in 0.7 mL ddH_2O and then filtered to remove excess salt. A clear, colorless solution was obtained at a concentration of 21 mM (based on an extinction coefficient of 1,420 $M^{-1}cm^{-1}$ for tyramine at 280 nm). The final product was confirmed by QTRAP LC-MS and ^1H NMR (AV300) in CD_3OD (Figure S6).

Synthesis of aminoxy-PEG5k-phenol. (Boc-aminooxy)acetic acid (28.4 mg, 1.5 eq) was dissolved in 5 mL of dry DCM in a flame dried vial. *N,N'*-Dicyclohexylcarbodiimide (DCC, 39 mg, 1.9 eq) and *N*-Hydroxysuccinimide (NHS, 27.6 mg, 2.4 eq) were added, and the reaction was stirred for 15 min at room temperature. The reaction was filtered through a 0.22 µm PVDF syringe into a flame-dried vial. Valeric acid-PEG5k-amine (200 mg, 1 eq) and triethylamine (TEA, 37 µL, 2.67 eq) were added to the filtered solution, and the reac-

tion was stirred at room temperature for 2 h. Solvent was removed by rotary evaporation, and then the product was put under high vacuum for 30 min. Quantitative conversion was assumed. The vial containing the NHS-activated PEG5k compound was flushed with N_2, and then the compound was dissolved in 6 mL of dry DCM. DCC (38.9 mg, 1.9 eq) and NHS (27.6 mg, 2.4 eq) were added, and the reaction was stirred for 15 min at room temperature. Tyramine (39 mg, 2.84 eq) and TEA (45 µL, 3.23 eq) were added to the filtered reaction and stirred overnight at room temperature. The reaction was filtered through celite and then a 0.22 µm PVDF syringe. Solvent was removed by rotary evaporation, and the product was placed under high vacuum until a white crystalline solid was obtained. The product was suspended in 8 mL of ddH_2O and filtered again through a 0.22 µm PVDF syringe before spin concentrating in 4 mL 3k MWCO spin filters (4,500 rpm for 10 min x2 and then 15 min x2). The concentrate was lyophilized to yield a fluffy white solid that was confirmed with ^1H NMR (AVQ 400) in $CDCl_3$ (Figure S7). Deprotection was carried out by dissolving the product in 1:1 DCM/TFA and allowing the reaction to proceed for 30 min at room temperature. Solvent was removed under N_2. The product was dissolved in ddH_2O and then adjusted to pH 7 with 1 M NaOH.

4.5 References

(1) Disposable Medical Sensors Market Size, Share & Trends Analysis Report By Product (Biosensors, Pressure, Accelerometer, and Temperature Sensor), By Type, By Application, And Segment Forecasts, 2018 - 2025. *Grand View Research* **2017**, Report ID: 978-1-68038-256-3.

(2) Dincer, C.; Bruch, R.; Costa-Rama, E.; Fernández-Abedul, M. T.; Merkoçi, A.; Manz, A.; Urban, G. A.; Güder, F. Disposable Sensors in Diagnostics, Food, and Environmental Monitoring. *Adv. Mat.* **2019**, *31* (30), 1806739.

(3) Li, H.; Steckl, A. J. Paper Microfluidics for Point-of-Care Blood-Based Analysis and Diagnostics. *Anal. Chem*. **2019**, *91* (1), 352–371.

(4) Martinez, A. W.; Phillips, S. T.; Whitesides, G. M.; Carrilho, E. Diagnostics for the Developing World: Microfluidic Paper-Based Analytical Devices. *Anal. Chem*. **2010**, *82* (1), 3–10.

(5) Credou, J.; Volland, H.; Dano, J.; Berthelot, T. A One-Step and Biocompatible Cellulose Functionalization for Covalent Antibody Immobilization on Immunoassay Membranes. J. *Mater. Chem. B* **2013**, *1* (26), 3277–3286.

(6) Pang, B.; Zhao, C.; Li, L.; Song, X.; Xu, K.; Wang, J.; Liu, Y.; Fu, K.; Bao, H.; Song, D.; Meng, X.; Qu, X.; Zhang, Z.; Li, J. Development of a Low-Cost Paper-Based ELISA Method for Rapid Escherichia Coli O157:H7 Detection. *Anal. Biochem.* **2018**, *542*, 58–62.

(7) Jarujamrus, P.; Tian, J.; Li, X.; Siripinyanond, A.; Shiowatana, J.; Shen, W. Mechanisms of Red Blood Cells Agglutination in Antibody-Treated Paper. *Analyst* **2012**, *137* (9), 2205–2210.

(8) Jeong, S.-G.; Kim, J.; Nam, J.-O.; Song, Y. S.; Lee, C.-S. Paper-Based Analytical Device for Quantitative Urinalysis. *Int. Neurourol. J.* **2013**, *17* (4), 155–161.

(9) Hong, W.; Jeong, S.-G.; Shim, G.; Kim, D. Y.; Pack, S. P.; Lee, C.-S. Improvement in the Reproducibility of a Paper-Based Analytical Device (PAD) Using Stable Co-

valent Binding between Proteins and Cellulose Paper. *Biotechnol. Bioproc. E* **2018**, *23* (6), 686–692.
(10) Arola, S.; Tammelin, T.; Setälä, H.; Tullila, A.; Linder, M. B. Immobilization–Stabilization of Proteins on Nanofibrillated Cellulose Derivatives and Their Bioactive Film Formation. *Biomacromolecules* **2012**, *13* (3), 594–603.
(11) ElSohly, A. M.; Francis, M. B. Development of Oxidative Coupling Strategies for Site-Selective Protein Modification. *Acc. Chem. Res.* **2015**, *48* (7), 1971–1978.
(12) Hooker, J. M.; Esser-Kahn, A. P.; Francis, M. B. Modification of Aniline Containing Proteins Using an Oxidative Coupling Strategy. *J. Am. Chem. Soc*. **2006**, *128* (49), 15558–15559.
(13) Behrens, C. R.; Hooker, J. M.; Obermeyer, A. C.; Romanini, D. W.; Katz, E. M.; Francis, M. B. Rapid Chemoselective Bioconjugation through Oxidative Coupling of Anilines and Aminophenols. *J. Am. Chem. Soc*. **2011**, *133* (41), 16398–16401.
(14) Obermeyer, A. C.; Jarman, J. B.; Netirojjanakul, C.; El Muslemany, K.; Francis, M. B. Mild Bioconjugation Through the Oxidative Coupling of *Ortho*-Aminophenols and Anilines with Ferricyanide. *Angew. Chem. Int. Ed.* **2014**, *53* (4), 1057–1061.
(15) Obermeyer, A. C.; Jarman, J. B.; Francis, M. B. N-Terminal Modification of Proteins with *o*-Aminophenols. *J. Am. Chem. Soc*. **2014**, *136* (27), 9572–9579.
(16) ElSohly, A. M.; MacDonald, J. I.; Hentzen, N. B.; Aanei, I. L.; El Muslemany, K. M.; Francis, M. B. *Ortho*-Methoxyphenols as Convenient Oxidative Bioconjugation Reagents with Application to Site-Selective Heterobifunctional Cross-Linkers. *J. Am. Chem. Soc.* **2017**, *139* (10), 3767–3773.
(17) Lobba, M. J.; Fellmann, C.; Marmelstein, A. M.; Maza, J. C.; Kissman, E. N.; Robinson, S. A.; Staahl, B. T.; Urnes, C.; Lew, R. J.; Mogilevsky, C. S.; Doudna, J. A.; Francis, M. B. Site-Specific Bioconjugation through Enzyme-Catalyzed Tyrosine–Cysteine Bond Formation. *ACS Cent. Sci.* **2020**, *6* (9), 1564–1571.
(18) Palla, K. S.; Hurlburt, T. J.; Buyanin, A. M.; Somorjai, G. A.; Francis, M. B. Site-Selective Oxidative Coupling Reactions for the Attachment of Enzymes to Glass Surfaces through DNA-Directed Immobilization. *J. Am. Chem. Soc*. **2017**, *139* (5), 1967–1974.
(19) Furst, A. L.; Smith, M. J.; Francis, M. B. Direct Electrochemical Bioconjugation on Metal Surfaces. *J. Am. Chem. Soc.* **2017**, *139* (36), 12610–12616.
(20) Maza, J. C.; Bader, D. L. V.; Xiao, L.; Marmelstein, A. M.; Brauer, D. D.; ElSohly, A. M.; Smith, M. J.; Krska, S. W.; Parish, C. A.; Francis, M. B. Enzymatic Modification of N-Terminal Proline Residues Using Phenol Derivatives. *J. Am. Chem. Soc*. **2019**, *141* (9), 3885–3892.
(21) Marmelstein, A. M.; Lobba, M. J.; Mogilevsky, C. S.; Maza, J. C.; Brauer, D. D.; Francis, M. B. Tyrosinase-Mediated Oxidative Coupling of Tyrosine Tags on Peptides and Proteins. *J. Am. Chem. Soc*. **2020**, *142* (11), 5078–5086.
(22) Bowman, M. D.; Jeske, R. C.; Blackwell, H. E. Microwave-Accelerated SPOT-Synthesis on Cellulose Supports. *Org. Lett.* **2004**, *6* (12), 2019–2022.
(23) Jin, L.; Li, W.; Xu, Q.; Sun, Q. Amino-Functionalized Nanocrystalline Cellulose as an Adsorbent for Anionic Dyes. *Cellulose* **2015**, *22* (4), 2443–2456.
(24) Hashem, A.; El-Shishtawy, R. M. Preparation and Characterization of Cationized Cellulose for the Removal of Anionic Dyes. *Adsorp. Sci. Tech.* **2001**, *19* (3), 197–

210.
(25) Pédelacq, J.-D.; Cabantous, S.; Tran, T.; Terwilliger, T. C.; Waldo, G. S. Engineering and Characterization of a Super-folder Green Fluorescent Protein. *Nature Biotech.* **2006**, *24* (1), 79–88.
(26) Yoo, H.; Jo, H.; Soo Oh, S. Detection and beyond: Challenges and Advances in Aptamer-Based Biosensors. *Mater. Adv.* **2020**, *1* (8), 2663–2687.
(27) Hooker, J. M.; Esser-Kahn, A. P.; Francis, M. B. Modification of Aniline Containing Proteins Using an Oxidative Coupling Strategy. *J. Am. Chem. Soc*. **2006**, *128* (49), 15558–15559.
(28) Mikulec, L. J.; Puleo, D. A. Use of P-Nitrophenyl Chloroformate Chemistry to Immobilize Protein on Orthopedic Biomaterials. *J. Biomed. Mater. Res.* **1996**, *32* (2), 203–208.
(29) Stöllner, D.; Scheller, F. W.; Warsinke, A. Activation of Cellulose Membranes with 1,1′-Carbonyldiimidazole or 1-Cyano-4-Dimethylaminopyridinium Tetrafluoroborate as a Basis for the Development of Immunosensors. *Anal. Biochem.* **2002**, *304* (2), 157–165.
(30) Byeon, J.-Y.; Limpoco, F. T.; Bailey, R. C. Efficient Bioconjugation of Protein Capture Agents to Biosensor Surfaces Using Aniline-Catalyzed Hydrazone Ligation. *Langmuir* **2010**, *26* (19), 15430–15435.
(31) Maza, J. C.; Ramsey, A. V.; Mehare, M.; Krska, S. W.; Parish, C. A.; Francis, M. B. Secondary Modification of Oxidatively-Modified Proline N-Termini for the Construction of Complex Bioconjugates. *Org. Biomol. Chem.* **2020**, *18* (10), 1881–1885.
(32) Koga, H.; Kitaoka, T.; Isogai, A. In Situ Modification of Cellulose Paper with Amino Groups for Catalytic Applications. *J. Mater. Chem*. **2011**, *21* (25), 9356–9361.
(34) Netirojjanakul, C.; Witus, L. S.; Behrens, C. R.; Weng, C.-H.; Iavarone, A. T.; Francis, M. B. Synthetically Modified Fc Domains as Building Blocks for Immunotherapy Applications. *Chem. Sci.* **2012**, *4* (1), 266–272.
(33) Vacondio, F.; Bassi, M.; Silva, C.; Castelli, R.; Carmi, C.; Scalvini, L.; Lodola, A.; Vivo, V.; Flammini, L.; Barocelli, E.; Mor, M.; Rivara, S. Amino Acid Derivatives as Palmitoylethanolamide Prodrugs: Synthesis, In Vitro Metabolism and In Vivo Plasma Profile in Rats. *PLOS ONE* **2015**, *10* (6), e0128699.

4.6 Supplementary Figures

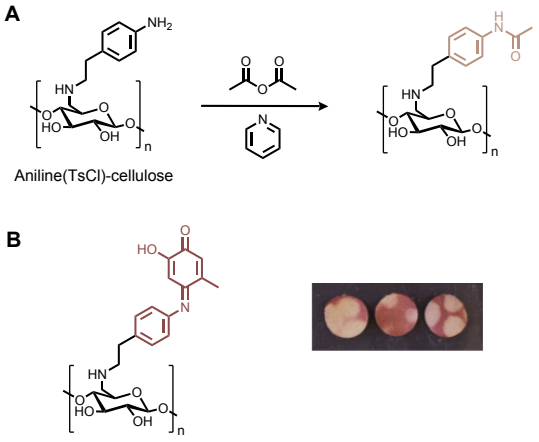

Figure S1. Blocking oxidative coupling on cellulose. (A) Aniline(TsCl)-cellulose was reacted with acetic anhydride in the presence of pyridine to acylate anilines and prevent oxidative coupling in specific sections of cellulose. (B) Subsequent oxidative coupling with 4-methyl catechol and $K_3Fe(CN)_6$ on blocked cellulose produced colored product only in regions of the aniline(TsCl)-cellulose that were not exposed to the acetic anhydride blocking solution.

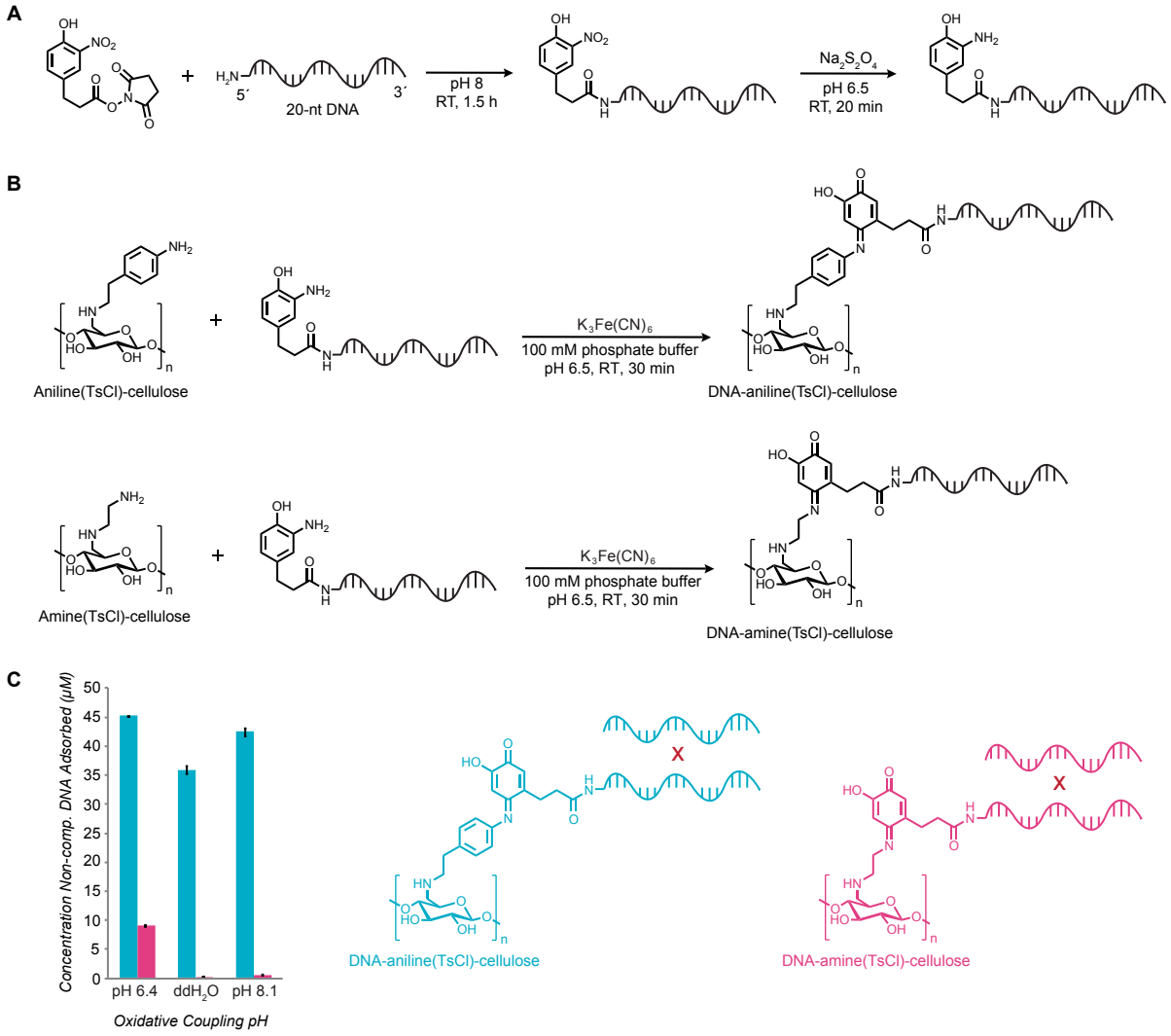

Figure S2. Synthesis and oxidative coupling of aminophenol-DNA. (A) Nitrophenol-NHS was reacted with commercially available 5' amine-DNA to generate nitrophenol-DNA, which was then reduced to aminophenol-DNA (AP-DNA) with sodium dithionite ($Na_2S_2O_4$). (B) Aniline(TsCl)-cellulose and amine(TsCl)-cellulose were oxidatively coupled to AP-DNA in the presence of K_3FeCN_6 (at various pH levels) to generate DNA-aniline(TsCl)-cellulose and DNA-amine(TsCl)-cellulose. (C) DNA-cellulose was exposed to ssDNA non-complementary to the AP-DNA sequence. To quantify the amount of ssDNA adsorbed, samples were exposed to 1 M NaOH and the resulting solutions were analyzed by determining absorbance at 260 nm.

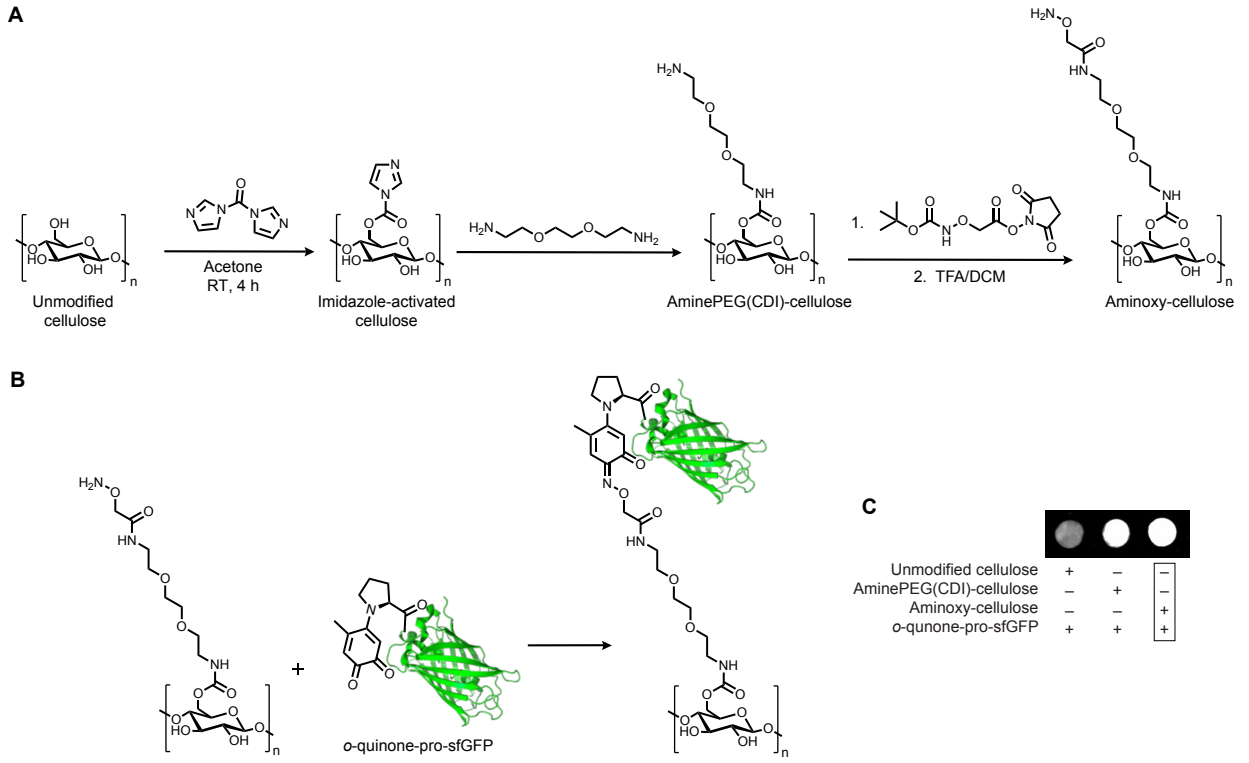

Figure S3. Generation of aminoxy-cellulose and ligation to *o*-quinone-pro-sfGFP. (A) Unmodified cellulose was activated with CDI to generate imidazole-activated cellulose. The imidazole was displaced through reaction with 1,8-diamino-2,6-dioxaoctane to generate aminePEG(CDI)-cellulose, which was then reacted with a boc-protected aminoxy-NHS compound. Deprotection of the aminoxy afforded aminoxy-cellulose. (B) Aminoxy-cellulose was ligated to *o*-quinone-pro-sfGFP to covalently immobilize sfGFP. (C) Strong fluorescence was observed when *o*-quinone-pro-sfGFP was exposed to either aminoxy-cellulose or aminePEG(C-DI)-cellulose. Immobilization on aminePEG(CDI)-cellulose may have resulted from alkylation with native lysine residues on sfGFP.

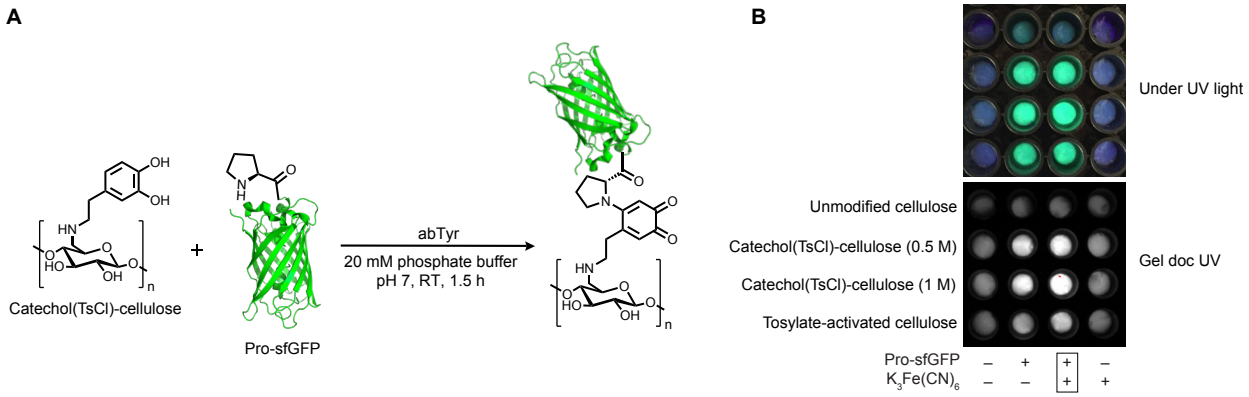

Figure S4. Oxidative coupling of pro-sfGFP to catechol(TsCl)-cellulose. (A) Catechol(TsCl)-cellulose was oxidized in the presence of abTyr and then coupled to pro-sfGFP. (B) Analysis by UV light revealed immobilization of pro-sfGFP on both catechol(TsCl)-cellulose (in the presence and in the absence of $K_3Fe(CN)_6$) and tosylate-activated cellulose.

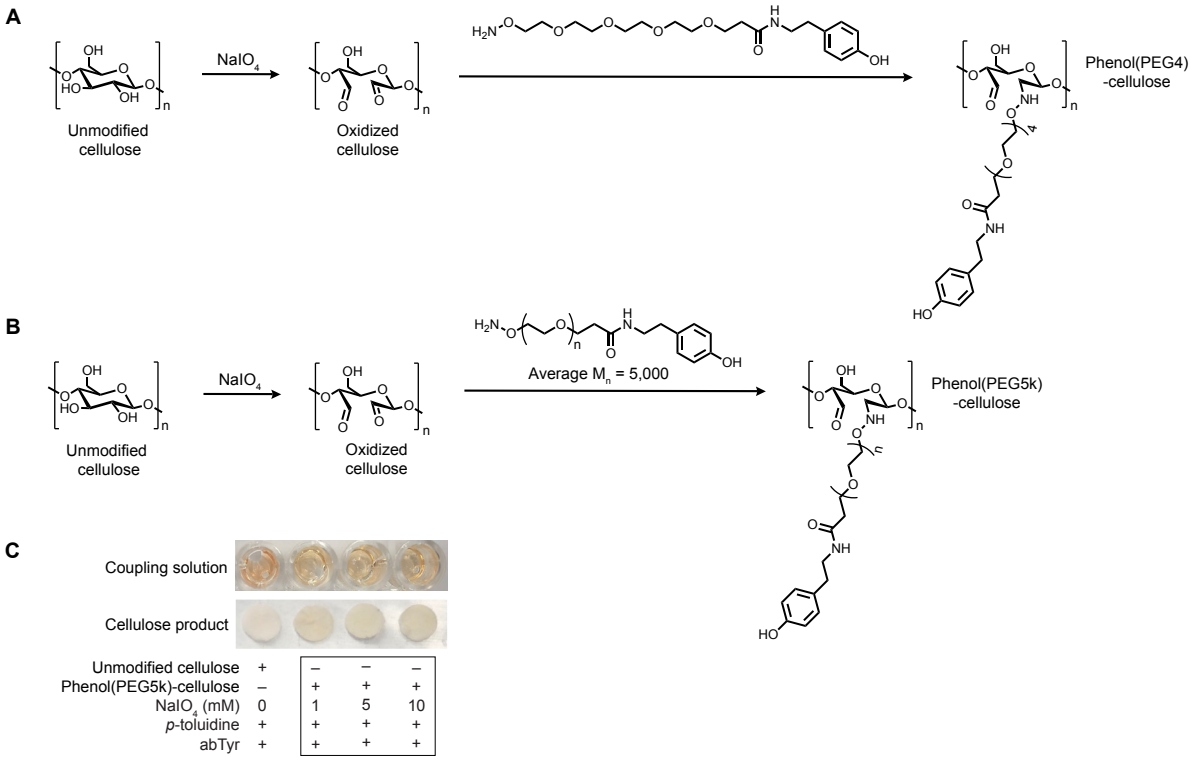

Figure S5. Phenol functionalization of cellulose through periodate oxidation. (A) Cellulose was exposed to sodium periodate ($NaIO_4$) to generate aldehydes. Subsequent ligation was carried out with an aminoxy-PEG4-aniline compound to generate phenol(PEG4)-cellulose. (B) Phenol(PEG5k)-cellulose was generated by first exposing cellulose to $NaIO_4$ and then subsequently ligating the generated aldehydes to an aminoxy-PEG5k-aniline compound. (C) Oxidative coupling of phenol(PEG5k)-cellulose to *p*-toluidine in the presence of abTyr produced an orange color in solution with little product on the cellulose surface.

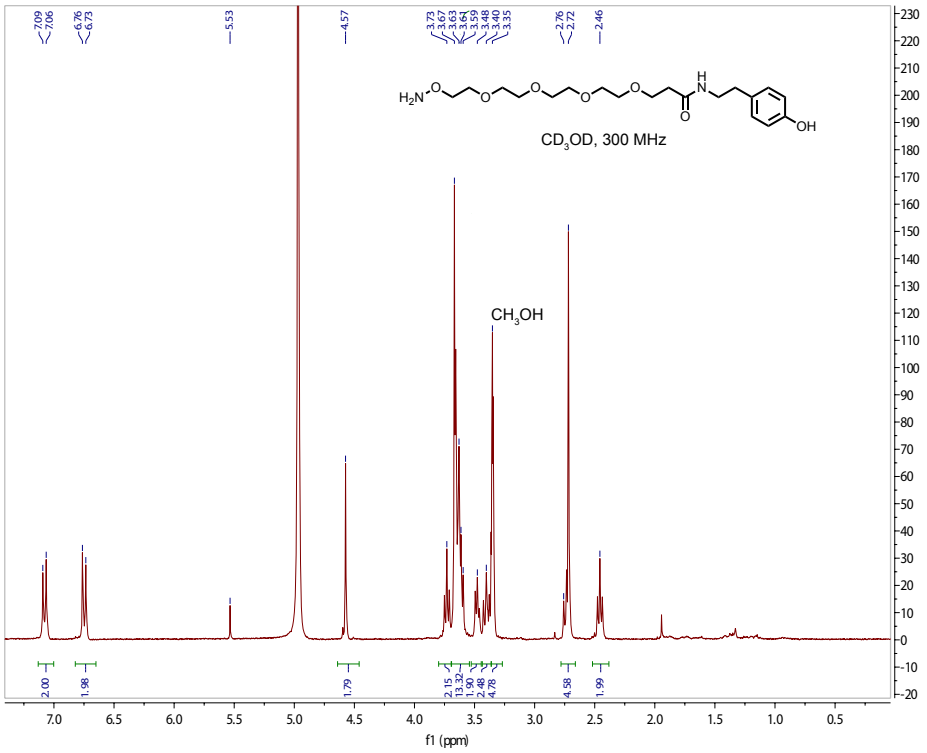

Figure S6. Characterization of aminoxy-PEG4-phenol via ^{1}H NMR.

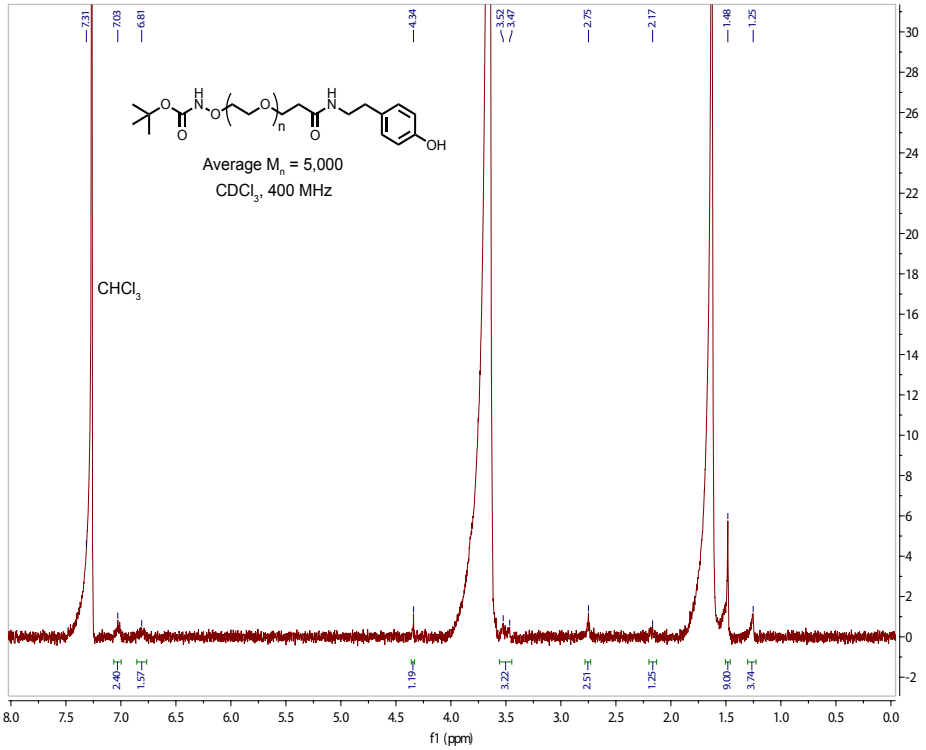

Figure S7. Characterization of boc-aminoxy-PEG5k-phenol via ^{1}H NMR.

Chapter 5

Progress Towards Regenerable SPR Chips and a Universal Biotinylation Strategy

Abstract

Surface Plasmon Resonance (SPR) is an important tool for studying protein-protein and protein-ligand interactions, but there are important limitations in current SPR technology that dampen the full application of this technique. To expand the utility of SPR, this chapter presents a new way to generate SPR sensor chips. The approach employs an oxidative coupling strategy to immobilize switchavidin, a mutant of streptavidin that exhibits reversible binding to biotin upon exposure to low pH/SDS conditions. The presented technique aims to produce chips that are (1) compatible with DNA-binding proteins and (2) can be regenerated for multiple analyses, two key limitations of the widely used Biacore sensing technology. Additionally, a new method is reported for protein biotinylation to enable subsequent SPR analysis or other applications where biotinylation is required. The biotinylation strategy relies on oxidative coupling between an engineered proline or tyrosine residue and biotin with a phenol or aniline functional group. Interleukin-1 beta is used as the model protein for these biotinylation studies. The fundamental theory and preliminary results are discussed for both regenerable sensor chip production and the biotinylation strategy.

5.1 Introduction

Surface Plasmon Resonance (SPR) is an optical technique used to study biological binding events.[1] The instrument set up for SPR involves a gold chip, a light source, a prism, and a detector (Figure 1A). The light source is directed through the prism toward the chip. When the beam of photons reaches the gold surface, two things happen: 1) the light is reflected toward the detector and 2) delocalized electrons in the gold atoms absorb some of the light. This absorption reduces the intensity of light encountered by the detector and produces a dip in the SPR Reflection Intensity Curve (Figure 1B). This intensity curve and its characteristic dips are also dependent on the resonance angle, which changes when a binding event occurs. SPR Reflection Intensity Curves are converted to resonance signal versus time graphs (Figure 1C) that can be correlated to characteristics of the sensor surface. Changes in the shape of resonance signal versus time graphs yield valuable insights into surface binding events.

SPR has found valuable application as a biosensor due to its ability to detect the binding of an analyte to a surface-immobilized recognition element.[2,3] SPR also enables the study of protein-ligand interactions and can even determine binding affinity and other kinetic parameters that are characteristic of a particular system.[1] Prior to exposure to a sample of interest, the gold surface must be functionalized with an appropriate biomole-

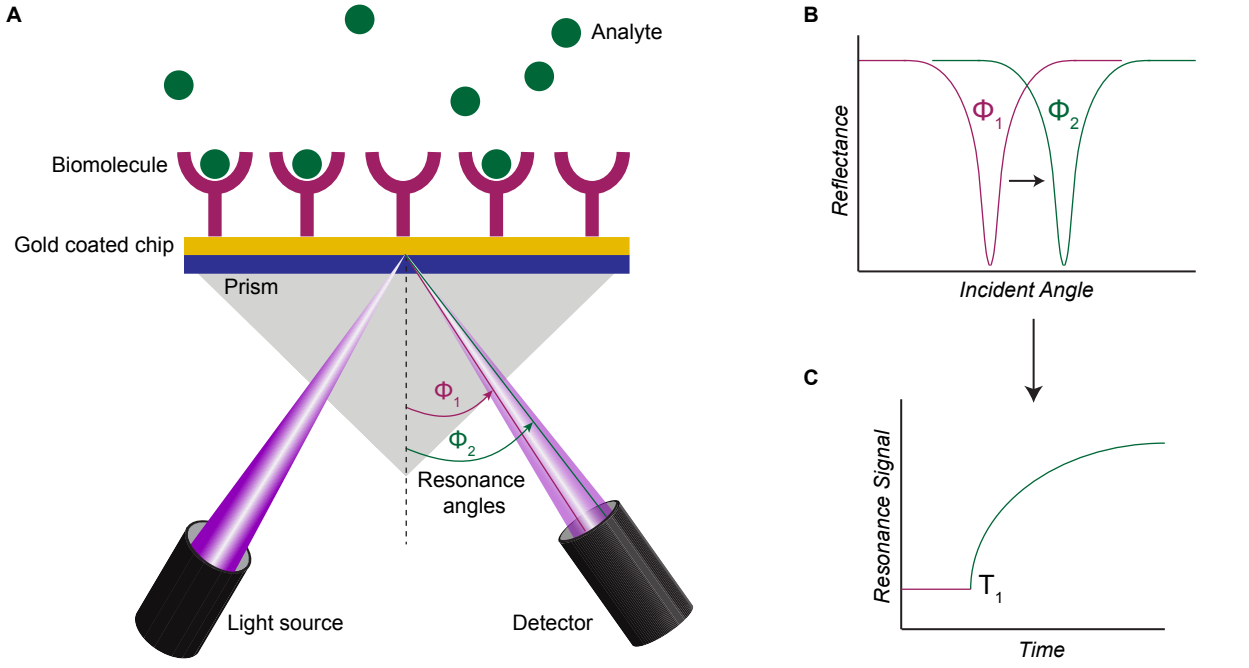

Figure 1. Surface Plasmon Resonance (SPR) analysis. (A) The instrument set-up for SPR consists of a gold chip coated with a biomolecule, a prism, a light source, and a detector. The incident light produced by the light source is reflected off of the gold chip toward the detector. The gold atoms in the chip absorb some of the light, resulting in reduced intensity of the reflected light. This produces a dip in the SPR Reflection Intensity Curve (B). The location of the dip depend on the resonance angle, which changes when a binding even takes place. For example, when binding of the analyte occurs, the maroon dip that corresponds to Φ_1 (absence of analyte) undergoes a shift that corresponds to the new resonance angle Φ_2 (green). (C) The SPR Reflection Intensity Curve can be converted into a Resonance Signal versus Time graph. These graphs provide valuable insight into the timing of binding events. For example, T_1 corresponds to the time at which analyte binding occurred.

cule, and it is imperative that the immobilization strategy does not affect the binding ability or affinity of the biomolecule.[4] Historically, immobilization has been achieved through chemisorption.[4] While easy to carry out, this method lacks control over biomolecule orientation, which can impact substrate binding. Additionally, chemisorption allows little control over the specific location of immobilization. Covalent immobilization approaches rely on formation of self-assembled monolayers on the sensor chip surface. These monolayers generate surfaces with maleimide,[5] aliphatic amine,[6] or NHS-ester[7] functional moieties for conjugation to protein cysteine, carboxylic acid, or lysine residues, respectively. These approaches are limited in that they may be reversible (in the case of maleimide surfaces) or lack site-specificity (in the case of aliphatic amine and NHS-ester surfaces). The overall deficiency of efficient chemistries for immobilizing biomolecules on gold surfaces can limit the performance and applicability of SPR analysis.

While there are a variety of sensor chips and systems available, one very commonly employed apparatus for studying molecular interactions is the Biocore system from Cytiva. This technology achieves sensing with the Biotin CAPture Kit ("CAP chip"), which relies on streptavidin-coated gold chips. The chips are first functionalized with ssDNA, which is then hybridized to a complementary strand that is covalently bound to streptavidin.[8] Biotinylated ligands or proteins are captured by the immobilized streptavidin, and the binding interactions are characterized by SPR. While this technology is successful, there are significant limitations. First, the nature of streptavidin immobilization makes the chips unsuitable for analysis of DNA-binding proteins. Second, the irreversible nature of streptavidin-biotin interactions limits the ability to regenerate a functional surface. Exposure of the chips to 8 M guanidine HCl and 1 M NaOH in a 3:1 ratio can denature the hybridized DNA and regenerate a DNA-coated surface. While useful, regenerating a surface for SPR analysis still requires subsequent hybridization to ssDNA-labeled streptavidin. This cumbersome step, which requires both conjugation of ssDNA to streptavidin and the hybridization, renders the costly CAP chips essentially single-use detection platforms. Additionally, even though the ssDNA surface can be regenerated, lack of compatibility with DNA-binding proteins is still a key limitation.

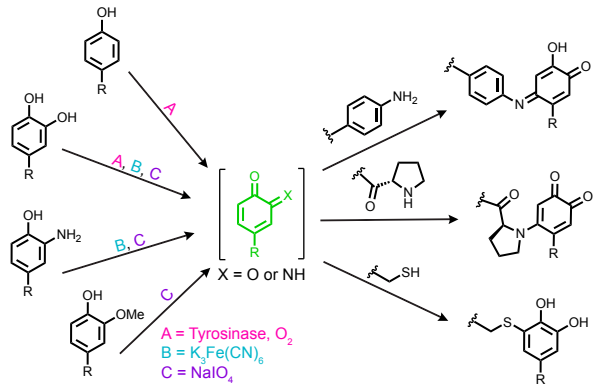

Figure 2. Oxidative coupling reactions. A variety of oxidants can be used to oxidize phenol based moieties to *ortho*-quinoid intermediates (green). These intermediates can undergo subsequent reactions with both amine- and thiol-based nucleophiles.

To address the obstacles faced with Biacore technology, we sought to develop more widely applicable and cost effective SPR chips that can be easily regenerated and used for multiple analyses. As an alternative to DNA hybridization for protein immobilization, we chose to employ our oxidative coupling strategy (Figure 2), which yields highly stable conjugates in a site-specific manner. In the oxidative coupling reaction, a phenol- or catechol-based electrophilic coupling partner is oxidized to an *ortho*-quinoid intermediate that can undergo subsequent

reaction with an amine-[9-14] or thiol-based[15] nucleophile. The reactive *o*-quinoid intermediate can be accessed by one of a variety of oxidants, depending on the identity of the electrophilic coupling partner. This versatile chemistry has enabled the construction of various bioconjugates that tether proteins, peptides, or nucleic acids to small molecules, other biomolecules, and even surfaces, such as glass[16] and gold electrodes.[17] More recently, we have developed an enzymatic version of the oxidative coupling reaction that allows *o*-quinones to be accessed from water soluble and highly stable phenols.[18] The enzyme, tyrosinase (abTyr), features a binuclear copper active site and is responsible for the formation of melanin. abTyr is isolated from the common button mushroom, *Agaricus bisporus*, and is commercially available in its active form. Past work has demonstrated that abTyr can oxidize phenols on a variety of substrates, including small molecules, peptides, and proteins. Our lab has also demonstrated successful oxidative couplings with a smaller (35.5 kDa versus ~120 kDa for abTyr) tyrosinase, megaTyr, from *Bacillus megaterium*.[19]

While oxidative coupling offers significant improvement over DNA-mediated immobilization, it does not directly enable functional gold chips to be regenerated. To achieve regeneration, we chose to employ the protein "switchavidin," a tetrameric variant of streptavidin that, like streptavidin, binds to biotin.[20,21] However, unlike streptavidin, which binds biotin essentially irreversibly, switchavidin binding can be reversed upon exposure to low pH/SDS conditions. Switchavidin exhibits five point mutations of the streptavidin gene sequence.[20] Two of these mutations are critical to the reversible nature of switchavidin (M96H and R114L) and the remaining three are neutralization mutations that aid in stability (K9E, R124H, and K127E). Switchavidin has been previously tested in the context of regenerable SPR sensor chips and found to be highly successful.[21] To immobilize switchavidin, two approaches are possible: (1) immobilization via binding to biotin-coated gold chips and (2) immobilization via direct covalent immobilization (Figure 3). Both approaches would allow DNA-binding proteins to be analyzed, but the first approach does not permit direct regeneration of functional surfaces and was thus explored as proof-of-concept for switchavidin immobilization and reversibility. This chapter reports progress towards each of these approaches, and further work will investigate both techniques in the context of SPR performance. Biotinylation of target proteins is another critical aspect of a functional SPR platform. Thus progress toward a universal protein biotinylation strategy is also discussed. Taken together, this work forms the foundation for generation of a broadly applicable and cost-effective SPR system that can enable the study of protein-ligand and protein-protein interactions.

5.2 Results and Discussion

5.2.1 Streptavidin Immobilization via Binding to Biotin-Coated Gold Chips

One approach to immobilize streptavidin is to first generate biotin-coated gold chips, which can then bind wild-type (WT) switchavidin (Figure 3A). Upon exposure to low pH/SDS conditions,[20] the biotinylated surface could be regenerated. We initially sought to generate phenol surfaces that could be coupled to aniline-containing biotin. This would

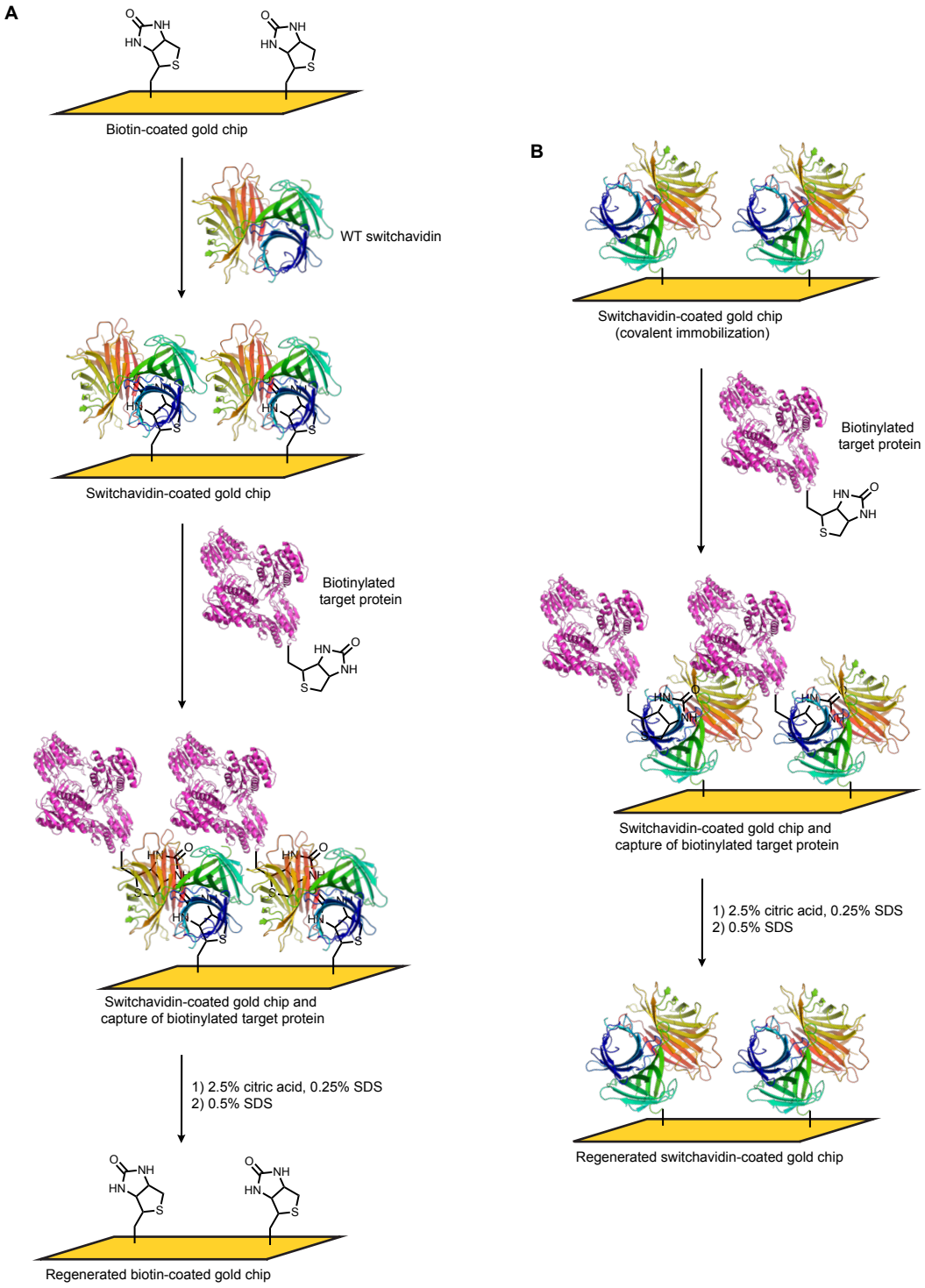

Figure 3. The two general approaches explored for regenerable SPR gold chips. (A) Functionalization of gold chips with biotin, followed by immobilization of WT switchavidin, would allow for regeneration of the biotin-coated surface after analysis of a biotinylated target protein. (B) Covalent immobilization of genetically engineered switchavidin on gold ships would allow for regeneration of the switchavidin-coated surface after analysis of a biotinylated target protein.

require oxidation of the surface phenols by abTyr, which was feasible based on successful activation of phenols on gold nanoparticle surfaces (see Chapter 3). To enable phenol functionalization of gold surfaces, a small thiol-phenol compound was synthesized by reacting tyramine with NHS-activated lipoic acid. After purification, the disulfide-C5-phenol compound was exposed to gold chips, along with 6-mercaptohexanol, to form self-assembled monolayers with varying ratios of phenols (Figure 4A). The ability to control the surface density of phenols is important in the context of switchavidin immobilization because phenol density will be directly correlated to biotin, and thus switchavidin, density. We envisioned that we would not need complete phenol surface coverage given that achieving high density of surface switchavidin does not necessitate a high degree of surface biotin. In fact, when switchavidin was previously immobilized on gold chips for SPR, a mixed monolayer of only 20% biotin was employed.[21] Additionally, high switchavidin surface density may not be required and could in fact be detrimental to the sensor chip performance since close clustering of switchavidin could hinder access to binding sites.

After generating the phenol-coated gold chips, the chips were exposed to abTyr and the aniline-containing biotin (Figure 4B). However, after reaction, the coupling solution was transparent orange in color. We have observed this in other instances of oxidative coupling when small molecule anilines were oxidized and subsequently polymerized. While abTyr binds more tightly to phenols, the enzyme can also accept aniline moieties as substrates, and, when in high enough concentration, anilines can out-compete phenols for binding. Thus we were concerned that abTyr was not able to access the surface phenols, leaving the aniline-biotin free in solution rather than coupled to the surface. To ex-

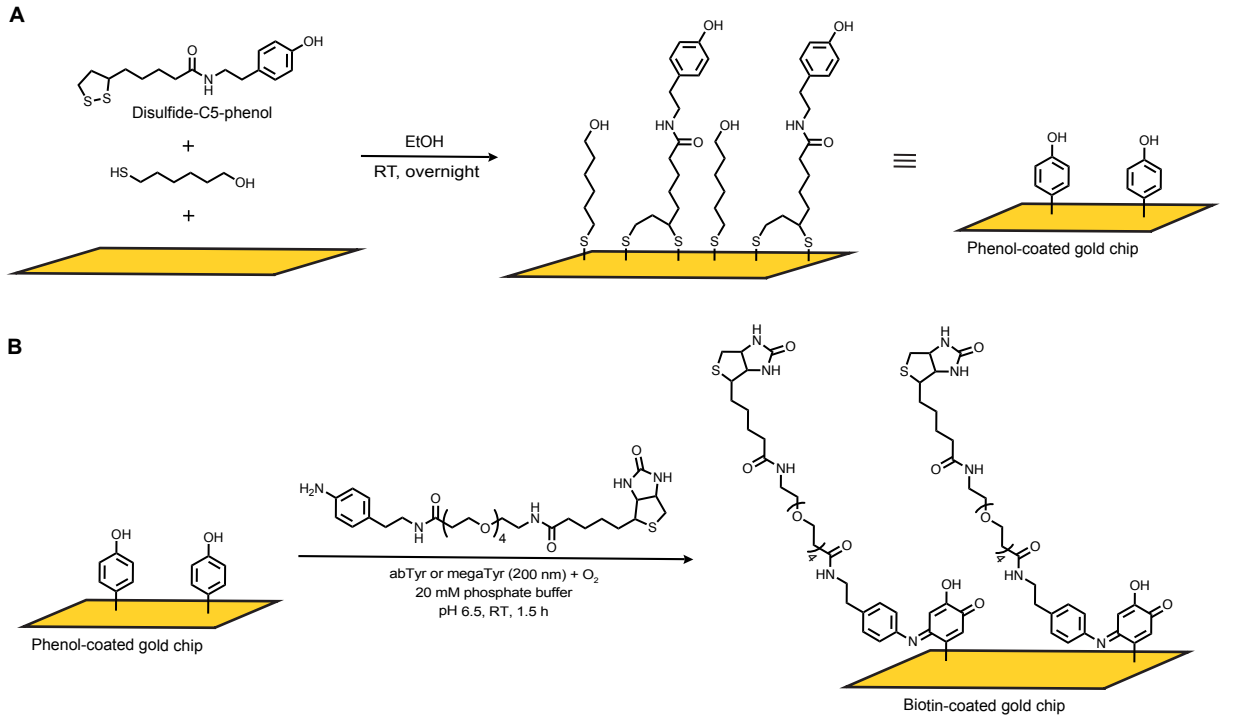

Figure 4. Generation of biotin-coated gold chips through phenol immobilization. (A) Exposure of gold chips to a mixture of disulfide-C5-phenol and 6-mercaptohexanol generated a mixed monolayer with phenol functional groups. (B) Oxidative coupling in the presence of abTyr or megaTyr and aniline-biotin may produce biotin-coated gold chips.

plore this further, we attempted to pre-activate the phenol surfaces by incubating the gold chips with abTyr for 30 min prior to the addition of aniline-biotin. However, the coupling solution still turned orange upon exposure of the pre-activated surface to aniline-biotin. It is possible that oxidative coupling on the surface was effective, and that the orange color resulted from polymerization of excess aniline-biotin in solution. It is important to point out, however, that in the context of gold nanoparticles, phenols were immobilized through a 5k PEG linker. In some cases, we have encountered steric- and charge-based limitations of phenol oxidation as the abTyr active site cavity is relatively small and features negatively charged residues. Thus the long linker employed for gold nanoparticles may be required for surface phenols to gain access to the sterically hindered active site of abTyr. Alternatively, the smaller megaTyr, which has a less sterically hindered active site and binds positive and negative substrates indiscriminately, may facilitate oxidative coupling directly on gold chip surfaces.

As an alternative method for generating biotin-coated chips, we synthesized a small molecule thiol-C5-aniline ligand in a manner analogous to that for the thiol-C5-phenol ligand. This compound was used to generate aniline-coated gold chips (Figure 5A), which were then oxidatively coupled to phenol-biotin in the presence of abTyr (Figure 5B). Similar to oxidative coupling of aniline-biotin, the solution turned orange, albeit lighter in color. However, it is still possible that oxidative coupling was successful and that the color resulted from polymerization of excess phenol-biotin. The success of this approach, as well as direct oxidation of surface phenols, will be determined by the ability of the functionalized chips to bind streptavidin (and eventually switchavidin) and subsequently facil-

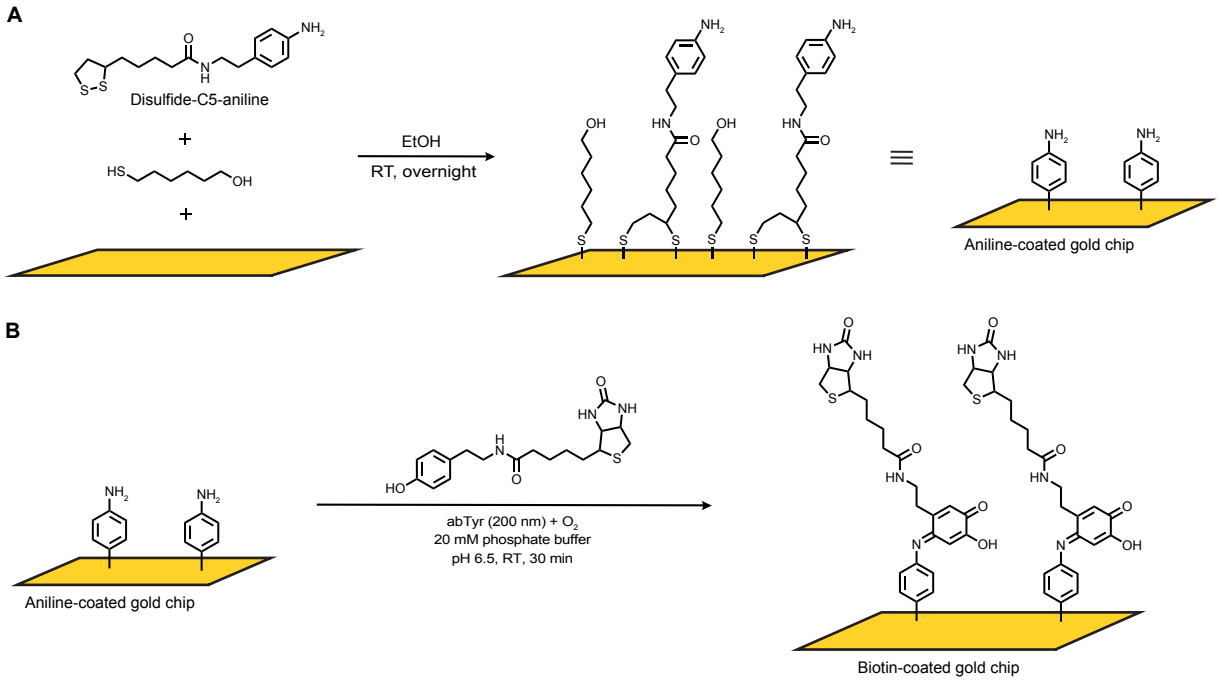

Figure 5. Generation of biotin-coated gold chips through aniline immobilization. (A) Exposure of gold chips to a mixture of disulfide-C5-aniline and 6-mercaptohexanol generated a mixed monolayer with aniline functional groups. (B) Oxidative coupling in the presence of abTyr and phenol-biotin may produce biotin-coated gold chips.

itate SPR analysis of biotinylated proteins.

5.2.2 Switchavidin Immobilization via Direct Covalent Conjugation

The other approach that we explored for switchavidin immobilization was direct covalent immobilization on the gold chip surfaces (Figure 3B). With the ability to generate either aniline- or phenol-coated gold chips, we designed two mutants of switchavidin: one with an N-terminal proline residue (pro-OmpA-SWA) for oxidative coupling to phenol-coated chips (assuming successful oxidation by abTyr or megaTyr, Figure 6A) and one with a C-terminal tyrosine tag (OmpA-SWA-SG_4Y) for oxidative coupling to aniline-coated chips (Figure 6B). Both switchavidin constructs contained OmpA, a bacterial signaling peptide that is reported to increase efficiency of protein production.[20] Golden Gate was used to clone the switchavidin gene (chicken avidin with the mutations previously described) containing an N-terminal OmpA sequence into a pET vector. Primers were designed to incorporate the N-terminal proline or C-terminal tyrosine tag into the OmpA-switchavidin gene. Gibson assembly was initially employed, but yielded no colonies. In contrast, the Golden Gate cloning was highly efficient and produced the desired clones, as confirmed by sequencing. WT switchavidin (WT-OmpA-SWA) was also cloned for immobilization on biotin-coated gold chips, as described in section 5.2.1. OmpA-SWA-SG_4Y and WT-OmpA-SWA were expressed according to the procedure previously reported for switchavidin expression in *E. coli*.[20] Once pro-OmpA-SWA is expressed, all constructs will be purified

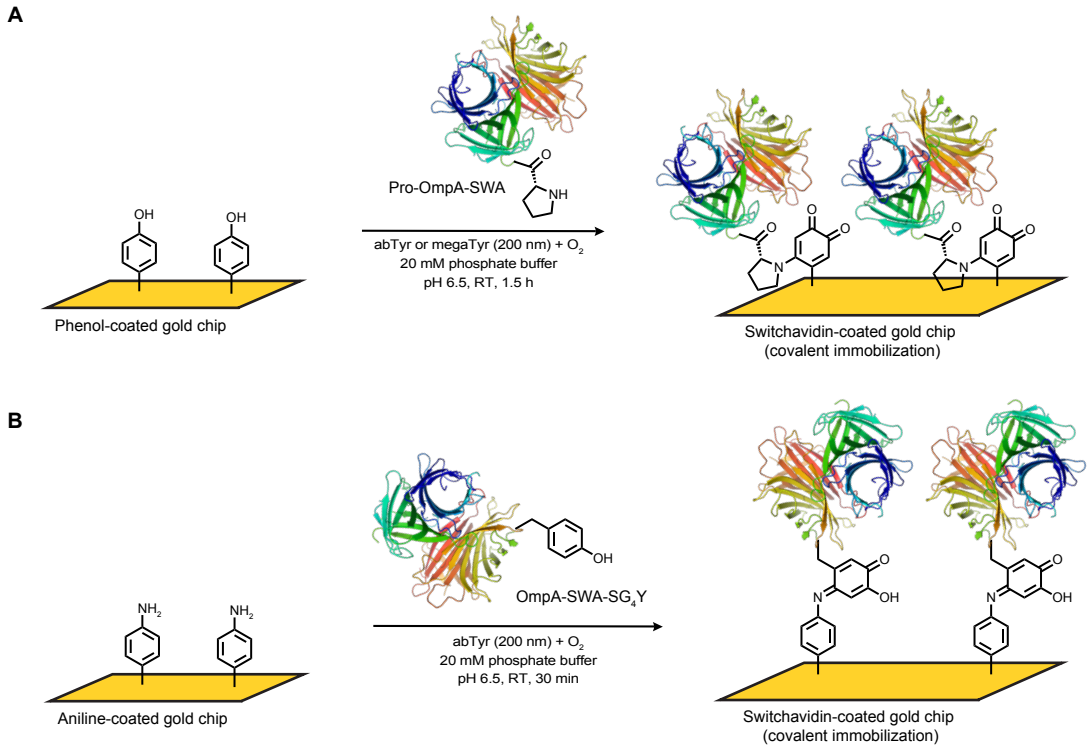

Figure 6. The two approaches explored for covalent immobilization of switchavidin. (A) N-terminal proline switchavidin can be oxidatively coupled to phenol-coated gold chips in the presence of abTyr or megaTyr. (B) C-terminal tyrosine switchavidin can be oxidatively coupled to aniline-coated gold chips in the presence of abTyr.

using 2-Iminobiotin Sepharose 4 Fast Flow.[20] The constructs will then be immobilized on phenol- or aniline-coated gold chips via enzymatic oxidative coupling and subsequently tested in the context of regenerable SPR surfaces (see Figure 3B).

5.2.3 Tyrosine-Tagged IL-1β Constructs for Universal Biotinylation

In order to bind to a streptavidin- or switchavidin-coated surface, the protein or ligand of interest must first be tagged with biotin.[22,23] Typically, this is carried out in a non-site-specific manner by targeting native lysine residues with an NHS-ester version of biotin.[24,25] Site-specificity, which is required to control orientation upon immobilization, can be achieved by reacting biotin-maleimide with engineered cysteine residues or by employing the enzymes sortase[26] or *E. coli* biotin ligase.[27,28] While labeling with these enzymes is effective, it requires incorporation of often lengthy recognition sequences during expression. This can significantly reduce the expression yield and can also affect the folding properties and activity of the purified protein. Thus, although critical in a variety of applications, protein biotinylation is actually non-trivial. As such, there is a need for new protein biotinylation methods.

The incorporation of a reactive tyrosine residue on proteins could enable quick biotin functionalization through subsequent oxidative coupling to biotin containing an aniline moiety. Alternatively, incorporation of an appropriate nucleophile would allow oxidative coupling to biotin containing a phenol moiety. Either approach could permit SPR analysis of substrate or analyte binding to the biotin-tagged target proteins. To investigate oxidative coupling as a method for protein biotinylation, Interleukin-1 beta (IL-1β) was used as a model protein. This would allow us to use SPR to monitor the effect of biotinylation and subsequent immobilization on protein function by testing the ability of IL-1β to interact with Interleukin-1 receptor.

The IL-1β sequence was equipped with a His6-tag and TEV cleavage site to allow for purification of the expressed proteins. During initial exploration, four variants of IL-1β were cloned containing: 1) an N-terminal proline, 2) an N-terminal tyrosine, 3) a C-terminal tyrosine, and 4) an N-terminal tyrosine and a C-terminal tyrosine. The N-terminal proline variant (pro-His6-TEV-IL1β) was designed to maintain the His6-tag and TEV cleavage site as we were concerned that incorporating the proline residue after the cleavage site might inhibit cleavage. Furthermore, we have previously left His6-tags uncleaved after purification and not observed deleterious affects on protein activity. However, all other constructs with N-terminal manipulation were mutated directly after the TEV cleavage site. The N-terminal proline mutant will allow oxidative coupling to phenol-biotin for an N-terminal biotin conjugate (Figure 7A). The N-terminal and C-terminal tyrosine tags (GYGGS-IL1β and IL1β-G_4Y, respectively) were constructed to generate both N- and C-terminal biotin conjugates (Figure 7B and 7C). Once immobilized, the activity of these conjugates will be compared to evaluate the effects on activity of immobilization via the N- versus C-terminus. The specific amino acid sequences used in these tags are based on tyrosine tags commonly employed by our lab.

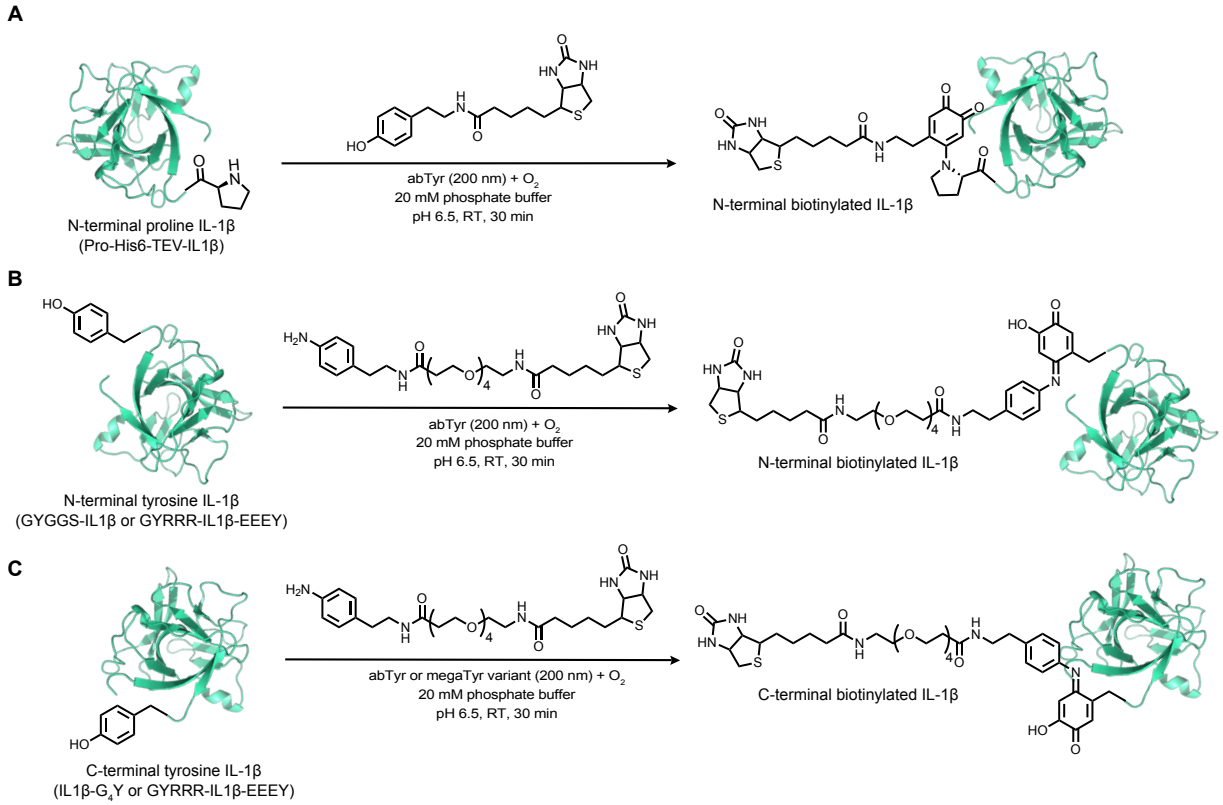

Figure 7. IL-1β mutants for site-selective biotinylation. Genetic manipulation of the IL-1β N-terminus to proline (A) or tyrosine (B) can enable selective biotinylation at the N-terminus through oxidative coupling with phenol- or aniline-biotin. In the case of GYRRR-IL1β-EEEY, the N-terminal tyrosine can be selectively oxidized by employing abTyr, which prefers positively-charged substrates. (C) Genetic manipulation of the IL-1β C-terminus to tyrosine can enable selective biotinylation at the C-terminus through oxidative coupling with aniline-biotin. In the case of GYRRR-IL1β-EEEY, the C-terminal tyrosine can be selectively oxidized by employing a variant of megaTyr that prefers negatively-charged substrates.

The final construct, with both N- and C-terminal tyrosine tags, was designed to exhibit a positively charged N-terminal tag and negatively charged C-terminal tag (GYRRR-IL1β-EEEY). We envisioned that by carefully choosing the right tyrosinase variant, we could selectively oxidize a single tyrosine residue at a specific terminus. For example, abTyr could be used for conjugation solely to the N-terminus (Figure 7B) while megaTyr mutants that prefer negatively charged substrates could be employed for conjugation solely to the C-terminus (Figure 7C). Selective oxidation will allow us to study the effect of orientation on binding further. The double mutant may also allow us to make two distinct modifications at both the N- and C-termini by carrying out sequential conjugations. This could be facilitated by first activating the N-terminus with a resin-bound version of abTyr,[29] which can be subsequently removed through filtration. The resulting conjugate could then be exposed to a megaTyr mutant for conjugation at the C-terminus.

Golden Gate cloning was used to successfully clone the genes for all four constructs into pET vectors (confirmed by sequencing), and expression was achieved by following an established procedure for IL-1β production in *E. coli*. Once purified with a nickel column, the IL-1β constructs will be oxidatively coupled to phenol- or aniline-containing

biotin. The resulting conjugates will be immobilized on switchavidin-coated gold chips, and their activity will be analyzed with SPR analysis.

5.3 Conclusion and Future Outlook

Application of the oxidative coupling strategy for immobilization of reversible streptavidin (termed “switchavidin”) has the potential to generate SPR sensor chips that are regenerable and compatible with a wider range of proteins than currently employed SPR technology. This chapter reports progress towards this goal and demonstrates synthesis of small molecule ligands for generation of functional gold chip monolayers, as well as successful cloning of WT switchavidin and switchavidin mutants that will allow covalent immobilization of switchavidin through enzymatic oxidative coupling. Additionally, a variety of IL-1β mutants have been successfully cloned. These mutants serve as a model system for the development of a universal biotinylation approach. Future work aims to use the synthesized small molecules for immobilization of biotin and subsequent binding of WT switchavidin, as well as formation of functional chips that will allow covalent immobilization of the switchavidin mutants. The resulting regenerable sensor chips will be used in combination with biotinylated IL-1β mutants to evaluate the efficacy of the SPR system. The optimized system will expand the scope and utility of SPR studies across a range of proteins and applications.

5.4 Materials and Methods

General methods and instrumentation

Unless noted otherwise, all reagents were obtained from commercial sources and used without further purification. Tyrosinase isolated from *Agaricus bisporus* (abTyr), aniline, tropolone, 6-mercaptohexanol, lipoic acid, 4-(2-aminoethyl)aniline, and tyramine were purchased from Sigma-Aldrich (St. Louis, MO). EZ-Link NHS-PEG4-biotin and EZ-Link NHS-biotin were purchased from Thermo Fisher (Waltham, MA). Doubly distilled water (ddH_2O) was obtained from a Millipore purification system. Gold chips were provided from the Biocore SIA Kit Au (product code: BR-1004-05). All primers and the OmpA-Switchavidin gene were obtained from Integrated DNA Technologies (Coralville, IA). The IL-1β plasmid was provided by Merck and Co. Phusion enzyme, T4 Ligase, and BsaI-HFv2 were purchased from New England Biolabs (Ipswich, MA).

NMR. ^{1}H spectra were recorded on a Bruker AV-300 (300 MHz) spectrometer.

Experimental procedures

Monolayer formation on gold chips. Gold chips were washed by submerging three times in EtOH. The washed chips were then submerged in 500 µL of a 250 µM ethanolic solution of disulfide-C5-phenol (or disulfide-C5-aniline) and 6-mercaptohexanol at various ratios (1:0, 9:1, 1:1, 1:9, and 0:1 of disulfide-C5-phenol:6-mercaptohexanol or disulfide-C5-aniline:6-mercaptohexanol). The chips incubated in the thiol solution for 24 h on a shaker

plate at room temperature. The chips were washed one time with EtOH, one time with ddH_2O, and one more time with EtOH, and then dried under a stream of N_2.

Oxidative coupling on phenol-coated gold chips. Gold chips prepared with phenol monolayers were subject to oxidative coupling with abTyr (200 nM) and aniline-PEG4-biotin (200 μM) in a 500 μL total reaction volume of 20 mM phosphate buffer at pH 6.5 (reactions were carried out in 20 mL scintillation vials). The reactions proceeded at room temperature, while shaking, for 1.5 h. The chips were then flipped over and reacted for another 1.5 h at room temperature. Quenching was carried out by adding tropolone (1 mM) and aniline (5 mM) and exposing the solution to each side of the chip for 10 min. The chips were washed one time with EtOH, one time with ddH_2O, and one more time with EtOH, and then dried under a stream of N_2. Note that only one side of the chips are coated with gold, and thus for future modification, only side of the chip needs to be exposed to the oxidative coupling solution.

Oxidative coupling on phenol-coated gold chips with pre-activation of surface phenols. Gold chips prepared with phenol monolayers were incubated with abTyr (200 nM) in 20 mM phosphate buffer at pH 6.5 (500 μL total reaction volume) for 30 min prior to adding aniline-PEG4-biotin (100 μM final concentration) and allowing to react an additional 1 h at room temperature. The reaction was quenched by the addition of tropolone (1 mM) and aniline (5 mM) and subsequent incubation for 10 min. The chips were washed one time with EtOH, one time with ddH_2O, and one more time with EtOH, and then dried under a stream of N_2.

Oxidative coupling on aniline-coated gold chips. Gold chips prepared with aniline monolayers were subject to oxidative coupling with abTyr (200 nM) and phenol-biotin (200 μM) in a 500 μL total reaction volume of 20 mM phosphate buffer at pH 6.5 (reactions were carried out in 20 mL scintillation vials). The reactions proceeded at room temperature, while shaking, for 30 min. The chips were then flipped over, exposed to fresh oxidative coupling solution (containing abTyr, phenol-biotin, and 20 mM phosphate buffer at pH 6.5), and reacted for another 30 min at room temperature. Quenching was not necessary. The chips were washed one time with EtOH, one time with ddH_2O, and one more time with EtOH, and then dried under a stream of N_2. Note that only one side of the chips are coated with gold, and thus for future modification, only side of the chip needs to be exposed to the oxidative coupling solution.

Assembly of sensor chips. Modified chips we assembled into sensor chip supports by following the protocol provided by the manufacturer. Chips were assembled in Series S format.

Switchavidin cloning

OmpA-switchavidin gene (used as template for all constructs; bold italic portion corresponds to the switchavidin gene; italic portion corresponds to the OmpA signaling peptide):
ATGAACAAGCCGTCTAAATTCGCTCTTGCATTAGCATTCGCTGCCGTAACTGCATC-

*GGGGGTCGCCTCAGCGCAGACTGTA**GCGCGTAAGTGTTCTTTGACCGGAGAGT-GGACGAACGATTTGGGTTCCAATATGACCATCGGTGCCGTGAATAGTCGTGGT-GAGTTCACAGGAACATATATCACTGCCGTTACAGCCACAAGTAACGAAATTAAA-GAGTCCCCTCTGCATGGAACGCAGAATACTATCAATAAGCGCACCCAGCCAA-CATTCGGGTTCACCGTAAATTGGAAGTTTTCGGAAAGCACCACCGTCTTCACCG-GACAGTGCTTCATTGATCGTAACGGGAAGGAGGTCTTGAAAACTCATTGGTTAT-TACGCAGTAGCGTTAATGACATTGGCGACGACTGGAAGGCTACATTAGTCGGCAT-TAACATCTTCACACGTCTTCACACGCAGGAGGAATAA***

Primers used for switchavidin constructs (all are from 5' to 3'; bold italic portions represent overlap to the OmpA-switchavidin gene):

Fwd WT primer: aGGTCTCaC***ATGAACAAGCCGTCTAAATTCGCTCTTG***
Rev WT primer: aGGTCTCaT***TTATTCCTCCTGCGTGTGAAGACGTG***

Fwd pro primer: aGGTCTCaC***ATGCCGAACAAGCCGTCTAAATTCGCTCTTGC***
Rev pro primer: Rev WT primer

Fwd SG_4Y primer: Fwd WT primer
Rev SG_4Y primer: aGGTCTCaT***TTAATAGCCGCCGCCGCCGCTTTCCTCCTGCGTGT-GAAGACGTG***

PCR (with Phusion enzyme) was used to generate the WT-OmpA-SWA, pro-OmpA-SWA, and OmpA-SWA-SG_4Y inserts from the OmpA-switchavidin gene and the appropriate primers. Golden Gate cloning (with T4 Ligase and BsaI-HFv2) was then used to insert the genes into a pET vector with a sfGFP insert and kanamycin resistance. The plasmids containing the SWA genes were transformed into *E. coli* DH5alpha cells using a standard heat shock protocol. After streaking on a LB/kanamycin agar plate, resistant colonies were grown overnight in LB containing kanamycin. Plasmids were isolated using a QIAprep Spin Miniprep Kit (Qiagen, Redwood City, CA). Sequences were confirmed with Sanger Sequencing at the UC Berkeley Sequencing Facility.

*IL-1*β *cloning*

Merck and Co. provided a plasmid containing the IL-1β gene with a His6-tag and TEV cleavage site at the N-terminus. The amino acid sequence for the IL-1β gene in the plasmid was as follows (with the native IL-1β sequence in bold):
MGSSHHHHHHSSGENLYFQGS***APVRSLNCTLRDSQQKSLVMSGPYEKALHLQGQD-MEQQVVFSMSFVQGEESNDKIPVALGLKEKNLYLSCVLKDDKPTLQLESVDPKNYP-KKKMEKRFVFNKIEINNKLEFESAQFPNWYISTSQAENMPVFLGGTKGGQDITDFT-MQFVSS***

Primers used for IL-1β constructs (all are from 5' to 3'; bold italic portions represent overlap to the His6-TEV-IL1β gene):

Fwd1 pro-His6-TEV-IL1β: aGGTCTCaC***ATGCCGGGCAGCAGCCATCATCATCACATC***
Rev1 pro-His6-TEV-IL1β: aGGTCTCaT***TTAGCTGCTAACGAACTGCATGGTGAAATC***

Fwd1 GYGGS-IL1β: aGGTCTCaC***ATGGGCAGCAGCCATCATCATCATCATCACAG-CAGCGGCGAAAACC***
Rev1 GYGGS-IL1β: aGGTCTCa***GTATCCCTGAAAATACAGGTTTTCGCCGCTGCTGT-GATG***
Fwd2 GYGGS-IL1β: aGGTCTCa***ATACGGCGGCTCCGCTCCGGTGCGTAGC***
Rev2 GYGGS-IL1β: Rev1 pro-His6-TEV-IL1β

Fwd1 IL1β-G_4Y: aGGTCTCaC***ATGGGCAGCAGCCATCATCATCATCATC***
Rev1 IL1β-G_4Y: aGGTCTCaT***TTAATAGCCGCCGCCGCCGCTGCTAACGAACTGCAT-GGTGAAATC***

Fwd1 GYRRR-IL1β-EEEY: aGGTCTCaC***ATGGGCAGCAGCCATCATCATCATCATCAC AGCAGCGGCGAAAAC***
Rev1 GYRRR-IL1β-EEEY: aGGTCTCa***GCGATATCCCTGAAAATACAGGTTTTCGC-CGCTGCTGTGATGATG***
Fwd2 GYRRR-IL1β-EEEY: aGGTCTCa***TCGCCGCCGCAGCGCTCCGGTGCGTAGC***
Rev2 GYRRR-IL1β-EEEY: aGGTCTCaT***TTAATATTCTTCTTCGCTGCTAACGAACTG-CATGGTGAAATC***

The His6-TEV-IL1β provided by Merck was used as the template for pro-His6-TEV-IL1β and IL1β-G_4Y during PCR amplification (with Phusion enzyme). For GYGGS-IL1β and GYRRR-IL1β-EEEY, the fwd2 and rev2 primers were combined with the template during PCR while the fwd1 and rev1 primers were exposed to PCR in the absence of template. Golden Gate cloning (with T4 Ligase and BsaI-HFv2) was then used to insert the genes into a pET vector with a sfGFP insert and kanamycin resistance. Two inserts were included for GYGGS-IL1β and GYRRR-IL1β-EEEY. The plasmids containing the IL-1β genes were transformed into *E. coli* DH5alpha cells using a standard heat shock protocol. After streaking on a LB/kanamycin agar plate, resistant colonies were grown overnight in LB containing kanamycin. Plasmids were isolated using a QIAprep Spin Miniprep Kit (Qiagen, Redwood City, CA). Sequences were confirmed with Sanger Sequencing at the UC Berkeley Sequencing Facility.

Switchavidin expression

Switchavidin expression was based on a literature protocol.[20] Miniprepped plasmid was transformed into *E. coli* BL21 DH3 cells using a standard heat shock protocol. After streaking on a LB/kanamycin agar plate, resistant colonies were grown overnight in LB containing kanamycin. Overnight cultures were added to pre-warmed LB containing kanamycin and 0.1% glucose (1 mL of overnight culture per 100 mL LB). Cultures were grown at 27 °C to an OD_{600} of ~0.3, after which IPTG and L-arabinose were added to final concentrations of 1 mM and 0.2% (w/v), respectively. The cultures continued to incubate at 27 °C overnight. The next morning, cells were pelleted at 7,000 rpm for 15 min at 4 °C. Pellets

were stored at -80 °C until purification.

*IL-1*β *expression*

IL-1β expression was based on a protocol provided by Merck and Co. Miniprepped plasmid was transformed into *E. coli* BL21 DH3 cells using a standard heat shock protocol. After streaking on a LB/kanamycin agar plate, resistant colonies were grown overnight in LB containing kanamycin. Overnight cultures were added to pre-warmed LB containing kanamycin (1 mL of overnight culture per 100 mL LB), and cultures were grown at 37 °C to an OD_{600} of ~0.7–0.8, after which IPTG was added to a final concentration of 0.5 mM. The cultures continued to incubate at 37 °C for 3 h, and then the temperature was reduced to 20 °C, and incubation proceeded overnight. The next morning, cells were pelleted at 7,000 rpm for 15 min at 4 °C. Pellets were stored at -80 °C until purification.

Synthetic procedures

Biotin-PEG4-aniline. EZ-Link NHS-PEG4-biotin (44 mM, 1.1 eq) was combined with 4-(2-aminoethyl)aniline (1 eq) in DMF. The mixture was rotated end-over-end overnight at room temperature. Formation of the product was confirmed with LC-MS. The solution was diluted to a concentration of 4.5 mM prior to use. QTOF-MS: m/z for $C_{28}H_{47}N_5O_7S$ $[M+H]^+$ 610.3, observed 610.3.

Biotin-phenol. Biotin-phenol was synthesized as previously described.[18] Briefly, EZ-Link NHS-biotin (50 mM, 1 eq) was combined with tyramine (55 mM, 1.1 eq) in DMF, and the reaction was rotated end-over-end at RT. The solution was diluted 10-fold with ddH_2O and allowed to stand at room temperature for 24 h before use.

Lipoic acid-NHS (based on previously reported procedure[30]). Lipoic acid (406 mg, 1 eq) and N-hydroxysuccinimide (230 mg, 1eq) were dissolved in 4 mL of dry DCM. Separately, N,N'-dicyclohexylcarbodiimide (DCC) (413 mg, 0.94 eq) was dissolved in 3 mL of dry DCM. The lipoic acid solution was added drop-wise to the DCC solution, and the mixture was stirred on ice for 1 h. The reaction was then stirred at 4 °C for 1 h, after which the stirring was stopped and the mixture was left overnight at 4 °C. The next morning, the mixture was placed in a -20 °C freezer for 30 min. The solution was then filtered with a Buchner funnel, and the collected solid was washed with two 3 mL portions of DCM that were pre-cooled to -20 °C. The filtrate was collected and subjected to rotary evaporation. The resulting pale-yellow solid was confirmed by ^1H NMR in $CDCl_3$ (NMR provided in Chapter 3, Figure S11).

Disulfide-C5-phenol. Tyramine (66 mg, 1 eq) was combined with lipoic acid-NHS (145 mg, 1 eq) in 5 mL of dry DCM. N,N-diisopropylethylamine (DIPEA, 187 µL, 1.5 eq) was added, and the mixture was stirred overnight at room temperature. The next day, the reaction was filtered through a 0.22 µm PVDF filter. Solvent was removed by rotary evaporation, and the resulting product was purified with silica flash chromatography using a solvent system of 8% methanol in DCM. After rotary evaporation, the resulting yellow oil

(141.5 mg) was confirmed by ^{1}H NMR in CD_3CN (Figure S1).

Disulfide-C5-aniline. 4-(2-aminoethyl)aniline (80 mg, 1 eq) was combined with lipoic acid-NHS (182 mg, 1 eq) in 5 mL of dry DCM. DIPEA (157 µL, 1.5 eq) was added, and the mixture was stirred overnight at room temperature. The next day, the reaction was filtered through a 0.22 µm PVDF filter. Solvent was removed by rotary evaporation, and the resulting product was purified with silica flash chromatography using a solvent system of 8% methanol in DCM. After rotary evaporation and drying under house vacuum, the resulting deep orange solid (171 mg) was confirmed by ^{1}H NMR in CD_3CN (Figure S2).

5.5 References

(1) Douzi, B. Protein–Protein Interactions: Surface Plasmon Resonance. In Bacterial Protein Secretion Systems: Methods and Protocols; Journet, L., Cascales, E., Eds.; *Methods in Molecular Biology*; Springer: New York, NY, **2017**, 257–275.

(2) Wang, X.; McKay, P.; Yee, L. T.; Dutina, G.; Hass, P. E.; Nijem, I.; Allison, D.; Cowan, K. J.; Lin, K.; Quarmby, V.; Yang, J. Impact of SPR Biosensor Assay Configuration on Antibody: Neonatal Fc Receptor Binding Data. *mAbs* **2017**, 9 (2), 319–332.

(3) Pattnaik, P. Surface Plasmon Resonance. *Appl. Biochem. Biotechnol.* **2005**, *126* (2), 79–92.

(4) Oliverio, M.; Perotto, S.; Messina, G. C.; Lovato, L.; De Angelis, F. Chemical Functionalization of Plasmonic Surface Biosensors: A Tutorial Review on Issues, Strategies, and Costs. *ACS Appl. Mater. Interfaces* **2017**, *9* (35), 29394–29411.

(5) Ferrero, V. E. V.; Andolfi, L.; Di Nardo, G.; Sadeghi, S. J.; Fantuzzi, A.; Cannistraro, S.; Gilardi, G. Protein and Electrode Engineering for the Covalent Immobilization of P450 BMP on Gold. *Anal. Chem.* **2008**, *80* (22), 8438–8446.

(6) Wong, L. S.; Khan, F.; Micklefield, J. Selective Covalent Protein Immobilization: Strategies and Applications. *Chem. Rev.* **2009**, *109* (9), 4025–4053.

(7) Baniukevic, J.; Kirlyte, J.; Ramanavicius, A.; Ramanaviciene, A. Application of Oriented and Random Antibody Immobilization Methods in Immunosensor Design. *Sensor Actuat. Chem-B* **2013**, *189*, 217–223.

(8) BIAcore application note “Biotin CAPtureKit”, GE data file 28-9577-47 AA.

(9) ElSohly, A. M.; Francis, M. B. Development of Oxidative Coupling Strategies for Site-Selective Protein Modification. *Acc. Chem. Res.* **2015**, *48* (7), 1971–1978.

(10) Hooker, J. M.; Esser-Kahn, A. P.; Francis, M. B. Modification of Aniline Containing Proteins Using an Oxidative Coupling Strategy. *J. Am. Chem. Soc*. **2006**, *128* (49), 15558–15559.

(11) Behrens, C. R.; Hooker, J. M.; Obermeyer, A. C.; Romanini, D. W.; Katz, E. M.; Francis, M. B. Rapid Chemoselective Bioconjugation through Oxidative Coupling of Anilines and Aminophenols. *J. Am. Chem. Soc*. **2011**, *133* (41), 16398–16401.

(12) Obermeyer, A. C.; Jarman, J. B.; Netirojjanakul, C.; El Muslemany, K.; Francis, M. B. Mild Bioconjugation Through the Oxidative Coupling of *Ortho*-Aminophenols and Anilines with Ferricyanide. *Angew. Chem. Int. Ed.* **2014**, *53* (4), 1057–1061.

(13) Obermeyer, A. C.; Jarman, J. B.; Francis, M. B. N-Terminal Modification of Proteins with *o*-Aminophenols. *J. Am. Chem. Soc*. **2014**, *136* (27), 9572–9579.

(14) ElSohly, A. M.; MacDonald, J. I.; Hentzen, N. B.; Aanei, I. L.; El Muslemany, K. M.; Francis, M. B. *Ortho*-Methoxyphenols as Convenient Oxidative Bioconjugation Reagents with Application to Site-Selective Heterobifunctional Cross-Linkers. *J. Am. Chem. Soc.* **2017**, *139* (10), 3767–3773.
(15) Lobba, M. J.; Fellmann, C.; Marmelstein, A. M.; Maza, J. C.; Kissman, E. N.; Robinson, S. A.; Staahl, B. T.; Urnes, C.; Lew, R. J.; Mogilevsky, C. S.; Doudna, J. A.; Francis, M. B. Site-Specific Bioconjugation through Enzyme-Catalyzed Tyrosine–Cysteine Bond Formation. *ACS Cent. Sci.* **2020**, *6* (9), 1564–1571.
(16) Palla, K. S.; Hurlburt, T. J.; Buyanin, A. M.; Somorjai, G. A.; Francis, M. B. Site-Selective Oxidative Coupling Reactions for the Attachment of Enzymes to Glass Surfaces through DNA-Directed Immobilization. *J. Am. Chem. Soc*. **2017**, *139* (5), 1967–1974.
(17) Furst, A. L.; Smith, M. J.; Francis, M. B. Direct Electrochemical Bioconjugation on Metal Surfaces. *J. Am. Chem. Soc.* **2017**, *139* (36), 12610–12616.
(18) Maza, J. C.; Bader, D. L. V.; Xiao, L.; Marmelstein, A. M.; Brauer, D. D.; ElSohly, A. M.; Smith, M. J.; Krska, S. W.; Parish, C. A.; Francis, M. B. Enzymatic Modification of N-Terminal Proline Residues Using Phenol Derivatives. *J. Am. Chem. Soc*. **2019**, *141* (9), 3885–3892.
(19) Marmelstein, A. M.; Lobba, M. J.; Mogilevsky, C. S.; Maza, J. C.; Brauer, D. D.; Francis, M. B. Tyrosinase-Mediated Oxidative Coupling of Tyrosine Tags on Peptides and Proteins. *J. Am. Chem. Soc*. **2020**, *142* (11), 5078–5086.
(20) Taskinen, B.; Zauner, D.; Lehtonen, S. I.; Koskinen, M.; Thomson, C.; Kähkönen, N.; Kukkurainen, S.; Määttä, J. A. E.; Ihalainen, T. O.; Kulomaa, M. S.; Gruber, H. J.; Hytönen, V. P. Switchavidin: Reversible Biotin–Avidin–Biotin Bridges with High Affinity and Specificity. *Bioconjugate Chem*. **2014**, *25* (12), 2233–2243.
(21) Zauner, D.; Taskinen, B.; Eichinger, D.; Flattinger, C.; Ruttmann, B.; Knoglinger, C.; Traxler, L.; Ebner, A.; Gruber, H. J.; Hytönen, V. P. Regenerative Biosensor Chips Based on Switchable Mutants of Avidin—A Systematic Study. *Sensor Actuat. Chem-B* **2016**, *229*, 646–654.
(22) Kodoyianni, V. Label-Free Analysis of Biomolecular Interactions Using SPR Imaging. *BioTechniques* **2011**, 50 (1), 32–40.
(23) Yang, N.; Su, X.; Tjong, V.; Knoll, W. Evaluation of Two- and Three-Dimensional Streptavidin Binding Platforms for Surface Plasmon Resonance Spectroscopy Studies of DNA Hybridization and Protein–DNA Binding. *Biosens. Bioelectron.* **2007**, *22* (11), 2700–2706.
(24) Muraoka, A.; Matsuura, Y.; Naitow, H.; Ihara, M.; Kunishima, N. Availability of NHS-Biotin Labeling to Identify Free Protein Lysine Revealed by Experiment and MD Simulation. *Anal. Biochem.* **2018**, *557*, 46–58.
(25) Strachan, E.; Mallia, A. K.; Cox, J. M.; Antharavally, B.; Desai, S.; Sykaluk, L.; O'Sullivan, V.; Bell, P. A. Solid-Phase Biotinylation of Antibodies. *J. Mol. Recognit.* **2004**, *17* (3), 268–276.
(26) Pishesha, N.; Ingram, J. R.; Ploegh, H. L. Sortase A: A Model for Transpeptidation and Its Biological Applications. *Annu. Rev. Cell and Dev. Biol.* **2018**, *34* (1), 163–188.
(27) Zhang, Y.; Park, K.-Y.; F. Suazo, K.; D. Distefano, M. Recent Progress in Enzymat-

ic rotein Labelling Techniques and Their Applications. *Chem. Soc. Rev.* **2018**, *47* (24), 9106–9136.
(28) Fairhead, M.; Howarth, M. Site-Specific Biotinylation of Purified Proteins Using BirA. *Methods Mol. Biol.* **2015**, *1266*, 171–184.
(29) Maza, J. C.; Ramsey, A. V.; Mehare, M.; Krska, S. W.; Parish, C. A.; Francis, M. B. Secondary Modification of Oxidatively-Modified Proline N-Termini for the Construction of Complex Bioconjugates. *Org. Biomol. Chem.* **2020**, *18* (10), 1881–1885.
(30) Capehart, S. L.; ElSohly, A. M.; Obermeyer, A. C.; Fran-cis, M. B. Bioconjugation of Gold Nanoparticles through the Oxidative Coupling of *Ortho*-Aminophenols and Anilines. *Bioconjugate Chem.* **2014**, *25* (10), 1888–1892.

5.6 Supplementary Figures

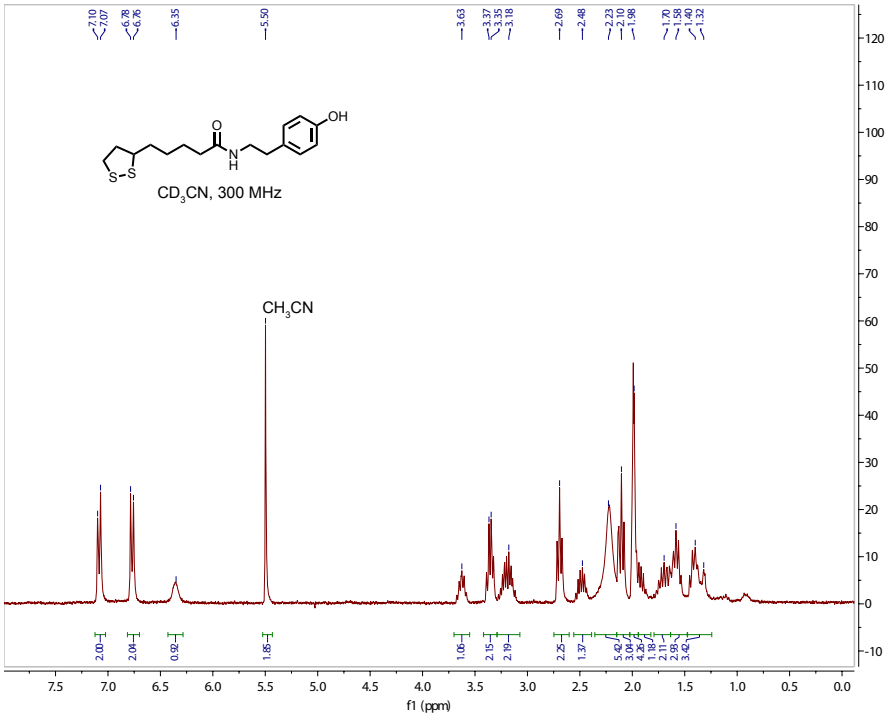

Figure S1. Characterization of disulfide-C5-phenol via ^{1}H NMR.

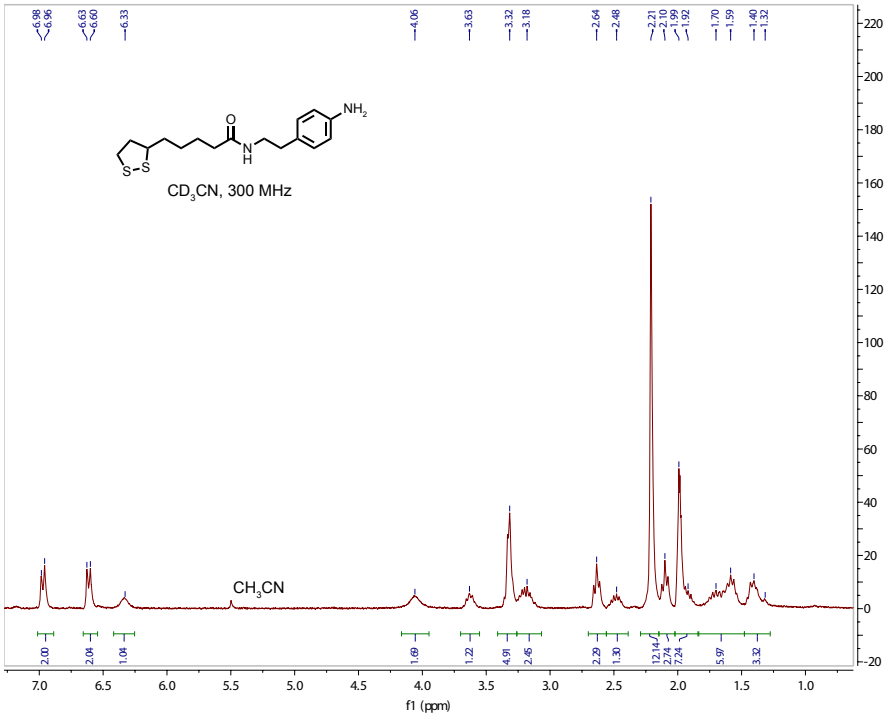

Figure S2. Characterization of disulfide-C5-aniline via ^{1}H NMR.